D66357'86

THE OPTICAL PROPERTIES OF OXIDE FILMS

ON COPPER AND COPPER ALLOYS

A thesis submitted to the
Council for National Academic
Awards in partial fulfilment
of the requirements for the
degree of Doctor of Philosophy

by

M.A. HAMILTON BA(OU), MSc

Department of Metallurgy and Materials Engineering
Sir John Cass Faculty of Physical Sciences and Technology
City of London Polytechnic
Whitechapel High Street
London E1

September 1985

DECLARATION

I, the undersigned MAVIS ALICE HAMILTON hereby
declare that the work contained in this
thesis has not been submitted before or
elsewhere for an academic qualification and
that I have not been, during my registration
with the CNAA for the PhD candidature,
registered with any other academic or
professional institution as a candidate.

Signed ...M. A. Hamilton.

CONTENTS

ABSTRACT

Suitable conditions were selected to allow thin, thermal oxide films consisting of cuprous oxide only to be grown on copper and dilute copper alloy substrates. The identity of the oxide was confirmed by X-ray diffraction and coulometry. Spectral measurements covering the wavelength range 350 - 750 nm were made using an automatic, self-nulling ellipsometer. From this data the optical constants and thickness of the oxide films were computed and compared to those of the bulk oxide. The optical constants of the oxide were found to depend on the thickness of the film and the identity of the alloying addition in the substrate. The effect of different substrates on the optical constants of cuprous oxide was tested by growing thin cuprous oxide films on gold and glass substrates. Optical property changes of the oxide are attributed to space-charge effects existing at the substrate/oxide interface.

1. <u>INTRODUCTION</u>

The optical properties of thin films are conveniently studied by ellipsometry. It provides a sensitive method of measuring the changes in the state of polarisation that light undergoes when it is reflected non-normally at a filmed surface. Ellipsometry has been widely used in oxidation studies of metals as a non-destructive, in-situ method of monitoring oxide growth. In most instances measurements have been made at a single or a limited number of wavelengths.

The oxidation products of metals are frequently found in nature as minerals and their optical properties have been measured by reflectance microscopy and used as reference standards for ellipsometric studies.

For this investigation thin films of cuprous oxide were produced on copper and dilute copper alloys in an attempt to compare the optical properties of thin films with those of the bulk material.

The optical constants of naturally occurring cuprite have been studied by the British Natural History Museum to check measuring techniques and to compare values of optical properties. Further work at the City of London Polytechnic has compared the optical properties of synthetic and natural bulk cuprite. Apart from the obvious value of these well documented studies of the optical properties of cuprite there were other reasons for choosing the copper/cuprous oxide system. The very thin air-formed films on copper have been identified as cuprous oxide and thicker films can be grown at low temperatures. Many thermal

oxidation studies of copper have been conducted and have related oxide composition and thickness to the oxidising conditions such as the partial pressure of oxygen, temperature, gas phase composition and impurities in the metal. The oxides of copper can be quantitatively reduced by cathodic polarisation and thus the oxide composition and thickness can be independently established. Since cuprous oxide is a semi-conductor, doping with foreign cations should produce changes in its electronic properties which should be detectable in the optical spectra.

For an absorbing material such as a metal oxide the optical constants are complex and involve a real and imaginary component i.e. $\bar{N} = n - ik$ where N is the complex refractive index, n is the ordinary refractive index for incident light normal to the surface, and k is the absorption coefficient. To determine the optical constants of a film of oxide on a metal substrate it is necessary to have accurate values of the optical constants of the metal and a precise value of the film thickness. The optical constants of the substrate are obtained by measuring Δ, the relative phase retardation and ψ, the relative phase change for light reflected non-normally from a surface. To satisfy the Drude-optical model, this surface must be clean, flat, specularly reflecting and unstrained. In practice such a condition is difficult to achieve since most metals are covered with surface layers of contaminants, oxides or adsorbed species and producing the required polished surface may involve deforming the outer layers.

Accurate values of the optical constants of thin films are difficult to obtain because of the problem of obtaining exact

measurements of the film thickness. The nature of the substrate, the state of the substrate surface, the surface roughness of the film and its defect structure will also affect the determination of the film optical constants and thickness. Many workers have reported anomalous values of the optical constants of thin films and several models have been proposed in an attempt to explain them. Through this investigation it is hoped to show that the optical constants of thin films of cuprous oxide change with thickness, foreign cation content and substrate. The results will be discussed with respect to some of the models proposed by other workers and will consider the algorithms used to evaluate them and their implicit assumptions.

2. LITERATURE SURVEY

2.1 The optical properties of copper

The optical properties of metals concern their interaction with electromagnetic radiation. The term is normally used to cover a wide range of wavelengths i.e. 1 to 10^6 nm (1 keV to 1 meV). The near infrared to the ultraviolet region, 350 - 750 nm is that of interest in this work.

Electromagnetic radiation acting on a metal induces transitions of electrons either within or between electronic energy bands. The excitation of electrons from one band to another is known as an interband transition. Observation of the absorption of light as a function of wavelength shows maxima and minima which indicate the energies of various electronic bands.

Predictions of optical and electronic properties are based on the calculated response of a simple atomic model. In this model an electron in an atom of the metal is presumed to be affected by the field created by the atomic cores (consisting of the nuclei and the inner-shell electrons) and the average field caused by all the other outer-shell electrons.

The classical models for the absorption and dispersion of light by metals and non-metals were proposed by Lorenz (1) and Drude (2). The Lorenz model, applicable to insulators, considers an atom with the electrons bound to the nucleus in a manner similar to a small mass connected to a larger mass by a spring. The dielectric function conveniently relates optical and electronic properties of materials.

thus
$$n = \left\{ \frac{1}{2} \left[\left(\epsilon_1^2 + \epsilon_2^2 \right)^{\frac{1}{2}} + \epsilon_1 \right] \right\}^{\frac{1}{2}}$$

and
$$k = \left\{ \frac{1}{2} \left[\left(\epsilon_1^2 + \epsilon_2^2 \right)^{\frac{1}{2}} - \epsilon_1 \right] \right\}^{\frac{1}{2}}$$

where ϵ_1 is the real part of the dielectric function and ϵ_2 is the imaginary part of the dielectric function. ϵ_1 and ϵ_2 are frequency dependent and can be related by the expression derived by, for example, Wooten (3)

$$\hat{\epsilon} = 1 + \frac{4\Pi e^2}{m} \sum_j \frac{N_j}{(\omega_j^2 - \omega^2) + i\Gamma_j \omega}$$

where
$$\hat{\epsilon} = \epsilon_1 - i\epsilon_2$$

ω is the frequency corresponding to the wavelength λ, i.e. $\omega = 2\Pi c/\lambda$ where c is the velocity of light in vacuo. N_j is the number of electrons per unit volume contributing to absorption in the jth absorption line, ω_j and Γ_j are the centre frequency and absolute line width of the jth oscillator, m is the electron mass and e is the charge on the electron.

The strength of the jth oscillator is given by

$$S_j = \frac{4\Pi e^2 N_j}{m\omega_j^2}$$

and
$$\Gamma_j^{relative} = \Gamma_j^{absolute}/\omega_j$$

The reflectivity of solids at normal incidences is given by

$$R = \frac{(n-1)^2 + k^2}{(n+1)^2 + k^2}$$

and the frequency dependent behaviour of the material can be described as reflecting, absorbing or transparent. When it is transparent $\omega \ll \omega_o$ (where ω_o is the natural frequency for excitation of the oscillator), $\varepsilon_2 = 2nk = 0$, $\varepsilon_1 = n^2 - k^2 > 1$ and therefore $k = 0$, $n > 1$ and $\varepsilon_1 = n^2$. Where the material can be described as absorbing, an appreciable amount of reflection may still occur but light not reflected is strongly absorbed. In the reflecting region $\omega \gg \omega_o$ and the electrons in the insulator behave as free electrons because the photon energy is greater than the binding energy. For good insulators this region lies beyond the ultra-violet. The fourth region is defined by $\varepsilon_1 = 0$ at what is known as the plasma frequency, ω_p, where $\omega_p \gg \omega_o \gg \Gamma$ and it can be shown that $\omega_p^2 = 4\Pi N e^2 / m$. The spectral dependence of n and k and the regions where the insulator is absorbing, reflecting or transparent are shown in Figure 2.1.

The Drude model for metals is obtained from the Lorenz model for insulators by equating the restoring force to zero. The metal can therefore be expected to behave in the same way as an insulator when $\omega > \omega_o$. For an ideal free-electron metal, reflectance is almost 100% below the plasma frequency. Above this frequency the metal is transparent. For real metals the plasma frequency is in the visible or ultra-violet part of the spectrum, typically corresponding to $\omega > 10^{15}$ sec^{-1}. The spectral dependence of n and k for a free electron metal and the regions where it is absorbing, reflecting or transparent
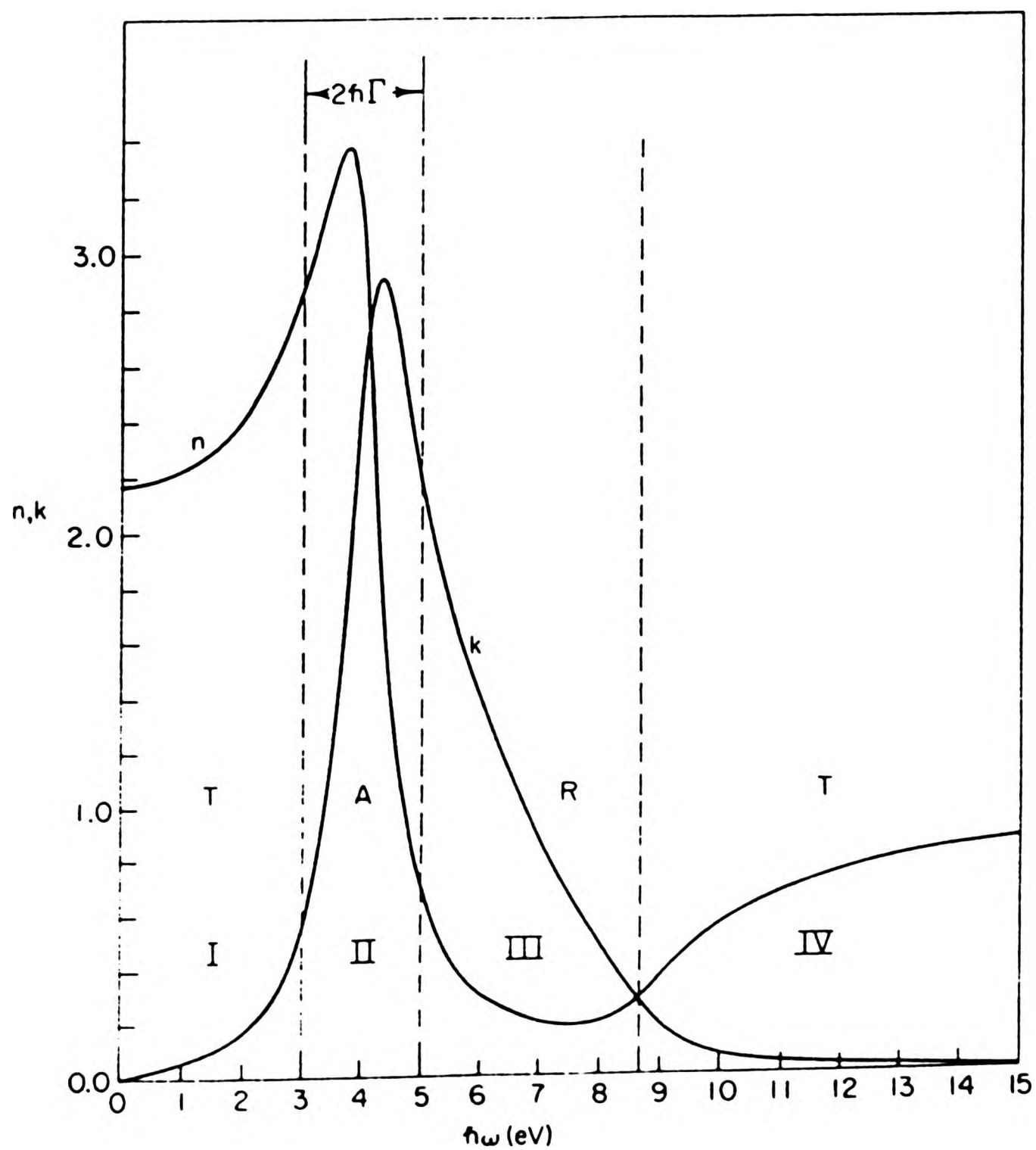
Figure 2.1 The spectral dependence of n and k for an insulator.
Regions I, II, III and IV are mainly transmitting (T), absorbing
(A), reflecting (R) and transmitting (T) respectively.
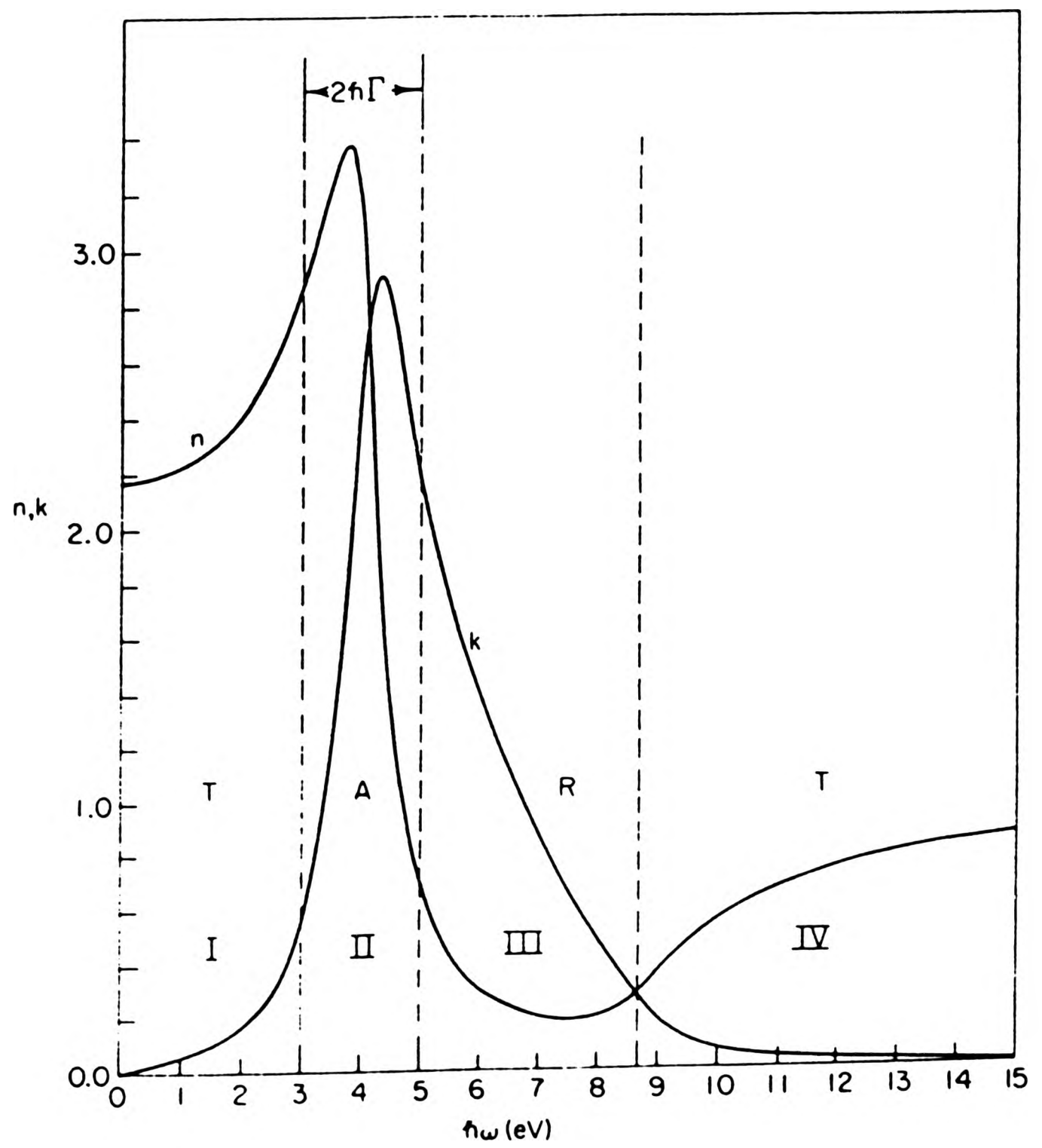
Figure 2.1 The spectral dependence of n and k for an insulator. Regions I, II, III and IV are mainly transmitting (T), absorbing (A), reflecting (R) and transmitting (T) respectively.

are shown in Figure 2.2. Real metals exhibit aspects of both
the Drude and Lorenz models.

Most of the electrical and optical properties of solids can be
explained qualitatively in terms of their band structure. When
atoms are sufficiently close quantum-mechanical forces become
effective and split the sharp energy levels of an isolated atom
into energy bands. Splitting of the energy levels shifts the
energy bands upwards and downwards lowering the potential
thresholds between neighbouring atoms. Electrons can move
freely within energy bands which are separated by forbidden
regions known as energy gaps. Of the complete band structure
it is the two highest bands which are most important. The upper
band, the conduction band has no electrons or has partly filled
energy levels. The lower band, called the valence band is
usually full and is separated from the conduction band by a
range of forbidden energies of width ΔE.

The band structure makes it possible to classify solids into
three classes; conductors, insulators and semiconductors
respectively. A conductor is a solid in which the conduction
band is partially filled and the electrons can move freely
under the influence of an applied field. The valence and
conduction bands may overlap so that electrons are shared
between them. In an insulator the conduction band is empty and
is separated from the valence band by $\Delta E \gg kT$ where kT is the
thermal energy. An applied field can not induce movement of
the electrons and no current flows. If the energy gap is of the
same order of magnitude as the thermal energy the solid is an
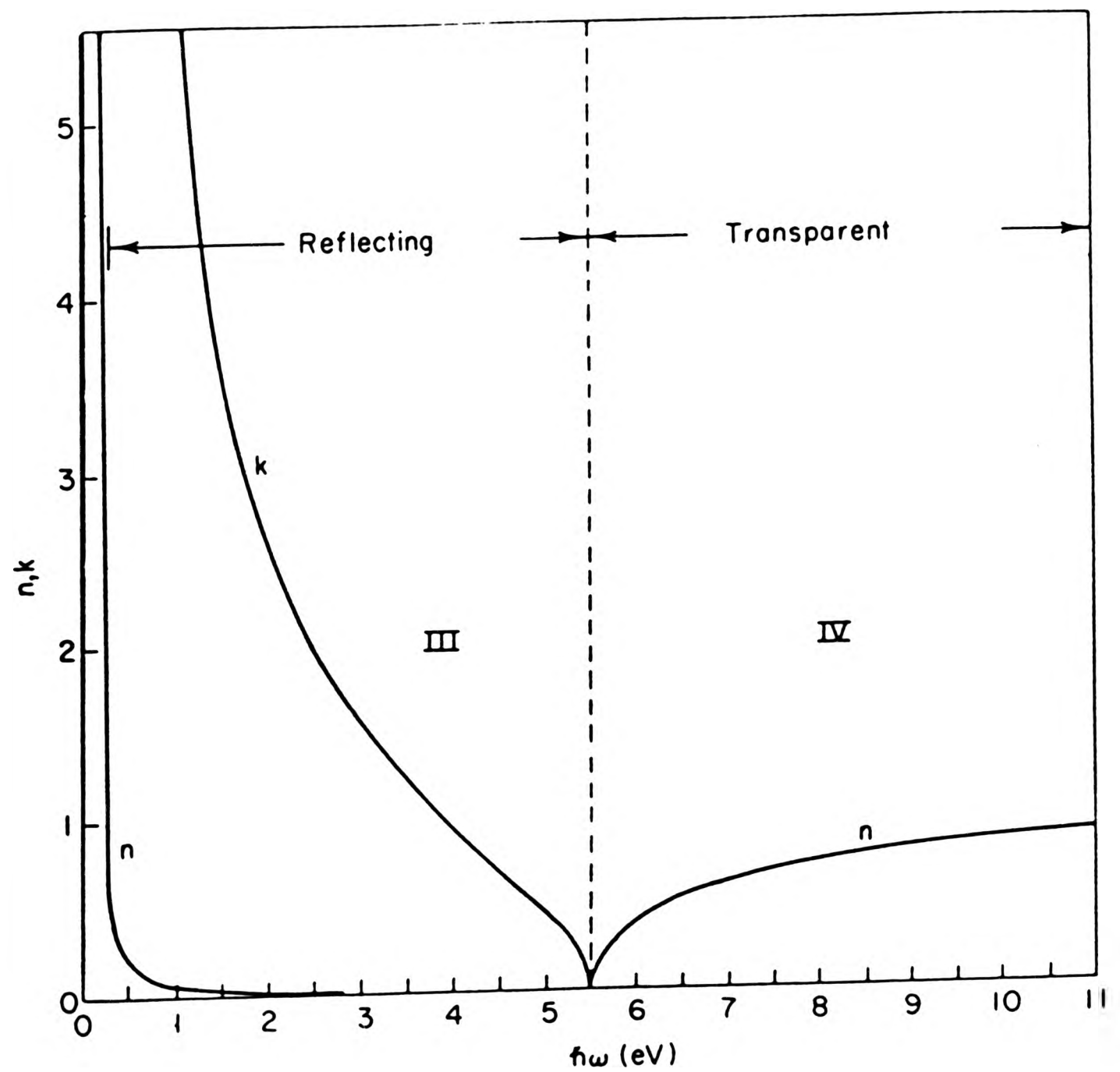
Figure 2.2 The spectral dependence of n and k for a free electron metal. Regions III and IV correspond to those of Figure 2.1. Region II, that of strong absorption is the range $0 \leq \hbar\omega$ which in this case is shown as 0.02 eV. Region I does not exist for metals.

intrinsic semiconductor showing electronic properties which are
temperature dependent. At low temperatures electrons are
excited into the conduction bands and the solid becomes conducting.
At zero Kelvin all the low lying energy states are full. The
energy at which this occurs is known as the Fermi level. The
optical excitation of an electron from below the Fermi level to
an energy level above it but within the same band is known as
an intraband transition. This type of transition is described
by the Drude model and can only occur in a metal. Insulators
have no partially filled bands which would allow an electron from
a filled state below the Fermi energy to be excited into an
empty state within the same band. Electrons can also be excited
by photons to another band. This type of transition is known as
an interband transition and has a threshold energy.

The dielectric function of a metal can be obtained from
reflectance measurements and can be split into bound electron
(Lorenz) and free electron (Drude) contributions, and interpreted
in terms of the band structure. Ehrenreich and Philipp (4)
presented the first detailed analysis of the absorption
spectrum of copper in 1962. They measured the reflectance over
the energy range 0-25 eV. Their measurements were made in air
but only fine detail has been added by later work done under
vacuum on film-free copper surfaces. The d-bands in copper
were found to lie some 2 eV below the Fermi level so only
interband transitions of the conduction electrons are possible
at low energies. Transitions from the d-bands to the higher
conduction bands start at about 600 nm. This strong absorption
means that the reflectance of copper starts to decrease in the

red region, ie. the highest reflectance occurs at the red end of
the visible spectrum giving copper its characteristic colour.
The origins of other peaks at 3.9 and 5 eV were disputed by many
workers including Mueller and Phillips (5), Seib and Spicer (6)
and Gerhardt (7). Reflectance measurements made by Fong et al
(8) on an electropolished single crystal of copper at 7 K
revealed finer details and confirmed the complex structure of the
5 eV peak.

Long before these electronic studies of copper many workers had
made optical measurements. In the period 1890 to 1936, Drude
(2), Minor (9), Tool (10), Foersterling and Freedericksz (11),
Margenau (12) and Lowery (13) all agreed that the degree of
polishing had a profound effect on the values of n, k and Rn
which they obtained. Annealing to produce a strain-free
surface was found to decrease values of n although its effect
on the magnitude and direction of changes in k was disputed.
Polishing was known to create surfaces with properties not
representative of the bulk material. Beilby (14) had suggested
that polishing produced an amorphous layer of metal up to 500 $\overset{\circ}{A}$
thick. Recent transmission electron microscopy studies by
Turley and Samuels (15) of copper surfaces polished with diamond
abrasives have shown no evidence of the Beilby layer. They
found that the surface layers were crystalline but showed signs
of plastic deformation. The degree of deformation decreased
with increasing fineness of abrasive. Surfaces polished with
6 μm diamond abrasive consisted almost entirely of small sub-
grains which indicated recrystallisation of severely deformed
material. They attributed this to the effect of temperatures

of 100-150°C reached during polishing on heavily deformed grains
at the surface. With finer abrasives there was less
recrystallisation probably because they cause less damage to
surface layers and lower temperatures are reached during
polishing. However, Roberts (16) found that this surface layer
had a higher electrical resistivity and larger values of n and
k than those of the bulk material. Electropolishing was used
to overcome this problem but the film of cuprous oxide which
forms on copper surfaces exposed to air caused difficulties for
many workers. Authors including Drude (2), Tool (10), Kretzmann
(17) and Archard et al (18) have reported that this film forms
in times varying from minutes to a period of hours. Winterbottom
(19), studying the surface films on copper, showed that they
were reduced by heating to a temperature above 460 K in hydrogen.
Roberts (16) improved on this by heating his specimens to 500 K
in a vacuum of 2×10^{-5} mm of mercury. He compared his results
with those of Ingersoll (20), Foersterling and Freedericksz (11),
Weiss (21) and Schultz (22) and found close agreement with those
of Schultz in the red and infra-red portions of the spectrum.
He attributed this to the annealing process used by Schultz and
his avoidance of oxide films.

Other methods of obtaining film-free surfaces included
solidification of the molten metal in a high vacuum and ion-
bombardment. Otter (23), using the former method, obtained
values of n and k at several wavelengths over the range 4700-
6750 Å. Although the surfaces produced in this way were
relatively clean, Smith (24) showed that they were not smooth.
He produced smooth, clean surfaces by mechanically polishing

the specimens for maximum smoothness and high temperature annealing in vacuo to remove oxide layers and surface damage. He followed these treatments with ion bombardment to remove contamination caused by segregation of impurities at the surface during the annealing process.

A comparison of the published data shows that improvements to the surface (resulting in closer approximation to the ideal Drude surface) have increased the value of n. The effect on k is less consistent as shown in Table 2.1.

Recent theoretical work on copper has suggested values for the dielectric function that have been compared with those derived from reflectance measurements. Roychaudhuri and Chatterjee (34) calculated the transition energy from the d-bands to the Fermi level to be 2.04 eV which they compared with Robert's (16) measured value of 2.5 eV. The calculated values of the optical constants evaluated depend on the assumptions of the model. So far no single model has been found which is in close agreement with experimental values over more than a very limited energy range. Robusto and Braunstein (35), for example, achieved a good match with the experimental values found by Schulz (22) over the range 4400-5500 $\overset{o}{A}$. Lässer et al (36) computed values of the dielectric function for energy values ≤ 2.5 eV and produced a theoretical spectrum similar in shape to that obtained experimentally by Lässer and Smith (37) but with sharper peaks which were shifted.

Table 2.1 Published optical constants for copper

Author	Ref	Form and preparation of specimen	Wavelength	n	k	Source of optical constants	Ref
S. Roberts, 1960	16	electropolished, vacuum annealed polycrystalline	546.1 632.8	0.82 0.11	2.71 3.66	ellipsometric measurements	
P.Q.S. Hayfield, 1961	25	electropolished	546.1	0.99	2.65	ellipsometric measurements	
M. Otter, 1961	33	solidified drop	546.1 632.8	0.89 0.10	2.76 3.70		
E.C. Butcher et al, 1968	26	bulk copper	546.1	1.101	2.165	ellipsometric measurements	
J.A.S. Green et al, 1970	27	electropolished	435.8	1.5	1-2.39	ellipsometric measurements	
P.B. Johnson, R.W. Christy, 1972	28	vacuum evaporated thin films	430.5 548.6 616.8	1.25 1.02 0.30	2.305 2.577 3.205	ellipsometric measurements	
G.W.C. Kaye, T.H. Laby, 1973	29		550.0	0.70	2.40		
J. Weaver, 1984	30		442.8 539.0 619.9	1.17 1.04 0.27	2.36 2.59 3.24	H.J. Hagemann et al, 1975	31

Table 2.1 contd. Published optical constants for copper

Author	Ref	Form and preparation of specimen	Wavelength	n	K	Source of optical constants	Ref
B.C. Alexander, 1976	32	electropolished single crystal	?	0.2766	3.178	ellipsometric measurements	
T. Smith, 1976	24	mechanically polished	546.1	0.89	2.67	ellipsometric measurements	
		vacuum annealed, ion bombarded	632.8	0.17	3.70		
J.S. Hartman, 1981	33	single crystal, electropolished ion bombarded	632.8	0.14	3.85	ellipsometric measurements	

2.2 The optical properties of cuprous oxide

The optical constants of cuprous oxide have been measured by
many workers for widely differing purposes. Cuprous oxide is
an intrinsic semi-conductor and optical studies have been used
as a way of studying the distribution of energy levels in the
crystal. Oxidation and corrosion studies of copper in a variety
of media have been carried out using ellipsometry which has
necessitated a knowledge of the optical constants of the oxides
of copper and, recently, cuprous oxide has become increasingly
important as a solar energy converter. This has generated
renewed interest in its optical properties.

Spectroscopic methods have been used for many years to provide
information on the structure of atoms and molecules. In the
1950s, attempts were made to develop a similar technique for
solid state physics to provide information on the band structure
of electronic states in solids. The spectral structure shows
thresholds and edges due to direct band to band transitions and
narrow peaks due to the formation of excitons. Phillips (38)
developed a method of interpreting absorption or reflection
spectra and hence constructing band structures from them. Before
this, Hayashi (39) had obtained absorption spectra for
polycrystalline cuprous oxide covering the visible part of the
spectrum at temperatures varying from -184°C to 150°C. He
found two sharp absorption edges forming a doublet with a
separation of 0.028 eV; hydrogen-like absorption lines adjoining
an absorption band and another absorption band at a wavelength
shorter than the hydrogen-like lines. Gross and Karryev (40)
reported a strong absorption in the short wave portion of the

spectrum which they assigned to the fundamental absorption of
the cuprous oxide lattice. There was a sharp decrease in
absorption at 6300 $\overset{o}{A}$. The edge of the absorption band was
found to be complex with absorption increasing step-wise with
decrease in wavelength. Two sharp edges were observed where the
absorption curve shows a break. The separation of these edges
was 0.027 eV at 20°C and was almost unchanged at 0.024 eV at
-200°C although the entire spectrum was shifted towards shorter
wavelengths. At -200°C the coefficient of absorption was
appreciably reduced and seven fine lines were observed which
converged at 5727 $\overset{o}{A}$. They interpreted these lines as evidence
for the existence of excitons. Nikitine, Perny and Sieskind
(41) observed three series of lines, of which at least two were
hydrogen-like in character. The first of these, in the green
part of the spectrum, was the most intense and was ascribed to
the fundamental exciton absorption. In 1959 Gorban (42) made
quantitative measurements on the intensity of absorption lines
as a function of impurity content at a temperature of -180°C.
He found that absorptions were independent of impurity level and
confirmed that the hydrogen-like series of absorptions in the
cuprous oxide spectrum was due to the fundamental absorption of
the crystal. Pastrnyak (43) in 1961, using a reflectance method
had identified reflection lines in the blue and dark blue
regions of the spectrum. Gross and Chang (44), working in the
same laboratory, and using an improved method, confirmed
Pastrnyak's findings and found further lines in the ultra-violet
part of the spectrum. They attributed them to excitons
associated with the excitation of electrons from the deeper
valence sub-bands to exciton levels near the higher conductivity

sub-bands.

Before the nature of the exciton spectra can be fully understood, the energy bands within the crystal must be known. Calculations made by Dahl and Swittendick (45) showed that the excitons in cuprous oxide are associated with copper ions rather than oxide ions. They were able to assign each of the exciton series to transitions within the energy bands of the crystal. Their calculated value of the band gap for cuprous oxide was 1.77 eV which they claimed to be in reasonable agreement with the experimentally determined value of 2.17 eV (46) thereby validating their model. The development of more sophisticated models using the increased capabilities of modern computers together with technological advances in experimental techniques has led to excellent agreement of theoretical and experimental values. Uihlein et al (47) calculated the even- and odd-exciton members of the yellow and green series using a model formulated by Lipari and Baldereschi (48). They compare their calculated results with experimental measurements obtained using a tuneable low-power laser combined with a fixed frequency high-power laser on highly pure, arc-image-grown cuprous oxide crystals at 4.5 K. They obtained spectra with high resolution covering the green and yellow exciton series. The differences between their calculated and measured exciton energies were negligible.

Many oxidation studies of copper have used optical methods either as a non-destructive means of measuring film thickness or for in-situ measurements at low temperatures. In most of these

studies a single wavelength has been used, usually 5461 $\overset{o}{A}$ using a
mercury lamp or 6328 $\overset{o}{A}$ using a helium-neon laser. In most cases
the films have been identified as cuprous oxide or conditions
have been selected to produce cuprous oxide. In later studies,
film-fitting computer programmes have been used to calculate film
thicknesses. The optical constants of both the substrate and
the film are generally required for these calculations, because
$k \neq 0$. Independent thickness measurements have been obtained in
a variety of ways. Rhodin (49) used a microbalance to determine
the thickness of oxide films on individual faces of a copper
single crystal and was able to correlate interference colours
with thickness. Gwathmey and Benton (50) also used interference
colours as a means of measuring oxide thickness. Later, Young,
Cathcart and Gwathmey (51) used a combination of interference
colours and the optical constants of cuprous oxide to calculate
the rates of oxidation of several faces of a single crystal of
copper. The values of the optical constants of cuprous oxide
which they used were obtained by Young (52) using a graphical
method but they are not stated in their paper. Coulometric
reduction was used by Wilhelm et al (53) to confirm film
thicknesses in a photo-electrochemical investigation of the semi-
conducting oxide films on copper. Table 2.2 shows some of the
values of the optical constants of cuprous oxide quoted by
these and other workers. Sources or derivations of the data
have been included when known.

Discrepancies between the optical constants computed for thin
films of cuprous oxide and those measured for the bulk material
are explained in terms of different stoichiometries (56, 61),

Table 2.2 Published optical constants of cuprous oxide

Author	Ref	Form of oxide	Wavelength λ/nm	n	k	Source of optical constants	Ref
S. Roberts (1960)	16	thin film	100	1.5	-	estimation	
P.C.S. Hayfield (1961)	25	thin film bulk	546.1 -	2.70-2.80 2.71	- -	polarimetric observations mineralogical data book	
E.C. Butcher, A.J. Dyer N.E. Gilbert (1968)	26	thin film	546.1	2.455	0.145	computed from ellipsometric measurements	
J.A.S. Green, H.D. Mengelberg H.T. Yolken (1970)	27	Cu$_2$O films on Cu and α-brass in aqueous ammonia	435.8	2.3-3.2	0.0-1.0	computed from ellipsometric measurements	
T. Smith (1977)	24	air formed films on copper	546.1	2.8	0.3		
K. Barwinkel, H.J. Schmidt (1979)	54	films > 300 Å thick	485 515	2.759 2.572	0.236 0.115	spectroreflectometry	
V.F. Drobny, D.L. Pulfrey (1979)	55	sputtered films 1000 Å thick	400-800	2.7 2.8-3.4		Weider and Czandera (1962) calculated from reflectance and transmittance measurements	56

Table 2.2 contd. Published optical constants of cuprous oxide

Author	Ref	Form of oxide	Wavelength λ/nm	n	k	Source of optical constants	Ref
P. Rastall (1980)	57	bulk synthetic cuprite	250	1.68	1.62	spectral ellipsometry	
			350	2.68	1.80		
			450	3.31	0.91		
			550	3.18	0.30		
			650	2.90	0.16		
			750	2.79	0.13		
			850	2.73	0.12		
G. Bartz, D. Kossel (1980)	58	Sputtered Cu_2O	450	2.03	0.44	Ernst Leitz GmbH, Wetzlar	59
			550	2.09	0.37		
			650	2.11	0.31		
H.C. Alexander (1976)	32	thin films	632.8	2.178	-	computed from ellipsometric measurements	
R Karlsson et al (1980)	60	solar absorbers		2.7	0.6	computed from reflectance data	
J.S. Hartzmann (1982)	33	thin films	532	2.65	0.206	computed from ellipsometric measurements	

defect structure (55), changes in substrate surface properties
due to chemisorption (62), anisotropy (32, 61), the presence of
foreign cations (63) or the use of inaccurate values of the
substrate optical constants (27, 54).

Much of the recent work on the oxides of copper concerns their
use in photo-voltaic cells. The films used in such cells being
of the order of μ metres in thickness. Aveline and Bonilla (64)
show that the optical properties of a layer of cuprous oxide on
a copper substrate can be modified to improve its suitability as
a selective surface. This is done by careful preparation of
the substrate and control of the oxidising conditions to avoid
the formation of cupric oxide, although they found that
comparatively thin layers of cupric oxide are undetectable.
Fortin and Sears (65) investigating the same type of photo-
voltaic back cell found that the cuprous oxide layer must be
around 1 μm thick to produce a cell of practical interest.
Karlsson et al (60) found that chemically oxidised copper
surfaces were more absorptive than those produced thermally.
In some areas the increased absorption was attributed to rougher
boundaries but cupric oxide was identified in such films and was
also thought to contribute to this effect.

It is clear that there are large differencies in the optical
constants measured or calculated by different workers. Many of
them have recognised sources of error and have tried, by careful
preparation of specimens, to eliminate them. Thus, control of
oxidising conditions will produce stoichiometric cuprous oxide
layers with smooth copper/cuprous oxide boundaries and smooth

surfaces (65). For the thicker films the possibility of a
surface layer of cupric oxide must be considered. Most of the
work on this subject has been done at elevated temperatures
but, Garnaud (66) found that there was always a higher oxide
present especially at the oxide/oxygen interface. Variation in
the optical constants of very thin films may be related to
inaccurate estimates of the film thickness. Comparisons between
the optical properties of thick and very thin films is further
complicated by the known anomalous properties of thin films.

2.3 The anomalous optical properties of thin films

In the preceding section it has been shown that there are almost
as many values of the optical constants of cuprous oxide available
from the literature as there are workers measuring them. The
majority of these values have been computed from measurements
made on thin films of cuprous oxide on a copper substrate. The
importance of accurate values of the optical constants of the
substrate has been stressed and a brief mention of other sources
of errors has been made. Some of these will be discussed in more
detail in this section.

The use of the Fresnel equations (section 2.4) to calculate the
refractive index of a reflecting surface by measuring the change
in state of polarisation of light reflected non-normally at the
surface is only valid when the surface is perfectly smooth.
Many workers have recognised that the surfaces which they have
examined have not fulfilled this requirement (67, 68).

Models of different types of roughness and methods of

compensating for them have been suggested. Fenstermaker and McCrackin (69) considered three types of roughness; square ridges, triangular ridges and pyramids, on substrates chosen to give a large range of values of both the real and the imaginary components of the refractive index. The range of roughness was 0 - 500 $\overset{o}{A}$ and they found that large errors in the determination of indices occurred for comparatively small values of roughness (50 $\overset{o}{A}$). They treated the surface as though it was a homogeneous film with an effective refractive index calculated from the proportions of the substrate and medium which made up the part of the system which they were considering as a film. Bodesheim and Otto (70) studied the limitations of some of the published theoretical calculations for the effect of surface roughness. They found that for surfaces with roughness of less than 10 $\overset{o}{A}$ these theories were satisfactory but for roughness greater than this, strong higher order scattering effects were observed.

Hunderi (71) identified three effects attributable to surface roughness they were:-

(1) The scattering of the incident light.

(2) The excitation of surface plasmons by the incident wave. This would alter transmission and reflection coefficients, particularly in the neighbourhood of the surface plasmon cut-off frequency.

(3) A larger effective surface area which would increase apparent inter- and intraband absorptions.

Brudzewski (72) prepared a strain-free substrate with controlled roughness by anodising a tungsten single crystal in sulphuric acid and then dissolving the oxide in dilute sodium hydroxide solution. The roughness was then measured by a stylus tracking device (Talystep) or light scattering. To investigate the effect of roughness on ellipsometric data for an oxide film on a metal, the tungsten samples were then anodised to give a wide range of film thicknesses. He found that the equivalent film theory proposed by Fenstermaker and McCrackin (69) can be applied when the surface irregularities and the distances between them are small compared with the wavelength of light. When this is not the case he suggested that the system of rough substrate/ rough film could be represented by two independent equivalent films, one with optical constants lying between those of the substrate and the film and the other with optical constants between those of the film and the medium, the two equivalent films being separated by a smooth film of oxide. This system is obviously very complex and he simplified it by dividing it into 200 homogeneous films of identical thickness with refractive indices which change with distance from the substrate. In this way he obtained good agreement between ellipsometric and Talystep estimations of surface roughness when the roughness was of the same order as the wavelength. Vorburger and Ludema (73) also compared ellipsometric and stylus measurements on rough surfaces. They used a set of nickel replicas of machined surfaces with random and periodic surface profiles and found that the ellipsometric angles Δ and ψ varied systematically with surface texture. The variations persisted even after the surface was changed by evaporating aluminium and then gold onto it. For

steeply sloped periodic surfaces the angles varied rapidly as
the angle of incidence was varied near a diffraction minimum.
This effect was ascribed to interference between singly and
doubly reflected light waves. However, although there were
trends related to surface geometry for the random surfaces they
were not able to correlate these trends with previous theories.
They concluded that the use of ellipsometry as a tool to
measure surface roughness would be problematical.

Recently, Smith (74) has shown that gross roughness can be
compensated for by considering its shadowing effect. He
describes three types of roughness - pits, ridges and bumps
which represent the types of roughness found on most real
surfaces. Thus etched surfaces are best described by the pits
model; rolled abraded surfaces by the ridge model and nucleation
and growth of films by the bump model. He prepared surfaces
with these configurations which had two levels of roughness, for
example, the pits themselves had roughness which was large
with respect to the light wavelength and within the pits there
was roughness on a scale small compared with the light wavelength.
McCrackin's computer program (75) was modified to take into
account correction factors for macroscopic and microscopic
roughness. Correction factors have been derived by several
authors (69, 76, 77) and Smith used one of these, having first
applied his own correction factor for macroscopic roughness.
He made measurements on sanded copper, etched aluminium and vapour
deposited aluminium/silicon and used the ridge, pits and bumps
models respectively to calculate their optical constants. By
considering the shadowing effects of the different forms of

roughness he obtained values for the optical constants of the
metals which were in close agreement with published data.

Zorin and Churaeva (78) have developed a method of establishing
the optical constants of a metal with a rough surface, and the
characteristics of the roughness. They show that the optical
constants of a metal, measured by ellipsometry, depend on the
refractive index of the medium with which it is in contact.
They attributed this to the presence of a transition layer
produced by roughness. By measuring the ellipsometric parameters
of the specimen in different media they found that they were
able to obtain the true optical constants of the metal and
information as to the nature of the roughness.

Roughness obviously complicates the interpretation of
ellipsometric data although to what extent is debatable.
Bodesheim and Otto (70) found differences with roughness of
about 10 $\overset{o}{A}$ while Fenstermaker and McCrackin (69) reported errors
associated with roughness of around 50 $\overset{o}{A}$. It seems likely that
differences in the optical constants of cuprous oxide computed
from ellipsometric measurements of films of cuprous oxide on
copper may be due to roughness in some cases. The smoothness
of the substrate and method of preparation of the oxide will be
important factors (24, 65).

Surface effects of other types have been considered by many
workers. Rastall et al (77), studying the optical properties
of cuprite, found that maxima and minima in spectral dispersions
of n and k were reduced by surface damage. They attributed

this to disorder in the crystal lattice produced by abrasion of
the surface layers during polishing. Hanekamp et al (61)
identified chemisorption of oxygen as a source of observed
optical anisotropy on copper single crystal surfaces. Clark (80),
reviewing the optical properties of semiconductor films mentions
grain boundaries, unwanted impurities, stoichiometric deviations
and point defects as sources of error in thin film and surface
studies. He considers some theoretical approaches to these
problems including Filinski's (81) study of the effect of
inhomogeneities on the reflectance of classical oscillators but
finds no model which deals with surface phenomena such as grain-
boundaries. Aspnes (82, 83) discusses the relationship between
the microstructure of thin films and their macroscopic dielectric
response. He suggests that voids reduce the polarisability per
unit volume of a surface and that oxide films or contamination
layers, which have dielectric constants smaller than those of
metal substrates, act to impedance match the substrate and ambient.
The presence of voids or films results in a reduction in the peak
of an ε_2 spectrum when compared to the true bulk value. This
observation can be used to monitor surface preparation techniques.

The atomic structure of a surface and the interdependence of a
film and substrate have also been considered. In 1964, Plumb
(84) suggested that the anomalous optical constants measured for
thin dielectric films on metal substrates could be ascribed to
a physical anomaly associated with the dielectric-metal interface.
He proposed that a diffuse electric double layer existing
between two distinct phases would produce a higher electrical
conductivity in the dielectric phase close to the metal than

that found in the bulk material. This variation in electrical
conductivity should be detectable as an increased optical
absorption. He supported his theories by ellipsometric
studies of gold surfaces covered with films of barium stearate
and found that the absorption coefficient of the film decreased
with increasing thickness. Roberts and Ross (85) re-examined
and extended this theory by considering other systems. They
found that the extent of the space-charge region for a thin
dielectric film on a metal substrate is directly proportional
to the dielectric constant of the film and inversely proportional
to the concentration of the electrons at the metal/film interface.
Opposite trends were observed when thin gold or silver films
were deposited on glass.

The geometric and electronic structure at the surface of a
crystal is often different from that of the bulk. This has been
demonstrated for substances with strong covalent bonds such as
silicon and germanium (86) and also for metals (87). LEED
and MEIS (medium energy ion-scattering) have shown that most
metal surfaces exhibit a tendency towards small bond length
between the first and next atomic layers, especially on less
close-packed faces. For clean metal surfaces with different
extents of contraction between the outer atomic layers
different values of the ellipsometric parameters Δ and ψ would
be expected. Habraken et al (62) calculate that the differences
in Δ and ψ for the (110) and (111) planes of copper measured
at 632.8 nm with an angle of incidence of 70° are 0.15 and
-0.01° respectively. Differences of this order of magnitude
could not reliably be attributed to variations in atomic

separation since it is unlikely that measurements on two apparently identical specimens would be that reproducible. They conclude that optical studies must be combined with other surface analytical techniques to establish surface cleanliness.

2.4 Ellipsometry

2.4.1 The fundamental equations

Detailed accounts of the theory of ellipsometry have been given by several authors (88, 89). A brief description outlining the theory and relating the calculated values of the optical constants to the measured angles A and P is given in this section.

The layout of the ellipsometer and the way in which measurements are obtained is described in Section 3.2.2. Δ, the relative phase retardation and ψ, the relative amplitude reduction of the electric field vectors measured in and normal to the plane of incidence are related to the measured angles, A and P respectively

i.e. $\qquad \Delta = 2A$ $\qquad\qquad$ (1)

$\qquad\qquad \psi = \pi/4 - P$ $\qquad\qquad$ (2)

These equations assume the optical arrangement shown in Figure 3.1 and a perfect quarter-wave plate. The reflection of polarised light from a filmed surface (shown schematically in Figure 2.3) can be described in terms of the complex reflection coefficients $\hat{R}_p$ and $\hat{R}_s$ where the subscripts p and s indicate

light vibration parallel and perpendicular respectively to the
plane of incidence. Figure 2.3 shows a system consisting of a
reflecting substrate with refractive index $\hat{N}_3$ covered with a
film of thickness d and refractive index $\hat{N}_2$ in a medium of
refractive index N_1, ϕ_1 is the angle of incidence, $\hat{\phi}_2$ is the
angle of refraction in the film; $\hat{\phi}_3$ is the angle of refraction
in the substrate and λ is the wavelength of the light in vacuo.
The medium is selected so that it has only a real component of
refractive index but $\hat{N}_2$ and $\hat{N}_3$ are usually complex. The
reflection coefficients are related to these parameters by the
following equations.

$$\frac{\hat{R}_p}{\hat{R}_s} = \tan \psi \; e^{i\Delta}$$

$$\hat{R}_p = \frac{\hat{r}_p^{12} + \hat{r}_p^{23} e^{-ix}}{1 + \hat{r}_p^{12} + \hat{r}_p^{23} e^{-ix}}$$

$$\hat{R}_s = \frac{\hat{r}_s^{12} + \hat{r}_s^{23} e^{-ix}}{1 + \hat{r}_s^{12} + \hat{r}_2^{23} e^{-ix}}$$

where
$$\hat{r}_p^{12} = \frac{\hat{N}_2 \cos \phi_1 - N_1 \cos \hat{\phi}_2}{\hat{N}_2 \cos \phi_1 + N_1 \cos \hat{\phi}_2}$$

$$\hat{r}_s^{12} = \frac{N_1 \cos \phi_1 - \hat{N}_2 \cos \hat{\phi}_2}{N_1 \cos \phi_1 + \hat{N}_2 \cos \hat{\phi}_2}$$

$$r_p^{23} = \frac{\hat{N}_3 \cos \hat{\phi}_2 - \hat{N}_2 \cos \hat{\phi}_3}{\hat{N}_3 \cos \hat{\phi}_2 + \hat{N}_2 \cos \hat{\phi}_3}$$

N_1

film
$\hat{N}_2$

substrate
$\hat{N}_3$
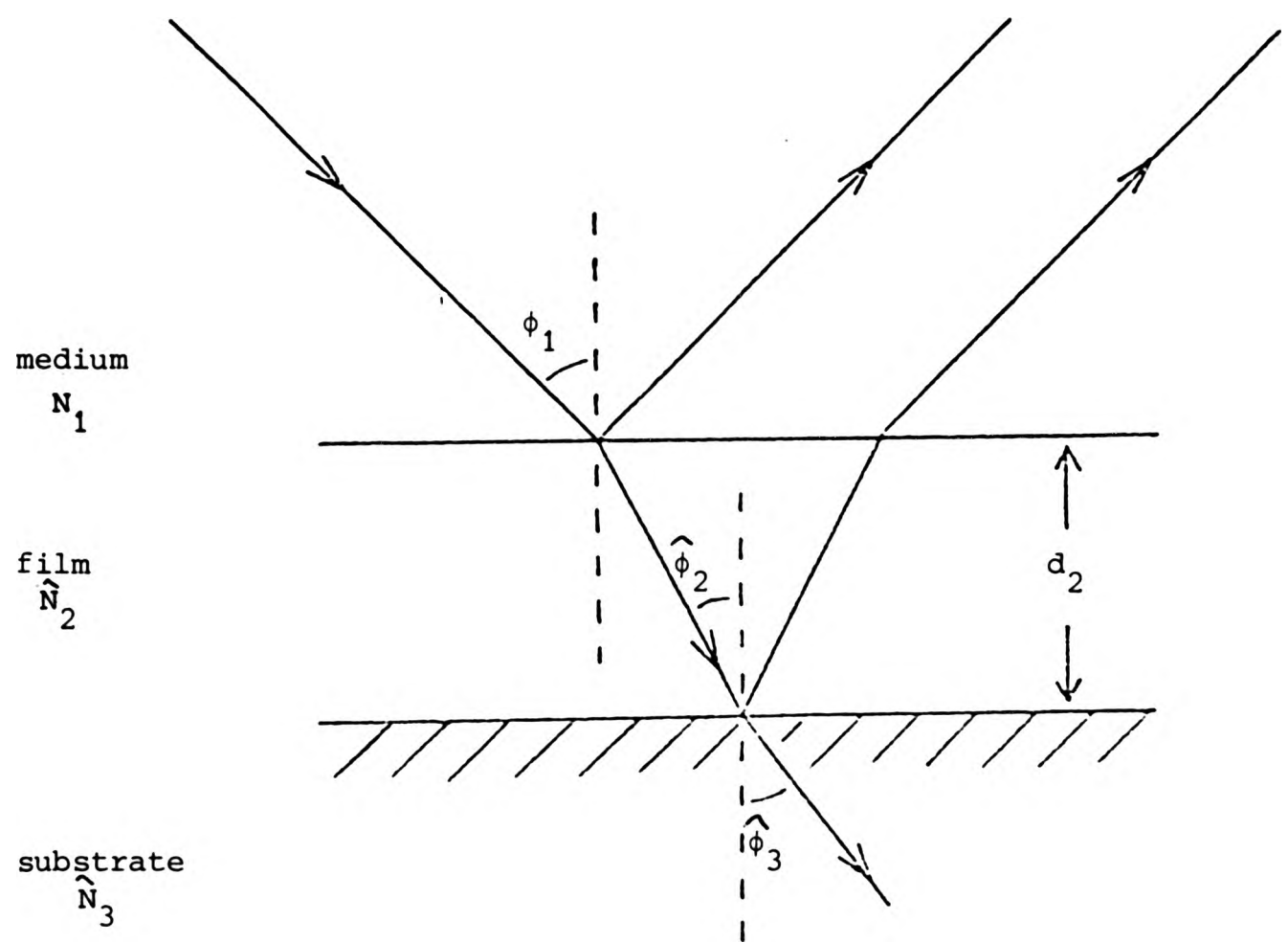
Figure 2.3   Reflection from a filmed surface

$$r_s{}^{23} = \frac{\hat{N}_2 \cos \hat{\phi}_2 - \hat{N}_3 \cos \hat{\phi}_3}{\hat{N}_2 \cos \hat{\phi}_2 + \hat{N}_3 \cos \hat{\phi}_3}$$

$$x = \frac{4 \Pi N_1 \, d \cos \phi_1}{\lambda}$$

$$\hat{N}_2 = n_2 - ik_2$$

$$\hat{N}_3 = n_3 - ik_3$$

For a film free surface, the refractive index of the surface is given by the simple expression

$$\hat{N}_3 = N_1 \tan \phi_1 \left[1 - \frac{4 \hat{\rho} \sin^2 \phi_1}{(1 + \hat{\rho})^2} \right]^{1/2}$$

where

$$\hat{\rho} = \hat{R}_p / \hat{R}_s$$

The calculation of $\hat{N}_2$ and d is more difficult. For an absorbing film there are three unknowns n_2, k_2 and d and only two measured quantities, Δ and ψ. To overcome this problem a series of refractive indices are assumed for a number of estimated film thicknesses. The corresponding values of Δ and ψ are calculated and compared with the experimentally derived values. The cumbersome nature and complexity of these equations have led to the introduction of computer programmes to evaluate the required parameters, (n_2, k_2, d).

$$r_s^{23} = \frac{\hat{N}_2 \cos \hat{\phi}_2 - \hat{N}_3 \cos \hat{\phi}_3}{\hat{N}_2 \cos \hat{\phi}_2 + \hat{N}_3 \cos \hat{\phi}_3}$$

$$x = \frac{4 \Pi N_1 \, d \cos \phi_1}{\lambda}$$

$$\hat{N}_2 = n_2 - ik_2$$

$$\hat{N}_3 = n_3 - ik_3$$

For a film free surface, the refractive index of the surface is given by the simple expression

$$\hat{N}_3 = N_1 \tan \phi_1 \left[1 - \frac{4 \hat{\rho} \sin^2 \phi_1}{(1 + \hat{\rho})^2} \right]^{1/2}$$

where $\qquad \hat{\rho} = \hat{R}_p / \hat{R}_s$

The calculation of $\hat{N}_2$ and d is more difficult. For an absorbing film there are three unknowns n_2, k_2 and d and only two measured quantities, Δ and ψ. To overcome this problem a series of refractive indices are assumed for a number of estimated film thicknesses. The corresponding values of Δ and ψ are calculated and compared with the experimentally derived values. The cumbersome nature and complexity of these equations have led to the introduction of computer programmes to evaluate the required parameters, (n_2, k_2, d).

2.4.2 The computer programs

McCrackin and Colson (90, 91) developed a method of solving

the reflection equations for a surface covered with a film of

unknown n, k and d. The solution for d will be complex i.e.

of the form $d = d_R + d_I$. The imaginary part d_I being assumed

to represent a measure of the error. Ideally, an exact solution

will exist when d_I is zero. To obtain a solution, a range of

values of n_2 and k_2 are taken which are assumed to include the

correct values. For each given value of k_2 there is probably a

value of n_2 for which d_I will ideally be zero. Near but either

side of it there will be values of n_2 which give values of d_I

of opposite signs. For a given value of k_2 a solution is

assumed to exist within the chosen range of n_2 if values of d_I

of opposite sign are found for the extremes of the range. Since

solutions can be found for more than one value of d, that giving

the lowest d_I is used. The real part of this thickness is then

used to compute values of Δ and ψ which are compared to the

experimental values. If the differences between calculated

and experimental values are less than the experimental error

these values of n_2, k_2 and d_R are accepted as a solution. If

the differences are larger than the experimental error, a new

value of n_2 is chosen and the calculation is repeated. The

procedure breaks down when n_2, k_2 and d are unknown and the

ranges of n_2 and k_2 are large. In this case the sign of d_I may

be the same at both ends of the n_2 range and it is assumed that

there is no solution, although this is not necessarily the

case. In practice this problem is overcome by limiting the range

of n_2 and k_2 values. Butcher et al (26) chose a graphical

method of limiting the range of n_2 values and then used the

McCrackin and Colson program (91) to evaluate n_2, k_2 and d as

before. For true dielectric films this problem does not exist

since k_2 is equal to zero. Shklyarevskii et al (92) made use

of this in finding the thickness of films which are transparent

in at least part of the spectrum. Schueler (93) produced a

powerful computer program to evaluate optical constants. He

used multiple angle of incidence measurements of ψ and Δ at a

single wavelength to overcome the problem of more than one

value of d appearing as a solution to the ellipsometric equations.

Pedinoff and Stafsudd (94) used a similar method for characterising

multiple layer films. The programm written by McCrackin (95)

has been the one used by most workers to evaluate the optical

constants of films. It was designed for data obtained at a

single wavelength at various angles of incidence. Clarke (96)

incorporated elements of McCrackin's program into one for use by

the ellipsometry group at the City of London Polytechnic. It

was designed to compute optical constants from spectral or multiple

angle measurements and like most of the other programs used

Powell's (97) method for minimising a sum of squares of non-

linear functions without calculating derivatives. Multiple

angle of incidence measurements ideally produce a single set of

values of n_2, k_2 and d. Similarly, spectral data should produce

a single value of d with self-consistent values of n_2 and k_2.

In both these cases the confidence limits of the computed value

of d are increased. With a single wavelength, single angle of

incidence measurement, there are three unknowns n_2, k_2 and d to

be evaluated and only two equations relating them. If n

separate wavelengths are used the uncertainty in d is

correspondingly decreased because there are now 2n equations

and (2n + 1) quantities to calculate as d is the same in each

case. Clarke's program has the advantage of being usable by
people with little or no knowledge of computing and allows data
to be output in tabular or graphical form.

3. <u>EXPERIMENTAL</u>

3.1 <u>Materials</u>

Oxygen-free high conductivity (OFHC) copper of more then 99.99%
purity was supplied by Yorkshire Imperial Metals Ltd. in the
form of annealed strip 1 mm thick. It had a small grain size
and was used as a comparative standard in optical measurements.

Broken cathode copper was supplied by Metal Crystals Ltd. and
used to prepare some dilute copper alloys. Metals Research
Ltd. supplied gallium, germanium and nickel of high purities
which were used as alloying additions. Table 3.1 shows the
details of the metals used.

<u>Table 3.1</u>

Specifications of materials used

Metal	Form	Grade	Typical analysis/ppm
copper	broken cathode	4N	Ag 50, Bi < 2.0, Pb 3.0, Cl 150
gallium	lump	6N	Mg < 0.1, Si < 0.3
germanium	broken ingot	5N	Ag < 0.2, Fe < 0.5, Se < 10
nickel	sponge	4N	C < 50, Si, Cu, Mn < 50, Fe < 400, O_2 100 approx, S 10-20, Mg < 50, Al < 50, Zn < 50, Pb > 50, Cr < 50

3. **EXPERIMENTAL**

3.1 **Materials**

Oxygen-free high conductivity (OFHC) copper of more then 99.99% purity was supplied by Yorkshire Imperial Metals Ltd. in the form of annealed strip 1 mm thick. It had a small grain size and was used as a comparative standard in optical measurements.

Broken cathode copper was supplied by Metal Crystals Ltd. and used to prepare some dilute copper alloys. Metals Research Ltd. supplied gallium, germanium and nickel of high purities which were used as alloying additions. Table 3.1 shows the details of the metals used.

Table 3.1

Specifications of materials used

Metal	Form	Grade	Typical analysis/ppm
copper	broken cathode	4N	Ag 50, Bi < 2.0, Pb 3.0, Cl 150
gallium	lump	6N	Mg < 0.1, Si < 0.3
germanium	broken ingot	5N	Ag < 0.2, Fe < 0.5, Se < 10
nickel	sponge	4N	C < 50, Si, Cu, Mn < 50, Fe < 400, O_2 100 approx, S 10-20, Mg < 50, Al < 50, Zn < 50, Pb > 50, Cr < 50

3.1.1 Preparation of dilute copper alloys

Three dilute copper alloys were prepared by Johnson-Matthey Ltd. 300 g of each alloy was made containing 0.5 atomic per cent of one of the following elements:- gallium, germanium, nickel. The copper/gallium and copper/germanium alloys were prepared by making copper/gallium and copper/germanium eutectic master-alloys which were added to the remaining melted copper. The copper/ nickel alloy was made by melting the copper and adding to it the nickel which was wrapped in copper foil. The alloys were cast into blocks measuring approximately 8 x 5 x 1 cm. A further 300 g of the broken cathode copper was melted and cast with no additions. Melting and casting were done under carbon monoxide. The castings were homogenised at 800°C under hydrogen. Finally, the alloys and the recast copper were rolled to a thickness of approximately 3 mm, annealed at 800°C for 30 minutes under hydrogen and then water quenched.

3.2 Physical properties of the metals

3.2.1 Optical microscopy

A specimen of each alloy, the OFHC copper and the recast cathode copper were mounted in bakelite, polished and etched with alcoholic ferric chloride to reveal structure, inclusions and gross defects. Micrographs were taken to facilitate and record the determination of the grain size.

3.2.2 Electron-probe microanalysis

Samples of germanium, nickel and the recast copper were mounted and polished for electron-probe microanalysis (EPMA). The gallium was not examined in this way because of its low melting point. The average number of counts per second (cs^{-1}), recorded

on a scintillation counter, at a number of random point locations
was measured for each of the pure alloying elements. A sample
of the recast copper was also mounted and polished and the
number of background counts for each alloying element recorded
at a number of sites.

To determine the composition of each alloy, the number of point
counts for the alloying element was measured. This value was
adjusted for the background count found for that element in the
recast cathode copper. The corrected value was then compared to
the value obtained for the pure alloying element. Hence the
proportion of the alloying element in the alloy can be calculated.

The homogeneity of each alloy was checked by recording line
scans across each mounted specimen. For these measurements only
the alloying element content was recorded. The beam traversed
the specimen at a relatively high speed (10 μm per minute) so
that representative portions of each alloy were examined.

3.2.3 The optical properties of the alloys and copper

Rectangular plaquettes measuring 2 x 1 x 0.3 cm of each alloy,
the OFHC copper and the recast copper were mounted in bakelite;
abraded on silicon carbide papers and successively polished on
6, 1 and $^{1}/4$ micron diamond polishing wheels. The specimens
were rinsed well with distilled water followed by ethanol and
then dried in a stream of warm air. The specimens were stored
in a dessicator until measurements were made.

The instrument used for spectral scanning was an automatic, self-

nulling ellipsometer which has been described by Roberts and
Meadows (98) and Clarke (96). Figure 3.1 shows the components
and layout of the instrument. The xenon-arc light source is
collimated by irises on the incident and reflection arms. The
air-gap Glan-Foucault analyser and polariser prisms are driven
by servo-operated stepping motors controlled by power oscillators
and phase-sensitive detectors.

Polychromatic light is plane polarised by the polariser prism
and modulated by a Faraday cell with a water-core. The quarter-
wave device produces elliptically polarised light which falls
on the specimen at 75° and is reflected as plane-polarised
light. After reflection the light passes through a second
Faraday modulator and the analyser prism to a Spex-Minimate
monochromator and photomultiplier. Two photomultipliers are
required to cover the spectral range from 350-750 nm. An EMI
9656 QR photomultiplier is used from 350-540 nm and an RCA 86
from 540-750 nm. A band gap of 5 nm was used with 1.25 mm slits
at the monochromator entrance and exit.

The instrument was optically aligned, in the straight-through
position, before use with a 0.5 mV Spectra Physics He-Ne laser
and mirror. The reflection arm was moved to give an angle of
incidence of 75° and the specimen was mounted on the back
plate which was adjusted until the specimen was accurately
located. The monochromator was set at 350 nm and the analyser
and polariser prisms were rotated until a minimum amount of
light emerged from the analyser. The angles, A and P, through
which the analyser and polariser respectively had to be rotated

1 Xenon arc source	7 Collimating iris	
2 Irises	8 Faraday cell	
3 Polariser prism	9 Analyser prism	
4 Faraday cell	10 Monochromator	
5 Quarter-wave device	11 Photomultiplier	
6 Specimen		
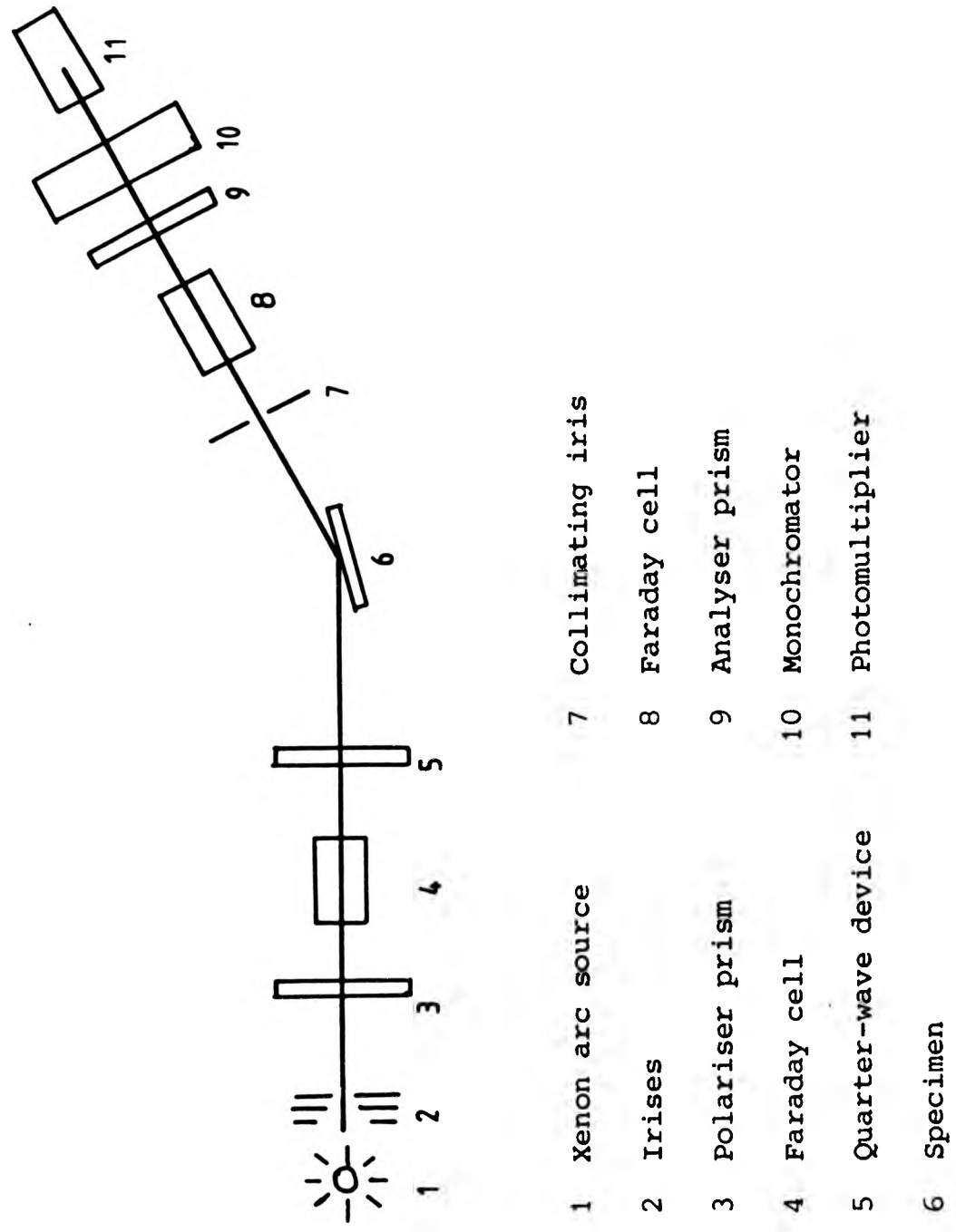
Figure 3.1 The ellipsometer

from the null position when the ellipsometer was set up in the
straight through mode were recorded. The angular positions of
the analyser and polariser prisms were displayed on digital
counters and were recorded at 5 nm intervals over the spectral
range 350-750 nm. The data was analysed on a DEC system 10
computer using a program written by Clarke (96). The program
computes the values of n (the real part of the complex
refractive index) and k (the imaginary part of the complex
refractive index or the absorption coefficient) for the equations
given by Muller (99). The C.I.E. chromaticity colour coordinates
are concurrently computed. The optical constants obtained in
this way are more correctly described as "pseudo constants"
since the surfaces examined are covered with thin air-formed
films of oxide. Attempts were made to establish true optical
constants by in situ ellipsometry during cathodic polarisation
of the specimen.

3.2.3.1 Spectral scanning of cathodically polarised specimens

A polished mounted specimen to which electrical contact had been
made (see Section 3.3.1) was placed in a specially constructed
cell, designed by Osborne (100) which fitted on to the
ellipsometer. Figures 3.2 and 3.3 show the cell and the kinematic
mounting device which ensures that the polished surface of the
specimen is aligned at 75° to the incident beam. 0.05 M sodium
tetraborate buffer solution was placed in the cell which was then
sealed. White spot nitrogen was bubbled through the cell
overnight to remove dissolved oxygen. The monochromator was
set at 525 nm and the specimen polarised at -690 mV with respect
to a standard calomel reference electrode (-450 mV$_{SHE}$) until
the analyser and polariser readings became constant. The
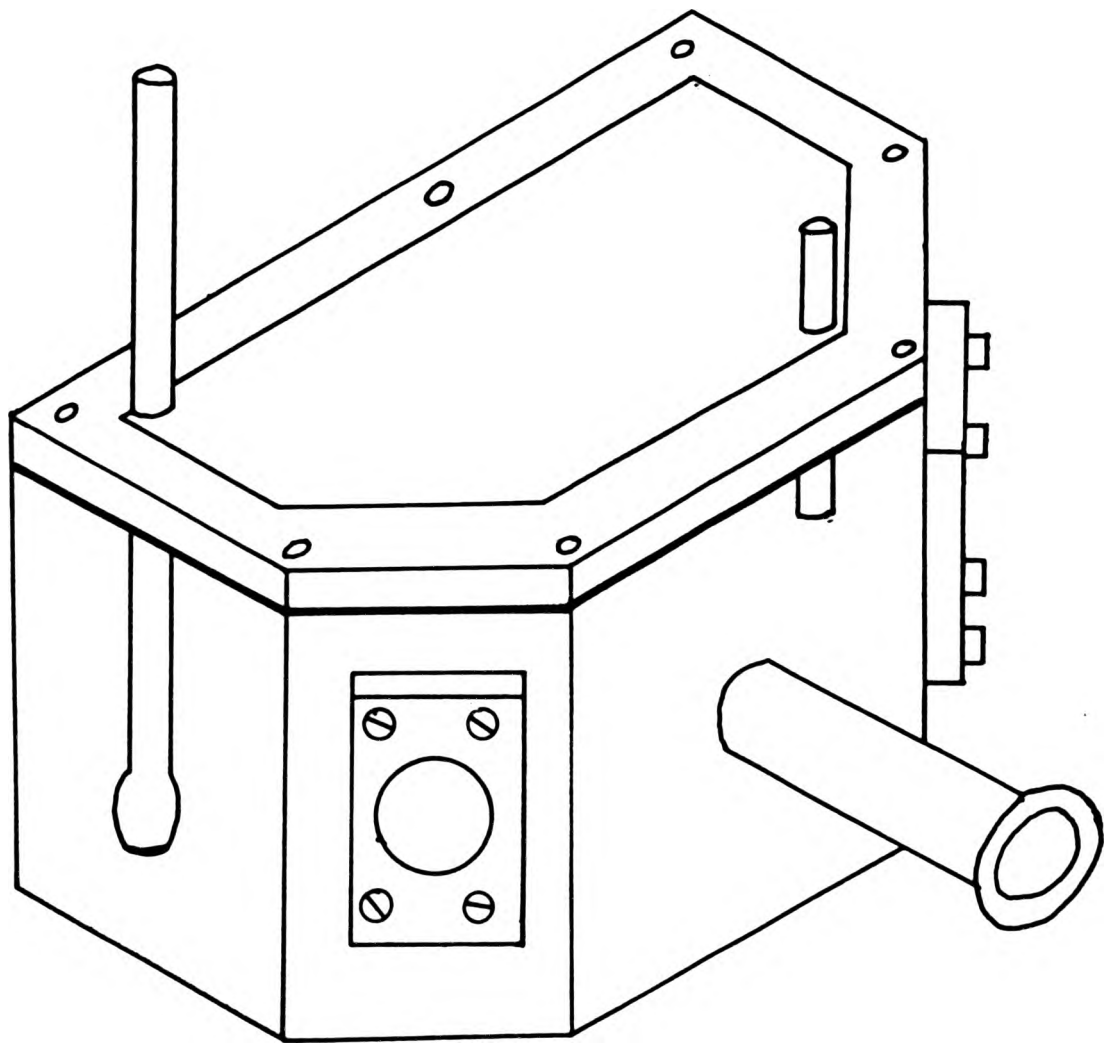
Figure 3.2   Electrochemical cell for use with the ellipsometer
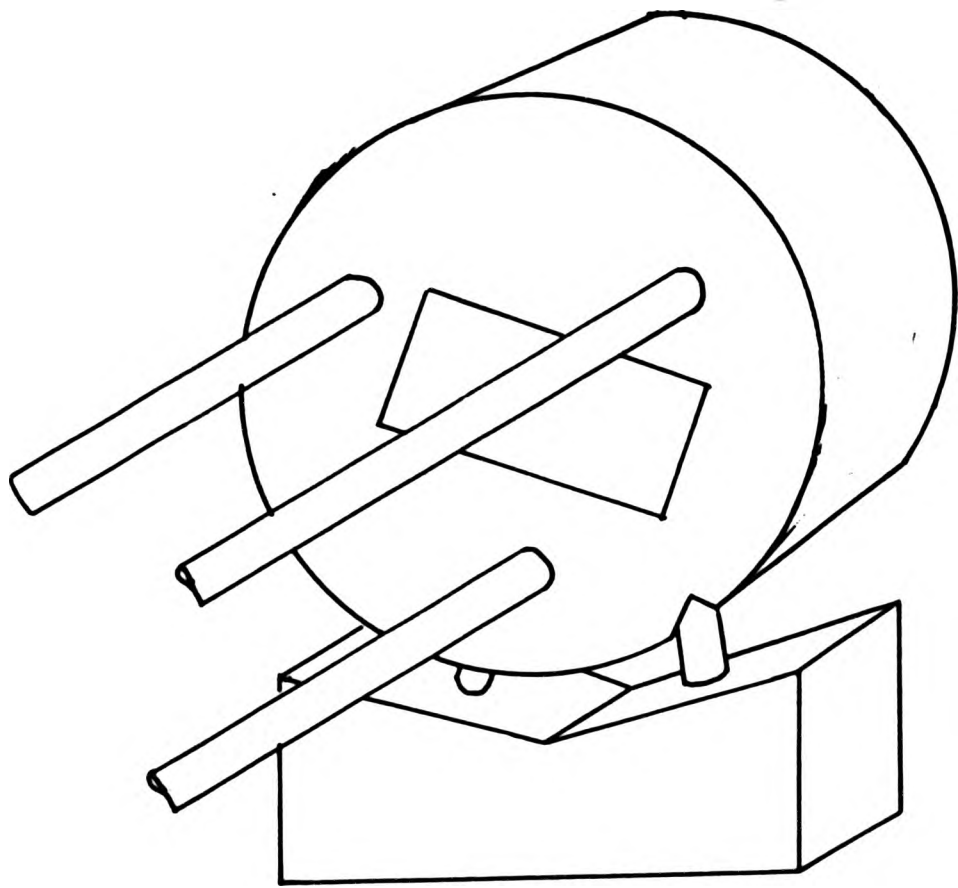
Figure 3.3   Kinematic mount

monochromator was then reset to 350 nm and analyser and polariser
readings were taken at 5 nm intervals to 750 nm.

3.3 Preparation of cuprous oxide films

Thin uniform films of cuprous oxide free of cupric oxide were
required for these experiments. The films also needed to be
compact and adherent and to approximate to an ideal Drude film.
Three methods of preparation were considered:-

(i)   anodic oxidation

(ii)   chemical oxidation

(iii)   thermal oxidation

3.3.1 Anodic oxidation

Electrical contact was made to the mounted specimen by drilling
through the bakelite mount to the metal. A copper wire dipped
in "Silver Dag" conducting cement was then pushed into the hole.
After the cement had set "Araldite" was used to strengthen the
connection. When the "Araldite" had hardened the edges of the
specimen and all but the free end of the copper wire were
painted with "Lacomite". The mounted specimen was placed in an
"H"-cell containing a suitable electrolyte and anodically
polarised using a Wenking potentiostat connected to a Wenking
linear-sweep generator. A platinum counter-electrode was used
in the other branch of the cell. The potential of the specimen
was measured with respect to a saturated calomel reference
electrode. The cell current was obtained by recording the change
in potential across a known resistance and applying Ohm's law.
The circuit used is shown in Figure 3.4. Specimens were
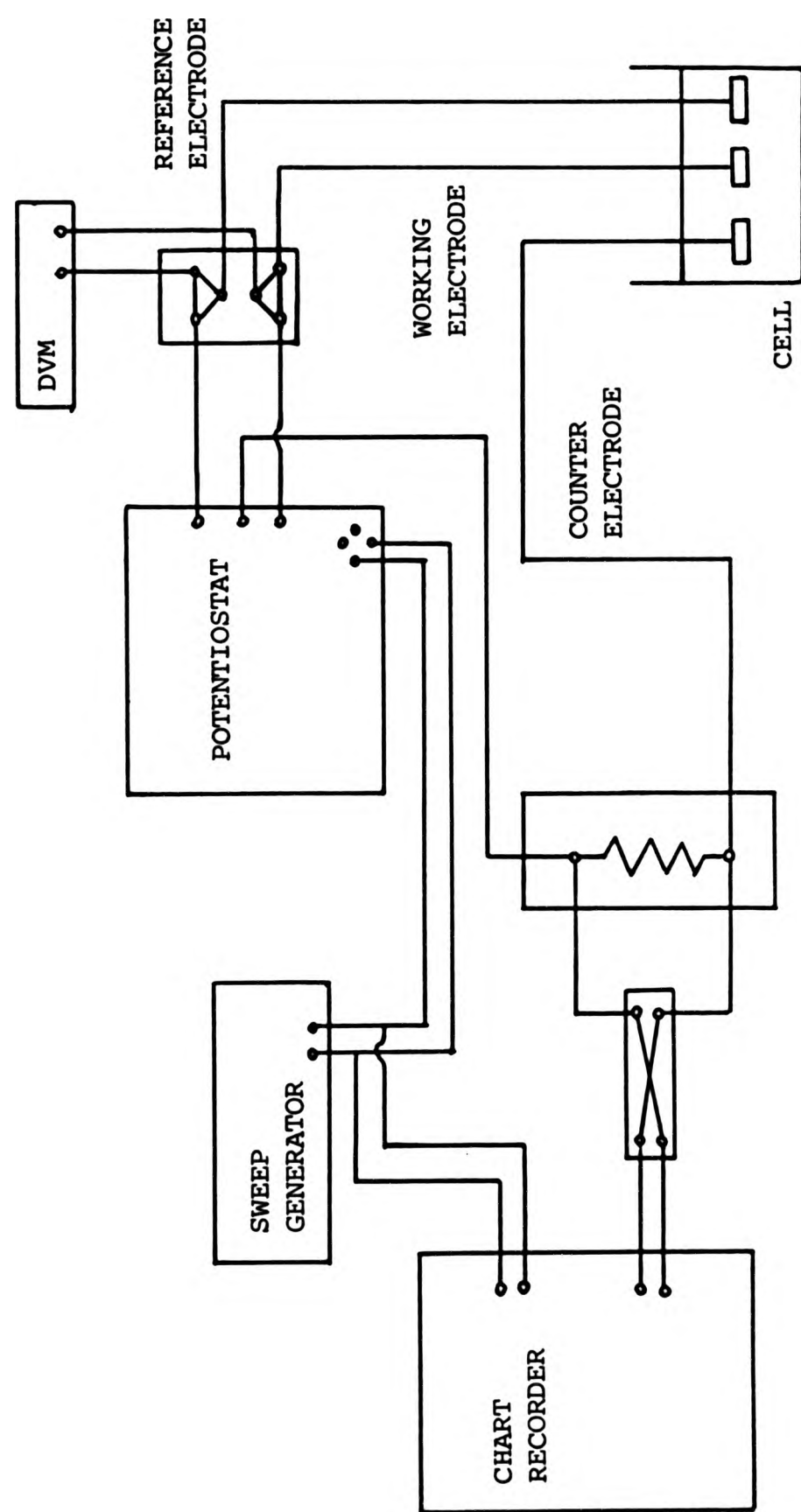
Figure 3.4 Anodic polarisation circuit

prepolarised at -0.2 $V_{(SHE)}$ for 30 minutes before anodic polarisation and the solution deoxygenated with white spot nitrogen. A constant sweep rate of 3.3 mV s^{-1} was used.

Graphs of cell current versus applied potential were plotted. From these it was possible to identify the potential at which the film had achieved a limiting thickness and to estimate the thickness of the film. By considering the Pourbaix diagram (101) for the copper/water system, shown in Figure 3.5, it was hoped to select an electrolyte of suitable pH to produce a film which fulfilled the previously stated requirements.

Anodic polarisation curves were obtained for copper and the dilute copper alloys using the electrolytes detailed in Table 3.2.

Table 3.2

Electrolytes used for anodic oxidation

Electrolyte	pH	Range of stability of $Cu_2O/V_{(SHE)}$
0.1 M KNO_3	5.7	0.15
0.05 M Na_2HPO_4 0.025 M NaH_2PO_4	7.0	0.07-0.28
0.05 M $Na_2B_4O_7$	9.2	0.00-0.81
0.01 M NaOH	11.6	-0.17-0.07
0.1 M NaOH	12.1	-0.20-0.03
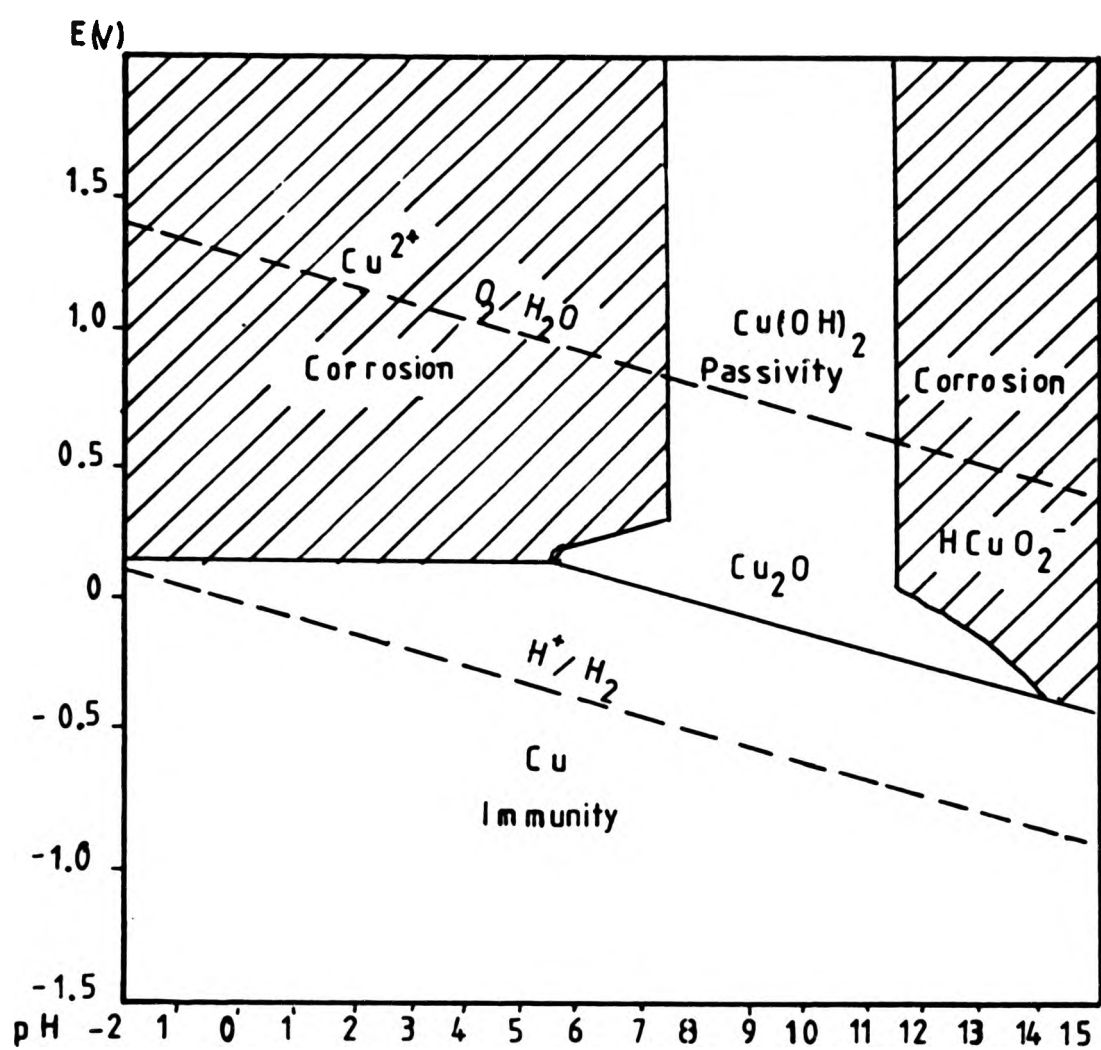
Figure 3.5 Pourbaix diagram for the copper/water system

From these curves conditions were chosen for growing cuprous oxide films. The films produced were reduced coulometrically to confirm their composition and thickness. This technique is described in full in a later section (3.5.3). For the thicker films X-ray diffraction was used to identify the constituents.

3.3.2 Chemical oxidation

Several aqueous oxidising agents were used to produce oxide films on polished specimens but coulometric reduction always showed that both oxides were present. Table 3.3 shows the composition of the solutions used and the proportion of cuprous oxide in the oxide films.

Table 3.3

Aqueous oxidising agents and composition of the oxide films

Solution	Composition of oxide/Cu_2O:CuO
1 M $KMnO_4$	2.59
~ 1 M H_2O_2	1.61
1 M $KClO_4$	1.89
H_2O/O_2 at 100°C	0.44

Mattsson's solution (102) has been used to produce tarnish films of cuprous oxide on brasses of varying composition (103) so polished specimens of copper and the alloys were immersed in Mattsson's solution for periods of 1 to 3 days.

3.3.3 Thermal oxidation

Initially a series of polished copper specimens was oxidised
over a temperature range of 50-200°C. The oxide films
produced in this way were subsequently reduced galvanostatically
in a buffer solution of 0.05 M sodium tetraborate. The potential
during reduction was measured with respect to a standard calomel
reference electrode. Plots of potential against time were used
to identify the oxide film. As a result of these experiments,
a temperature of 80°C was selected for all the other thermal
oxidation experiments.

3.3.4 Identification of the oxide

The films used in this study were too thin to identify using an
X-ray diffractometer and electrochemical methods of dissolving
the copper to leave the oxide for examination by transmission
electron microscopy would have affected the oxide composition.
An alternative method of producing a thin film of the oxide was
therefore adopted. A thin film of copper was evaporated onto
a freshly cleaved surface of a rock-salt crystal. The crystal
was then placed in distilled water so that the copper foil
floated off. It was collected on copper grids and carefully
rinsed with distilled water followed by alcohol and dried on
filter paper. The grids were then placed in an oven at 80°C
for 24 hours. They were then examined in an electron microscope
(AEI EM6G Model) and diffraction patterns were obtained as
quickly as possible.

3.4 Preparation of oxidised specimens

3.4.1 On copper and dilute copper alloy substrates

Specimens of the recast cathode copper, the OFHC copper and the alloys measuring 2 x 1 x 0.3 cm were mounted and polished and had electrical contacts made to them as described in Section 3.1.1. The specimens were placed with their polished surfaces horizontal in an oven containing dessicant and maintained at 80°C. They were withdrawn at intervals over a period of several days and visually inspected. Only specimens showing uniform oxidation were scanned ellipsometrically over the spectral range 350-750 nm at 5 nm intervals.

After spectral scanning the oxide films were reduced coulometrically as described in Section 3.5.3.

A further series of specimens, again measuring approximately 2 x 1 x 0.3 cm, were cut and polished without mounting. Electrical contact was made by cementing a copper wire to the back of each specimen. All but the polished surface and the free end of the copper wire was covered with a chlorinated rubber paint. The specimens were oxidised at 80°C for varying periods of time. This group of specimens was used to provide additional oxidation rate data.

3.4.2 Preparation of cuprous oxide films on glass

The back of a glass-slide was roughened with fine silicon carbide paper. It was then washed and degreased and a thin copper film evaporated onto it. The slide was placed in an oven at 80°C for seven days to oxidise the copper. It was

then aligned on the ellipsometer and the analyser and polariser positions at the null were noted at 525 nm. To ensure that the film was completely oxidised, the slide was returned to the oven for a further 24 hours after which the analyser and polariser positions were rechecked. Spectral scanning of the oxidised specimens covering the range 350-750 nm was carried out as described in Section 3.2.3.1.

Attempts were made to produce copper films of varying thickness by changing the time allowed for evaporation.

3.4.3 Preparation of cuprous oxide films on gold

Thick gold films were evaporated onto glass slides and heat treated at 150°C for one hour to relieve stress. Copper films of varying thickness were then evaporated on to the gold and oxidised as described in the previous section (3.4.2). Spectral scanning was carried out as before.

3.5 Determination of oxide film thickness

Calculations of the optical constants of a film covering a substrate using ellipsometric data require values of the optical constants of the substrate and a measurement of the film thickness.

The first method described in this section assumes that the optical constants of the thin film are those of the bulk material. The numerical method makes similar assumptions but by considering a set of data produces an average thickness value and estimates its accuracy. The third method provides

an independent measurement of thickness.

3.5.1 A graphical method

The relative phase retardation, Δ, and the relative amplitude ratio, ψ, between the electric field vectors, measured in and normal to the plane of incidence, are the two parameters involved in measuring changes in the state of polarisation of light reflected at a surface. Theoretical values of Δ and ψ were computed for a copper substrate overlaid with films of cuprite (bulk cuprous oxide prepared and measured by Rastall (57)) of thicknesses varying from 10 to 1000 $\overset{o}{A}$ for the spectral range 350 to 750 nm. ψ and Δ are related to A and P by the simple expressions

$$\psi = \pi/4 - A \qquad\qquad (1)$$

$$\Delta = 2P \qquad\qquad (2)$$

Spectral values of ψ and Δ for oxidised specimens were plotted and compared to the theoretical curves. The thickness of the film was estimated from the relative positions of the experimental and theoretical curves.

3.5.2 A numerical method

The computer program written by Clarke (96) compares experimental data for a filmed system with data computed for a theoretical substrate covered with an appropriate film of oxide. For each experimentally derived wavelength used the computer will produce values of n_f, k_f and d_f (the refractive index, the

absorption coefficient and the thickness respectively of the film). At the end of execution an average value of the thickness is produced together with a root-mean-square error and standard deviation for the complete set of data. The accuracy of this estimated thickness can be improved by an iterative method which will be described in a later section (3.6).

3.5.3 A coulometric method

The oxidised specimen was made the cathode in a cell especially designed for coulometric reduction (Figure 3.6). 0.05 M sodium tetraborate buffer solution was used as the electrolyte. The platinum counter electrode was separated from the cell by glass frits to prevent oxygen diffusion which would affect the efficiency of the cathode reaction. White-spot nitrogen was bubbled through the apparatus overnight to remove dissolved oxygen. A standard calomel reference electrode was connected to the cell by a salt-bridge and Luggin capillary to prevent the introduction of chloride ions. A constant current of approximately 20 μ A cm^{-2} for thin films or 40 μ A cm^{-2} for thicker films was maintained by adapting a potentiostat for galvanostatic use. Figure 3.7 shows the circuit used. The potential of the specimen with respect to the reference electrode was recorded during reduction and plots of potential against time were used to determine the time taken for reduction of the oxide film. Faraday's laws were then applied to calculate the film thickness.
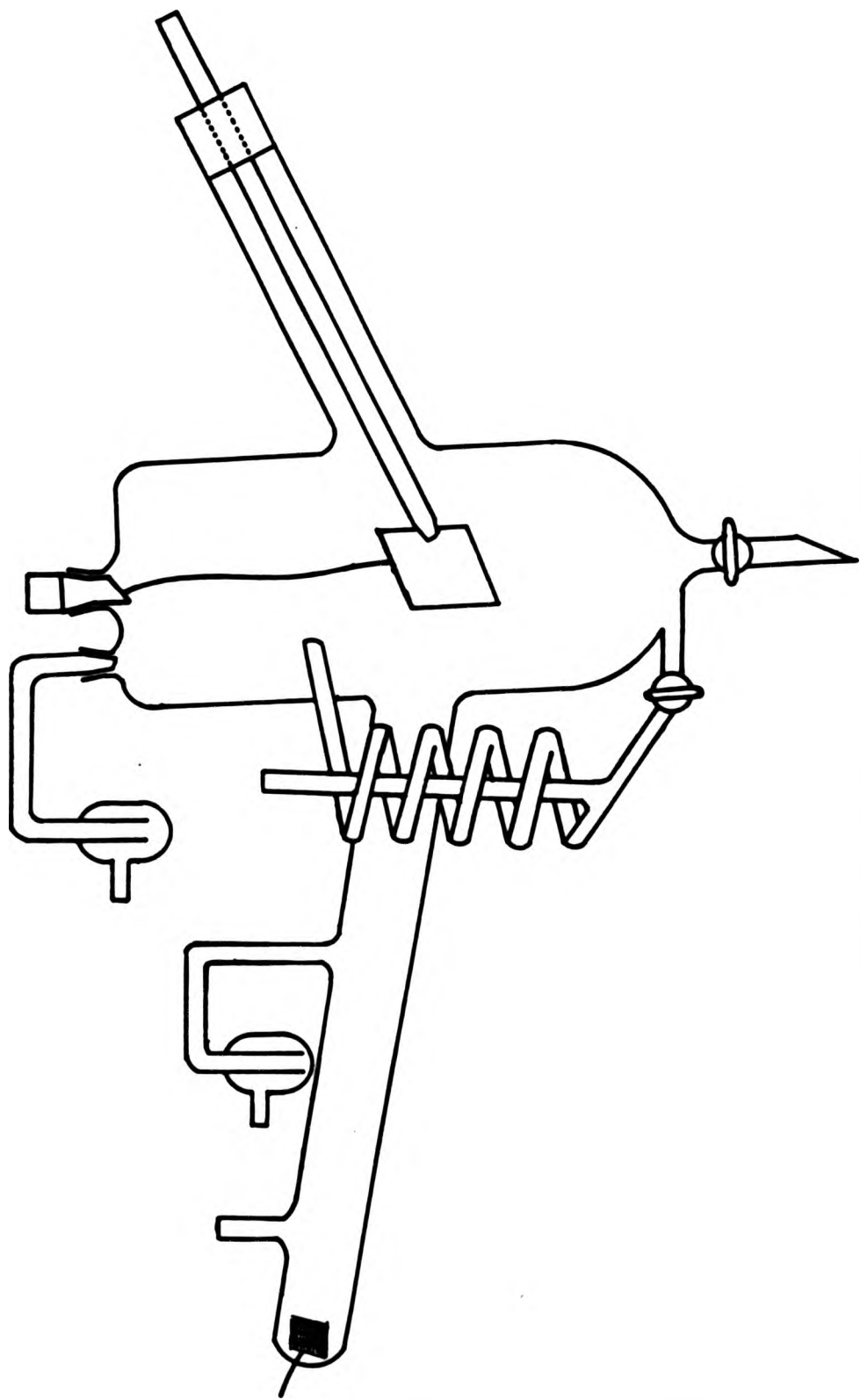
Figure 3.6 Coulometric cell
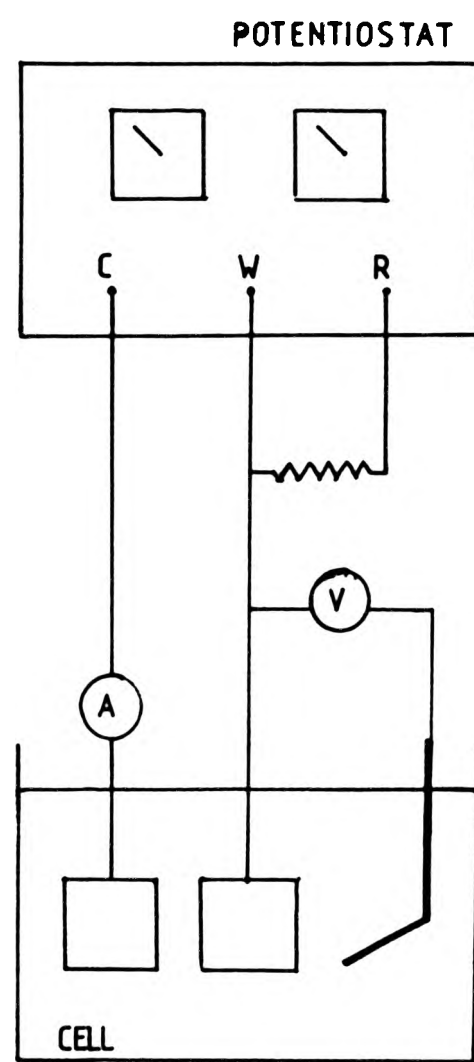
Figure 3.7 Coulometry circuit

3.6 Evaluation of the optical constants of an oxide film

The program described in Section 3.5.2 can be used to evaluate
the optical constants and thickness of an oxide film when the
only data available are the optical constants of the substrate
and a set of experimentally derived A and P values for the
filmed system. In this case there is no set of theoretical
values for the substrate covered with an appropriate oxide film
which can be compared with experimental data.

The program asks for information about the substrate, film and
film thickness and requires a "true" or "false" declaration for
each. The problems associated with providing answers to these
questions are dealt with under the headings:-

(1)   Substrate

(2)   Film

(3)   Film thickness

(1)   Substrate

The experimental data cover the spectral range 350-750 nm and
readings are taken at 5 nm intervals. The optical constants,
n and k, for a clean copper substrate are required at the same
intervals over the same wavelength range. The copper specimens
examined on the ellipsometer are covered with an air-formed
film of oxide and only pseudo-optical constants are obtained by
spectral scanning in air. Cathodic polarisation combined with
ellipsometry failed to give the required clean substrate values
and it was, therefore, necessary to use those obtained by other
workers. n and k for oxide - free copper surfaces measured in

vacuo (24) were plotted against wavelength and interpolated to provide the required data. These values are listed in Appendix 1 together with the data from which they were compiled.

Substrate n and k values for glass were obtained by spectral scanning of a glass-slide with the back roughened to prevent reflections from it. Similarly, a glass-slide bearing a thick evaporated gold layer was used to provide the optical constants of a gold substrate.

(2) Film

The optical constants of bulk cuprite have been measured by Rastall (57) and, while it is unlikely that those of a thin film of cuprous oxide will be identical to them, they will serve as a first approximation. The optical constants of bulk cuprite are listed in Appendix 2.

(3) Thickness

The graphical method described in Section 3.5.1, using theoretical values of ψ and Δ calculated for a copper substrate overlaid with films of cuprite, provides the first value of thickness used in the iterative process to evaluate both the optical constants of the film and its thickness.

Appendix 3 shows how the film-fitting program is used. The program is run with the chosen thickness estimate and using the bulk cuprite values for the film optical constants. These parameters are not fixed i.e. they are followed by "F" (false). At the end of the program an average thickness together with

the standard deviation and the root-mean square (RMS) error for
each wavelength is printed. The program is then rerun using
this average thickness. The process is repeated until the
average thickness values generated by successive repeats are
within 0.01 nm. The tables included in Appendix 3 show how
the thickness is now fixed by changing "F" to "T" (true) and
now the program produces n and k values for the oxide film.
The accuracy of the results can be checked by using the MNEMON
program which was also written by Clarke (96). Values of ψ and
Δ are calculated for a copper substrate overlaid with a film,
which has the optical constants and thickness established by
computer, and compared with the experimental data.

3.7 Surface roughness

Surface roughness is an important factor in the measurement of
surface phenomena. To assess the topography of the surfaces
used in these experiments replicas of some of them were made.
Acetate film was softened with acetone and pressed onto the
surface. When it had dried it was removed from the specimen and
shadowed with carbon. The carbon coated acetate was cut into
small pieces and placed in acetone to dissolve the acetate. The
carbon replicas were collected on copper grids and examined in
a transmission electron microscope.

Polished and oxidised specimens were also examined in a
scanning electron microscope (Model Philips 501).

4. RESULTS

4.1 Properties of the alloys

4.1.1 Optical microscopy

Examination of the alloys by optical microscopy showed that they were equiaxed and had similar grain-sizes. Measurements on micrographs of the alloys showed that the copper/nickel alloy had a grain-size rather smaller than that of the recast copper or the other alloys which were all very similar in size. Table 4.1 shows the variation in grain-size of the metals.

Table 4.1

Grain sizes of the alloys and recast copper

Metal	Grain-size/μm
recast copper	30
Cu/Ga alloy	30
Cu/Ge alloy	35
Cu/Ni alloy	20

4.1.2 Electron-probe microanalysis

Tables 4.2, 4.3 and 4.4 summarise the results of EPMA measurements on mounted samples of the elements, the recast cathode copper and the alloys respectively.

Table 4.2

EPMA measurements on germanium and nickel

Element	LiF crystal angle	cs^{-1}	mean value
		9072	
Ge	36° 11'	9277	9213
		9289	
		12426	
Ni	48° 39'	12466	12409
		12334	

Table 4.3

EPMA measurements on recast cathode copper

LiF crystal angle	element	cs^{-1}	mean value
		38.5	
38° 52'	Ga	43.8	40.6
		39.5	
		42.9	
36° 20'	Ge	41.8	40.8
		37.7	
		41.5	
48° 39'	Ni	43.1	40.9
		38.2	

Table 4.4

EPMA measurements on dilute copper alloys

Alloy	LiF crystal angle	cs^{-1}	mean value
		73.7	
CuGa	38° 52'	77.1	75.2
		74.9	
		94.8	
CuGe	26° 20'	92.5	92.2
		89.2	
		123.0	
CaNi	48° 39'	118.9	118.8
		114.4	

The concentration of the alloying element in each alloy can be calculated by subtracting the number of counts recorded for that element in the cathode copper (Table 4.3) from that for the same element in the alloy (Table 4.4) and comparing this value with that for the pure element (Table 4.2).

Thus for the Cu/Ge alloy:-

$$\text{Ge content} = \left(\frac{92.2 - 40.8}{9213}\right) \times 100\%$$

$$= 0.56\%$$

Similarly for the Cu/Ni alloy:-

$$\text{Ni content} = \left(\frac{118.8 - 40.9}{12409}\right) \times 100\%$$

$$= 0.63\%$$

Linear scans of the alloys showed them to be homogeneous. A section of the scan across the Cu/Ge alloy is shown in Figure 4.1. It shows the cs^{-1} varying from 60-87 cs^{-1}. Some of this variation in peak height can be attributed to "noise" due to the effect of other electrical equipment and the thermionic valves used in the system ($2 - 3\ cs^{-1}$). Atmospheric ionisation causes a fluctuation of similar magnitude. Thus the scan shows that the germanium is uniformly distributed within the alloy. Scans across the other alloys showed similar homogeneity.

4.1.3 Ellipsometric measurements

Spectral scans of the recast copper and the alloys showed that they were optically very similar. Small variations in the experimental variables, ψ and Δ, were observed and these are listed in Tables 4.5 and 4.6 together with the average value for all the metals at each wavelength.
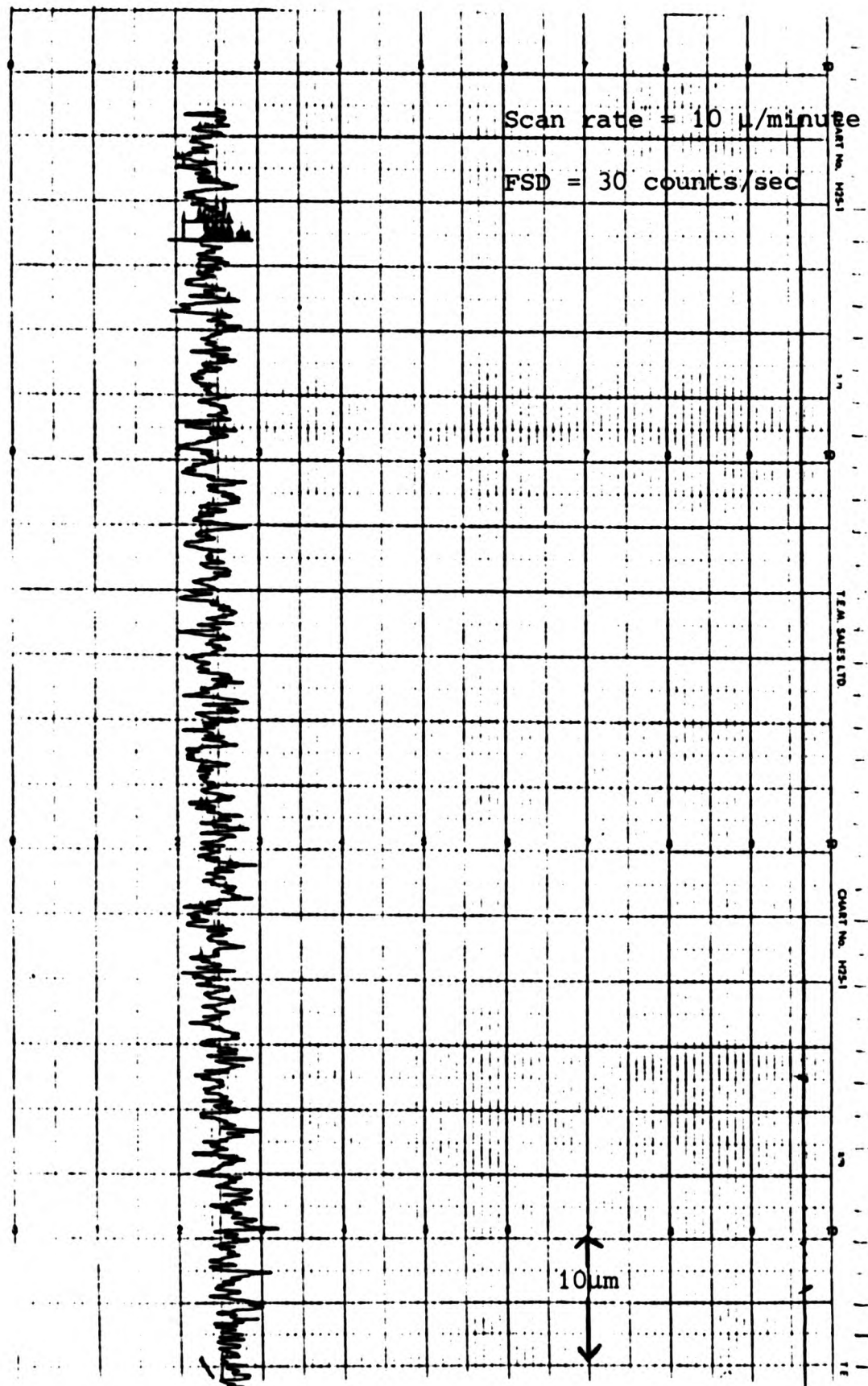
Figure 4.1 E.P.M.A. of Cu/Ga alloy

Table 4.5

Variation of ψ with wavelength

Wavelength λ/nm	Substrate ψ/°				
	Cast Cu	Cu/Ga	Cu/Ge	Cu/Ni	Mean
350	32.23	32.11	32.15	32.11	32.15
375	32.78	32.73	32.79	32.69	32.75
400	33.34	33.33	33.40	33.23	33.33
425	33.92	33.93	33.98	33.78	33.90
450	34.46	34.41	34.44	34.23	34.39
475	34.79	34.75	34.73	34.53	34.70
500	34.93	34.98	34.97	34.79	34.92
525	35.39	35.41	35.42	35.15	35.34
550	36.75	36.89	36.79	36.50	36.73
575	39.99	40.09	39.82	39.67	39.69
600	41.74	41.82	41.53	41.52	41.65
625	42.24	42.24	42.02	42.03	42.17
650	42.35	42.37	42.20	42.15	41.27
675	42.41	42.45	42.37	42.20	42.36
700	42.43	42.49	42.42	42.23	42.29
725	42.32	42.34	42.35	42.19	42.30
750	42.05	42.09	42.09	41.83	42.02

Table 4.6

Variation of Δ with wavelength

Wavelength λ/nm	Alloy Δ/°				
	Cast Cu	Cu/Ga	Ca/Ge	Cu/Ni	Mean
350	56.10	55.48	54.94	57.04	55.87
375	58.04	57.56	56.92	59.38	57.98
400	60.32	59.90	59.26	61.60	60.27
425	62.90	62.46	61.88	64.20	62.86
450	65.48	65.08	64.52	66.90	65.50
475	67.70	67.34	66.72	69.12	67.72
500	69.20	68.86	68.26	69.12	67.72
525	69.66	69.40	68.82	71.06	69.74
550	68.82	68.80	68.26	70.32	69.05
575	70.56	70.72	70.24	71.92	70.86
600	76.72	76.78	75.98	77.90	76.85
625	81.96	81.96	80.98	93.22	81.94
650	86.00	86.26	85.06	87.30	86.16
675	89.32	89.64	88.40	90.68	89.51
700	92.06	92.44	91.32	93.58	92.35
725	94.36	94.60	93.62	96.02	94.50
750	95.48	95.72	95.06	97.20	95.87

Figure 4.2 is a graph of mean ψ against mean Δ for the metals. Values of ψ and Δ for a clean copper surface (Appendix 1) and for copper overlaid with 25 $\overset{o}{A}$ and 50 $\overset{o}{A}$ of cuprous oxide are
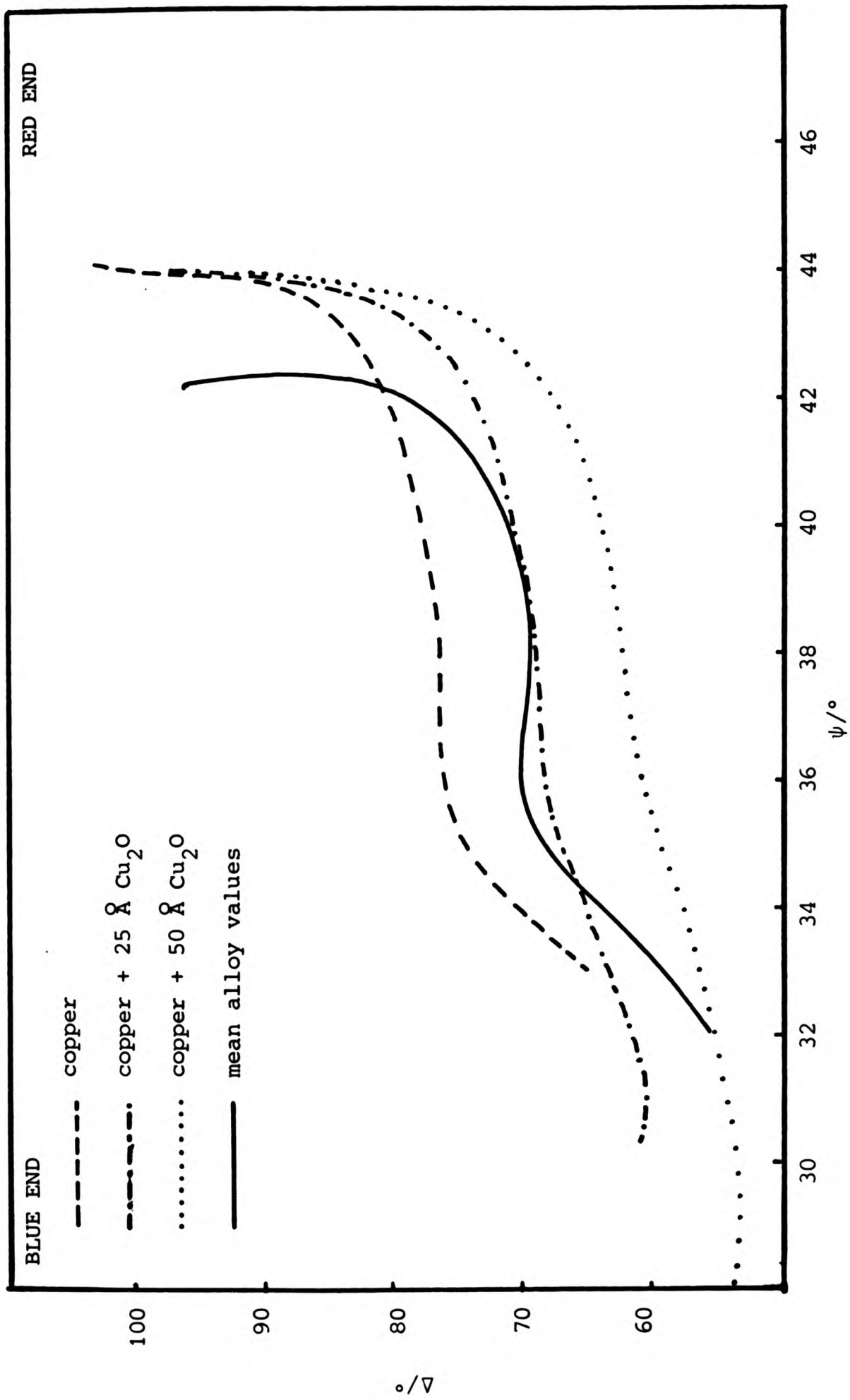
Figure 4.2 Variation of Δ with ψ

included for comparison.

Figures 4.3, 4.4 and 4.5 compare the computed values of the pseudo optical constants, n and k, and the reflectance, R_N, of the metals with those of clean copper. In each case the shaded area represents the range of values for the alloys. Table 4.7 lists the corresponding CIE chromaticity coordinates.

Table 4.7

CIE chromaticity coordinates

Metal	X	Y	Luminance	Dominant wavelength/nm	Saturation /%
recast Cu	.3601	.3396	67.24	588.2	19.68
CuGa	.3610	.3408	67.46	587.8	20.24
CuGe	.3603	.3405	66.53	587.8	19.99
CuNi	.3582	.3382	67.17	588.5	18.81
Copper (in vacuo)	.3599	.3384	74.52	588.8	19.35

The air-formed films on these specimens were coulometrically reduced to establish their thicknesses which are listed in Table 4.8.
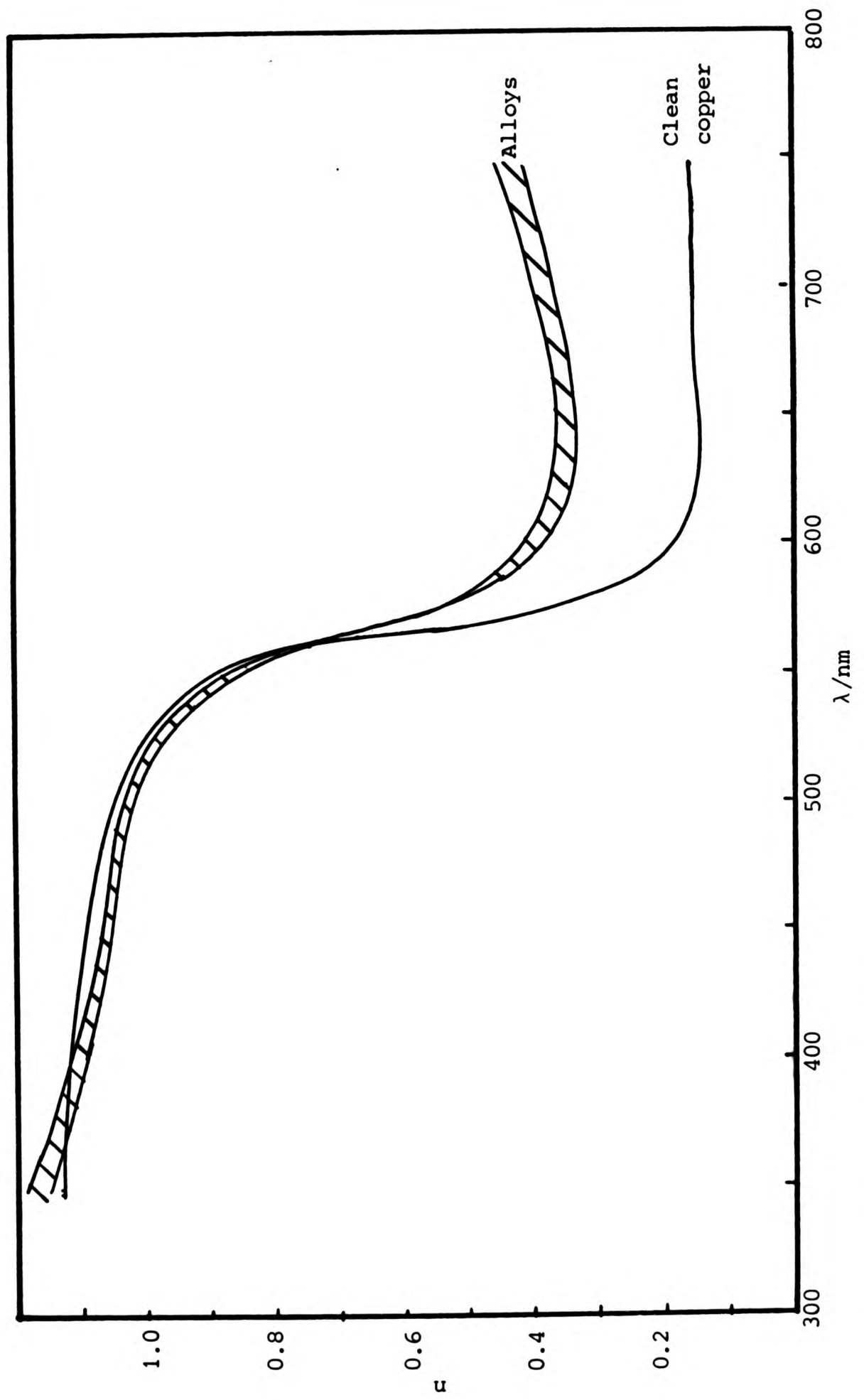
Figure 4.3 Variation of n with wavelength
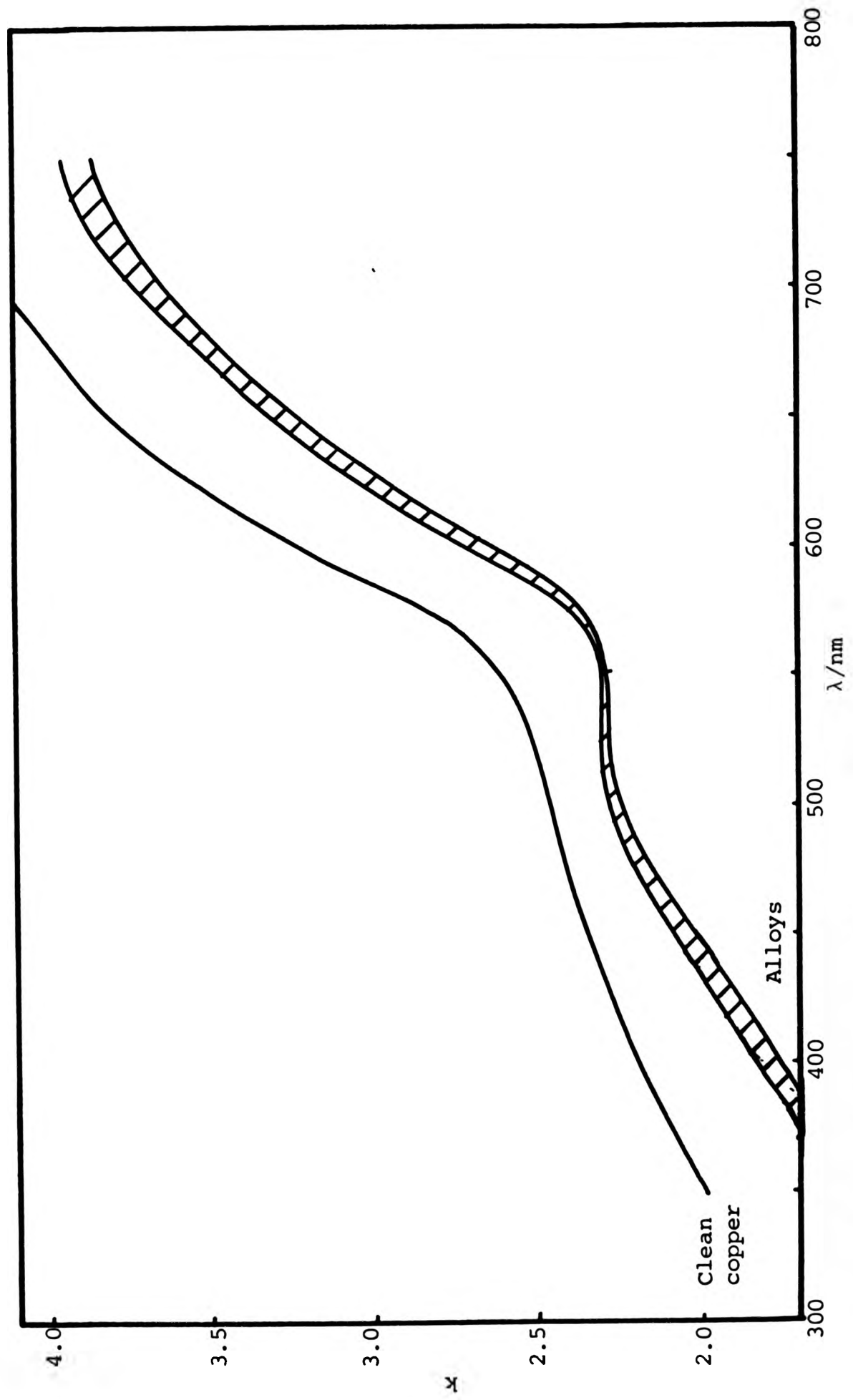
Figure 4.4 Variation of k with wavelength
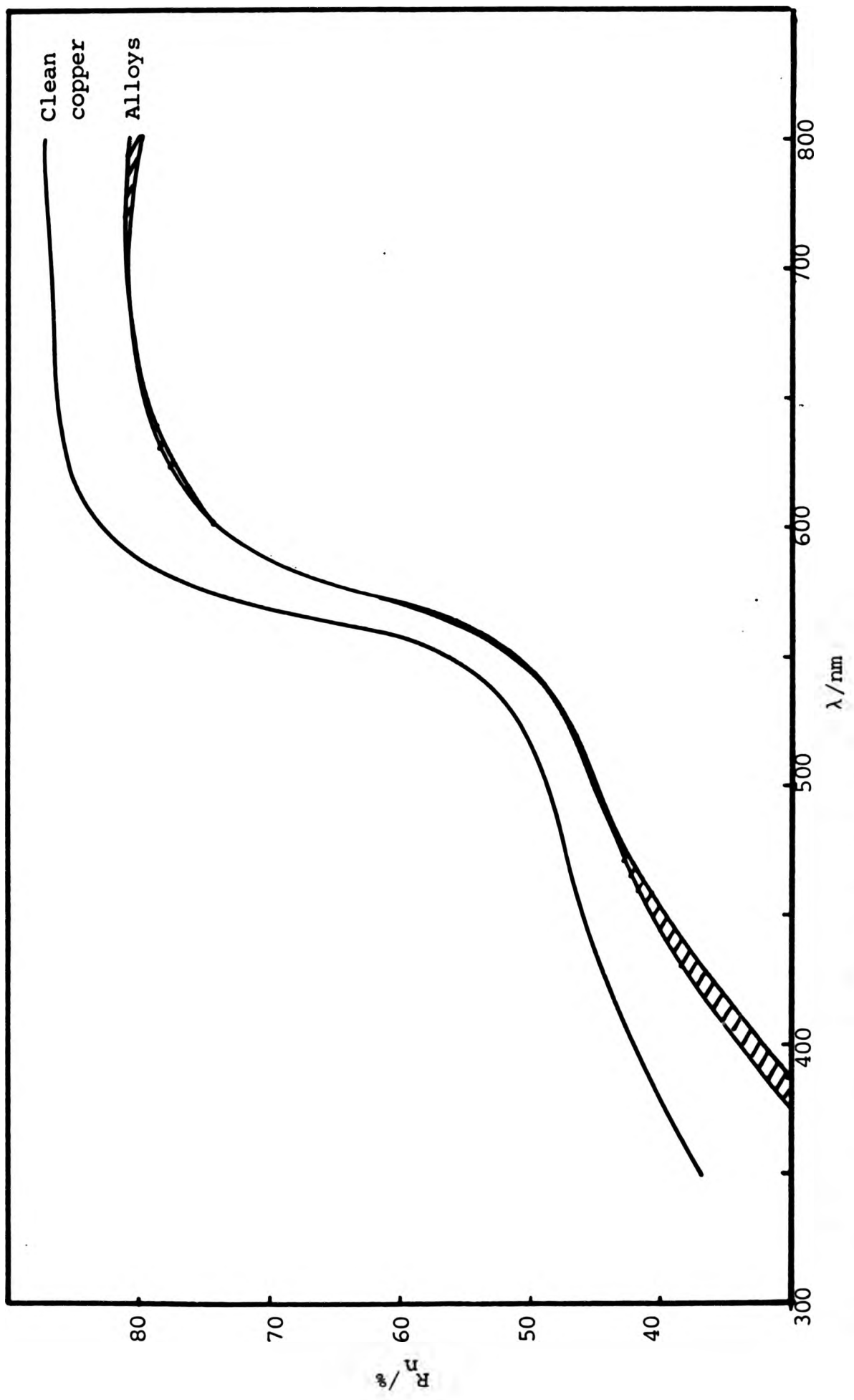
Figure 4.5 Variation of reflectance with wavelength

Table 4.8

Thicknesses of air-formed films

Metal	Area/cm^2	Current/μA	Reduction	Thickness/$\overset{\circ}{A}$
Cu	1.44	18.00	120	18.5
CuGa	1.44	18.33	172	27.0
CuGe	1.44	18.00	226	35.0
CuNi	1.28	20.00	140	27.0

4.1.4 Spectral scans of cathodically polarised specimens

When a copper specimen was first aligned in the cell and
immersed in 0.05 M sodium tetraborate solution, the analyser and
polariser positions at 525 nm were 8.59° and 28.63° respectively.
After deoxygenating the solution and polarising at -690 mV$_{(SCE)}$
for 16 hours these positions had changed to 8.45° and 32.25°
respectively. No further changes were observed. Table 4.9
lists the values of ψ and Δ recorded for a copper specimen
polarised at -690 mV$_{(SCE)}$ together with computed values for
clean copper immersed in a medium of refractive index 1.335.
(The refractive index of 0.05 M sodium tetraborate solution
was found to be 1.335 at 20°C).

Table 4.9

Computed and measured values of ψ and Δ for copper immersed in a medium of refractive index 1.335

Wavelength/nm	Computed		Measured	
	$\psi/°$	$\Delta/°$	$\psi/°$	$\Delta/°$
350	35.59	52.90	35.31	52.02
375	35.79	54.68	35.56	54.52
400	35.92	56.21	35.72	57.14
425	36.07	57.73	35.92	59.60
450	36.25	58.90	36.06	61.60
475	36.45	60.70	36.17	64.46
500	36.64	60.70	36.17	64.46
525	36.96	61.58	36.55	64.50
550	38.30	62.18	37.99	63.56
575	41.94	65.87	41.18	65.28
600	43.67	71.06	42.76	71.48
625	43.96	76.14	43.20	76.46
650	44.00	79.75	43.06	80.36
675	44.03	81.72	43.13	83.60
700	44.06	83.95	43.22	86.28
725	44.09	86.06	43.09	88.30
750	44.11	88.05	42.80	88.82

Figure 4.6, a graph of ψ against Δ, shows clearly how the measured variables differ from those predicted especially
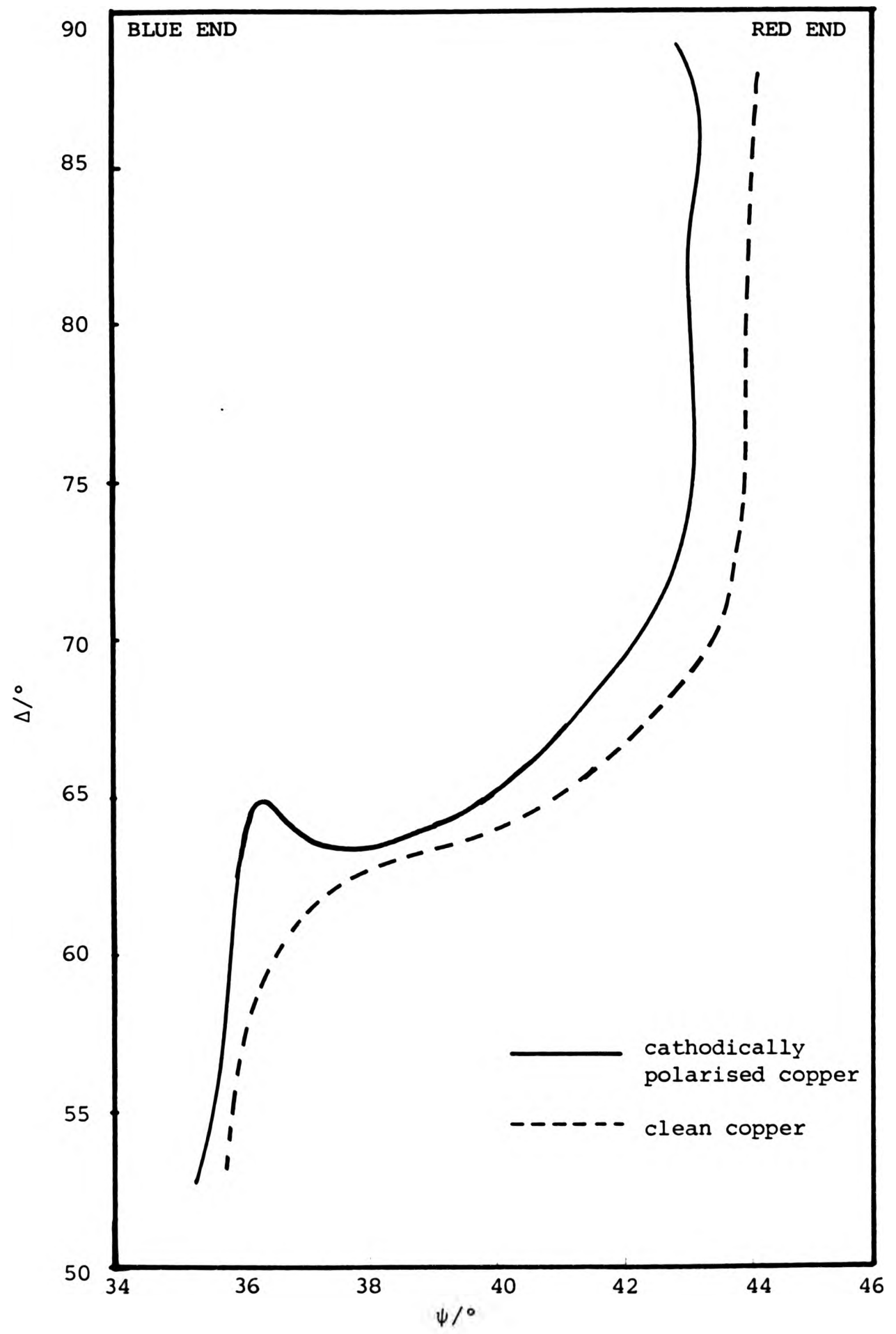
Figure 4.6 Variation of Δ with ψ for clean and cathodically
polarised copper in borate buffer solution

at the longer wavelengths.

4.2 Oxide films

4.2.1 Anodic oxide films

Experimental anodic polarisation curves for copper and the alloys
indicated that passive regions existed in solutions of pH 7 or
more. In potassium nitrate solution of pH 5.7 there was very
little indication of film formation and this electrolyte was
discarded. Thick films were seen to form in strongly alkaline
solutions, i.e. 0.1 M and 0.01 M sodium hydroxide solutions, but
they were loosely adherent and contained blue copper compounds.
X-ray diffraction revealed the presence of CuO, Cu_2O and
$Cu(OH)_2$. The films obtained in the phosphate buffer solution of
pH 7 were thin and became blue at higher potentials. Keeping
the applied potential below 1.0 $V_{(SCE)}$, produced dark films
which were too thin for identification by X-ray diffraction.
However, coulometric reduction showed that they were a mixture
of cuprous and cupric oxides. Figure 4.7 compares the shape of
the anodic polarisation curves obtained in electrolytes of
different pH. It can be seen that polarisation in borate
buffer solution of pH 9 results in the formation of a film
intermediate in thickness between those in solutions of pH 7 and
pH 11.6 (indicated by the value of i passive). The film was
adherent and brown in colour although it would become blue if
the potential was allowed to reach 1.0 V
to estimate the thickness, from a linear plot of current against
applied potential, if it was assumed that formation of the film
was the only anodic process taking place. Figure 4.8 is a
diagrammatic representation of such a graph. A-B represents
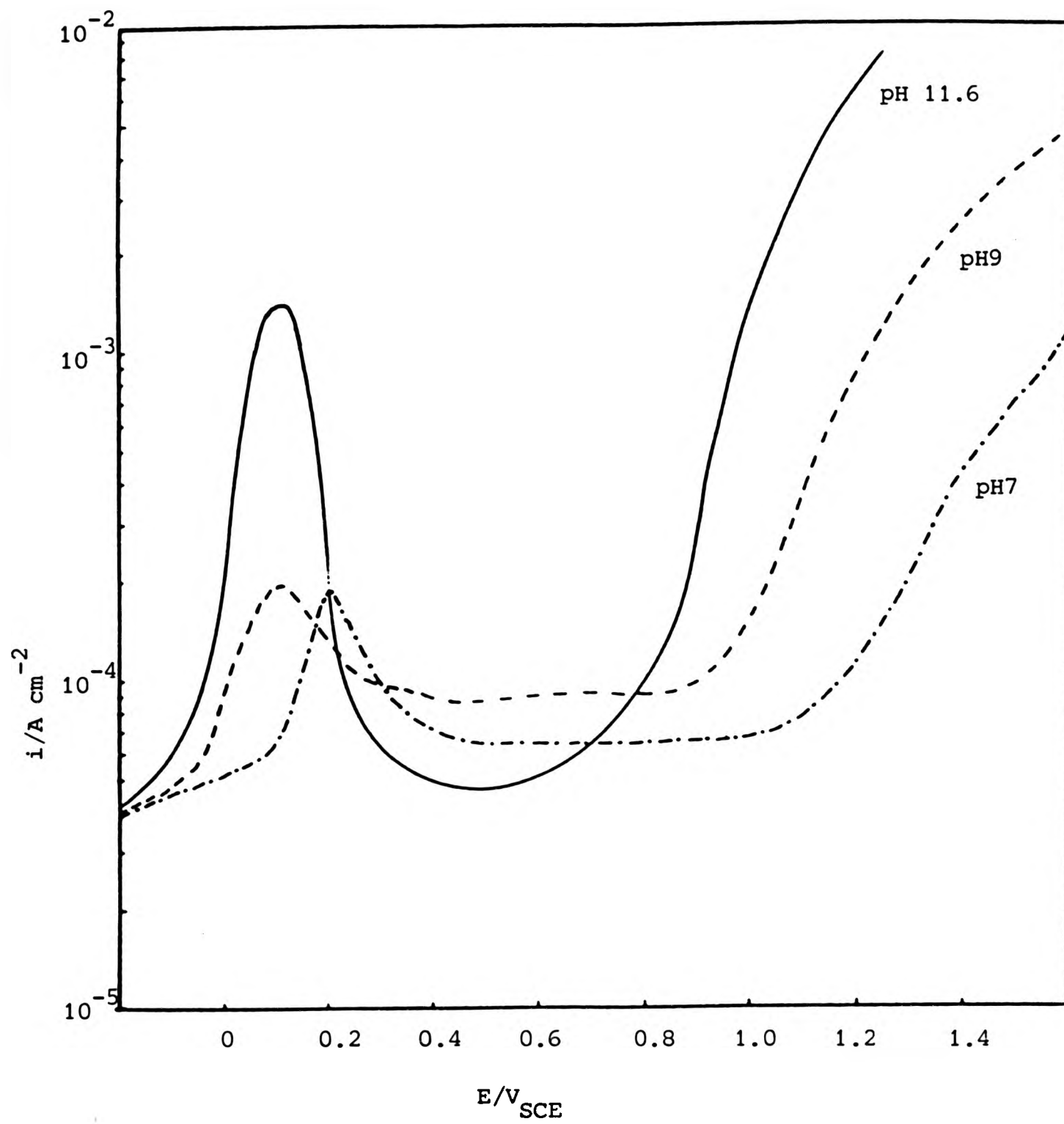
Figure 4.7 Potentiostatic anodic polarisation curves for copper in solutions of different pH
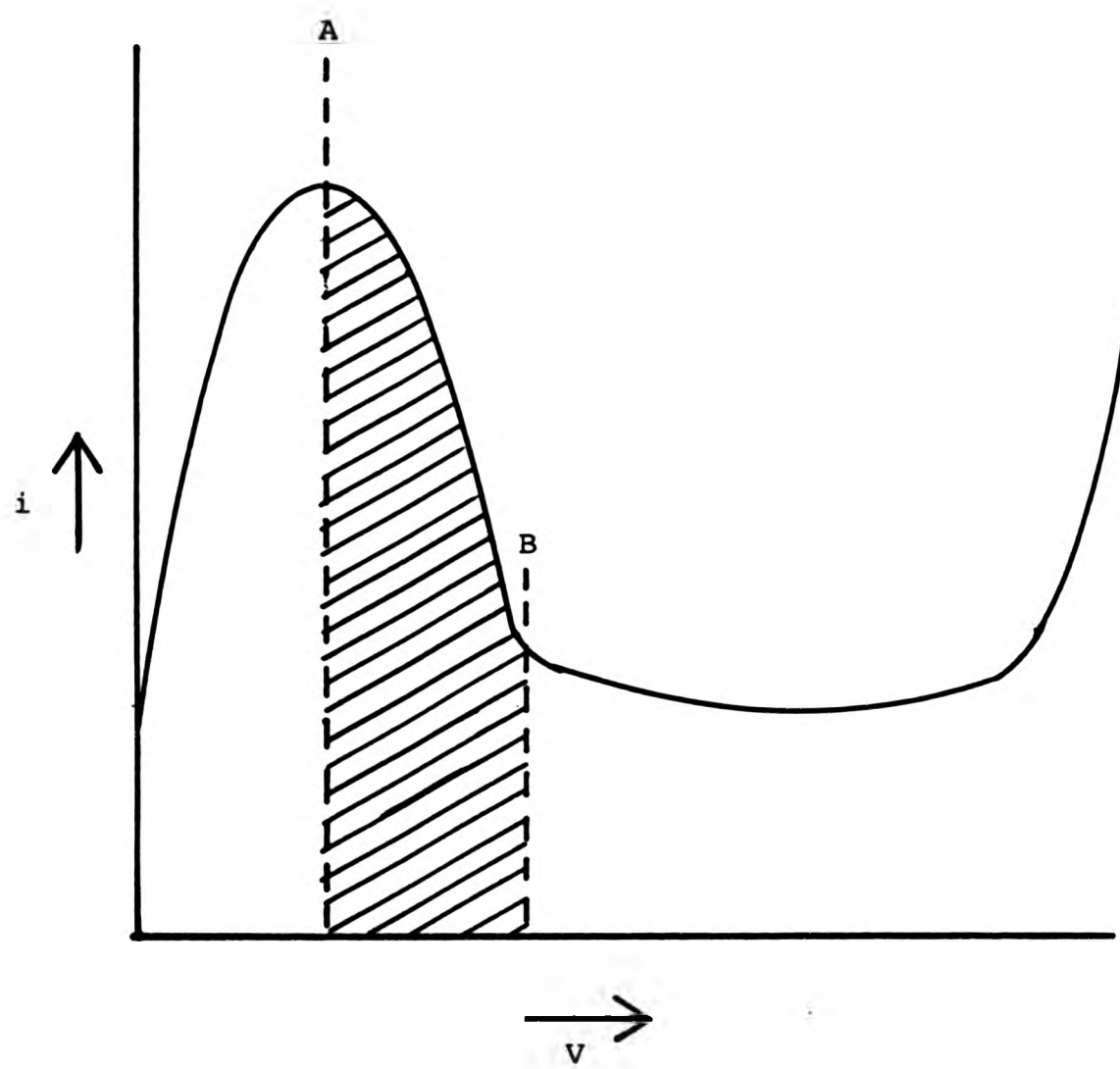
Figure 4.8 Typical anodic polarisation curve used to determine oxide film thickness

the region of film growth. A constant sweep rate of 3.3 m V s^{-1}
was used for these experiments and hence the horizontal axis
can be related to the number of coulombs used for film growth
and the thickness of the film can be calculated by applying
Faraday's laws. The film thicknesses estimated in this way
were between 60 and 100 $\overset{o}{A}$. Coulometric reduction of these
films revealed that they were mainly cuprous oxide with small
amounts of cupric oxide. Microscopic examination revealed small
blue crystallites. These films were dull and therefore
unsuitable for ellipsometric measurements and were too thin to
polish.

Polarisation of the alloys revealed small but significant
differences in their anodic behaviour and these are illustrated
in Figure 4.9.

During anodic polarisation diffusion layers were observed
adjacent to the electrode surface.

4.2.2 Chemically oxidised specimens

Table 3.3 lists the oxidising agents used and the composition
of the resulting films. Not only were the films unsuitable as a
result of their composition but they were also powdery and
therefore non-reflecting. Specimens which had been immersed in
Mattsson's solution developed visible oxide films after about
24 hours. Figure 4.10 shows photographs of specimens which had
been immersed in Mattsson's solution for 48 hours; then removed,
rinsed with distilled water and acetone and dried. The films on
copper specimens were red-brown in colour and were mainly of
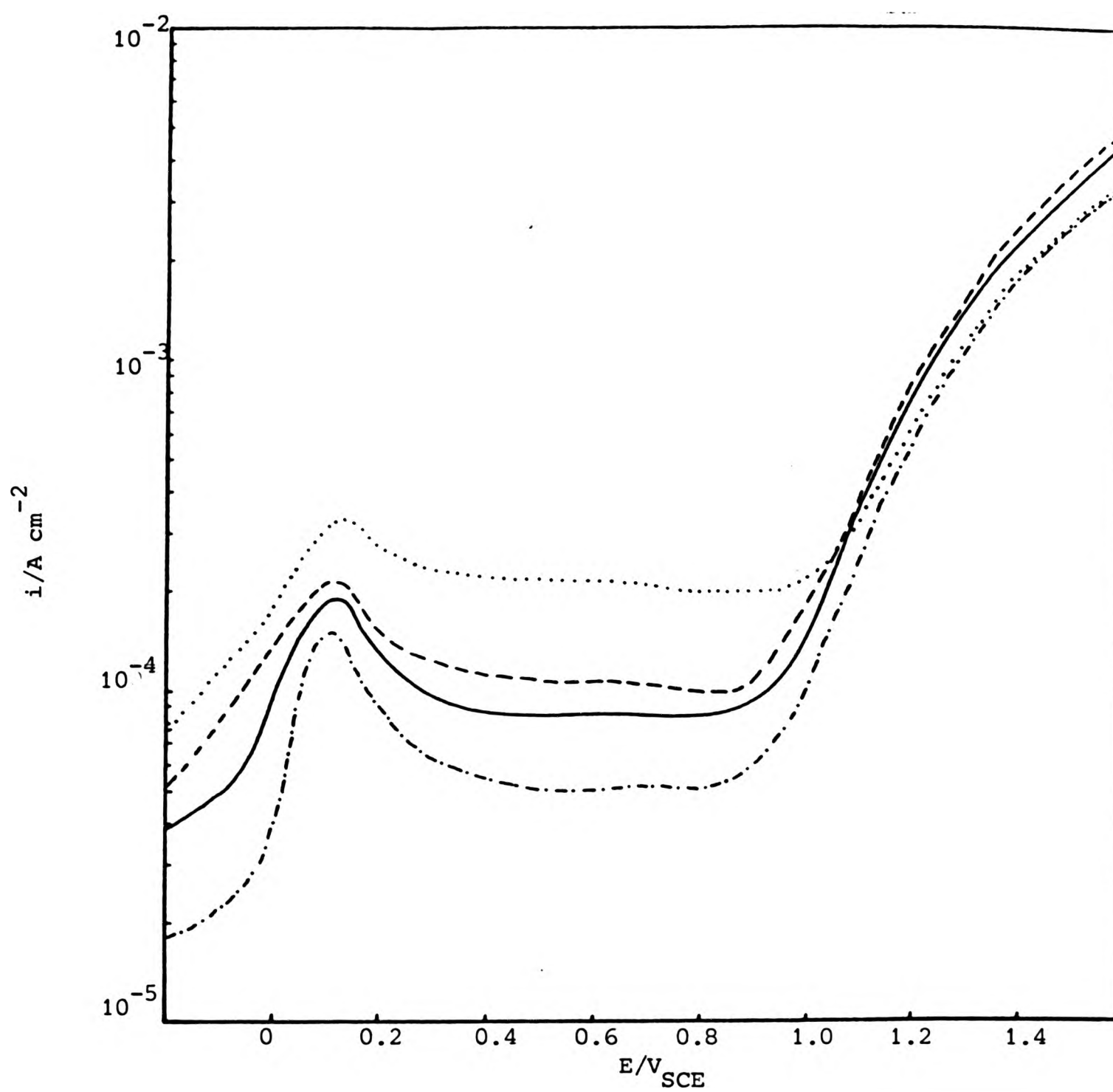
Figure 4.9 Anodic polarisation curves for copper and dilute copper alloys in pH9 buffer solution

.... Cu/Ni alloy

------- Cu/Ga alloy

——— Cu

—·—·—· Cu/Ge alloy
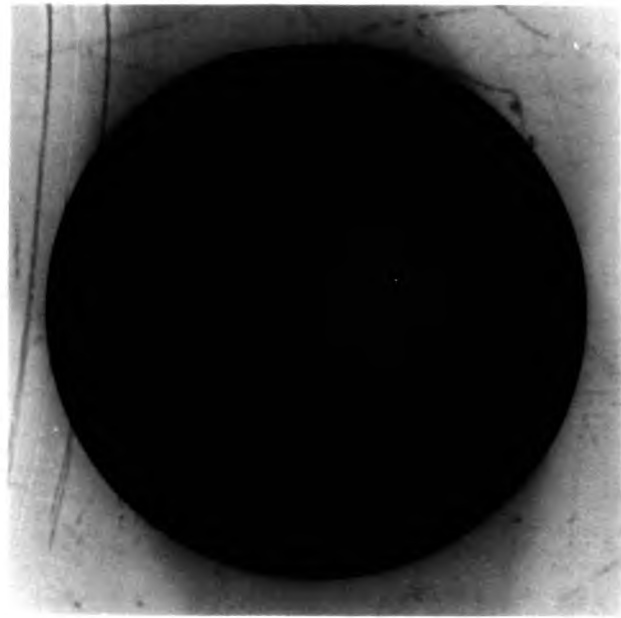
copper

copper/gallium alloy
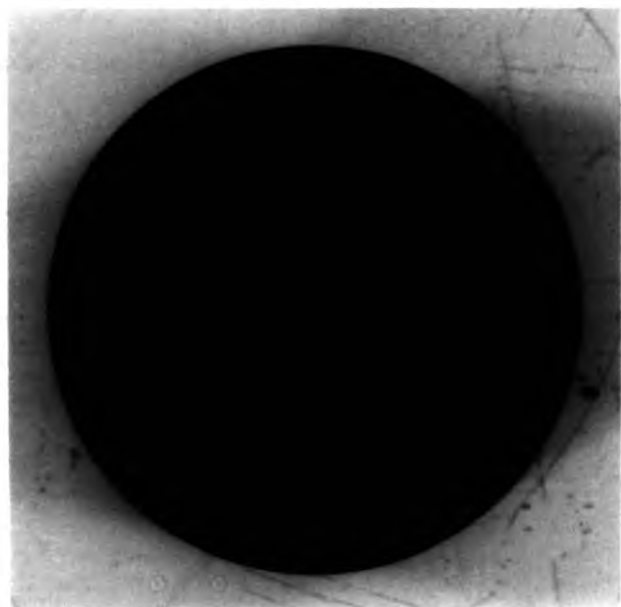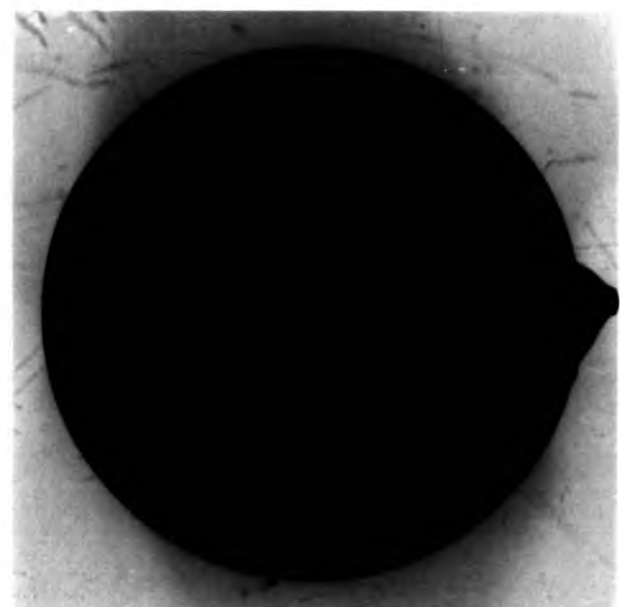
copper/germanium alloy

copper/nickel alloy

Figure 4.10   Copper and dilute copper alloy specimens after 48 hours

in Mattsson's solution
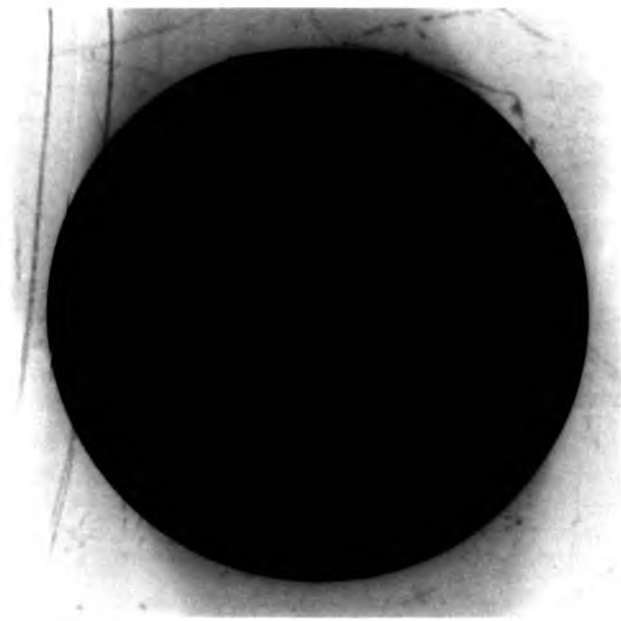
copper   copper/gallium alloy
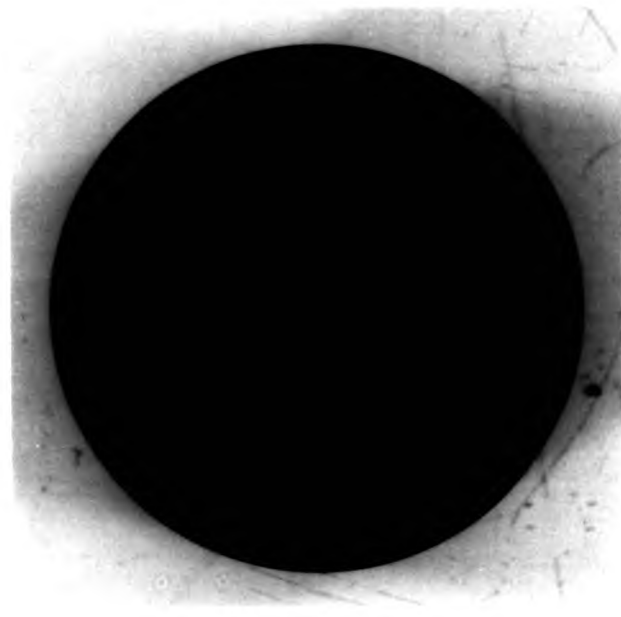
copper/germanium alloy   copper/nickel alloy

Figure 4.10   Copper and dilute copper alloy specimens after 48 hours
              in Mattsson's solution
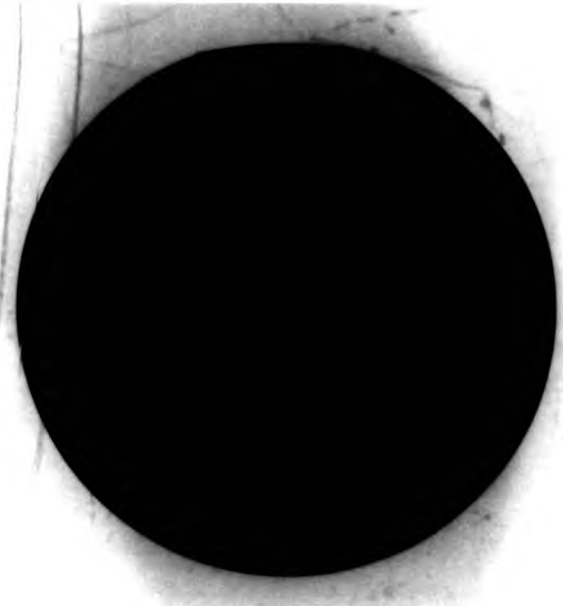
copper   copper/gallium alloy
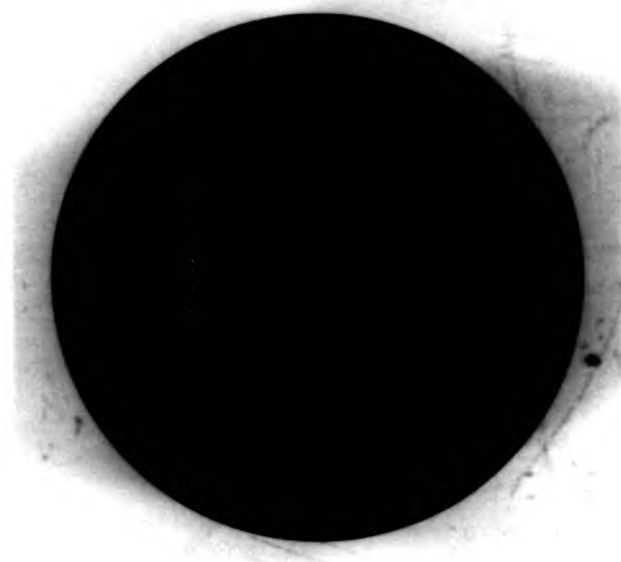
copper/germanium alloy   copper/nickel alloy

Figure 4.10   Copper and dilute copper alloy specimens after 48 hours

in Mattsson's solution

cuprous oxide whereas, those forming on the alloys were yellowish and contained appreciable quantities of blue, crystalline copper salts.

4.2.3 Thermal oxide films

Oxidation of polished specimens at 80°C resulted in the formation of films which were uniform and reflecting. Within 24 hours the surface of the specimen darkened and as oxidation progressed the normal range of interference colours appeared. Table 4.10 lists approximate oxidation times and corresponding colours for the various specimens.

Table 4.10

Approximate oxidation times and corresponding interference colours.

Oxidation time/ days	Colour	
	Copper	Alloys
1	darkened	darkened
2	slightly bronzed	bronze
3	bronze	bronze-magenta
4	"	"
5	"	magenta-bronze
6	"	magenta
7	bronze-magenta	magenta-blue

The composition of these films was established by coulometric analysis.

4.3 Composition and thickness of the oxide films

4.3.1 Coulometry

Cuprous and cupric oxide are quantitatively reduced to copper when a cathodic current is applied if certain precautions are observed. These include:-

(i)   a low current density to avoid excessive cathodic polarisation

(ii)   the exclusion of oxygen which would otherwise be reduced, giving an incorrect value of the quantity of electricity used for reduction of the oxide film

(iii)   the use of a buffer solution which does not dissolve or react with the oxide film.

Under these circumstances the oxides are reduced as:-

$$Cu_2O + 2H^+ + 2e = 2Cu + H_2O \tag{1}$$

$$CuO + 2H^+ + 2e = Cu + H_2O \tag{2}$$
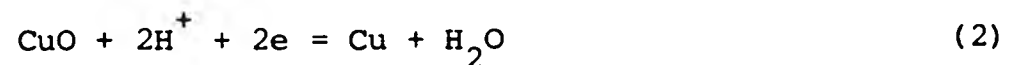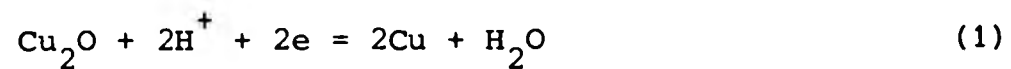
The potentials at which the two reactions occur are different and by the application of Faraday's law, the thickness of each layer may be calculated. Thus,

$$d = \frac{M \ I \ t \ x \ 10^8}{n \ F \ A \ \rho}$$

where d = thickness in Ångstroms

M = relative molecular mass of oxide

I = current in ampères

t = time in seconds

F = Faraday constant

A = area of specimen in cm^2

ρ = density of oxide in $g \ cm^{-3}$

n = number of electrons

It was found that cupric oxide was reduced at potentials between -40 and -190 $mV_{(SCE)}$ and cuprous oxide at potentials between -190 and -610 $mV_{(SCE)}$ in the borate buffer solution used. These potentials were found to be the same for the oxide films on copper or dilute copper alloys although the final potential for hydrogen evolution on the metal did vary slightly. The potentials for hydrogen evolution at the metal surfaces are listed in Table 4.11.

Table 4.11

Potentials for hydrogen evolution on copper and dilute alloys
in 0.05 M sodium tetraborate solution.

Metal	Potential/$V_{(SCE)}$
Cu	-1.084
Cu/Ga	-0.920
Cu/Ge	-1.108
Cu/Ni	-0.890

Figure 4.11 shows a typical coulometric reduction curve
obtained when both cuprous and cupric oxides were present. This
oxide was produced by heating the copper specimen at 95°C.
Similar curves were obtained for reduction of all oxide films
prepared at temperatures of 95°C or more.

Figure 4.12 shows a typical reduction curve obtained when cuprous
oxide only was present. This curve is typical of those obtained
by reduction of oxide films prepared at 80°C.

Tables 4.12, 4.13, 4.14 and 4.15 list the oxidation time and the
thickness of oxide films determined coulometrically and/or
ellipsometrically for copper and dilute copper alloy specimens
(Section 4.4). Relevant coulometric data are also included.
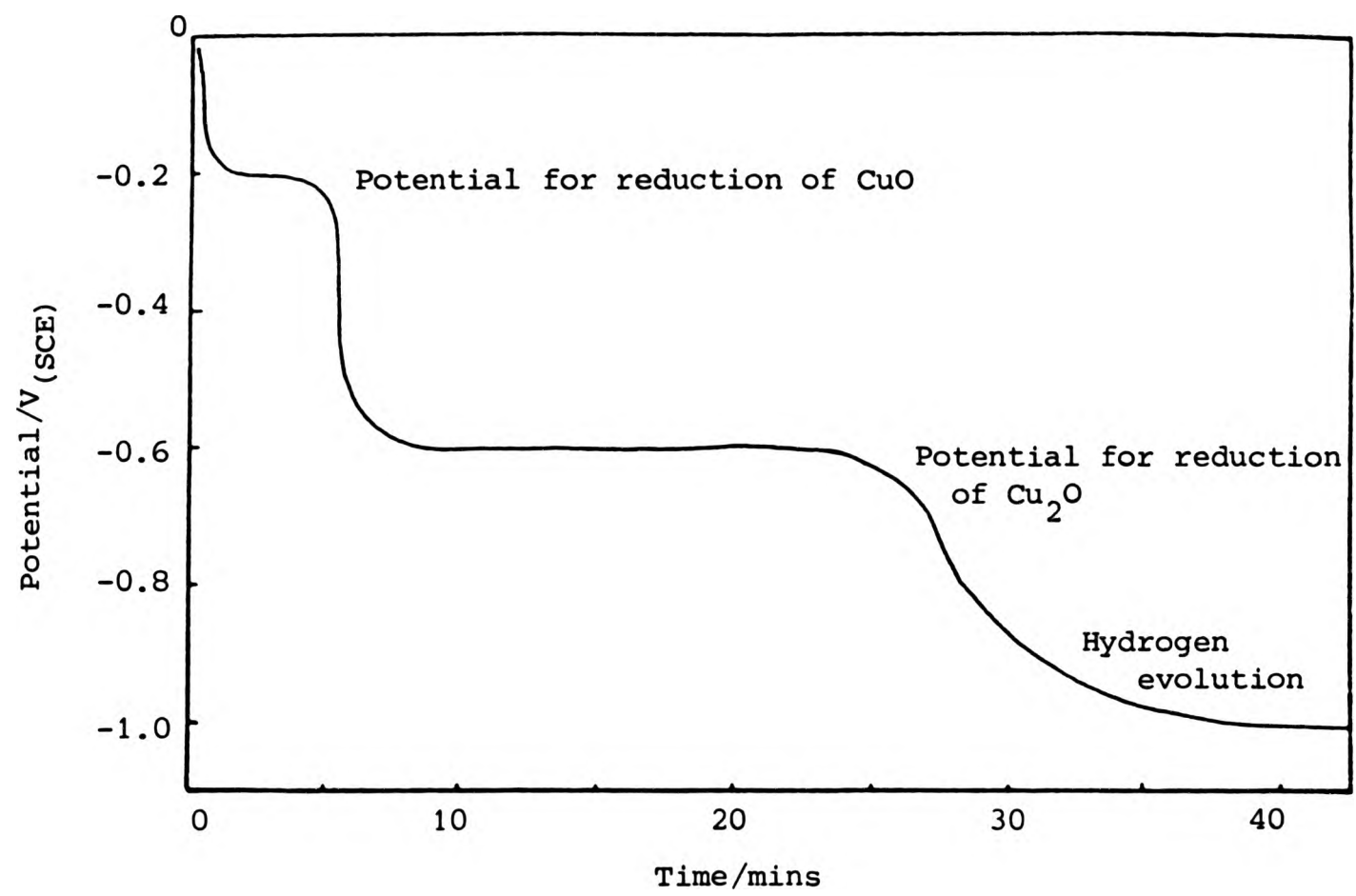
Figure 4.11. A typical coulometric reduction curve for a mixed oxide film.
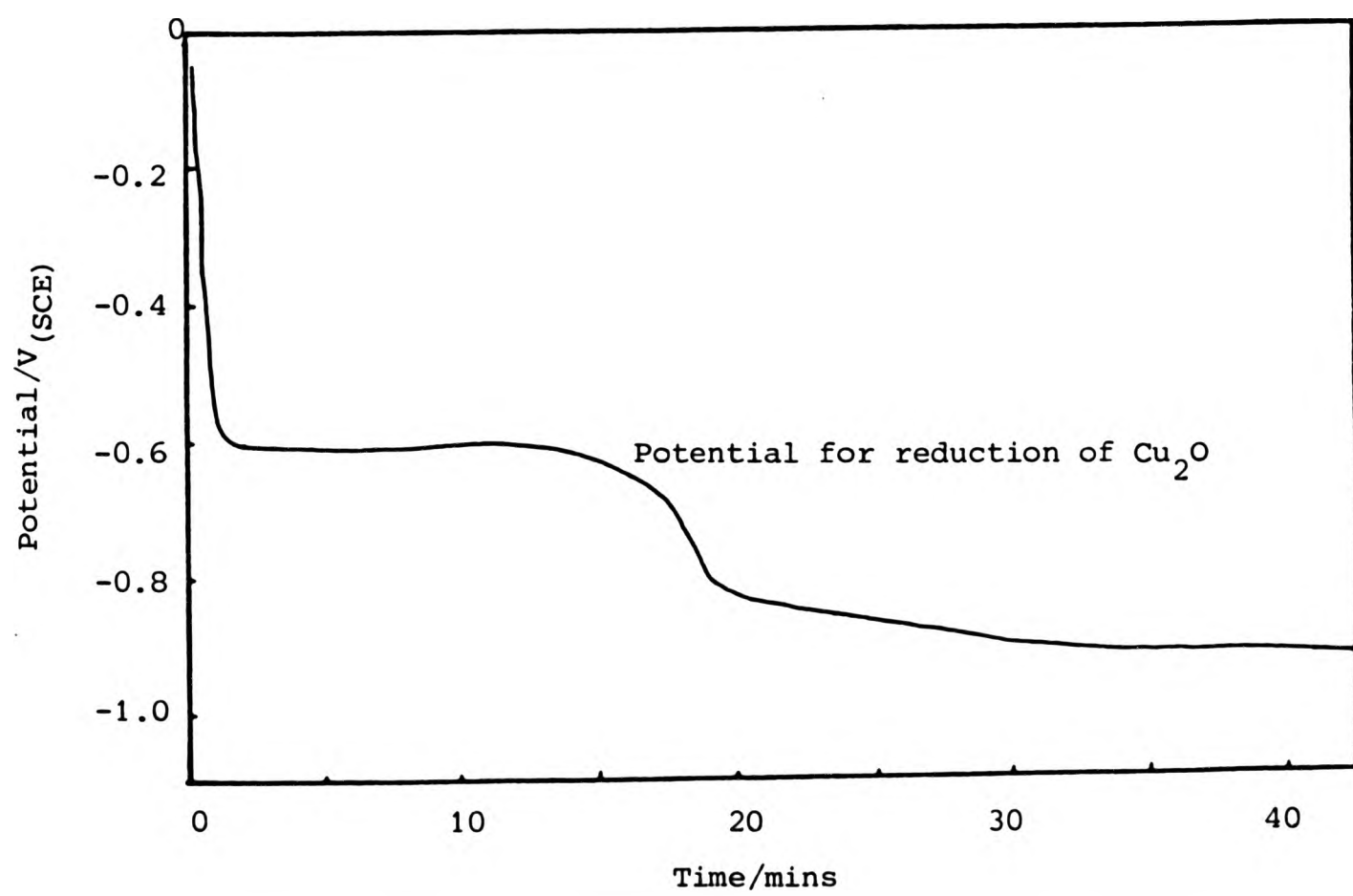
Figure 4.12. A typical coulometric reduction curve for a cuprous oxide film.

Table 4.12

Oxide films on copper prepared at 80°C

Period of oxidation/ hrs	$I/\mu A$	A/cm^2	t/secs	Thickness /$\overset{\circ}{A}$	
				coulometric	ellipsometric
Air formed	18.00	1.44	120	18.5	26
4	39.25	2.24	390	85	41
6	-	-	-	-	43
9	39.73	2.24	705	155	51
13	-	-	-	-	59
16	39.38	2.24	810	176	71
24	39.42	2.24	1200	261	77
24	-	-	-	-	87
36	15.00	1.80	2240	310	90
40	39.27	2.31	1620	341	-
48	-	-	-	-	116
48	39.77	2.19	1675	376	110
72	70.52	2.24	1171	457	140
91	-	-	-	-	158
144	60.00	1.92	1820	703	-

Table 4.13

Oxide films on the copper/gallium alloy prepared at 80°C.

Period of oxidation/ hrs	$I/\mu A$	A/cm^2	$t/secs$	Thickness /$\overset{\circ}{A}$	
				coulometric	ellipsometric
Air formed	18.33	1.44	172	27	26
4	39.35	2.34	720	112	63
7	39.37	2.23	570	124	71
10	-	-	-	-	81
15	39.72	2.34	1110	233	94
16	39.24	2.36	1140	234	-
24	39.36	2.23	1440	314	-
30	38.74	2.36	780	290	117
40	-	-	-	-	178
72	-	-	-	-	347

Table 4.14

Oxide films on the copper/germanium alloy prepared at 80°C.

Period of oxidation/ hrs	$I/\mu A$	A/cm^2	$t/secs$	Thickness / $\overset{\circ}{A}$	
				coulometric	ellipsometric
Air formed	18.00	1.44	226	35	29
4	39.24	2.26	510	110	54
6	39.35	2.05	630	150	-
8	39.67	2.26	1050	228	-
16	39.47	1.90	900	231	84
24	40.34	2.05	990	241	130
40	70.61	2.26	735	284	-
48	70.95	1.90	630	292	213
72	70.58	2.05	870	370	251

Table 4.15

Oxide films on the copper/nickel alloy prepared at 80°C

Period of oxidation/ hrs	$I/\mu A$	A/cm^2	t/secs	Thickness / $\overset{\circ}{A}$	
				coulometric	ellipsometric
Air formed	20.00	1.28	140	27	22
4	39.36	2.19	450	100	40
4	39.45	2.18	480	107	-
6.5	-	-	-	-	62
10	-	-	-	-	77
16	39.25	2.19	930	206	97
20	-	-	-	-	154
24	39.39	2.19	1500	333	173
36	-	-	-	-	183
40	39.42	2.17	1890	424	-
72	70.59	2.19	2400	956	-

Graphs showing how the oxide thickness increased with time were plotted for each substrate (Figures 4.13, 4.14, 4.15 and 4.16). Figures 4.17, 4.18, 4.19 and 4.20 show the relationship between ellipsometrically and coulometrically determined thicknesses for the oxide films on the four substrates. In some cases a film thickness was experimentally determined by both methods. Where this data was not available interpolated values from Figures 4.13, 4.14, 4.15 and 4.16 are used. A least square analysis, using experimental data only, was used to fix the position of each line.
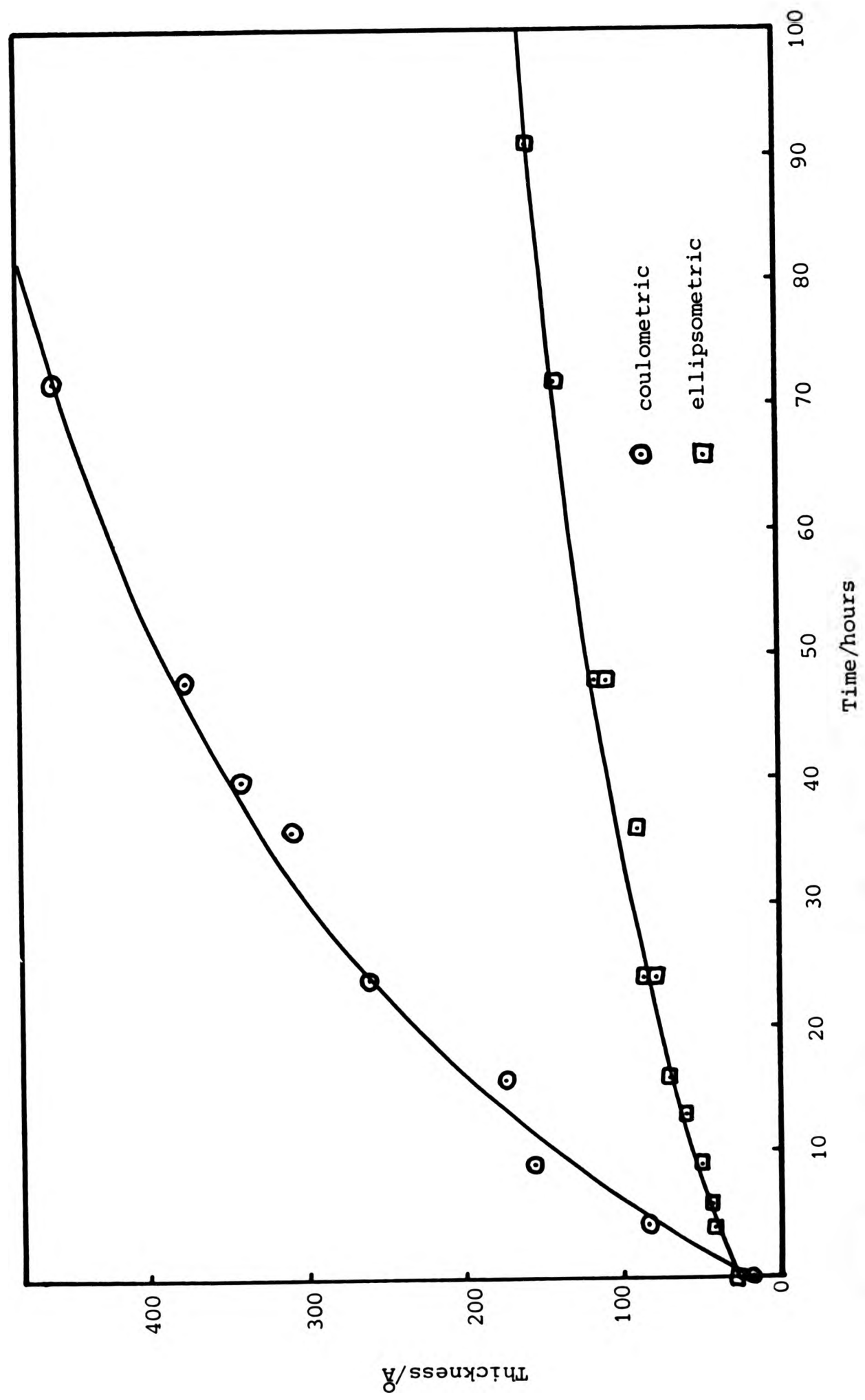
Figure 4.13. Oxide formation on cast copper at 80°C.
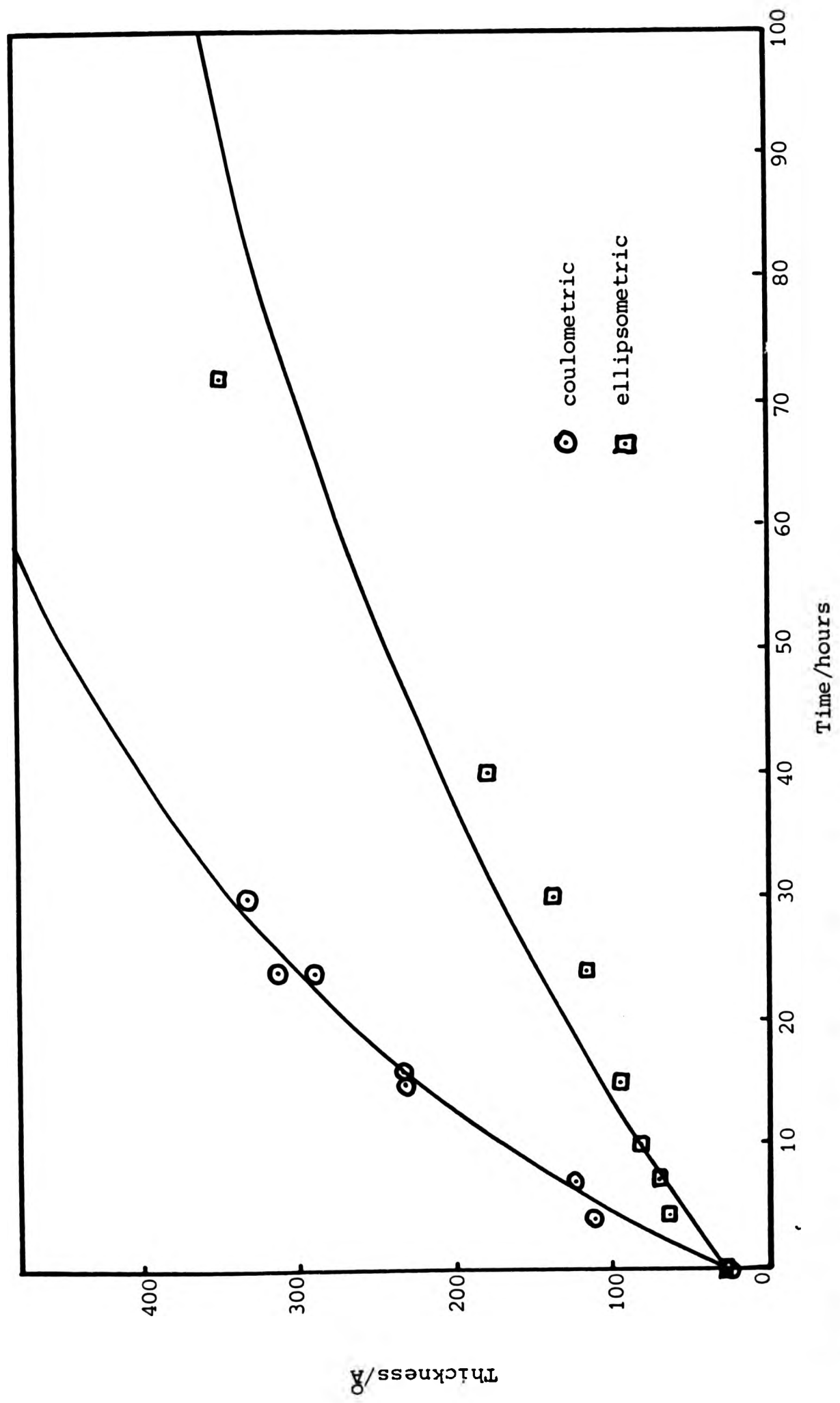
Figure 4.14. Oxide formation on copper/gallium alloy at 80°C.
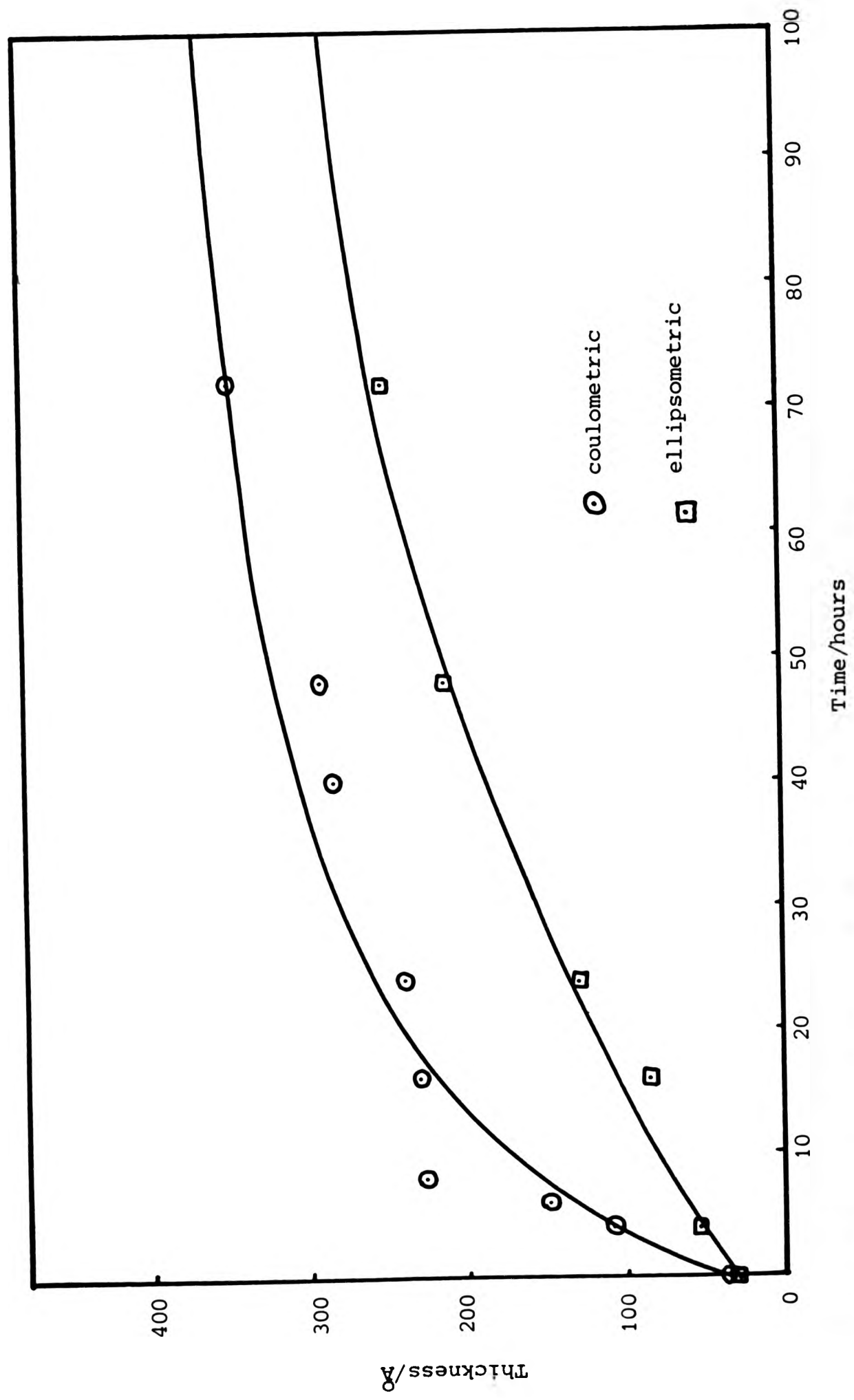
Figure 4.15. Oxide formation on copper/germanium alloy at 80°C.
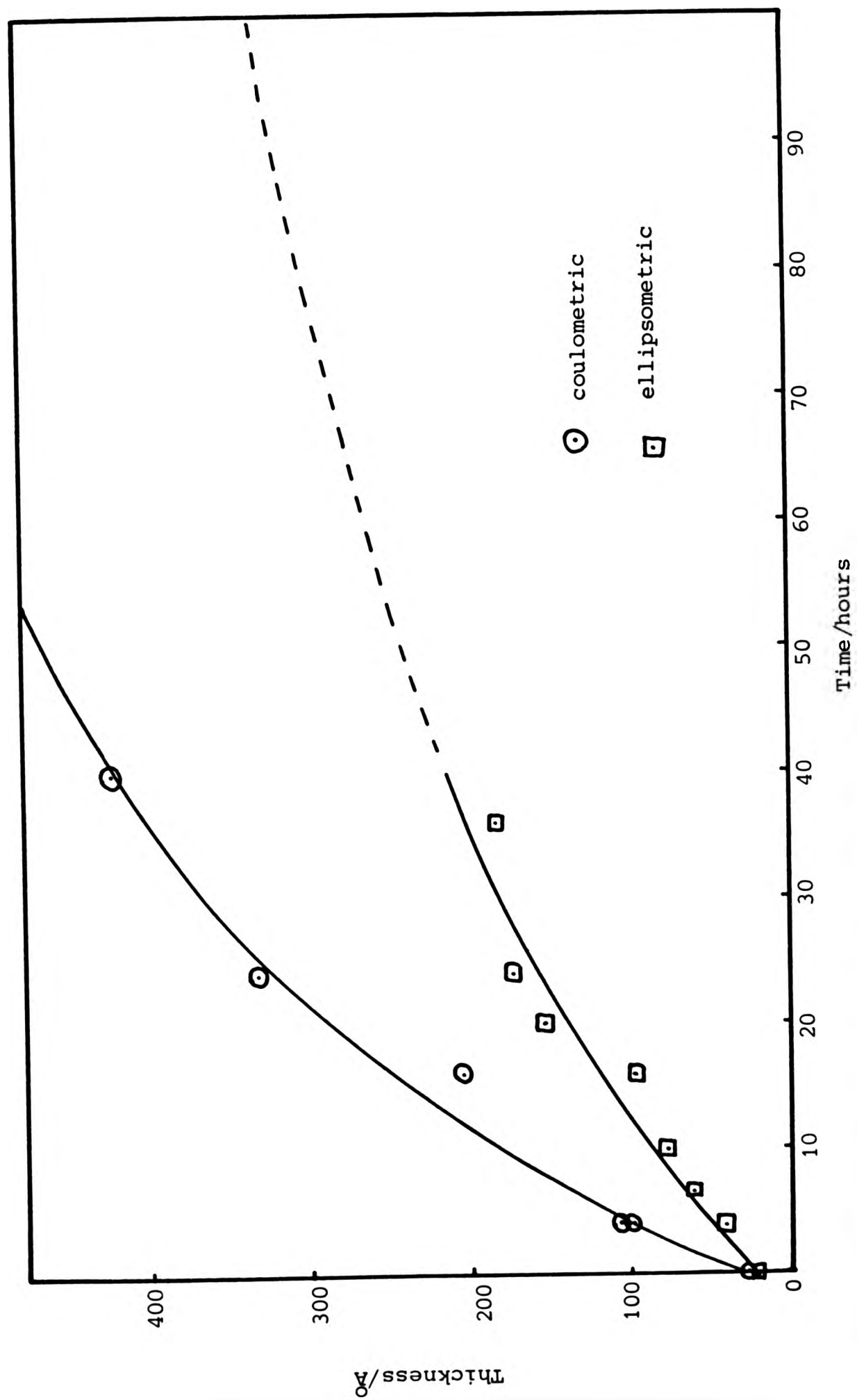
Figure 4.16. Oxide formation on copper/nickel alloy at 80°C.
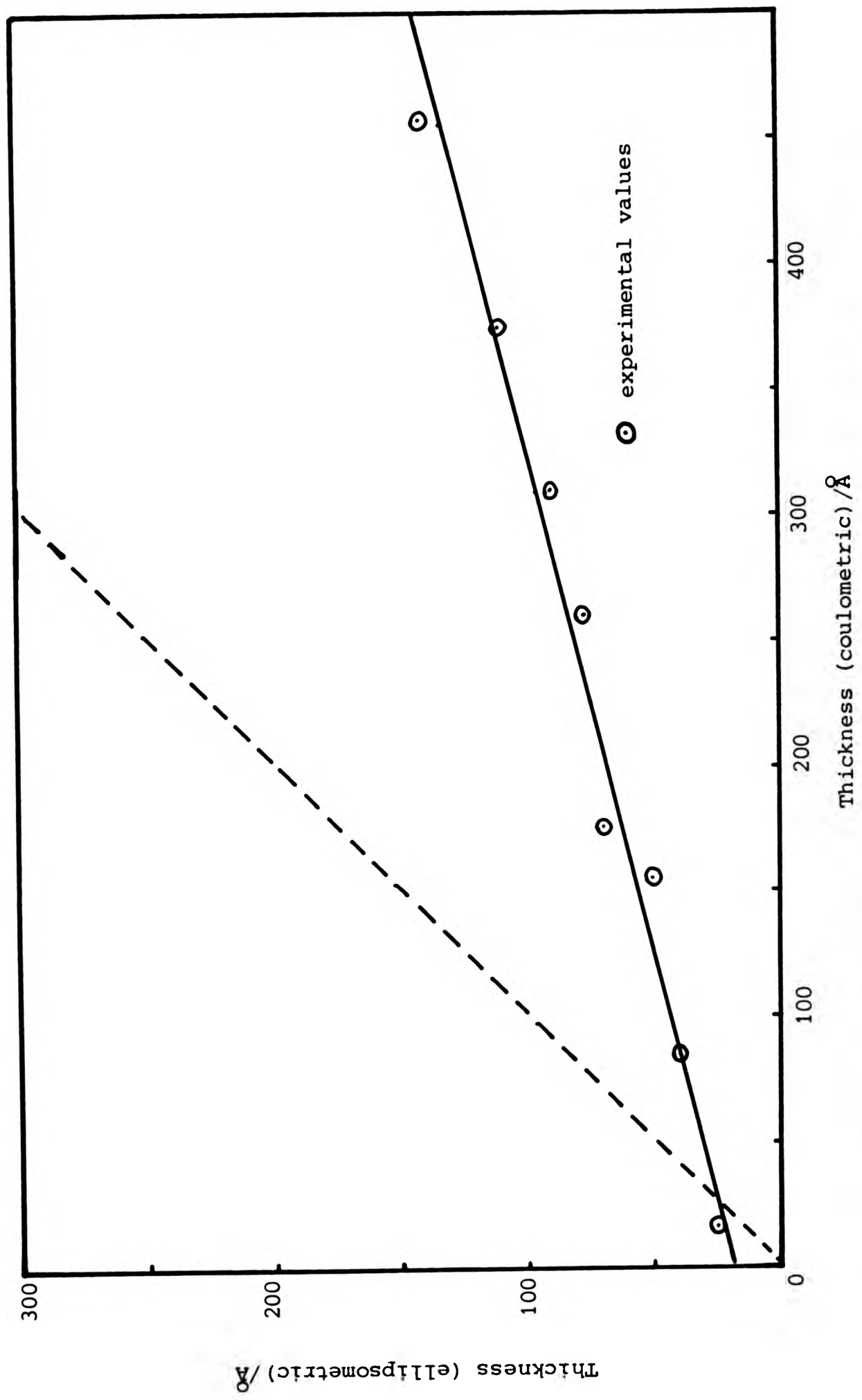
Figure 4.17. Ellipsometric and coulometric measurement of oxide thickness on cast copper.
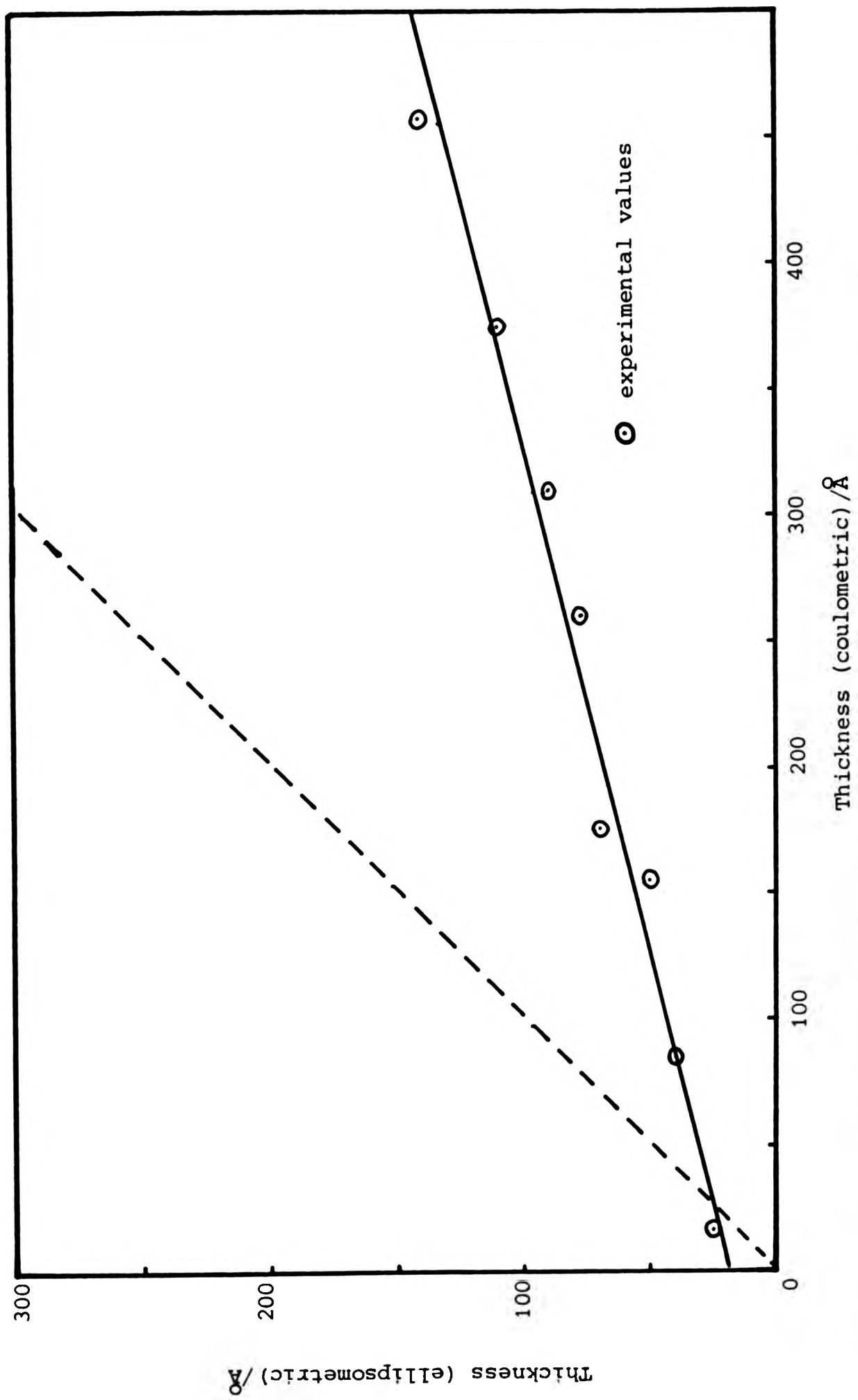
Figure 4.17. Ellipsometric and coulometric measurement of oxide thickness on cast copper.
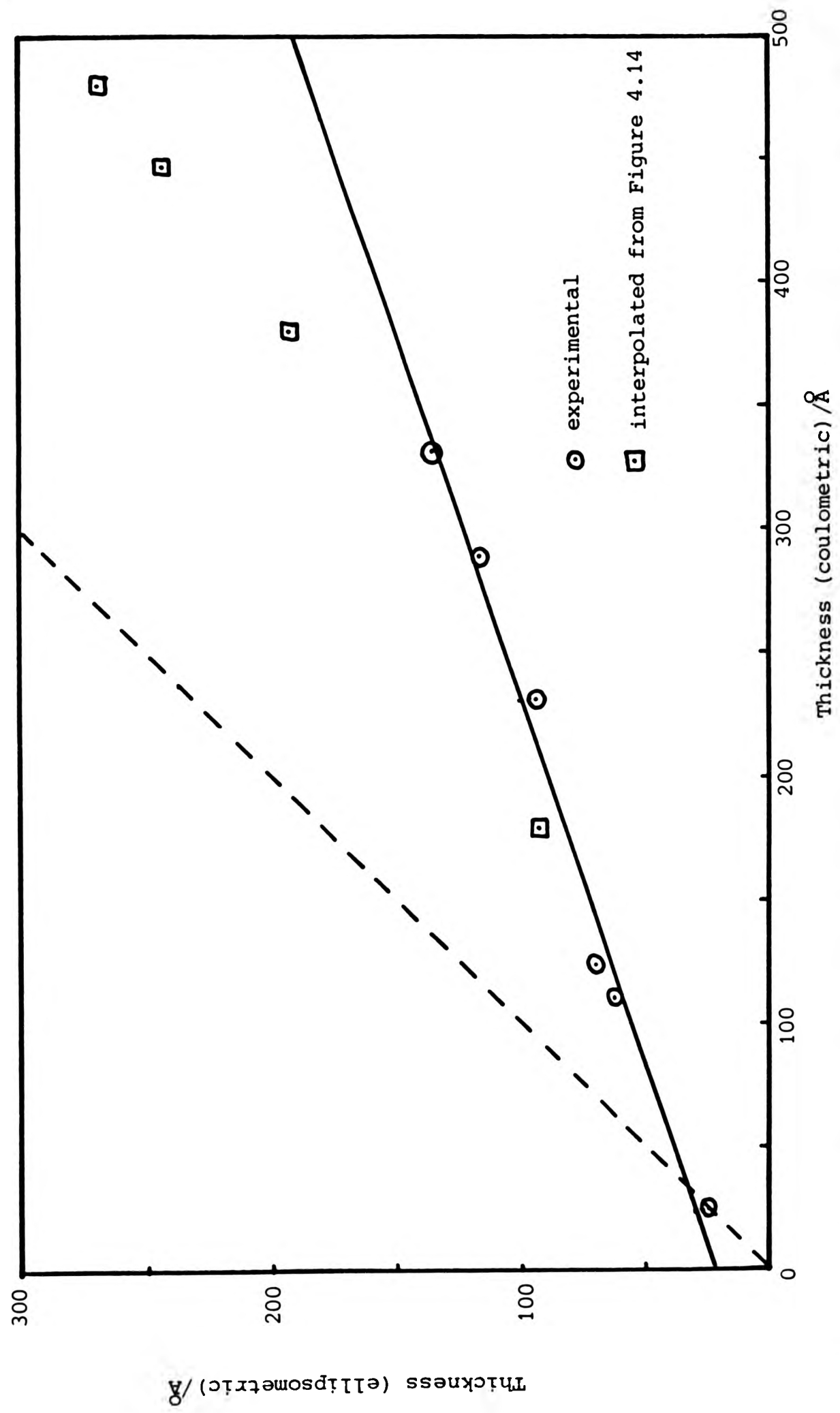
Figure 4.18. Ellipsometric and coulometric measurement of oxide thickness on copper/gallium alloy.
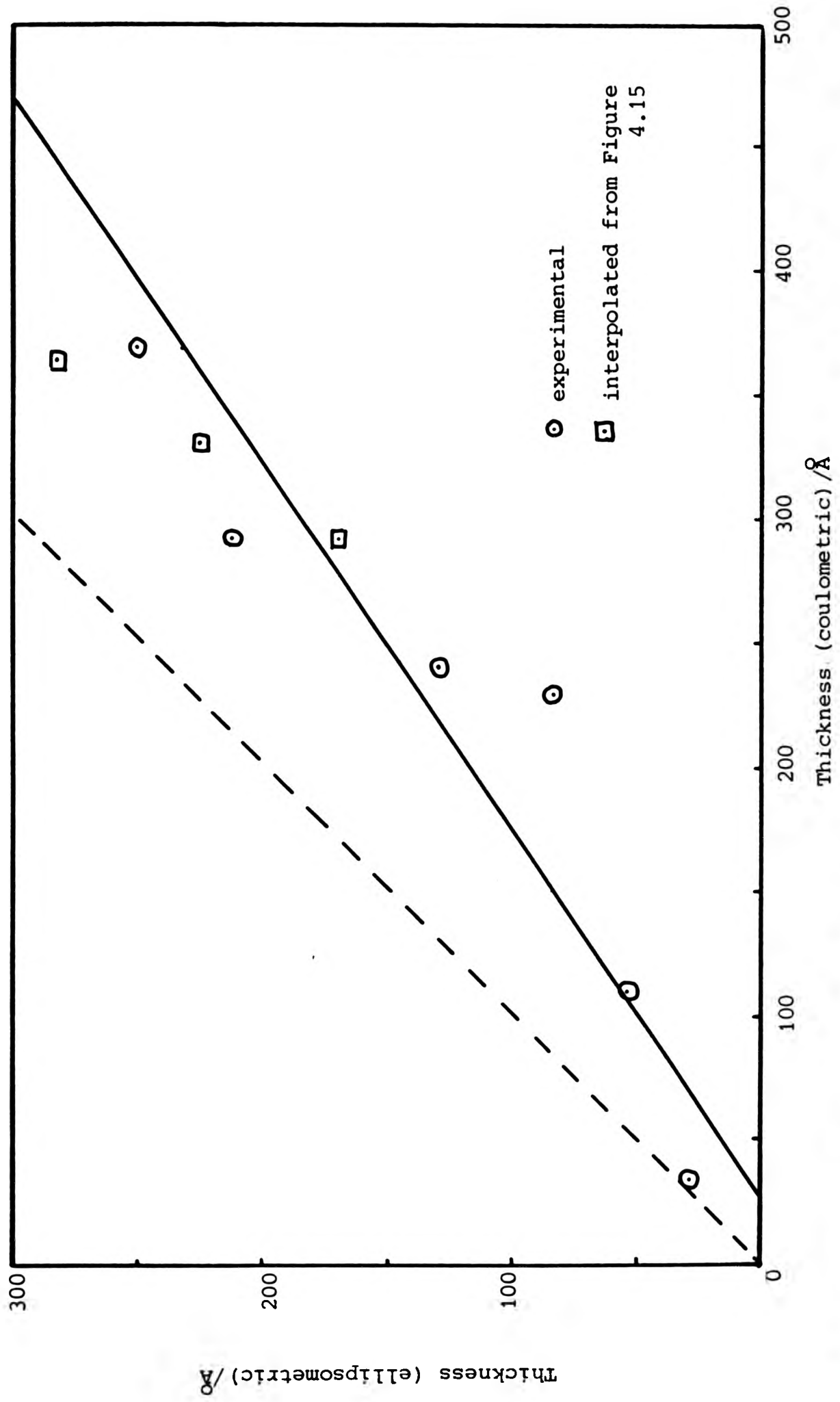
Figure 4.19. Ellipsometric and coulometric measurement of oxide thickness on copper/germanium alloy.
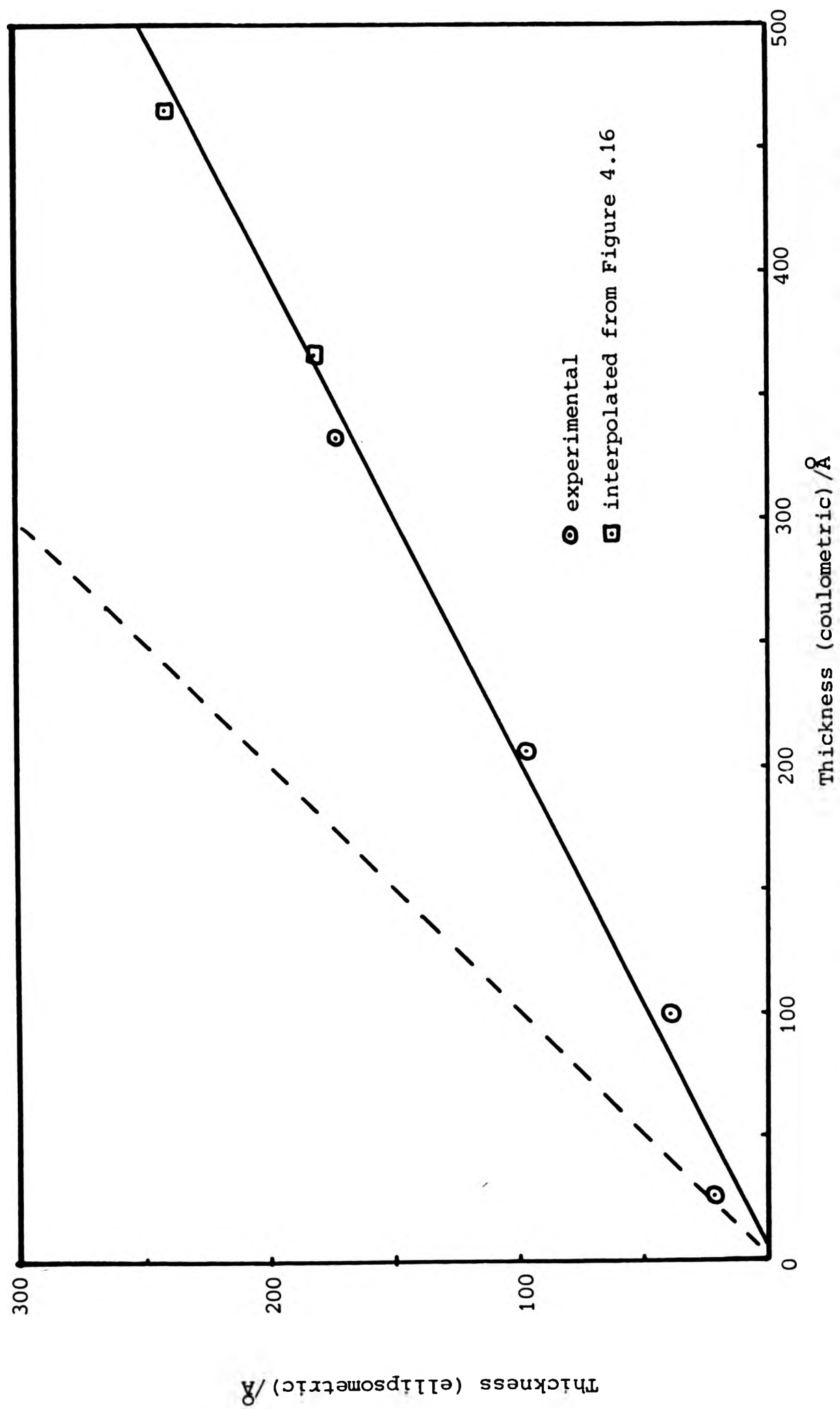
Figure 4.20. Ellipsometric and coulometric measurement of oxide thickness on copper/nickel alloy.

4.3.2 Transmission electron microscopy

Figures 4.21 and 4.22 are electron micrographs of a copper foil before and after oxidation at 80°C for 24 hours. Figures 4.23 and 4.24 are the corresponding diffraction patterns. The diffraction patterns consist of rings indicating that the foil and the oxide are composed of very small crystallites. The diameter of each ring of the diffraction pattern was measured and the lattice spacing, d, was calculated from the expression $d = K/s$ where d is the lattice spacing in Ångstroms, K is the camera constant (3.837 at 100 kV) and s is the diameter of the ring in centimetres. Tables 4.16 and 4.17 list the diameters of the rings and the corresponding values of d for the two diffraction patterns.
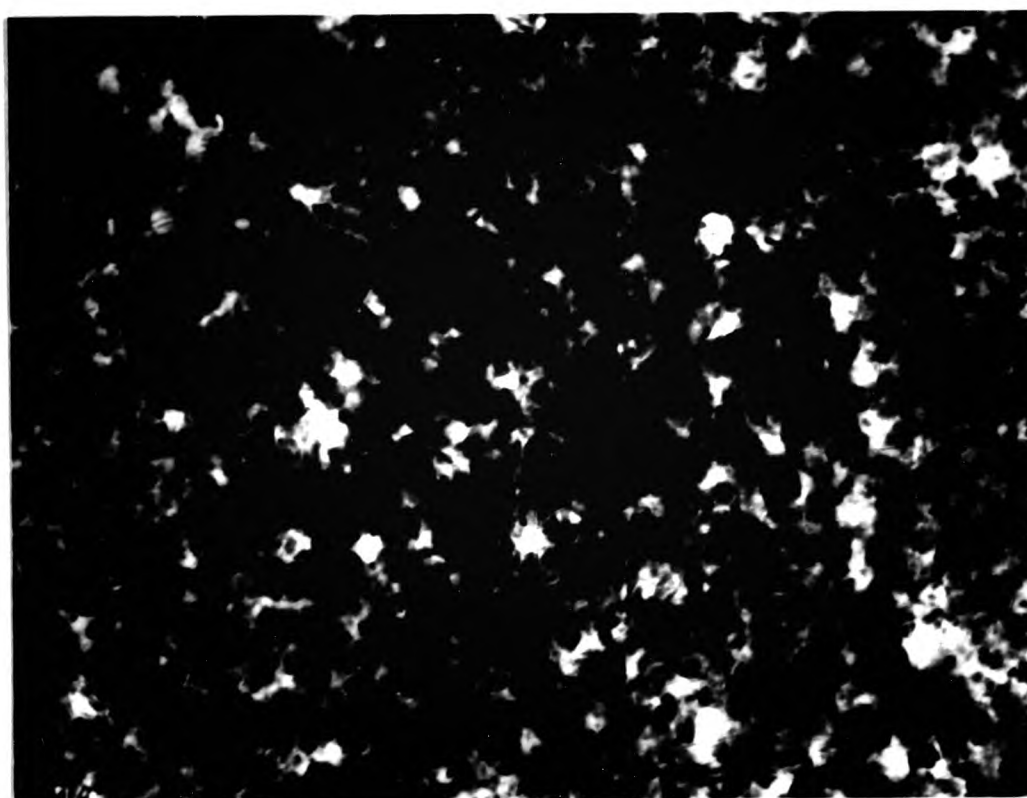
Figure 4.21   Transmission electron micrograph of a thin copper foil
(x 28,000).
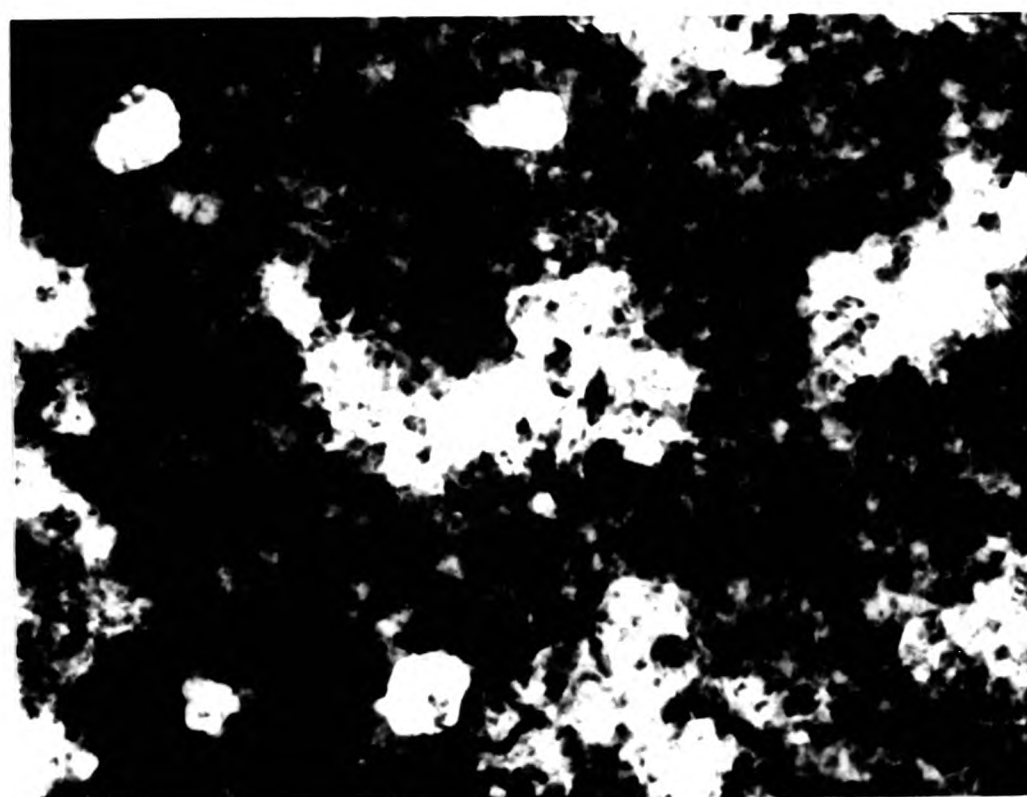
Figure 4.22   Transmission electron micrograph of an oxidised
copper foil (x 28,000).
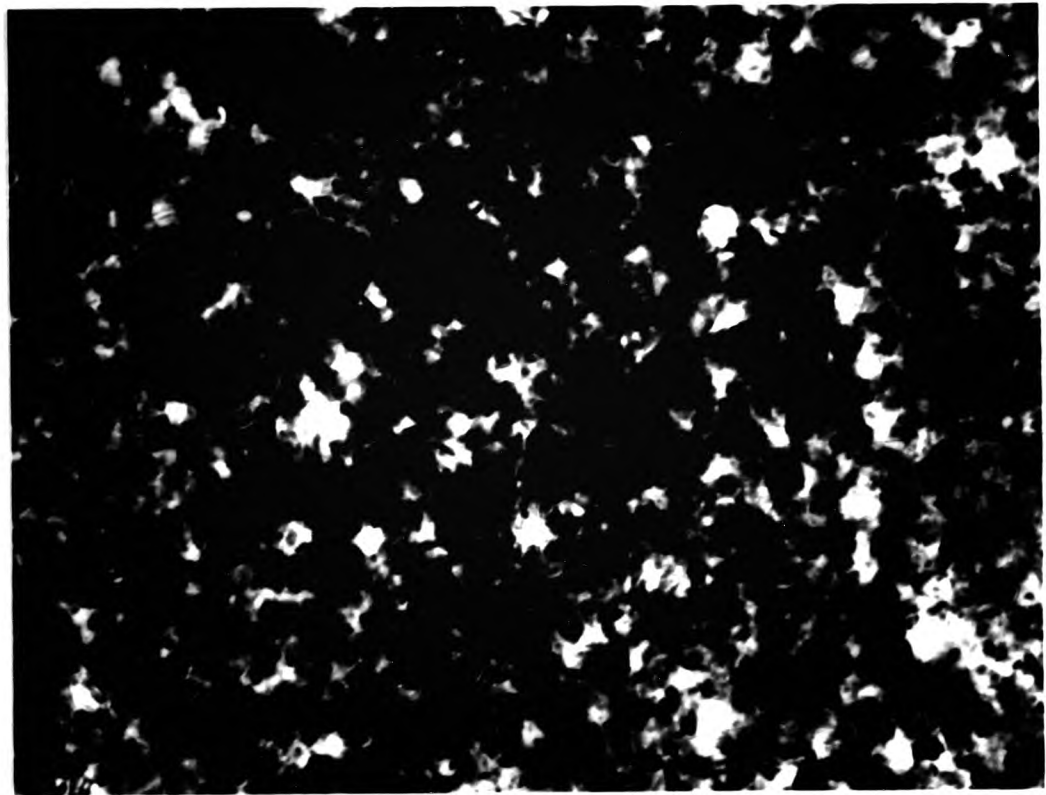
Figure 4.21   Transmission electron micrograph of a thin copper foil (x 28,000).
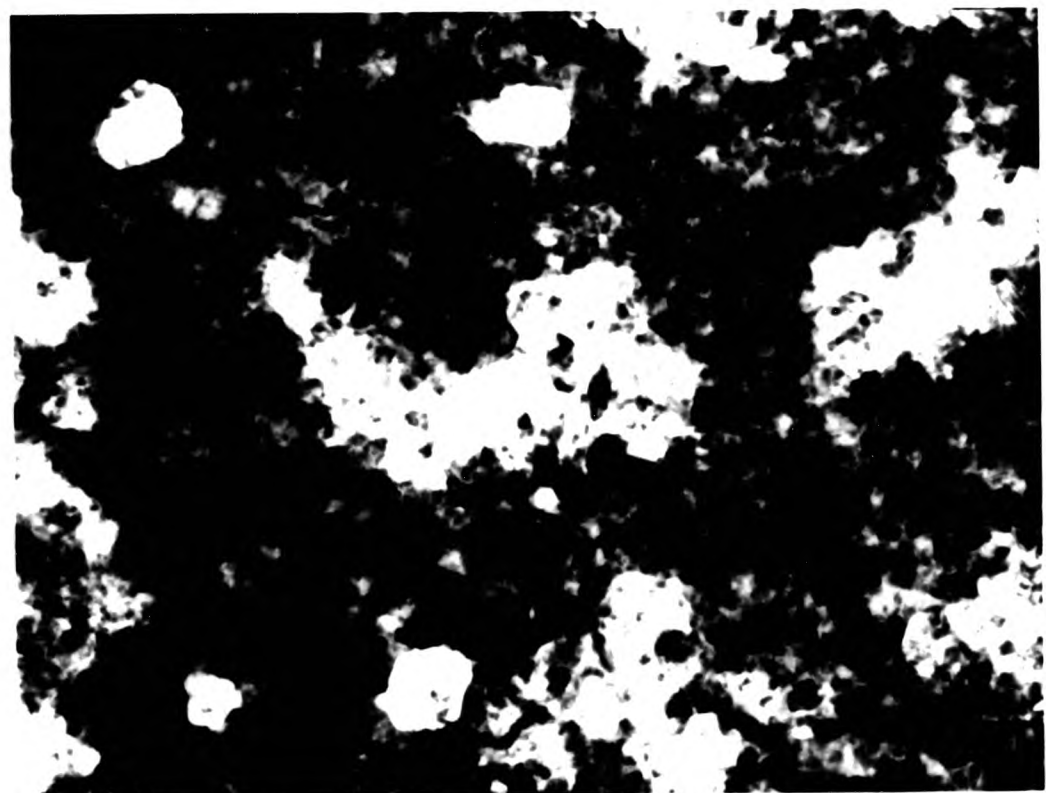
Figure 4.22   Transmission electron micrograph of an oxidised copper foil (x 28,000).
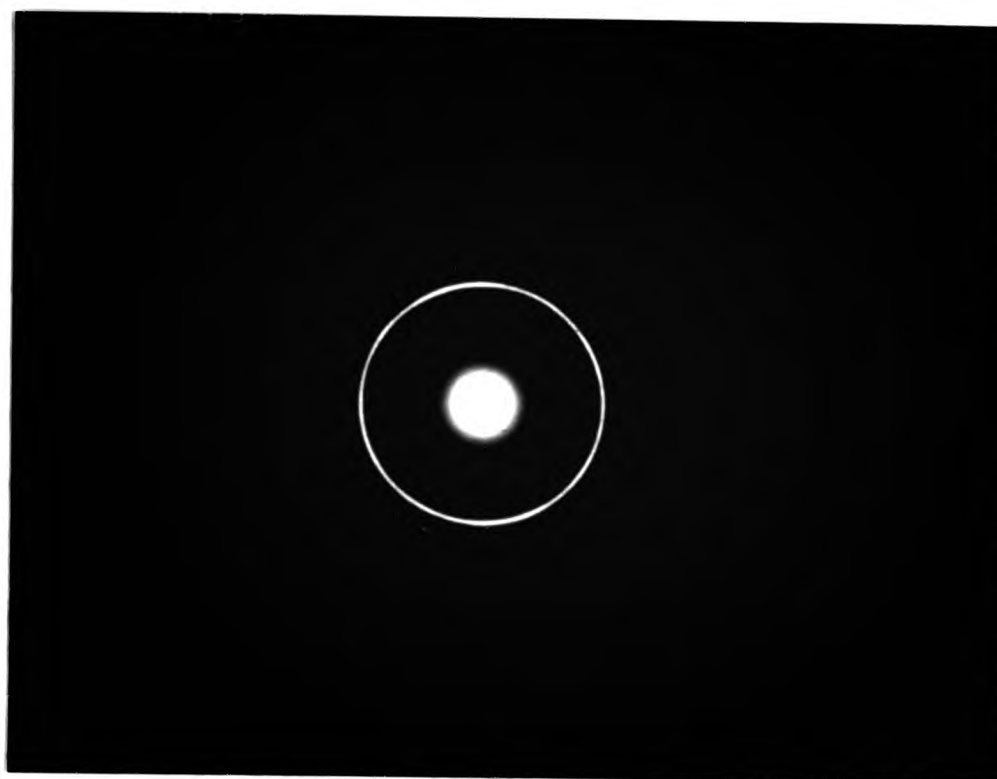
Figure 4.23   Electron diffraction pattern from a thin copper foil.

Figure 4.24   Electron diffraction pattern from an oxidised copper foil.
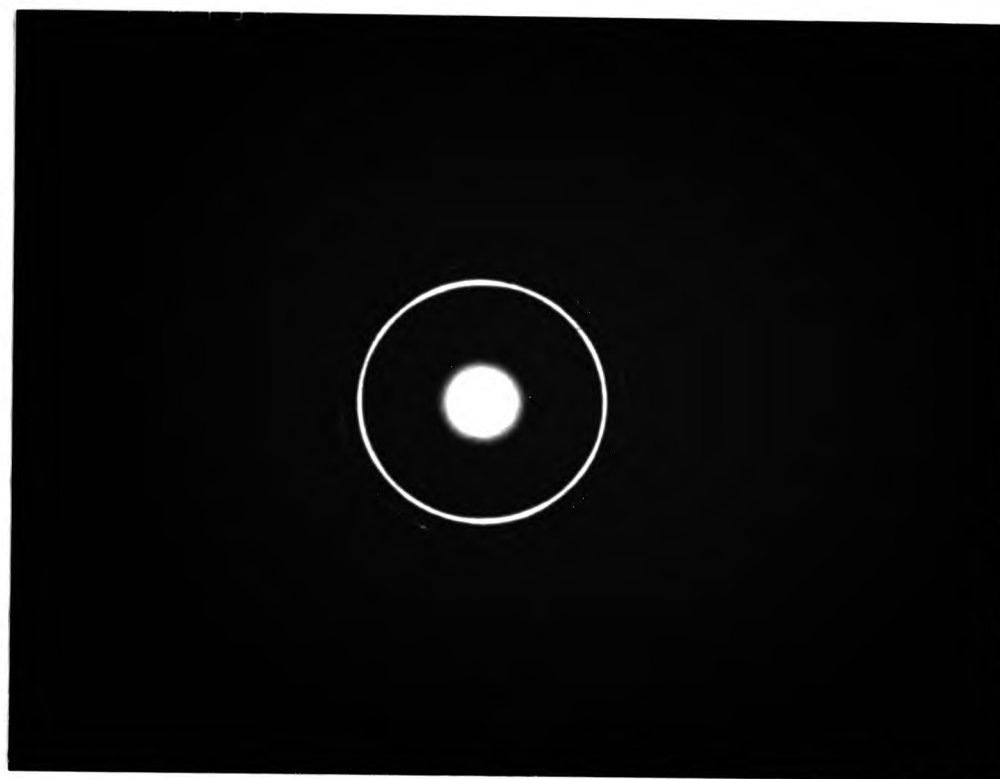
Figure 4.23   Electron diffraction pattern from a thin copper foil.

Figure 4.24   Electron diffraction pattern from an oxidised copper foil.

Table 4.16

Lattice parameters measured from Figure 4.23

Diameter of ring/cm	Intensity	Lattice spacing/Å
1.57	weak	2.44
1.84	strong	2.09
2.12	medium	1.81
2.54	v. weak	1.51
3.02	medium	1.27
3.56	medium	1.08
3.70	weak	1.04

Table 4.17

Lattice parameters measured from Figure 4.24

Diameter of ring/cm	Intensity	Lattice spacing/Å
1.25	medium	3.07
1.55	strong	2.48
1.81	strong	2.12
2.12	weak	1.81
2.51	medium	1.53
2.94	medium	1.29
3.02	v.weak	1.27

4.3.3 Graphical estimates of oxide film thickness

Figure 4.25 shows the variation of ψ and Δ calculated for several thicknesses of cuprite on a copper substrate together with experimental results for four oxidised specimens. It is clear that there is some similarity between predicted and experimental values although there is no complete match over the spectral range used. This indicates a difference in the optical constants of thin films of cuprous oxide and bulk cuprite which means that the graphical method cannot be used to fix absolutely, the thickness of a thin oxide film. The choice of thickness depends on the visual interpolation of the curves which is made difficult by the uneven distribution of the experimental points. This is clearly illustrated on the plot for specimen C where values of Δ and ψ at 50 nm intervals are indicated by circles. Interpolation is also made more difficult by the way in which the curves converge at longer wavelengths and diverge at shorter ones. However this method provides an initial, approximate value which can then be used in the numerical method. Thus in Figure 4.25 it can be seen that specimen A bears a film which is approximately 50 $\overset{o}{A}$ thick. Table 4.18 lists the estimated thicknesses of the oxide films on the specimens whose spectral data is plotted in Figure 4.25.

Figure 4.25. The variation of ψ and Δ for copper overlaid with cuprite.

_____ theoretical values for copper overlaid with cuprite of the
indicated thickness

- - - - experimental values for copper oxidised at 80°C
A oxidised for 9 hours
B   "   "   48   "
C   "   "   72   "
D   "   "   91   "

Table 4.18

Estimated thicknesses of oxide films

Specimen	Limits of film thickness/$\overset{o}{A}$	Estimated value/$\overset{o}{A}$
A	∿50	50
B	>100	120
C	∿150	150
D	>150	160

4.3.4 Numerical estimates of oxide film thickness

Like the graphical method, this assumes that the optical constants
of cuprite are the same whatever its form but uses each of the
81 spectral measurements to calculate the film thickness. The
reliability of the numerical method depends partly on the
accuracy of the initial thickness estimate used. An estimate
within the range 0.5 to 2.0 times the actual thickness is
acceptable. The computer program will list a thickness value and
the root-mean-square error associated with the data for each
wavelength at which measurements were taken. It will also
produce an average film thickness together with the average
root-mean-square error and the standard deviation for the set
of experimental data.

Without the graphical method trial-and-error has to be relied
on for the initial value and inspection of the magnitude of the
errors used to assess the accuracy of the average thickness

computed. Thus the graphical method saves computing time.

Tables 4.19, 4.20, 4.21 and 4.22 list the thickness estimates obtained using the graphical method, and the average thickness generated by using them in the numerical method for oxide films on copper, copper/gallium, copper/germanium and copper/ nickel alloys respectively. The errors associated with these values are also listed.

Table 4.19

Thicknesses of oxide films on copper specimens obtained by the numerical method.

Graphical thickness estimate/$\overset{\circ}{A}$	Average thickness /$\overset{\circ}{A}$	Average RMS error per angle	Standard deviation/$\overset{\circ}{A}$
20	27	0.932	7
40	44	1.144	8
40	46	1.335	9
50	54	1.486	10
60	63	1.712	12
65	67	1.782	13
80	82	2.262	17
120	126	3.742	26
150	153	4.553	28
160	171	5.171	32

Table 4.20

Thicknesses of oxide films on copper/gallium alloy specimens obtained by the numerical method.

Graphical thickness estimate/$\overset{\circ}{A}$	Average thickness /$\overset{\circ}{A}$	Average RMS error per angle	Standard deviation/$\overset{\circ}{A}$
20	27	0.937	6
60	66	1.962	11
70	74	2.226	13
90	101	3.100	27
120	129	4.151	31
140	149	5.097	30
180	191	8.561	36
350	448	5.420	159

Table 4.21

Thicknesses of oxide films on copper/germanium specimens obtained by the numerical method.

Graphical thickness estimate/$\overset{o}{A}$	Average thickness /$\overset{o}{A}$	Average RMS error per angle	Standard deviation/$\overset{o}{A}$
20	30	1.024	7
50	57	1.896	11
75	79	2.373	17
130	144	4.781	32
200	228	5.097	35
250	265	4.475	60

Table 4.22

Thicknesses of oxide films on copper/nickel specimens obtained
by the numerical method

Graphical thickness estimate/Å	Average thickness /Å	Average RMS error per angle	Standard deviation/Å
20	22	0.922	6
40	42	1.152	8
60	66	1.801	14
75	82	2.314	17
100	103	3.183	21
150	175	4.279	28
175	189	8.365	38
200	201	7.946	43

4.4 Evaluation of the optical constants of oxide films

The graphical and numerical methods described in Section 3.5
assumed that the optical constants of the oxide film were those
of cuprite in an attempt to establish its thickness. However,
it is obvious that this is not the case (see Figure 4.25). The
computer program written by Clarke (96) and used in the
numerical method can be used to evaluate n, k and d for the
film but unless the estimate of the thickness was close to its
actual value the program would not run or alternatively
produced results which were clearly incorrect. This was

especially the case with specimens bearing thicker films where
the value of Δ falls outside the range $90° > \Delta > 0°$. In these
circumstances discontinuous values of n, k and/or d were
frequently produced when the program was used. By using the
average thickness found as the estimated value in the next run
of the program and repeating this several times, the thicknesses
found gradually converge to a constant value (see Appendix 3).
Clarke's program was therefore modified by the Computer Support
Unit of the City of London Polytechnic so that it was automatically
repeated until the average thickness found by successive repeats
was within a specified limit which was normally 0.01 nm. Having
established the thickness of the film Clarke's original program
was used with the thickness fixed at the value given in the final
iteration so that spectral values of n and k for the oxide film
are produced.

4.4.1   The optical constants of cuprous oxide films on copper and
        dilute copper alloys

Tables 4.23, 4.24, 4.25 and 4.26 list the thicknesses of the
oxide films on the recast copper and the copper/gallium, copper/
germanium and copper/nickel alloys respectively. The number of
iterations and the errors associated with these results are
also included.

Table 4.23

Thickness of oxide films on recast copper.

Graphical estimate /$\mathring{A}$	Numerically determined value/$\mathring{A}$	Final value /$\mathring{A}$	Number of iterations	Average RMS error per angle	Standard deviation /$\mathring{A}$
20	27	26	5	0.006	4
40	44	41.2	5	0.010	4
40	46	43.3	3	0.007	5
50	54	51.1	3	0.008	6
60	63	58.7	3	0.011	7
65	67	62.9	3	0.011	7
80	82	76.6	4	0.013	9
120	126	115.8	7	0.019	16
150	153	140.2	10	0.020	17
160	171	157.5	4	0.019	18

Table 4.24

Thickness of oxide films on the copper/gallium alloy.

Graphical estimate /Å	Numerically determined value/Å	Final value /Å	Number of iterations	Average RMS error per angle	Standard deviation /Å
20	27	26	8	0.009	4
60	66	62.9	7	0.009	6
70	74	70.7	5	0.013	7
80	86	80.6	3	0.017	10
90	101	93.9	7	0.035	11
120	129	117.0	6	0.020	16
140	149	135.6	7	0.024	18
180	191	178.2	11	0.031	18
350	448	347.3	12	0.478	20

Table 4.25

Thickness of oxide films on the copper/germanium alloy.

Graphical estimate /Å	Numerically determined value/Å	Final value /Å	Number of iterations	Average RMS error per angle	Standard deviation /Å
20	30	28.8	8	0.007	4
50	54	53.8	10	0.008	6
75	79	83.8	4	0.016	9
130	144	130.5	13	0.022	19
200	228	213.2	7	0.024	19
250	265	251.1	15	0.249	30

Table 4.26

Thickness of oxide films on the copper/nickel alloy

Graphical estimate /$\overset{\circ}{A}$	Numerically determined value/$\overset{\circ}{A}$	Final value /$\overset{\circ}{A}$	Number of iterations	Average RMS error per angle	Standard deviation /$\overset{\circ}{A}$
20	22	22.1	6	0.016	4
40	42	39.7	3	0.005	4
60	66	61.5	3	0.009	8
75	82	76.5	9	0.013	9
100	103	96.6	6	0.018	12
150	175	172.6	4	0.033	21
175	189	182.7	7	0.028	22

Using the thicknesses listed in the preceeding tables, spectral values of n and k were generated for each of the oxide films. The average root-mean-square error per angle was zero in all but two cases. The 347.3 $\overset{\circ}{A}$ film on the copper/gallium alloy and the 251.1 $\overset{\circ}{A}$ film on the copper/germanium alloy had errors of 0.990 and 0.022 respectively associated with them.

Figures 4.26, 4.27 and 4.28 show the variation of n, k and R_n respectively for some of the oxide films on recast copper. Values for bulk cuprite are included for comparison.
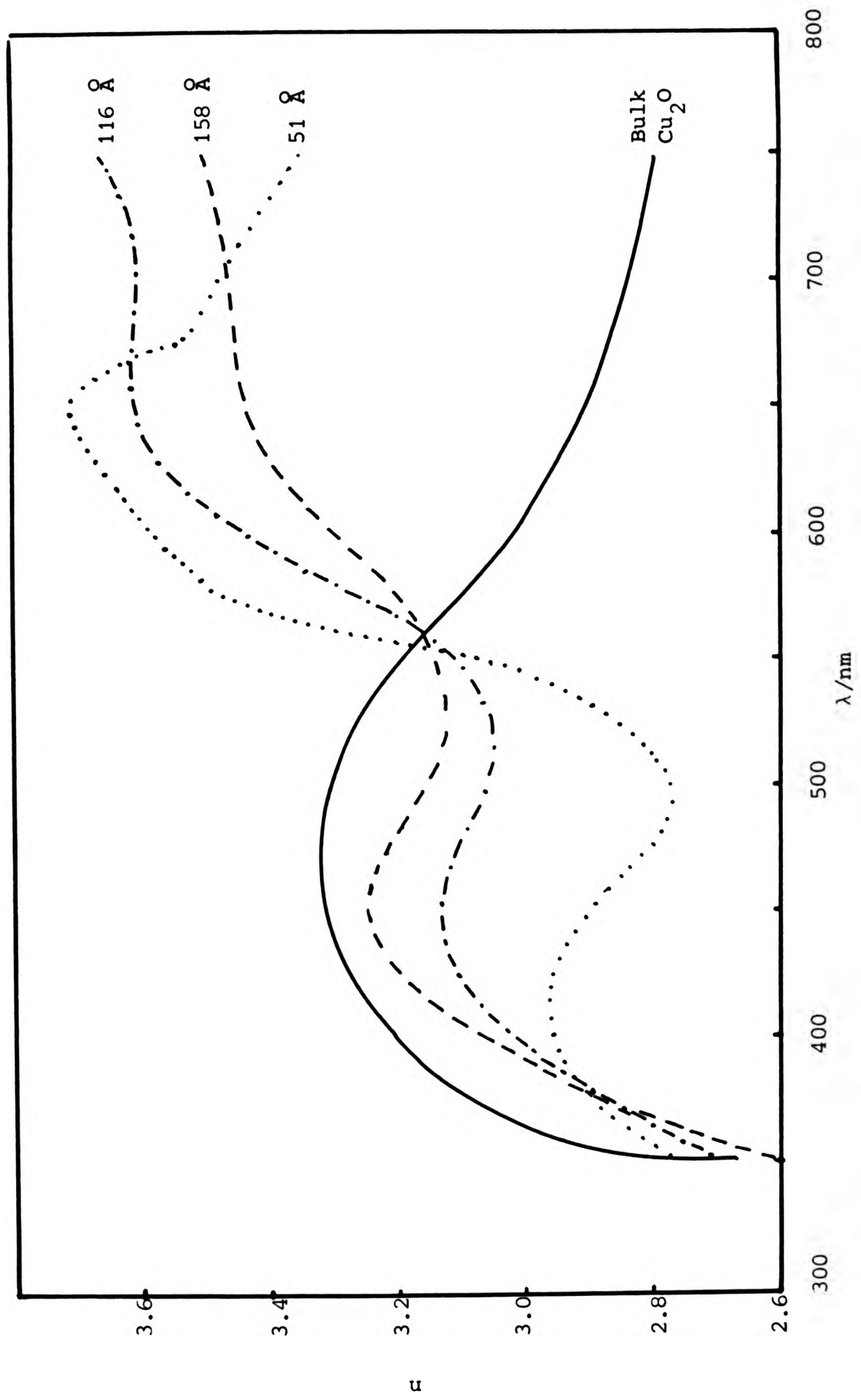
Figure 4.26. Spectral variation of n for cuprous oxide films of various thickness on copper.
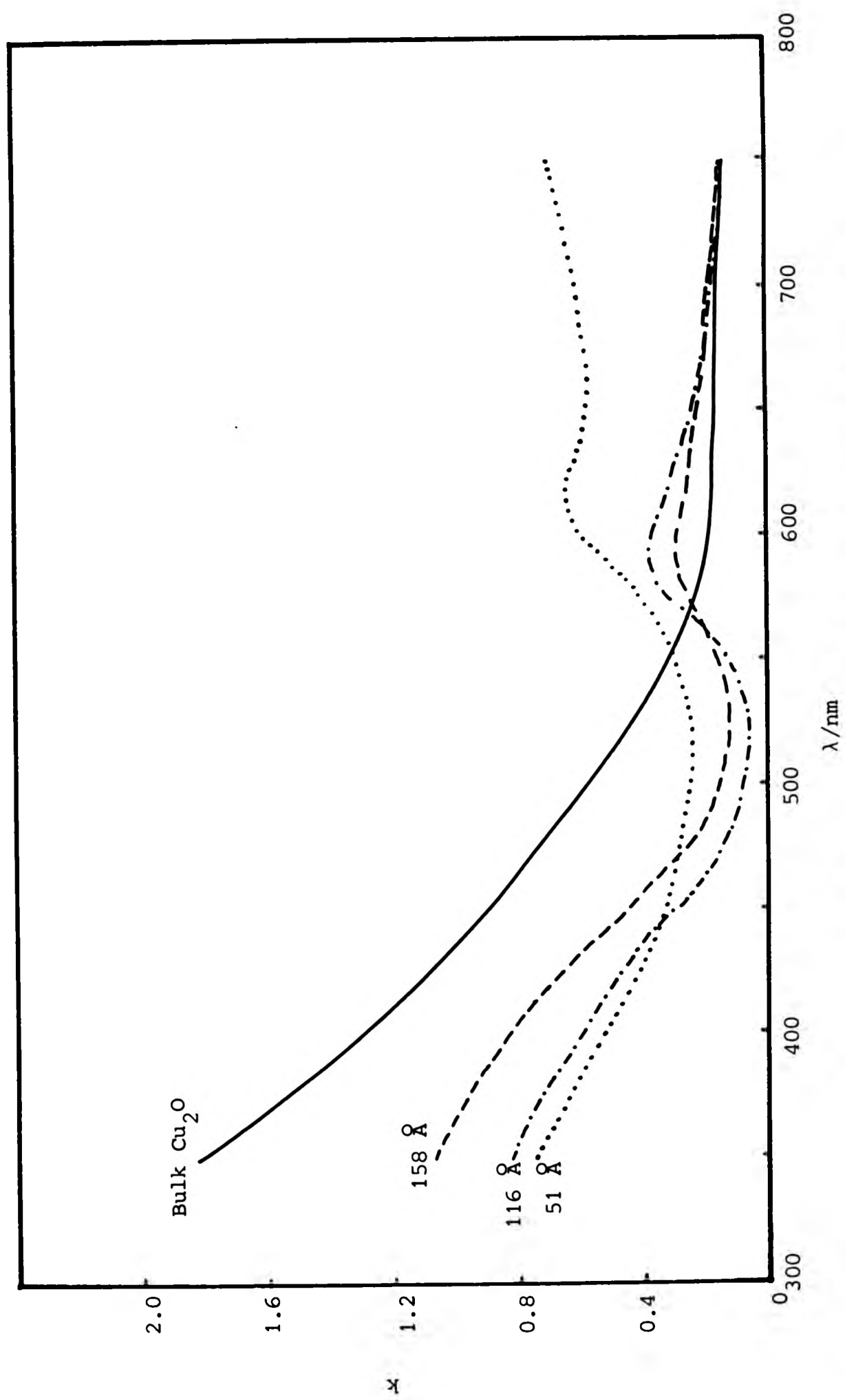
Figure 4.27. Spectral variation of k for cuprous oxide films of various thickness on copper.
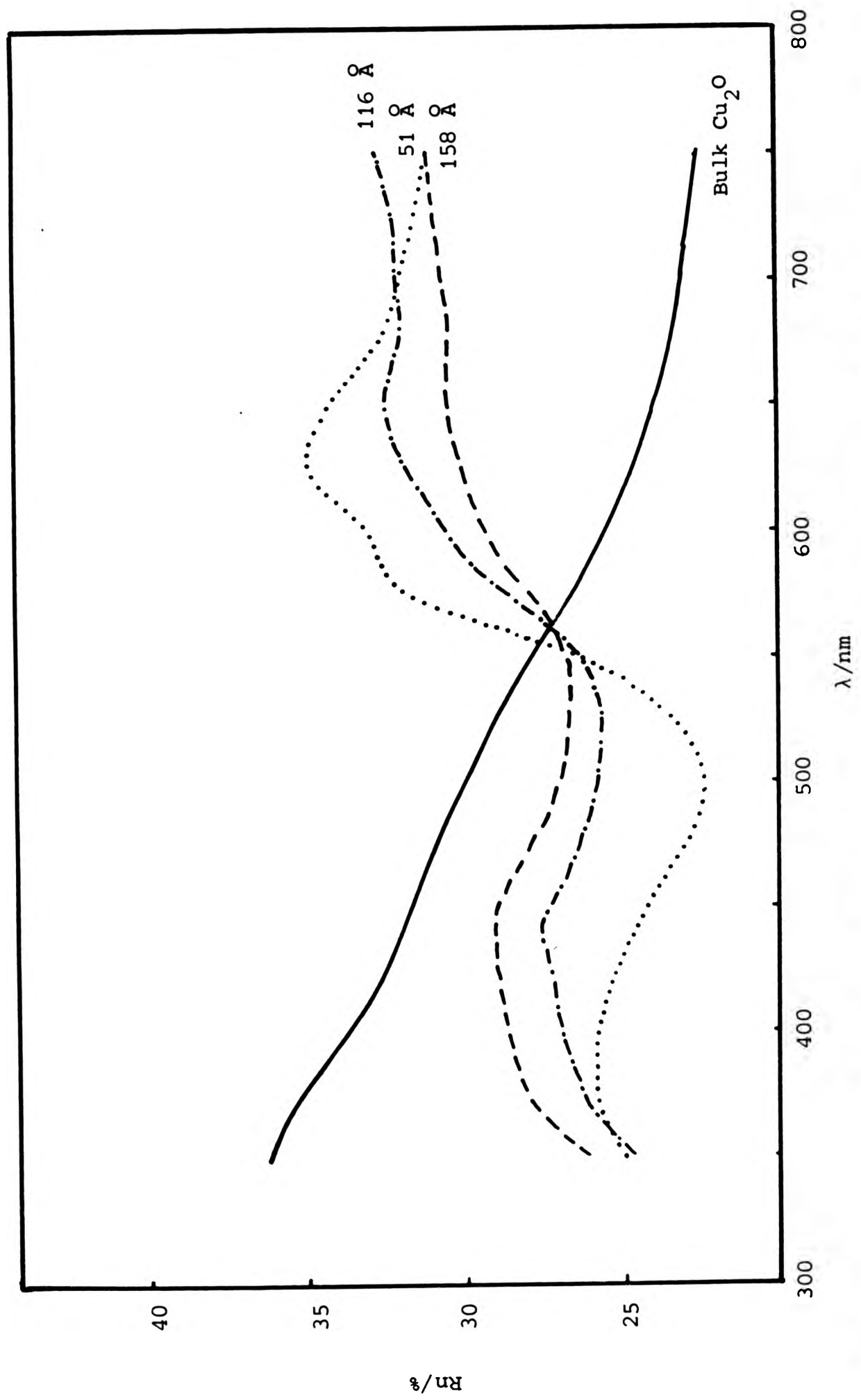
Figure 4.28. Spectral variation of reflectance for cuprous oxide films of various thickness on copper.

Similar spectral curves were obtained for the oxide films on the alloys. The small differences observed for individual substrates will be discussed in Section 5. For films 200 Å or more in thickness, the optical constants were found to approach more closely those of bulk cuprite. This is illustrated in Figure 4.29 where spectral values of n and k for an oxide film 347 Å thick are compared with those of cuprite. Conversely, there are greater differences between the optical constants of the thin air-formed films and those of bulk cuprite as shown in Figures 4.30 and 4.31.

4.4.2 The optical constants of cuprous oxide films on glass

The optical constants of the glass used as the substrate in these experiments are listed in Table 4.27.
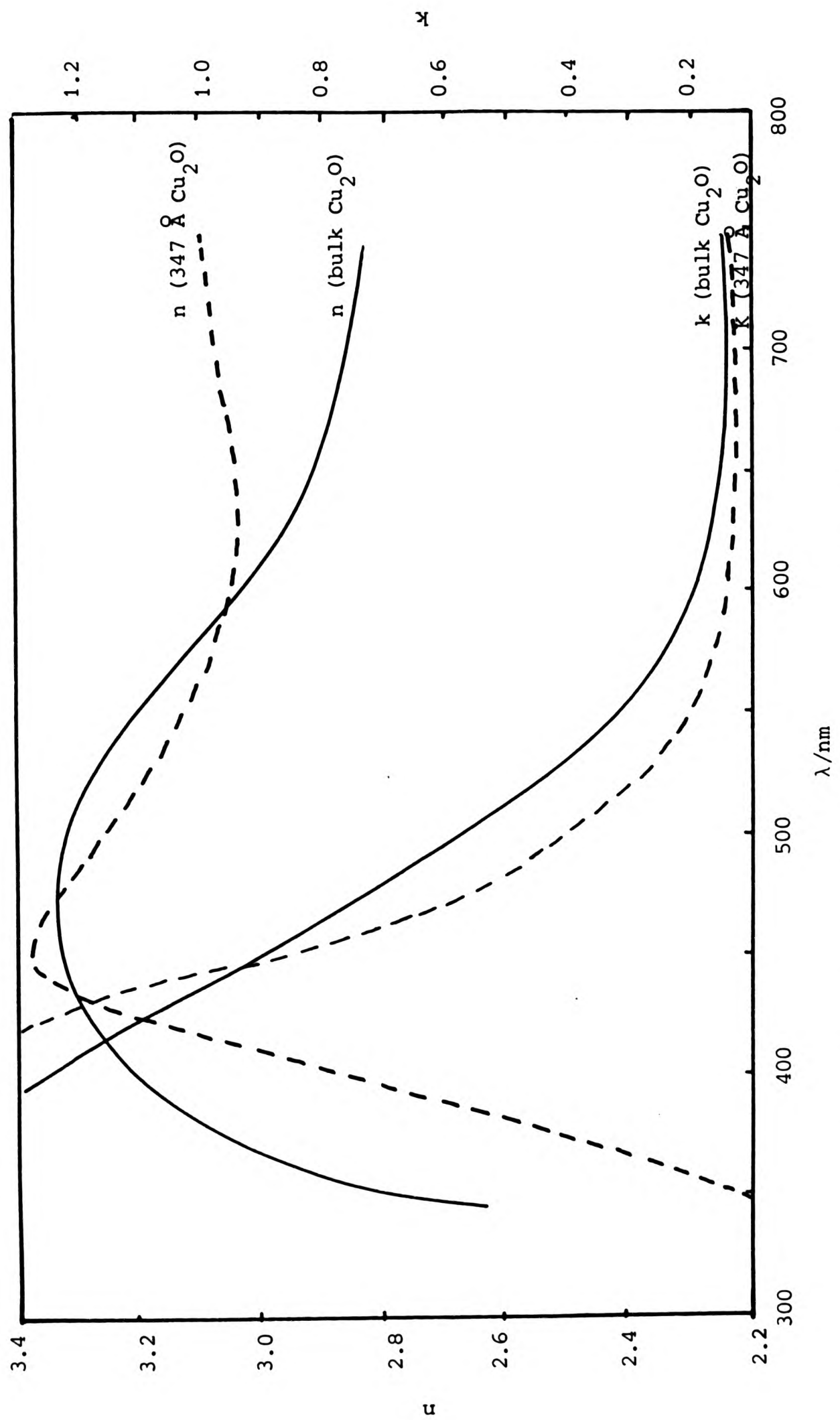
Figure 4.29. Spectral variation of n and k for a thick cuprous oxide film.
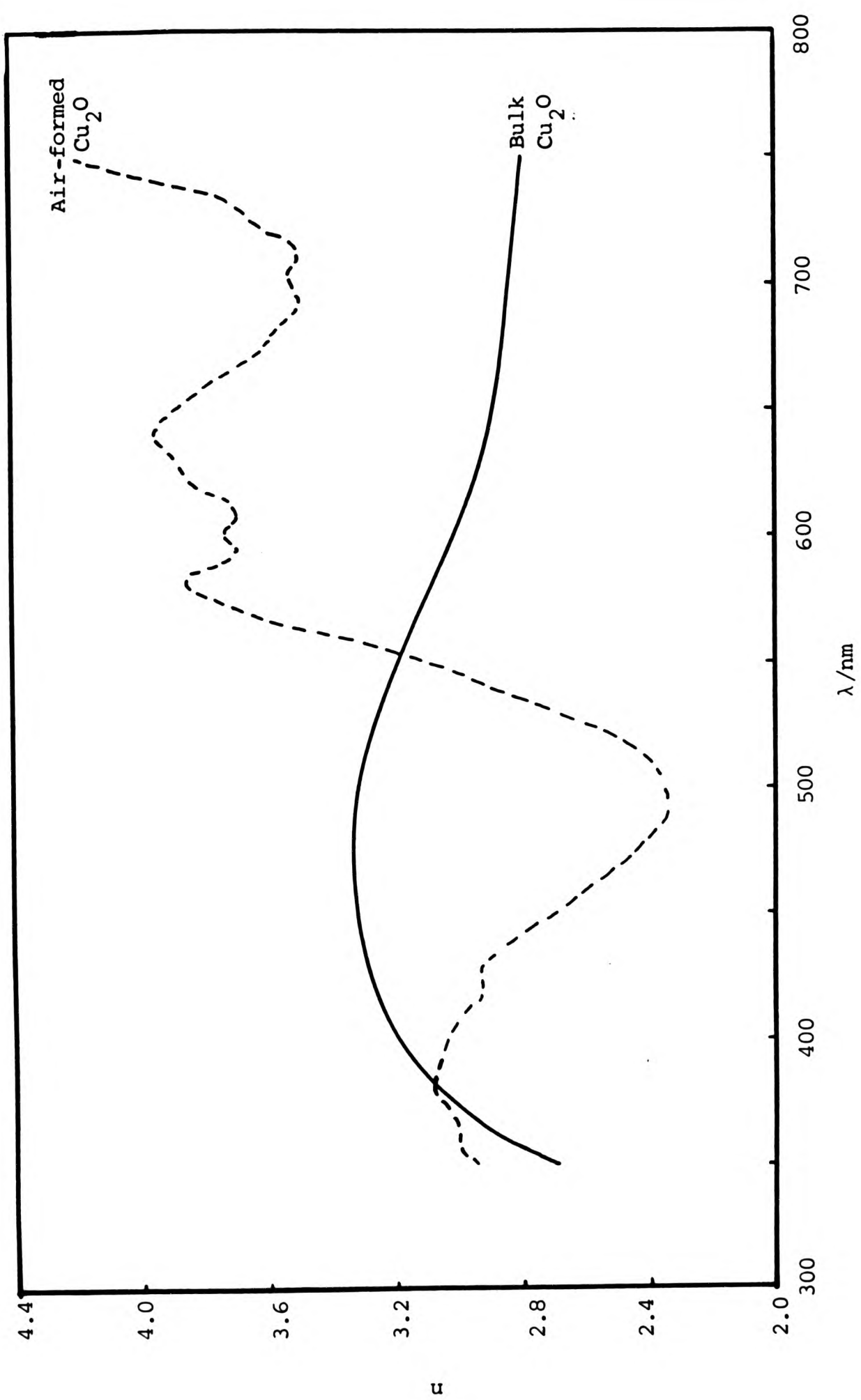
Figure 4.30. Spectral variation of n for an air formed film of cuprous oxide.
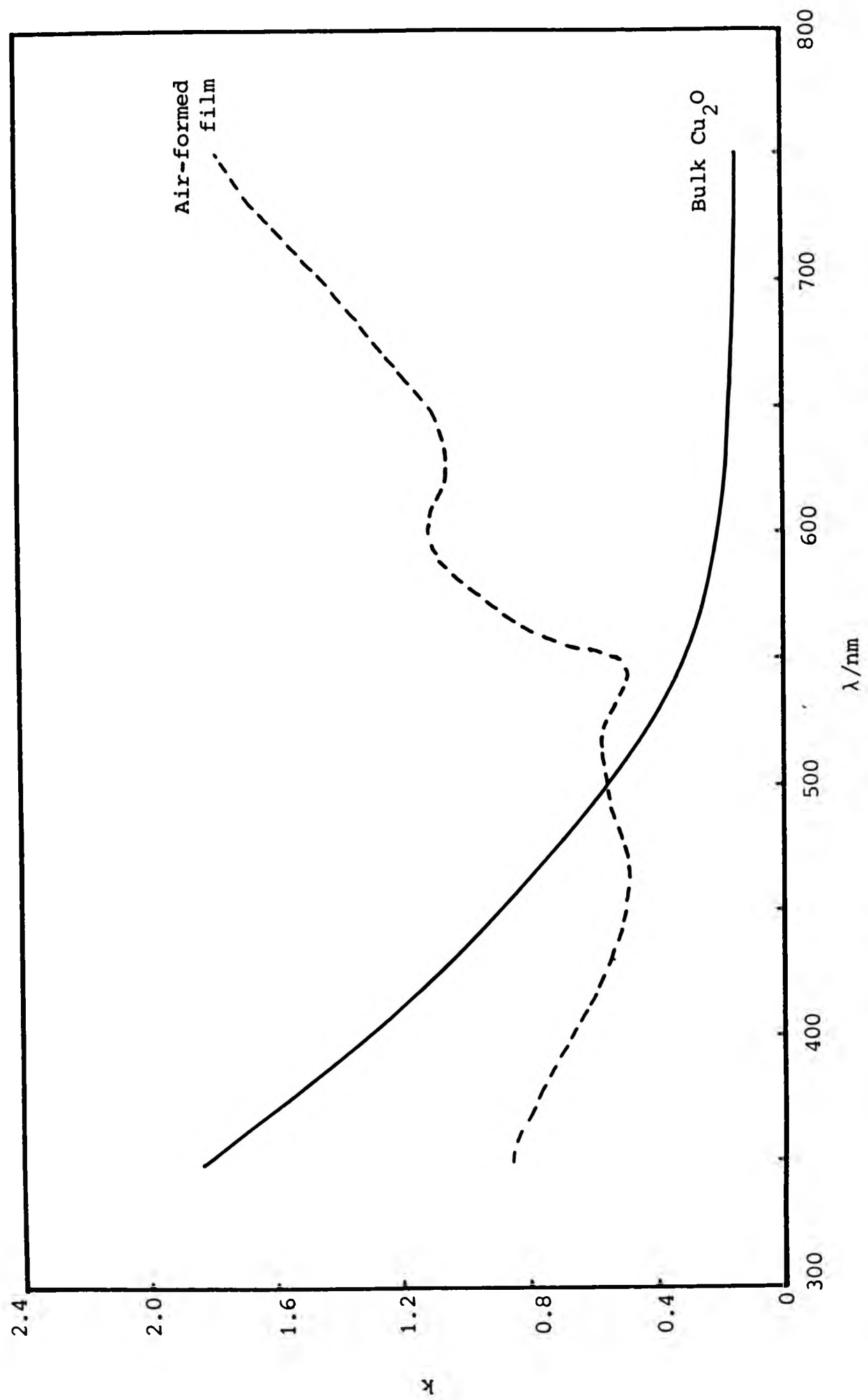
Figure 4.31. Spectral variation of k for an air-formed film of cuprous oxide.

Table 4.27

The optical constants of the glass substrate

λ/nm	n	k
350	1.53	0.03
400	1.52	0.03
450	1.52	0.02
500	1.52	0.02
550	1.51	0.02
600	1.51	0.02
650	1.51	0.02
700	1.51	0.02
750	1.50	0.02

These values compare well with those quoted for this type of glass in the literature. (104)

Using these values, the thickness and optical constants of the cuprous oxide films were computed using the iterative method described earlier. It had been hoped to produce cuprous oxide films covering a range of thicknesses up to about 500 Å by varying the time of deposition of the copper. However, the films measured were all found to be less than 150 Å thick. Details of the film thickness determinations are given in Table 4.28.

Table 4.28

Cuprous oxide films on glass

Thickness/$\overset{\circ}{A}$	Average RMS error per angle	Standard deviation/$\overset{\circ}{A}$
8.9	0.051	1
9.3	0.039	1
50.0	0.004	17
110.0	0.018	16

Values of n and k for these films were computed. Figures 4.32 and 4.33 compare the optical constants for two of these films with those of bulk cuprite.

4.4.3 The optical constants of cuprous oxide films on gold

The optical constants of the gold substrate listed in Table 4.29 were sufficiently close to those of other workers to indicate that the gold film was clean, continuous and thick enough to be treated as a bulk gold layer. (105, 106)
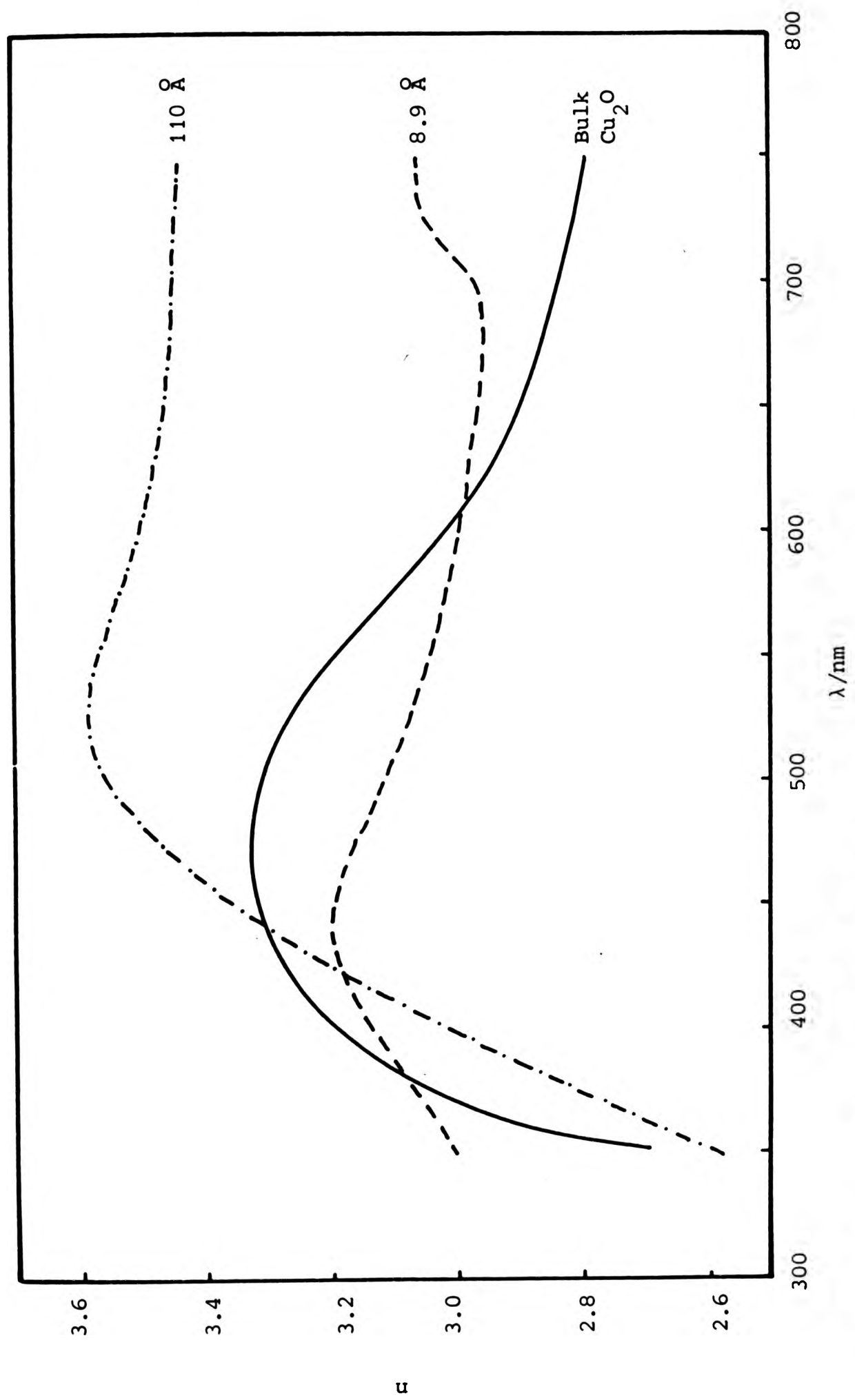
Figure 4.32. Spectral variation of n for cuprous oxide films on glass.
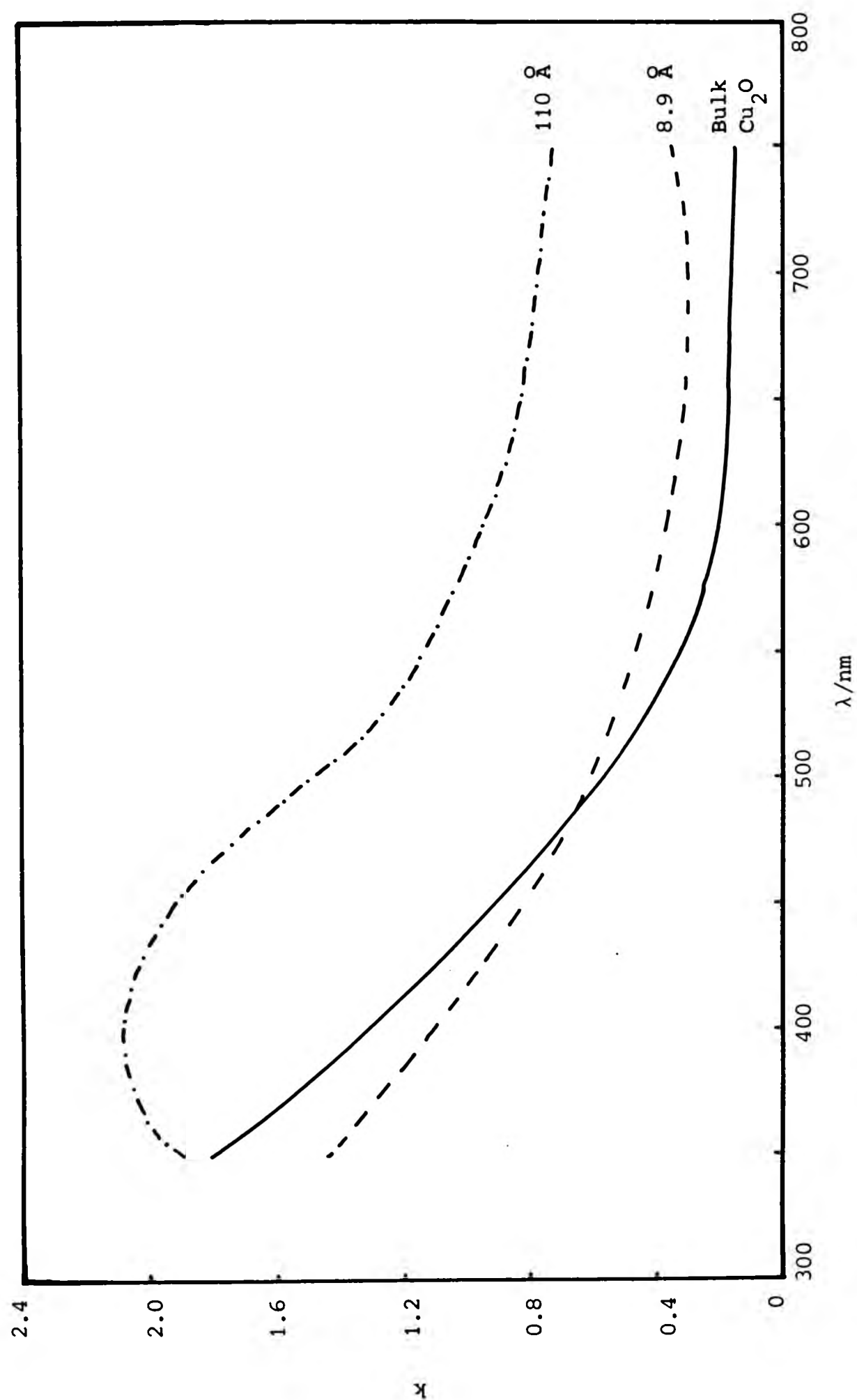
Figure 4.33 Spectral variation of k for cuprous oxide films on glass.

Table 4.29

Optical constants of gold substrate

λ/nm	n	k
350	1.64	1.67
400	1.60	1.75
450	1.52	1.73
500	1.05	1.71
550	0.68	2.32
600	0.63	2.82
650	0.64	3.25
700	0.67	3.63
750	0.72	3.97

Attempts were made to establish the oxide film thicknesses using the graphical and numerical methods described in 3.5.1 and 3.5.2 respectively and using the optical constants of gold as those of the substrate. This proved to be impossible. The possibility of diffusion between the gold and copper layers was considered and data were computed for copper/gold alloy substrates. Using these it was possible to evaluate the optical constants of the oxide films. Table 4.30 summarises the results of these calculations.

Table 4.30

Oxide films on gold/copper alloy substrates

Alloy composition /% gold	Average film thickness/Å	Average RMS error per angle	Standard deviation/Å
95	67	0.909	16
90	51	1.144	9
90	60	0.884	16

Values of n and k for these films were computed. Figures 4.34 and 4.35 compare the optical constants of one of these films with those of bulk cuprite.

4.5 Surface roughness

Figure 4.36 shows two of a series of scanning electron micrographs of an oxidised copper surface. They show a surface which is largely flat and featureless. These particular micrographs were selected because the presence of the pores illustrates the flatness of the remainder of the surface which might not otherwise be clear.

Figure 4.37 and 4.38 are transmission electron micrographs obtained from carbon replicas of a polished copper specimen and a similar specimen which had been oxidised at 80°C for 24 hours respectively. Scratches are visible on both although the profiles of the scratches are different.
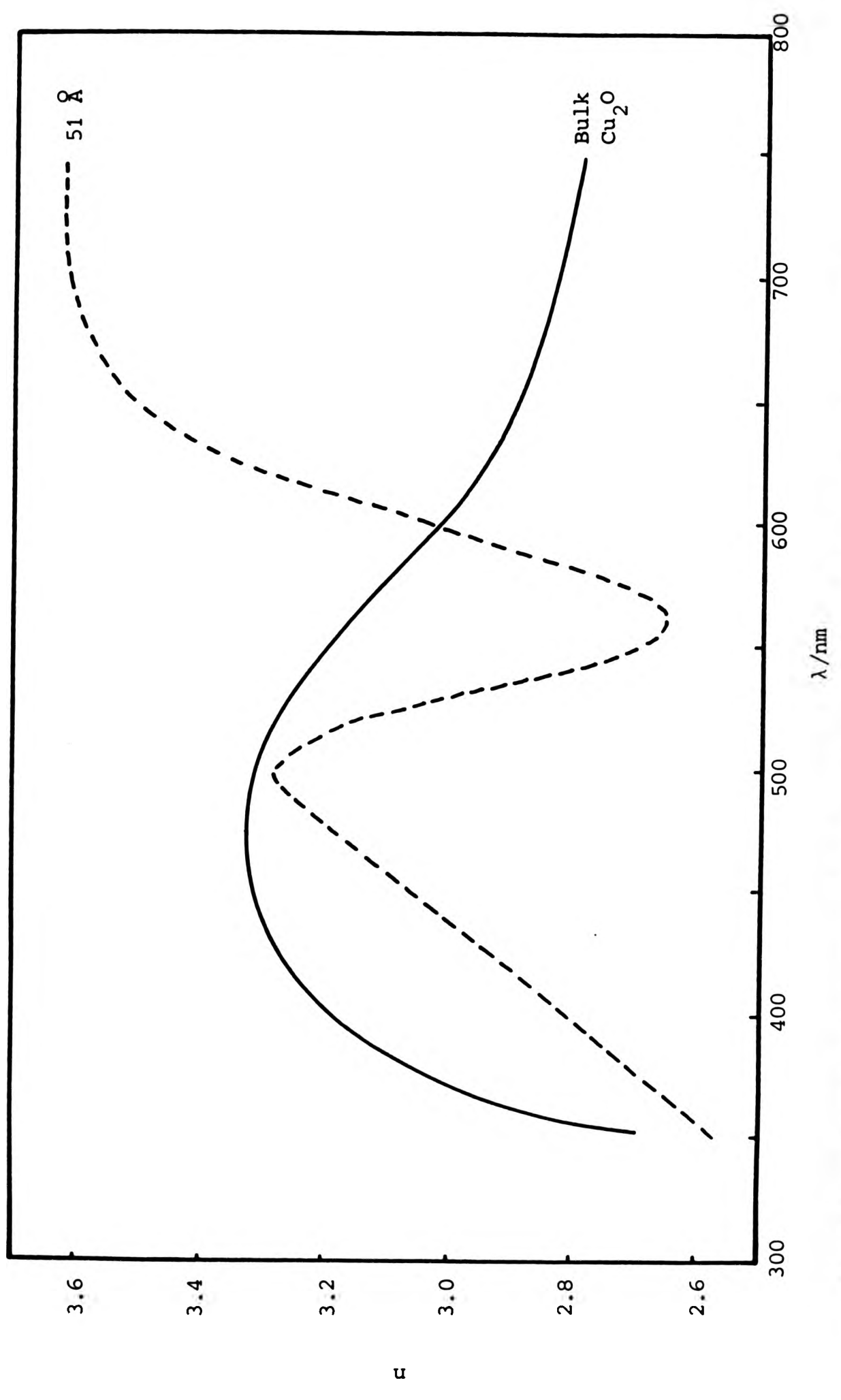
Table 4.34. Spectral variation of n for a cuprous oxide film on gold/copper alloy.
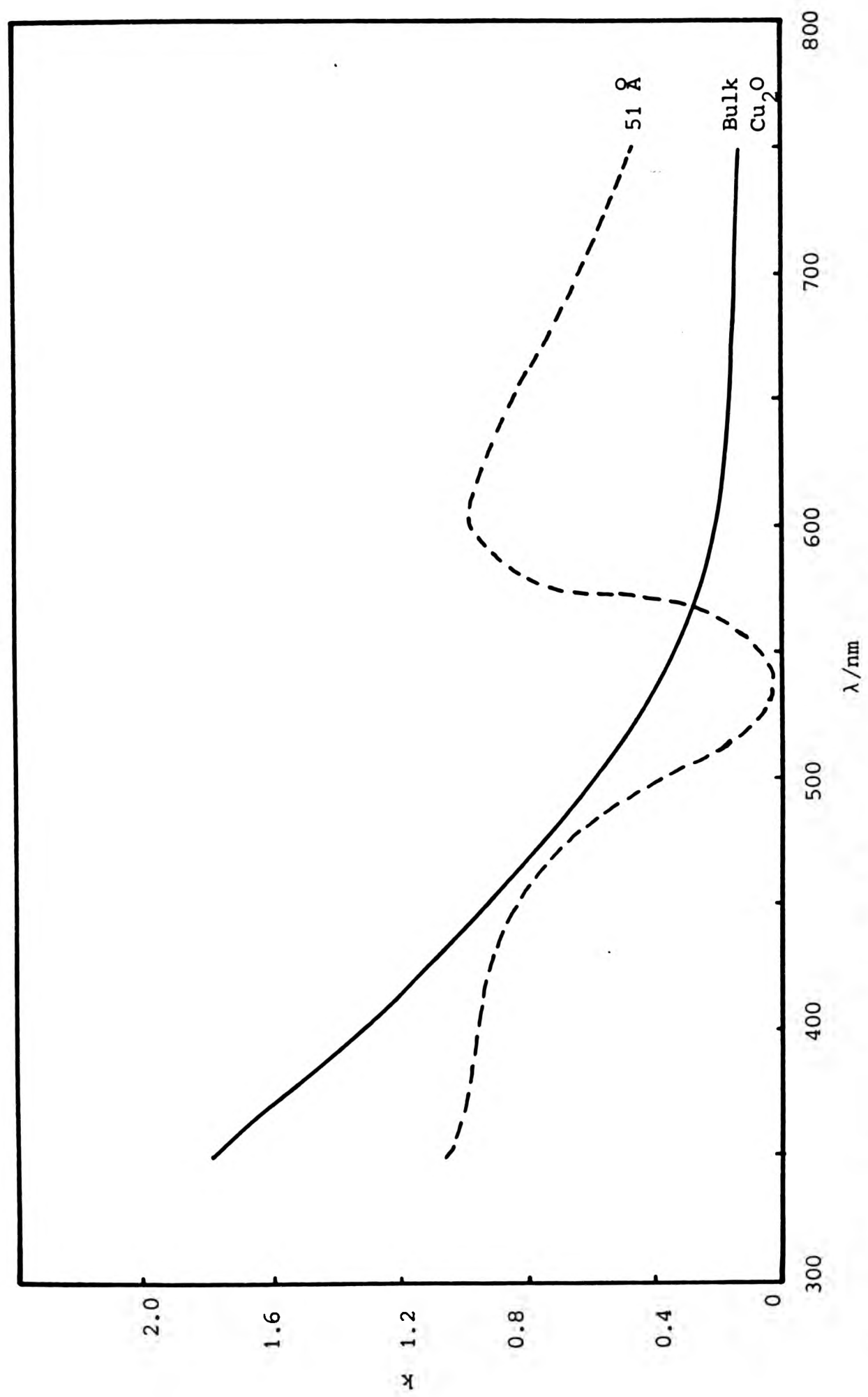
Figure 4.35   Spectral variation of k for a cuprous oxide film on gold/copper alloy.
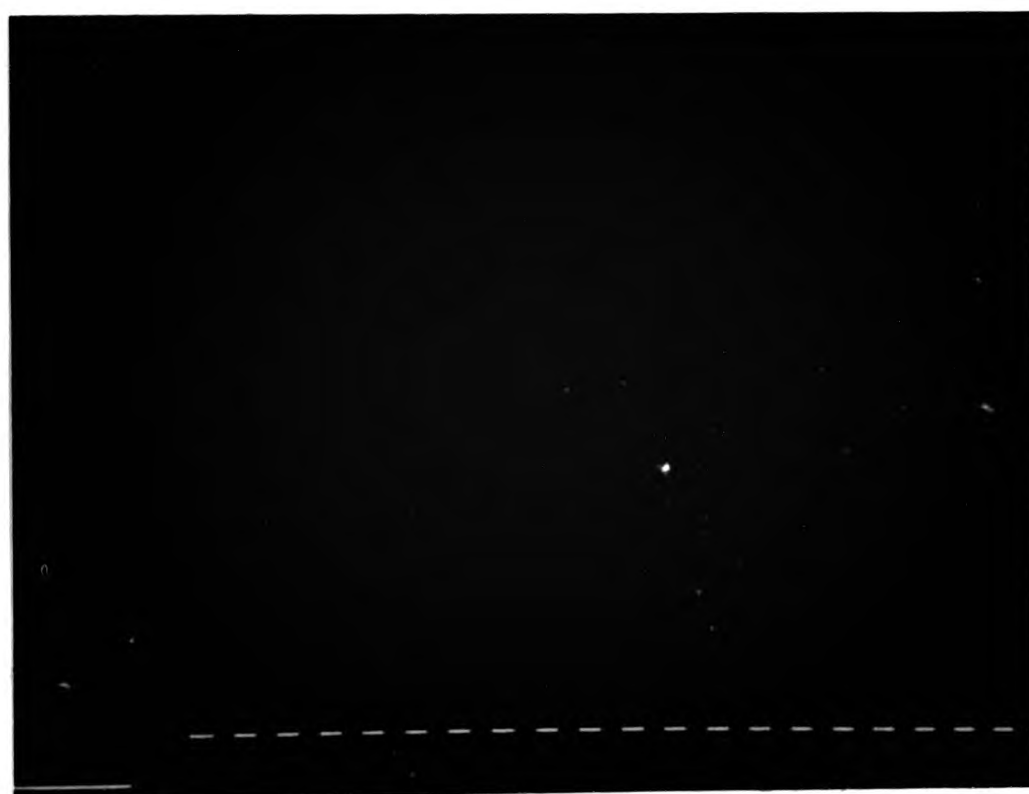
Figure 4.36   Scanning electron micrographs of an oxidised copper
specimen (x 2500).

Figure 4.36   Scanning electron micrographs of an oxidised copper
specimen (x 2500).

Figure 4.37   Transmission electron micrograph from a carbon replica of a polished copper specimen (x 28,000).

Figure 4.38   Transmission electron micrograph from a carbon replica of an oxidised polished copper specimen (x 28,000).
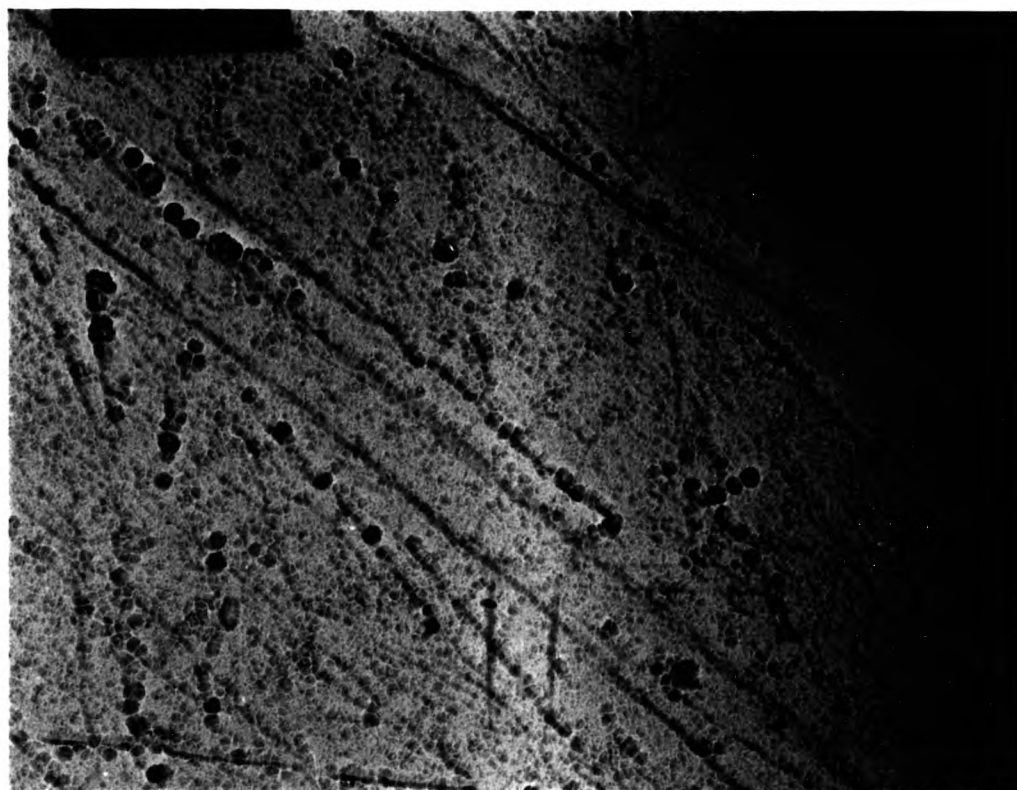
Figure 4.37   Transmission electron micrograph from a carbon replica
of a polished copper specimen (x 28,000).
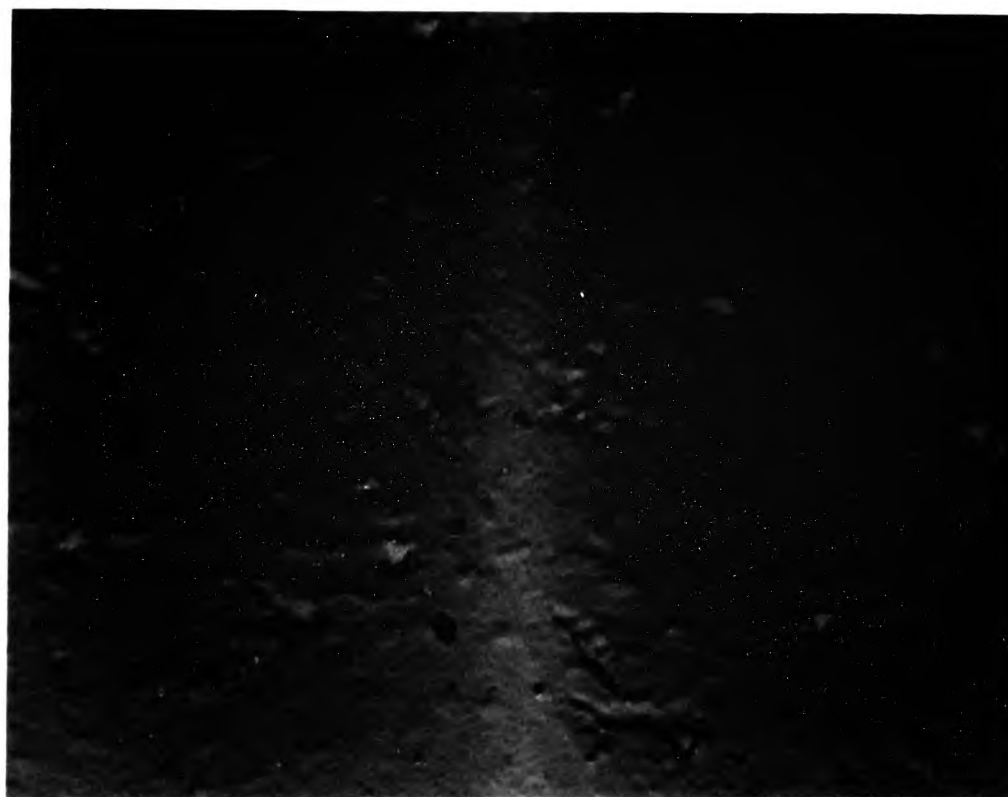
Figure 4.38   Transmission electron micrograph from a carbon replica
of an oxidised polished copper specimen (x 28,000).

5. DISCUSSION

5.1 Introduction

In preceding sections the need for flat specularly reflecting
surfaces of both metal and oxidised metal specimens has been
emphasised. Details of the techniques used to obtain them have
been described together with methods of assessing their success.
In the first part of this section the nature of the surfaces will
be examined in relation to ideal Drude conditions. This will be
followed by a discussion of the composition and thickness of the
oxide films and will consider the different values of the
thickness given by the different ways of measuring them. The
optical properties of the oxide films will be compared to those
of bulk cuprite and related to their thickness and to the presence
of the different alloying elements in the copper substrate.
Finally, the effect of different types of substrates on the
optical properties of thin films of cuprous oxide will be
considered.

5.2 The surface

To calculate optical constants from the measured ellipsometric
angles, Δ and ψ, it is necessary to know the value of the angle of
incidence (set at 75° for all these experiments). However, a
rough surface effectively changes the angle of incidence as
illustrated in Figure 5.1.

(a) $\angle i = 75°$ (b) $\angle i \neq 75°$
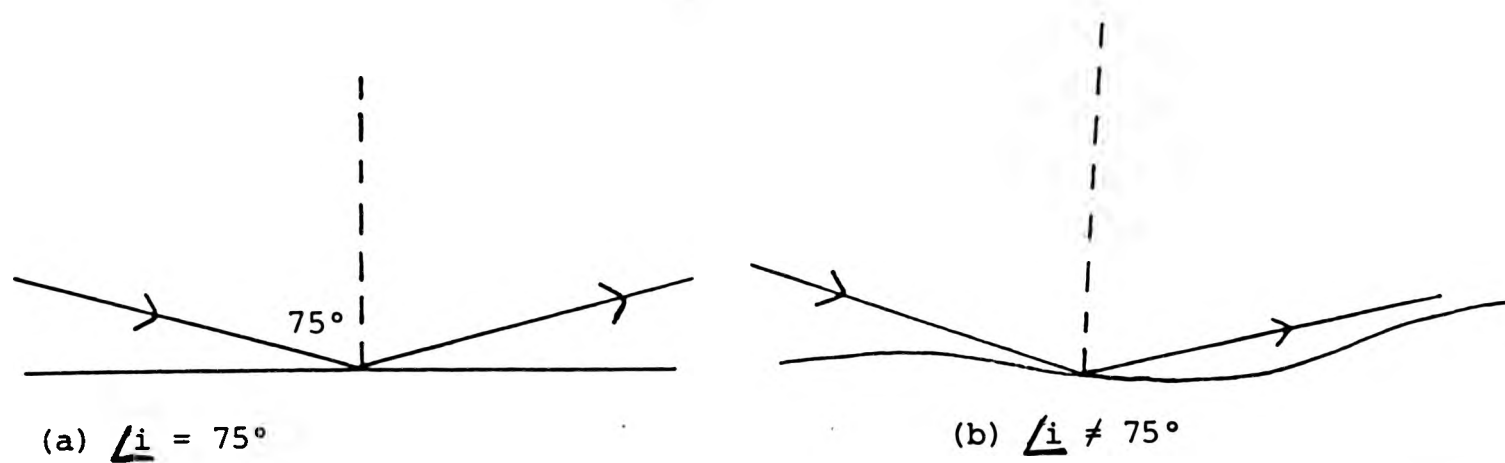
Figure 5.1 Change in angle of incidence related to surface
roughness

The extent to which ellipsometric measurements are affected
depends on the type of roughness. The light beam is narrow
(approximately 2.5 mm in diameter) and will either not be
reflected from some forms of roughness or the reflected beam
will miss the photomultiplier at the end of the reflection arm.
This is illustrated in Figure 5.2.

(a)   (b)

(c)   (d)
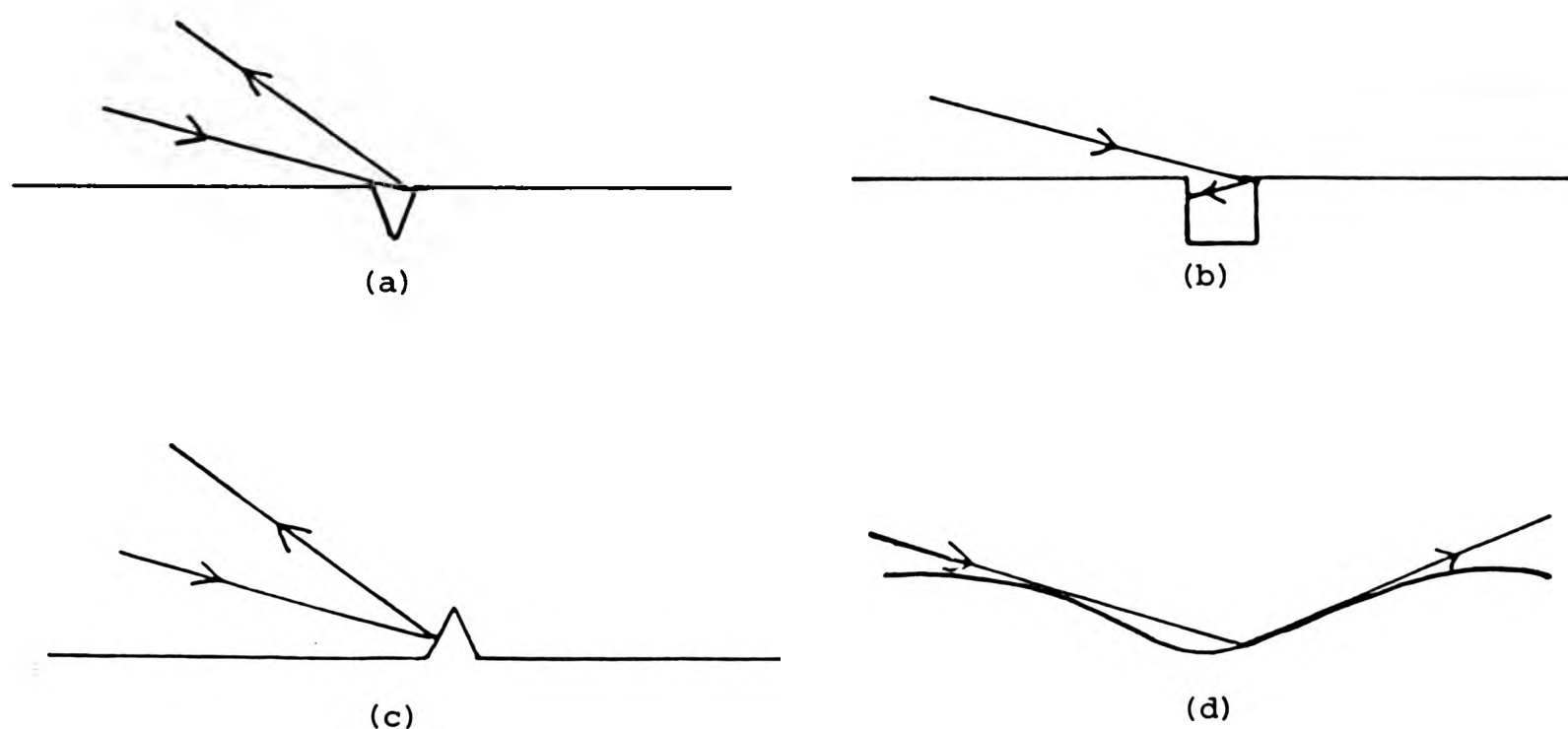
Figure 5.2 Types of surface roughness

In Figure 5.2 (a), (b) and (c) the incident beam will be reflected in such a way that it will not hit the first iris on the reflection arm. In Figure 5.2 (d) the angle of incidence changes continuously with the surface profile. If the angle of incidence on part of the surface is changed from 75° by surface roughness, a fraction of the beam will not pass normally through the optical components on the reflection arm. As it passes through the Faraday cell and the analyser prism the divergence from the normal will increase. The aperture of the irises is kept small (approximately 2 mm in diameter) so light reflected from areas of significant roughness will not reach the photomultiplier. The intensity of the beam will obviously be reduced where the surface is rough but this will not affect the measurement of the angles Δ and ψ. The scanning electron micrographs in Figure 4.36 show that there are indeed surface defects of the types illustrated in Figure 5.2 but they are only a small fraction of the surface and can therefore be regarded as insignificant. A transmission electron micrograph (Figure 4.38) from a replica of an oxidised copper surface shows smoothing of the scratches which will lead to the type of roughness depicted in Figure 5.2 (d). The oxide film on the specimen from which the replica was made was about 50 $\overset{o}{A}$ thick and appears to be continuous. Thus although the surface is obviously not "perfectly smooth" it is clearly sufficiently smooth for ellipsometric measurements to be made with confidence.

5.3 The composition of the oxide film

Films consisting of cuprous oxide only were required for this
work and oxidising conditions were carefully investigated and
controlled to provide them. The extent to which they were
successful has been assessed by coulometric reduction and
transmission electron microscopy.

5.3.1 Coulometric assessment of the oxide film

Coulometric reduction of the oxide film produced potential/time
curves which consisted of a single plateau indicating the
presence of one oxide only. The potential at which it was
reduced ($\sim$ -600 mV $_{(SCE)}$) is consistent with a film of cuprous
oxide (107). Although this reduction potential was reached in a
short space of time there is the slight possibility of there
being a very thin film of cupric oxide which is reduced at a
higher potential during this period. Assuming a maximum of 90
seconds before the cuprous oxide reduction potential is reached,
a density of 6.4 gcm^{-3} for cupric oxide (29) and a current of
20 $\mu A\, cm^{-2}$, such a film would have a thickness of 15 $\overset{o}{A}$.

5.3.2 Identification of the oxide by transmission electron
microscopy

Tables 5.1, 5.2 and 5.3 list the lattice parameters of copper,
cuprous oxide and cupric oxide respectively.

Table 5.1

The lattice parameters of copper (108)

d/Å	I/I_1	hkl
2.088	100	(111)
1.808	46	(200)
1.278	20	(220)
1.090	17	(311)
1.044	5	(222)

Table 5.2

The lattice parameters of cuprous oxide (108)

d/Å	I/I_1	hkl
3.020	9	(110)
2.465	100	(111)
2.135	37	(200)
1.743	1	(211)
1.510	27	(220)
1.287	17	(311)
1.233	4	(322)

Table 5.3

The lattice parameters of cupric oxide (108)

d/Å	I/I_1	hkl
2.751	12	(110)
2.530	49	(002)
2.523	100	($\bar{1}$11)
2.323	96	(111)
2.312	30	(200)
1.959	3	($\bar{1}$12)
1.866	25	(202)
1.788	2	(112)
1.714	8	(020)
1.581	14	(202)
1.505	20	($\bar{1}$13)
1.418	12	(022)
1.410	15	(311)(310)

In Tables 5.4 and 5.5 the lattice parameters of a copper foil and an oxidised copper foil respectively are related to the data listed in Tables 5.1, 5.2 and 5.3.

Table 5.4

Assignment of the lattice parameters measured from a copper foil

	d-spacings		hkl	
measured/Å	literature values/Å		(108)	
2.44	2.465		Cu_2O	(111)
2.09	2.088		Cu	(111)
1.81	1.808		Cu	(200)
1.51	1.510		Cu_2O	(220)
1.27	1.278		Cu	(220)
1.08	1.090		Cu	(311)
1.04	1.044		Cu	(222)

Table 5.5

Assignment of the lattice parameters measured from an oxidised copper foil

d-spacings		hkl	
measured/Å	literature values/Å	(108)	
3.07	3.020	Cu_2O	(110)
2.48	2.465	Cu_2O	(111)
2.12	2.088	Cu	(111)
1.81	1.808	Cu	(200)
1.53	1.510	Cu_2O	(220)
1.29	1.287	Cu_2O	(311)
1.27	1.278	Cu_2O	(220)

Stable air - formed films of cuprous oxide, which had developed over a period of several days, were found to have a thickness of about 25 Å (Section 4.3.1). The air - formed oxide film on the freshly prepared copper foil was probably rather thinner than this but was clearly revealed in the electron diffraction pattern obtained from the foil. After oxidation for 24 hours at 80°C the foil would be expected to bear an oxide film about 80 Å thick (Table 4.12). There is no evidence for the existence of any cupric oxide. Diffraction rings arising from the CuO ($\bar{1}$11) and (111) planes, with d-spacings of 2.523 and 2.323 Å respectively, would be the most intense (Table 5.3) and would have diameters of 1.52 and 1.65 cm respectively. Although

Table 5.5

Assignment of the lattice parameters measured from an oxidised copper foil

| d-spacings | | hkl | |
measured/Å	literature values/Å	(108)	
3.07	3.020	Cu_2O	(110)
2.48	2.465	Cu_2O	(111)
2.12	2.088	Cu	(111)
1.81	1.808	Cu	(200)
1.53	1.510	Cu_2O	(220)
1.29	1.287	Cu_2O	(311)
1.27	1.278	Cu_2O	(220)

Stable air - formed films of cuprous oxide, which had developed over a period of several days, were found to have a thickness of about 25 Å (Section 4.3.1). The air - formed oxide film on the freshly prepared copper foil was probably rather thinner than this but was clearly revealed in the electron diffraction pattern obtained from the foil. After oxidation for 24 hours at 80°C the foil would be expected to bear an oxide film about 80 Å thick (Table 4.12). There is no evidence for the existence of any cupric oxide. Diffraction rings arising from the CuO ($\bar{1}$11) and (111) planes, with d-spacings of 2.523 and 2.323 Å respectively, would be the most intense (Table 5.3) and would have diameters of 1.52 and 1.65 cm respectively. Although

there is a ring with a diameter of 1.56 cm arising from the Cu_2O (111) plane it is unlikely that it would mask both these others. Since a very thin film of cuprous oxide was identified on the copper foil it would be reasonable to expect to be able to detect a similarly small proportion of cupric oxide in a film of cuprous oxide. As none was detected it may be assumed that no cupric oxide is present in the oxide films produced on copper at 80°C.

5.4 The thickness of the oxide films

5.4.1 Interference colours of the oxide films

Interference colours arise from the diffraction of incident light by oxide films of varying thickness. Attempts have been made to correlate particular colours with film thicknesses established by coulometric or gravimetric analysis. Table 5.6 lists film thicknesses and the corresponding interference colours found by Campbell and Thomas (109).

Table 5.6

The interference colours of oxide films on copper

Thickness/$\overset{\circ}{A}$	Colour
180	darkened
270	light rose
300	deep rose
395	light blue
730	yellow I
990	orange II

A problem in using the listed interference colours to measure film thickness is the subjective assessment of colour. Table 4.10 lists the colours exhibited by specimens of copper and the dilute copper alloys after varying periods of oxidation at 80°C. Tables 5.7 and 5.8 correlate these oxidation times with the thickness of the films using the information in Table 5.6.

Table 5.7

Interference colours and thickness of oxide films on copper

Oxidation time /hours	Colour	Thickness/$\overset{\circ}{A}$
24	darkened	< 180
48	slight bronze	
72	bronze	
96	"	
120	"	
144	"	180
168	bronze - magenta	270

Table 5.8

Interference colours and thickness of oxide films on dilute copper alloys

Oxidation time /hours	Colour	Thickness/$\overset{\circ}{A}$
24	darkened	< 180
48	bronze	180
72	bronze - magenta	270
96	"	
120	magenta - bronze	
144	magenta	300
168	magenta - blue	< 395

Although these are very rough estimates of thickness, there is closer agreement between them and the ellipsometric estimates than those derived coulometrically.

5.4.2 Coulometric determination of oxide film thickness

There are considerable differences between the estimates of the film thickness obtained by coulometry and ellipsometry. Plots of coulometric versus ellipsometric values show a linear relationship between them. Inspection of these results and comparison with the interference colour estimates suggests that there is an overestimate in the coulometric values. By assuming that the ellipsometric result is a true value, the quantity of

Table 5.8

Interference colours and thickness of oxide films on dilute copper alloys

Oxidation time /hours	Colour	Thickness/$\overset{\circ}{A}$
24	darkened	< 180
48	bronze	180
72	bronze - magenta	270
96	"	
120	magenta - bronze	
144	magenta	300
168	magenta - blue	< 395

Although these are very rough estimates of thickness, there is closer agreement between them and the ellipsometric estimates than those derived coulometrically.

5.4.2 Coulometric determination of oxide film thickness

There are considerable differences between the estimates of the film thickness obtained by coulometry and ellipsometry. Plots of coulometric versus ellipsometric values show a linear relationship between them. Inspection of these results and comparison with the interference colour estimates suggests that there is an overestimate in the coulometric values. By assuming that the ellipsometric result is a true value, the quantity of

Table 5.8

Interference colours and thickness of oxide films on dilute copper alloys

Oxidation time /hours	Colour	Thickness/$\overset{\circ}{A}$
24	darkened	< 180
48	bronze	180
72	bronze - magenta	270
96	"	
120	magenta - bronze	
144	magenta	300
168	magenta - blue	< 395

Although these are very rough estimates of thickness, there is closer agreement between them and the ellipsometric estimates than those derived coulometrically.

5.4.2 Coulometric determination of oxide film thickness

There are considerable differences between the estimates of the film thickness obtained by coulometry and ellipsometry. Plots of coulometric versus ellipsometric values show a linear relationship between them. Inspection of these results and comparison with the interference colour estimates suggests that there is an overestimate in the coulometric values. By assuming that the ellipsometric result is a true value, the quantity of

electricity used to reduce the film, Q_e, can be calculated using Faraday's Laws. If Q_t is the total quantity of electricity given by $Q_t = I \times t$, where I is the current in Amps and t is the reduction time in seconds, (Tables 4.12 - 4.15), the quantity $(Q_t - Q_e)$ is found to increase with time for similar values of I. A more valid comparison can be made by calculating what the reduction time would have been for a constant current of 40 µA in each case. Table 5.9 lists data calculated in this way from Tables 4.12 - 4.15.

Table 5.9

Quantities of electricity and times for reduction of oxide
films calculated from Tables 4.12 - 4.15

$I/\mu A$	$t/$ secs	$t(I=40\mu A)$ /secs	d_c /Å	d_e /Å	$Q_t/\mu C$	$Q_e/\mu C$	$(Q_t - Q_e)/\mu C$
18.00	120	54	18.5	26	2160	3036	876
39.25	390	383	85	41	15320	7390	7930
39.73	705	700	155	51	18000	9213	18787
39.38	810	793	176	71	31720	12796	33360
39.42	1200	1183	261	77	47320	13960	33360
15.00	2240	830	310	90	33600	9755	23845
39.77	1675	1665	376	110	66600	19484	47116
70.52	1171	2064	457	140	82560	25292	57268
18.33	172	79	27	26	3160	3043	117
39.35	720	708	112	63	28320	15930	12390
39.37	570	561	124	71	22440	12849	9591
39.72	1110	1102	233	94	44080	17783	26297
38.74	780	755	290	117	30200	12184	18016
18.00	226	102	35	29	4080	3381	699
39.24	510	500	110	54	20000	9818	10182
39.47	900	888	231	84	35520	12916	22604
40.34	990	998	241	130	39920	21534	18386
70.45	630	1110	292	213	44400	32388	12012
70.58	870	1535	870	370	61400	26113	35287

Table 5.9 contd.

I/μA	t/ secs	t(I=40μA) /secs	d_c /Å	d_e /Å	Q_t/μC	Q_e/μC	$(Q_t - Q_e)$/μC
20.00	140	70	27	22	2800	2281	519
39.36	450	443	100	40	17720	7088	10632
39.25	930	913	206	97	36520	17196	19324
39.39	1500	1477	333	173	59080	30693	28387

Figure 5.3 relates the charge difference $(Q_t - Q_e)$ for reduction of the two different film thicknesses (coulometric and ellipsometric) to time. The linear relationship suggests that part of the charge is being used for a reaction other than reduction of the oxide film. The most likely reaction would be the reduction of oxygen not completely removed by deaeration of the system with white-spot nitrogen. The oxygen reduction reaction is:-

$$O_2 + 4H_2O + 4e = 4OH^-$$
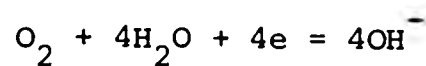
Using a typical coulometric reduction result from Table 4.12, a current of 39.77 μA reduced the oxide film in 1675 seconds. The film thickness calculated by Faraday's Law is 376 Å but the ellipsometric estimate was only 110 Å. The total charge passed was 39.77 x 1675 = 66615 μ Coulombs while the charge required to reduce a film of 110 Å would be $\frac{66615 \times 110}{376}$ = 19500 μ Coulombs, leaving 47115 μ Coulombs for the reduction of oxygen. Using Faraday's Law this charge would reduce 3.9 x 10^{-6} g oxygen which
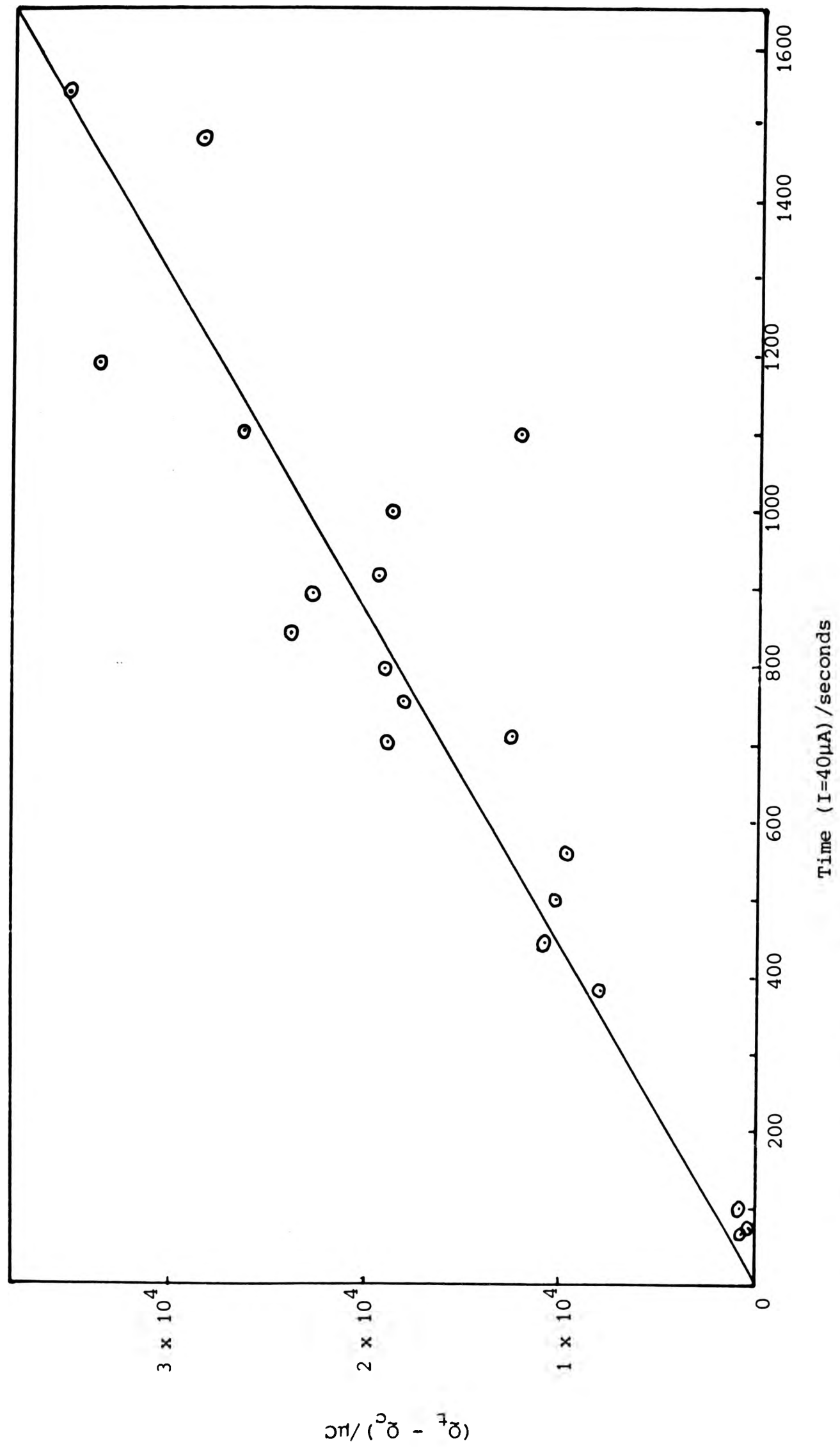
Figure 5.3 Plot of charge difference against reduction time

is equivalent to less than 0.01 ppm of oxygen in the solution.
Since the nitrogen used for deaeration contains 1-5 ppm oxygen
it is unlikely that this problem can be eliminated without
redesigning the equipment and using high purity gases. When
thicker oxide films over larger surface areas are reduced the
effect of such small quantities of oxygen becomes less
significant.

5.4.3 Ellipsometric estimates of film thickness

Unless a reasonable estimate of thickness can be included in
the data used to compute film thicknesses it is possible for
false values to be generated (Section 2.4.2). It was for this
reason that coulometry was used in an attempt to obtain an
independent measurement. However, there are good reasons
(detailed in the previous section) for suspecting that the values
found in this way are over-estimates. Nevertheless, they
provided the "initial guess" required for the KCNEP1 program
(Appendix 3). The iterative use of the program described in
Section 3.6 was found to give the same final thickness even when
quite different starting values were selected provided they were
within an order of magnitude of the true value (Appendix 3,
Table A7).

When plots of Δ and ψ for oxidised specimens were compared with
computed values for copper overlaid with layers of cuprous oxide
(Figures 4.2 and 4.25) it was found that the thickness value
generated by the computer program was consistent with the relative
positions of the experimentally and theoretically derived curves
over a considerable part of the wavelength spectrum examined.

Indeed, these thickness values were used as "initial guesses" for the KCNEP1 program when coulometric values were not available.

The agreement between ellipsometric values and those suggested by interference colours has already been discussed (5.4.1). Furthermore there is good agreement between oxidation rates calculated using ellipsometric results and those compiled by other workers. These will be examined more closely in the next section. Thus, the higher coulometrically derived thicknesses can be discounted.

5.4.4 Oxidation rates

The thermal oxidation of copper is well documented for a wide range of temperatures and oxidising conditions. Low temperature studies have been carried out by several workers including Rhodin (49), Young et al (51) and Pinnel et al (110). They all established parabolic growth kinetics of the type, $y^n = kt$. Pinnel et al (110) found that this relationship applies over the temperature range 50 to 150°C with n = 2 at 150°C, n $\cong$ 2.5 at 100°C and n > 3 between 50 and 75°C. They found that the data could be represented by a single equation, $(y - c)^2 = kt$, where c $\cong$ 10 $\overset{o}{A}$ over the range of temperatures and times which they used. They also found that impurities in the atmosphere could increase the oxidation rate by up to a factor of 8. In Figure 5.4 the ellipsometric values of the thickness of the oxide films on copper from Table 4.12 were used as Pinnel et al (110) suggested. A straight line is obtained although there is less agreement for the oxide films on the alloys as shown in Figures 5.5 - 5.7.
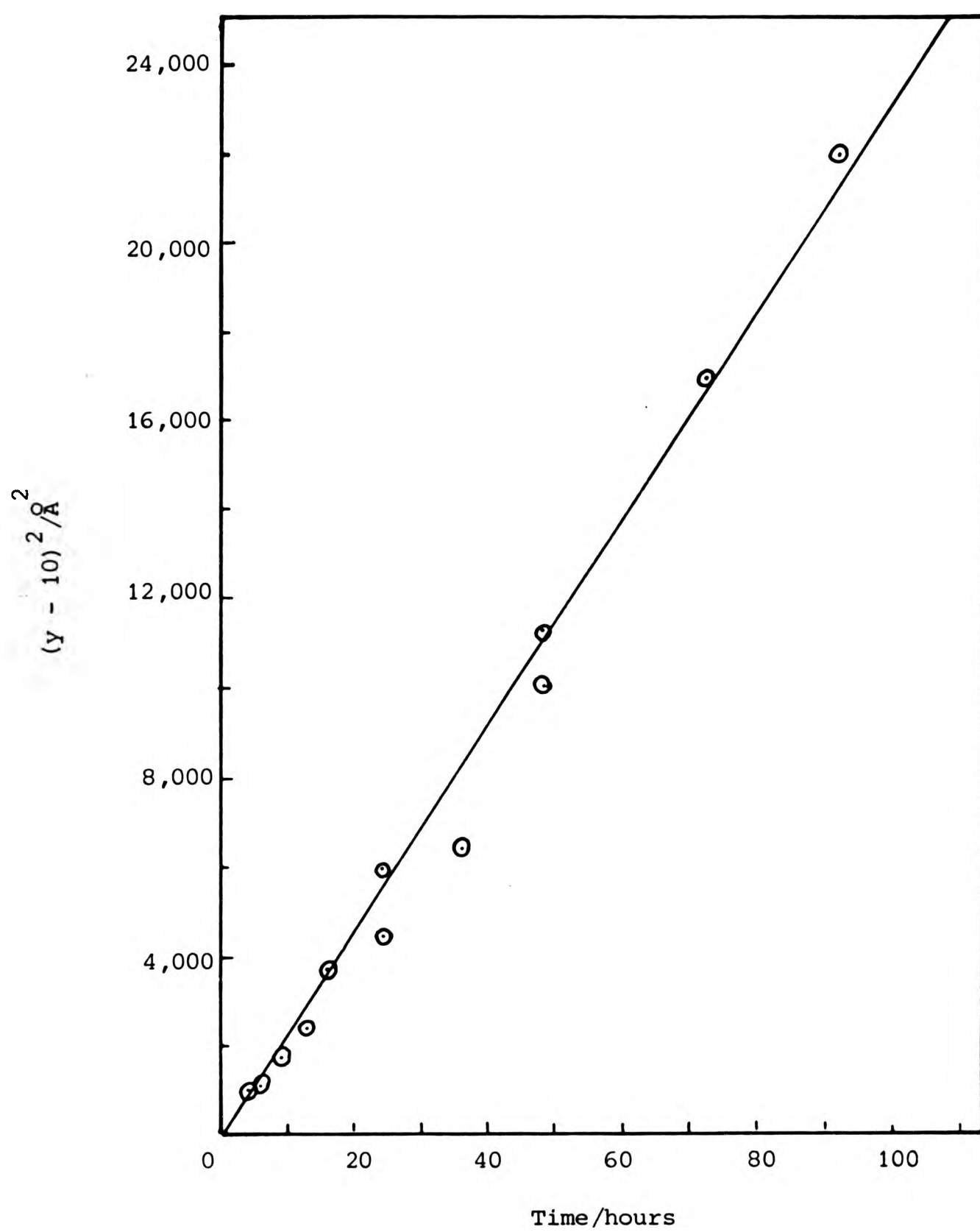
Figure 5.4 Oxidation of copper
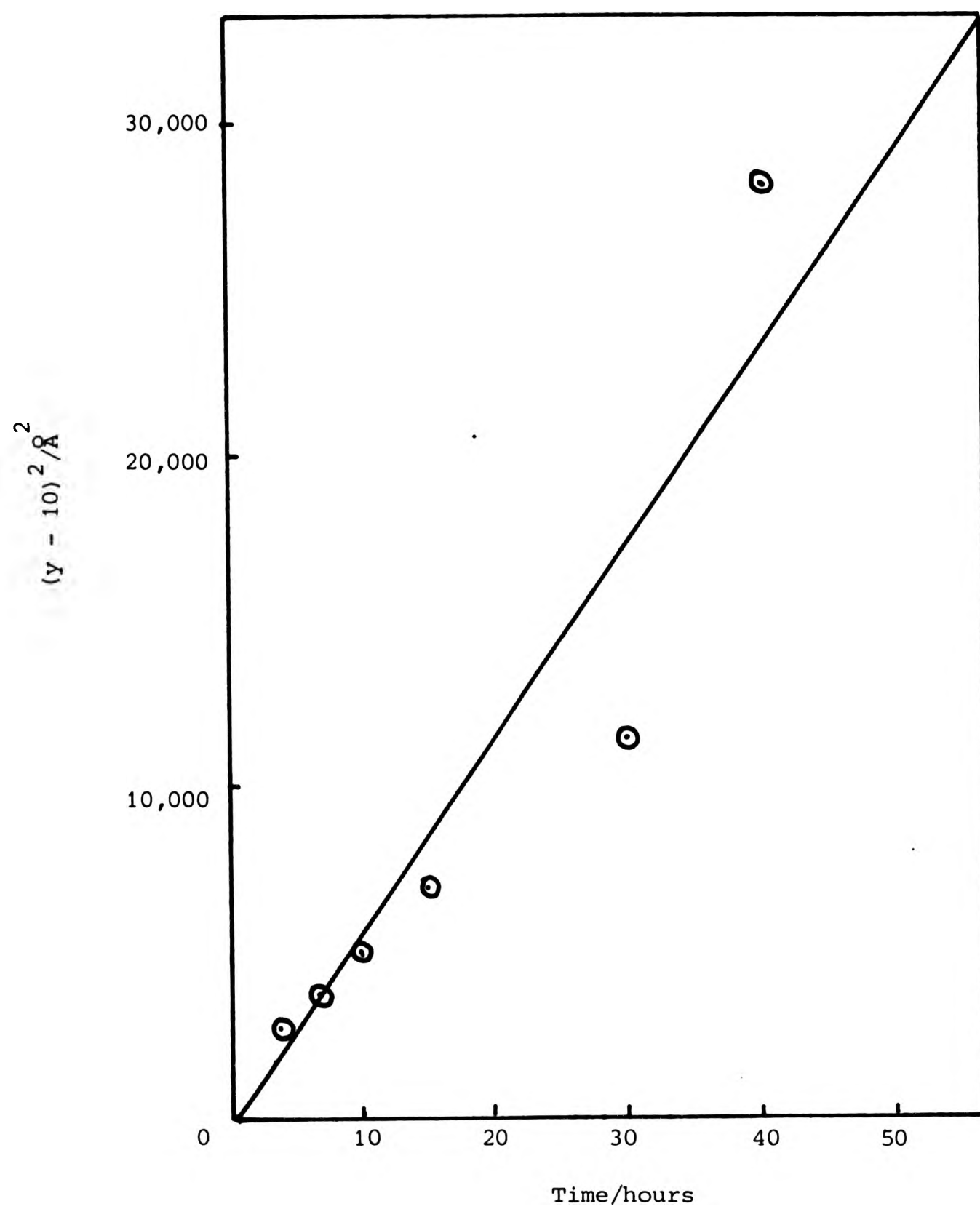
Figure 5.5 Oxidation of copper/gallium alloy
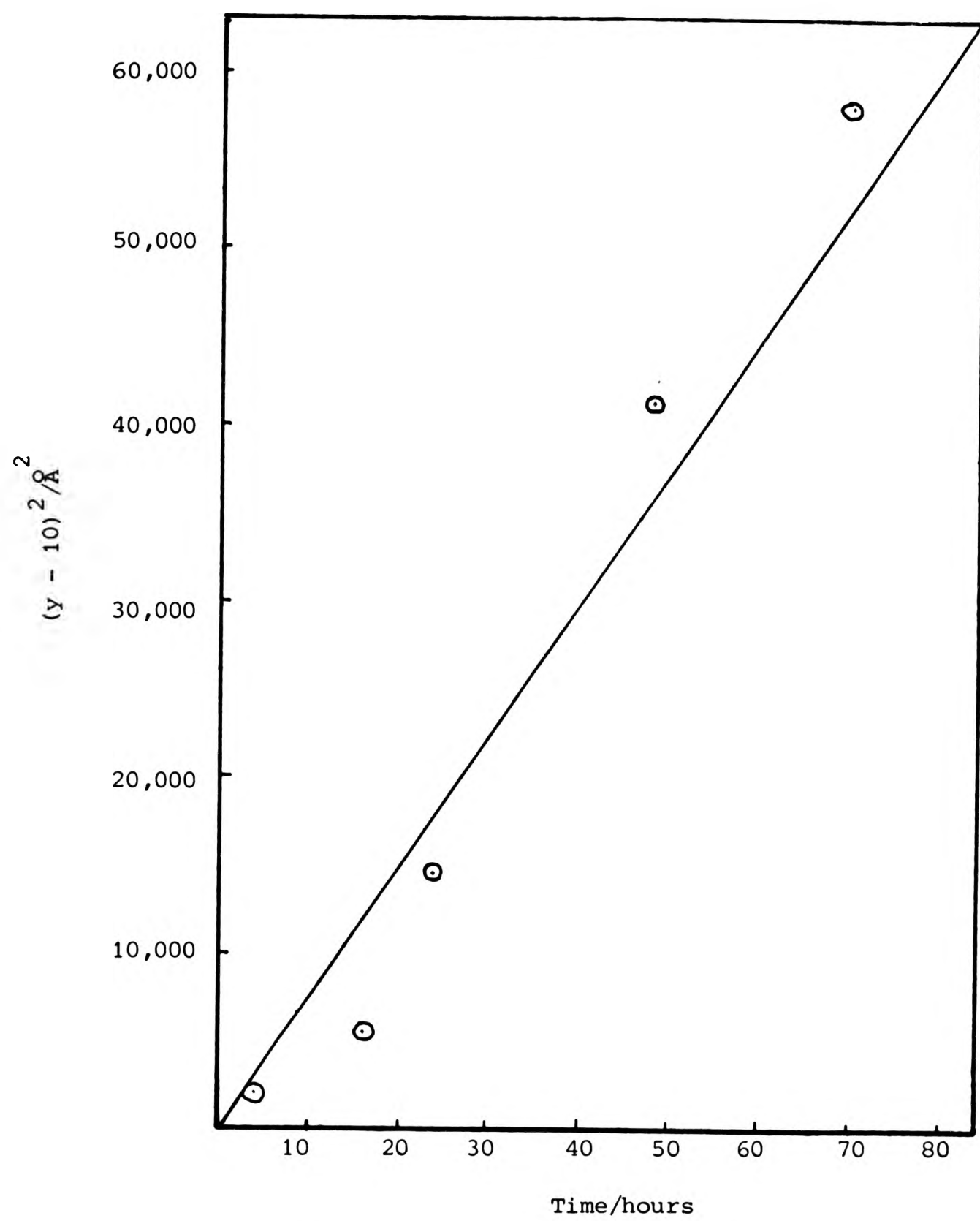
Figure 5.6   Oxidation of copper/germanium alloy
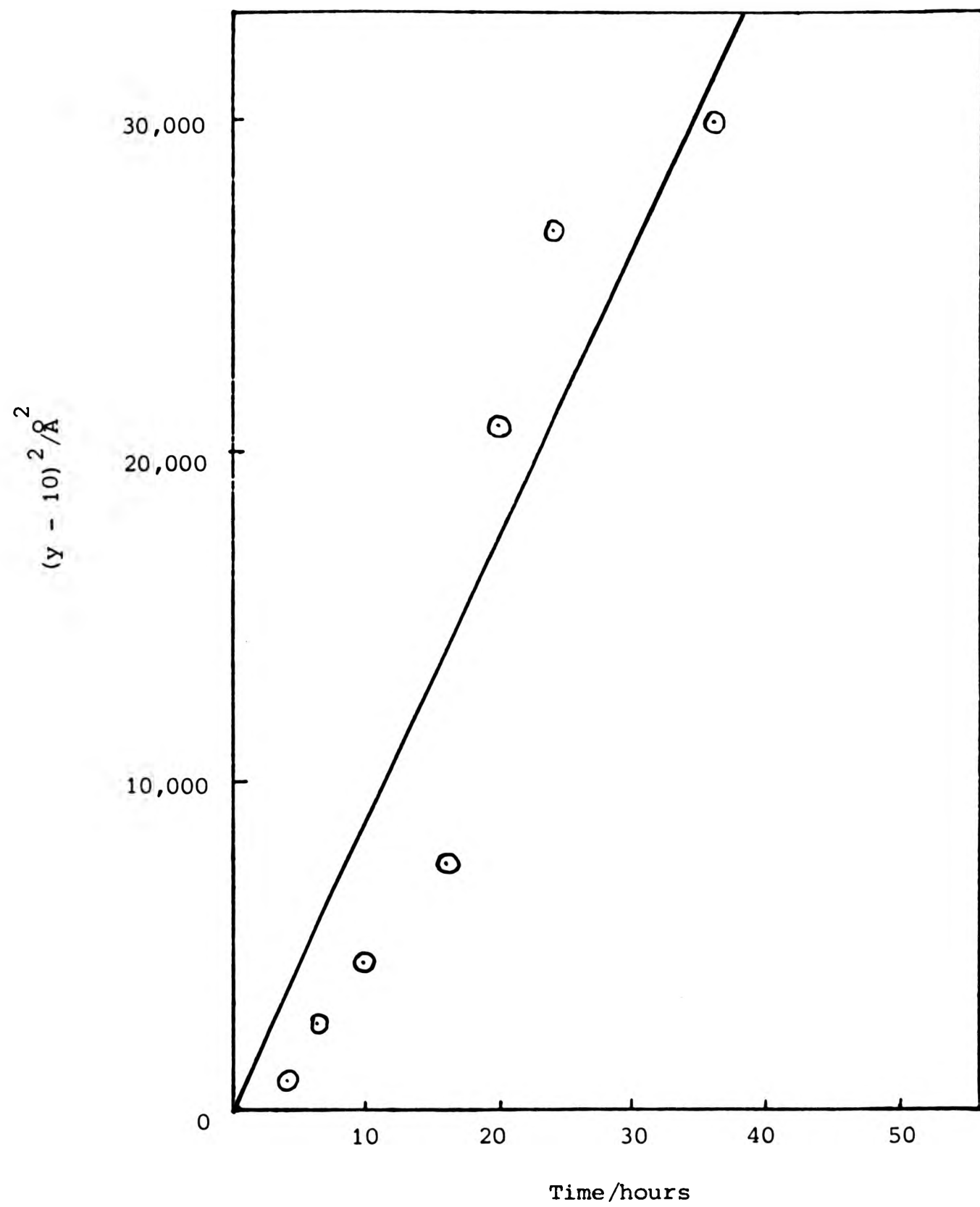
Figure 5.7 Oxidation of copper/nickel alloy

5.4.5 Summary of oxidation data

The evidence obtained by transmission microscopy and coulometry indicate the presence of cuprous oxide films. The film thicknesses obtained by ellipsometry fit the oxidation laws suggested by Pinnel et al (110) and it would appear that the higher values of thickness given by coulometry should be adjusted to compensate for current loss. Interference colours, though only useful as crude indicators of thickness, also confirm the ellipsometric values.

5.5 The optical properties of the oxide films on copper based alloys

5.5.1 Introduction

The MNEMON computer program written by Clarke (96), processes data and gives optical properties in terms of the complex dielectric function, $\bar{\varepsilon} = \varepsilon_1 + i\varepsilon_2$, or the optical constants n and k. n and k are related to ε_1 and ε_2 by the simple relationships $\varepsilon_1 = (n^2 - k^2)$ and $\varepsilon_2 = 2nk$. Reflectance, Rn, may also be calculated and, being a function of both n and k, is often a more convenient quantity to use for comparing the cumulative variation in n and k. Kappa, κ, also relates n and k by the relationship $\kappa = k/n$.

The chromaticity colour coordinates of the oxide films were calculated using the CIE 1931 system. This involves computing the reflectivity of the surface at enough wavelengths in the visible spectrum to accurately define the spectral reflectance curve. This curve is then combined with physiological data on the "average" human eye (the CIE 1931 Standard Observer), and

data on the spectral distribution of the illumination of particular interest. The illumination used for the results in this work was the CIE Standard Illuminant C. The X and Y coordinates of a colour fix its location on the CIE chromaticity chart (Figure 5.8).

5.5.2 The optical constants of the copper and copper alloy substrates

The optical constants of copper measured by Smith (24) were used as substrate values for calculating the optical properties and thickness of all the oxide films. Attempts to measure the true optical constants of copper by in situ ellipsometry of cathodically polarised specimens were not successful. The values of n_s and k_s obtained in this way were not greatly different from the literature values especially at shorter wavelengths (Figures 4.3 and 4.4). However, when they were used to compute oxide film data, the KCNEP1 program could not match substrate and filmed system data or produced nonsensical values of n_f, k_f and film thickness.

Cathodic polarisation of copper at -690 mV$_{(SCE)}$ is known to result in oxide free surfaces (111, 112) but it also produces diffusion layers within the electrolyte which are often visible to the naked eye and which must therefore have refractive indices different from that of the bulk electrolyte. Stedman (113) found significant changes in the optical parameters Δ and ψ which were attributable to the electrical double layer. These changes could be modelled as an increase in the refractive index of a 6 $\overset{o}{A}$ layer of the electrolyte; a change in the surface of the electrode
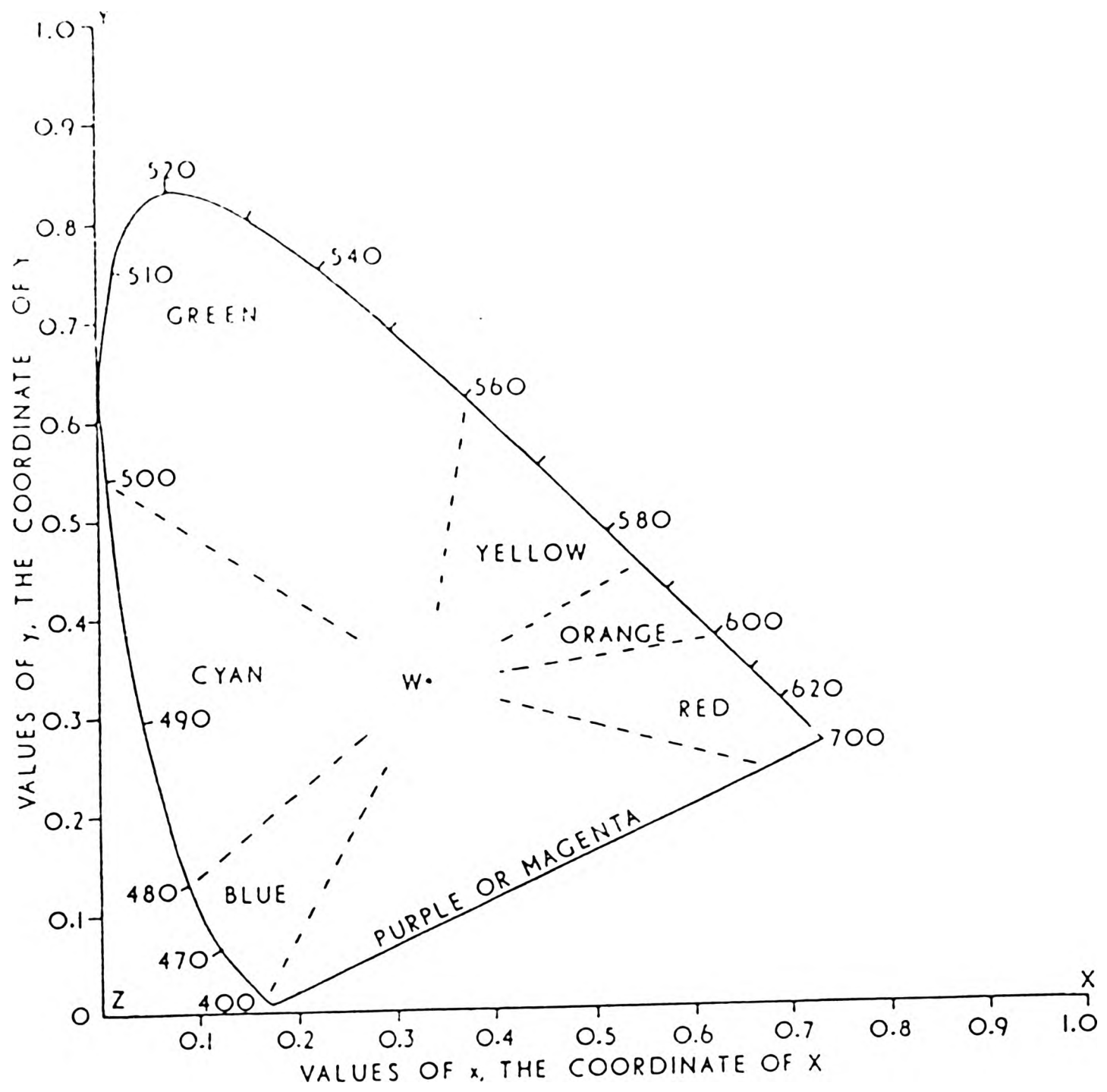
Figure 5.8   The CIE colour coordinate system (illuminant C)

and the presence of an adsorbed layer of ions. Since the refractive index of the medium must be known in order to calculate the optical constants of the metal, the existence of such a double layer will account for the differences between the measured optical constants and their true values.

A further problem arises with the dilute alloys. Cathodic polarisation would not necessarily produce the required oxide free alloy surfaces. The resulting surface could be pure copper or enriched alloy depending on the relative electrochemical behaviour of the copper and the alloying additions.

The pseudo-optical constants of copper and the alloys freshly polished, but still with a thin air-formed oxide film were found to have very similar values (Figures 4.3, 4.4 and 4.6). Anodic polarisation curves indicated that the oxide films on the alloys were of similar thickness to those on a copper substrate (Figure 4.9). Clarke (96) measured the optical constants of various solid solution binary alloys and found that there were slight differences when the minority element exceeded 1%. The alloys used in these experiments contained 0.5 at/o alloying additions and it is therefore assumed that the true constants of the alloys will be very similar to those of copper and so the optical constants of copper (24) have been used as substrate values throughout.

5.5.3 The optical constants of the oxide films

Since there were only slight differences between the calculated

optical constants of the oxide films on copper and those on

the copper alloys, the first part of this section will

concentrate on the similarities. Differences will be discussed

in a later section.

The spectral variation of n for bulk cuprite shows a maximum

at about 470 nm (Figure 4.26). This has been assigned to the

3d $\rightarrow$ 4s interband transitions (114). In the thin films this

peak is displaced to shorter wavelengths indicating a higher

energy requirement for this transition.

Rastall (57) investigated the effect of polish damage on the

optical properties of cuprite and found that a highly defective

lattice structure, such as that associated with thin films,

tends to initiate interband transitions at lower energies.

Thus it would appear that a different effect is manifested here.

In a thicker film (Figure 4.29) the maximum in n_f is closer to

that of the bulk material. At longer wavelengths the values of

n_f are considerably higher than those of cuprite. They start

to increase from minima which occur between about 500 nm, for

a film 51 $\overset{o}{A}$ thick, and about 550 nm for a film 158 $\overset{o}{A}$ thick.

Since the absorption edge for copper starts at about 540 nm it

is probable that these higher values of n_f are attributable to the

substrate.

The spectral distribution of k for bulk cuprite follows a smooth

curve and has a value close to zero at the red end of the
spectrum. The oxide films all have higher k_f values in this
region which are probably the result of the presence of the
metal substrate underlying a very thin, nearly transparent
film of oxide (this hypothesis will be examined later). Thin
films of thicknesses up to about 200 Å, show minima at about 515
nm and maxima between 580 and 610 nm.

A comparison of the reflectance of oxidised specimens with
theoretical values computed for copper overlaid with cuprite of
comparable thicknesses (Figures 5.9 and 5.10) shows an overall
similarity in the shape of the curves but with distinct broadening
of the region in which reflectance changes rapidly with wavelength.
The classical interference peak at about 600 nm for a theoretical
film of 200 Å is broadened and displaced to a shorter wavelength
in the experimental system. Again the effect of the substrate
is clearly dominant and is more significant with thin, probably
defective films of cuprite than with thin films of bulk cuprite.

Combining n and k values by the relationship $\kappa = k/n$ and
plotting log κ against the wavelength, λ, makes it possible to
compare the spectral variation of κ for bulk cuprite, copper and
the oxide films. Figure 5.11 shows the spectral distribution of
κ for copper, cuprite and four oxide films ranging in thickness
from 26 to 158 Å. The spectra of the two thinnest films show
marked similarities in shape to that of copper although the
numerical values of κ are closer to those of cuprite. Similar
trends are seen with the oxide films on all the alloy substrates

curve and has a value close to zero at the red end of the
spectrum. The oxide films all have higher k_f values in this
region which are probably the result of the presence of the
metal substrate underlying a very thin, nearly transparent
film of oxide (this hypothesis will be examined later). Thin
films of thicknesses up to about 200 Å, show minima at about 515
nm and maxima between 580 and 610 nm.

A comparison of the reflectance of oxidised specimens with
theoretical values computed for copper overlaid with cuprite of
comparable thicknesses (Figures 5.9 and 5.10) shows an overall
similarity in the shape of the curves but with distinct broadening
of the region in which reflectance changes rapidly with wavelength.
The classical interference peak at about 600 nm for a theoretical
film of 200 Å is broadened and displaced to a shorter wavelength
in the experimental system. Again the effect of the substrate
is clearly dominant and is more significant with thin, probably
defective films of cuprite than with thin films of bulk cuprite.

Combining n and k values by the relationship $\kappa = k/n$ and
plotting $\log \kappa$ against the wavelength, λ, makes it possible to
compare the spectral variation of κ for bulk cuprite, copper and
the oxide films. Figure 5.11 shows the spectral distribution of
κ for copper, cuprite and four oxide films ranging in thickness
from 26 to 158 Å. The spectra of the two thinnest films show
marked similarities in shape to that of copper although the
numerical values of κ are closer to those of cuprite. Similar
trends are seen with the oxide films on all the alloy substrates
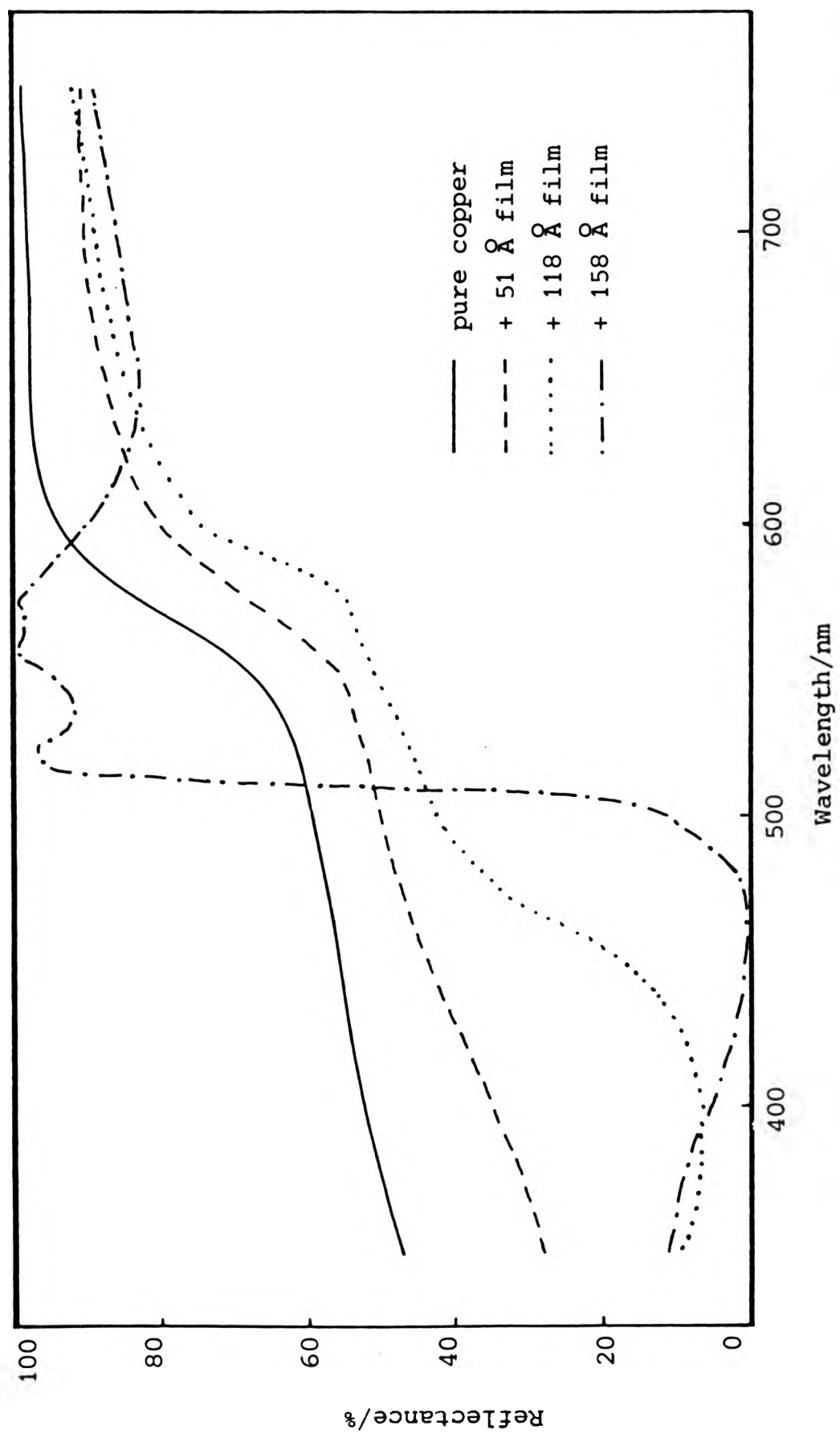
Figure 5.9   The experimental spectral reflectance of oxidised copper specimens bearing films of varying thickness.
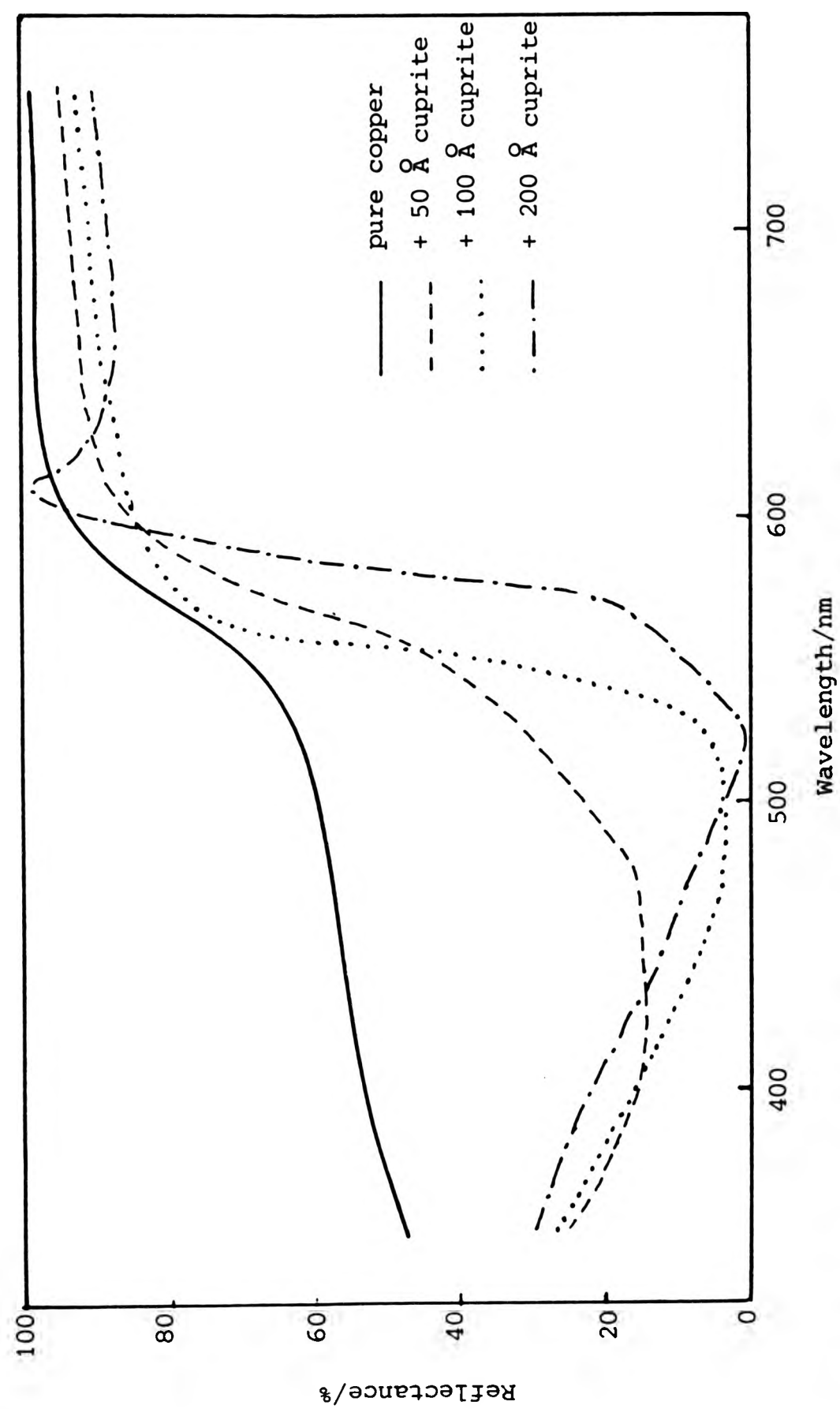
Figure 5.10 Computed spectral reflectance of copper bearing films of cuprous oxide
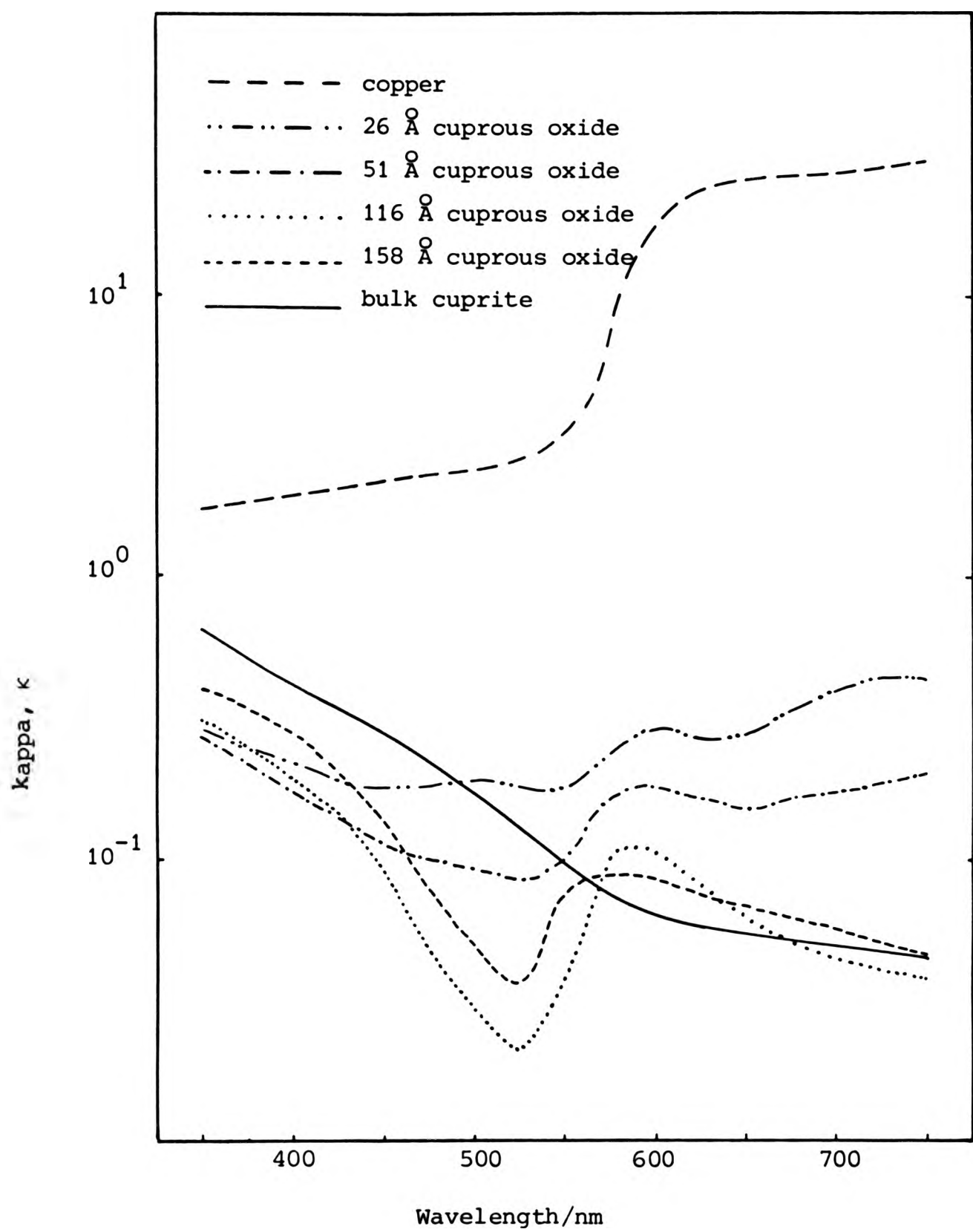
Figure 5.11   The spectral variation of log kappa for cuprous oxide
films.

(Figures 5.12 to 5.14). When values of κ for thicker films are plotted (Figures 5.12 and 5.13) they are found to lie closer to the bulk cuprite spectrum although they still exhibit minima at about 525 nm. Only in the immediate vicinity of the maximum at 580 nm are the values of κ found to occur in order of thickness. It is clear from Figures 5.11 to 5.14 that the optical constants of very thin films of cuprous oxide on copper or 99.5 at/o copper alloy are appreciably affected by the substrate and that the effect of the substrate diminishes with the thickness of the film. A possible explanation of this phenomenon will be developed later.

5.5.4 The colours of the oxide films

Chemical oxidation of copper and the dilute copper alloys in Mattsson's solution (102) resulted in the formation of oxide films which, though loose and powdery and therefore of no use for ellipsometric studies, showed interesting variations in colour (Figure 4.10). The blue crystallites result from the aqueous environment and are of no significance. The colour of the thermally oxidised specimens has already been noted but these colours were caused by interference effects depending on the thickness of the film rather than the true colour of the oxide. The true (i.e. non-interference) CIE colour coordinates of the oxide films on copper and dilute alloy substrates were computed and were found to vary with the thickness of the film (Figures 5.15 - 5.17). Insufficient data were available for the oxide films on the copper/germanium alloy for it to be possible to plot the corresponding graph for this substrate. For film thicknesses of 50 to 200 $\overset{o}{A}$ there is a linear dependence
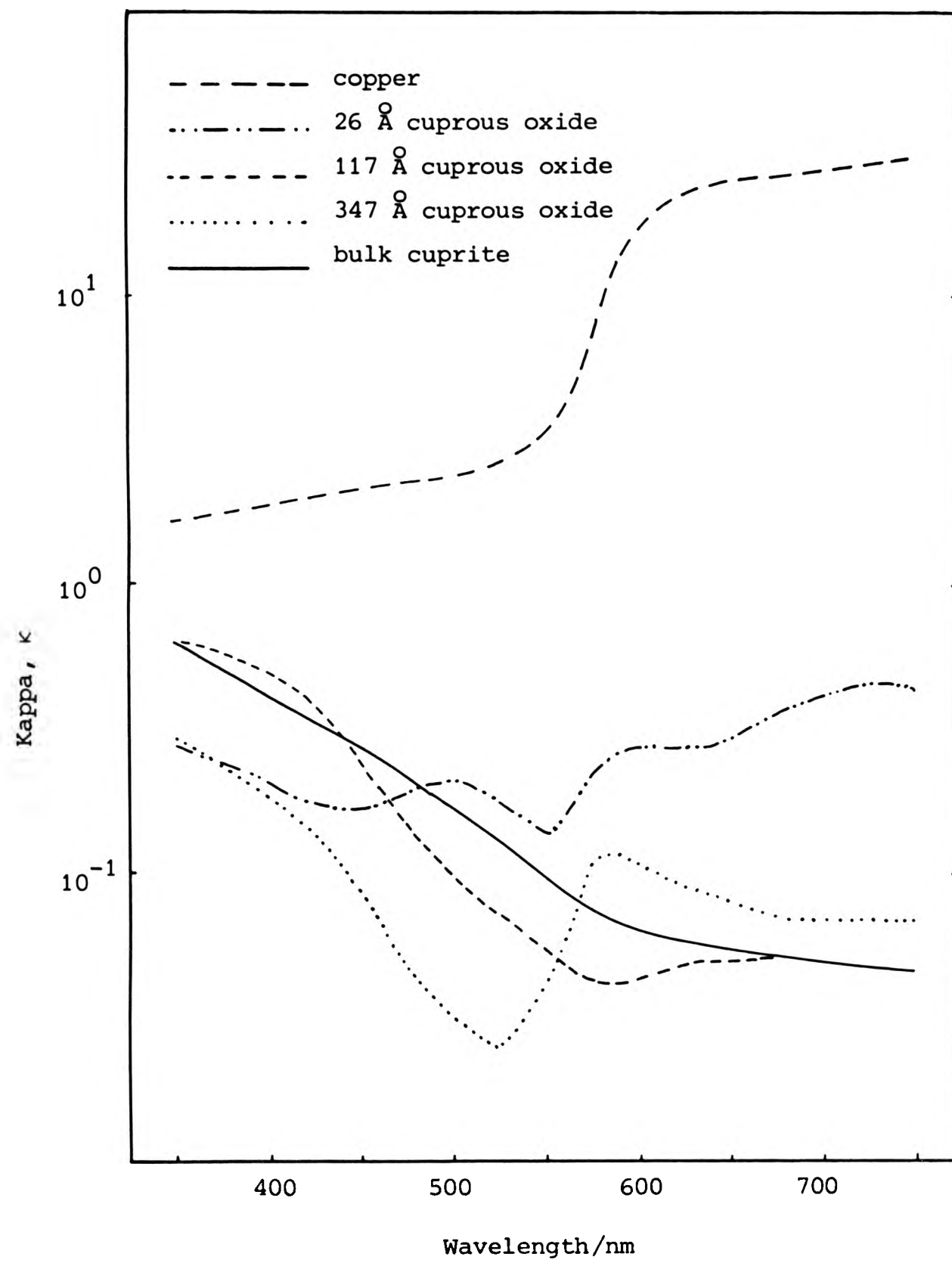
Figure 5.12 The spectral variation of log kappa for cuprous oxide
films on copper/gallium alloy.
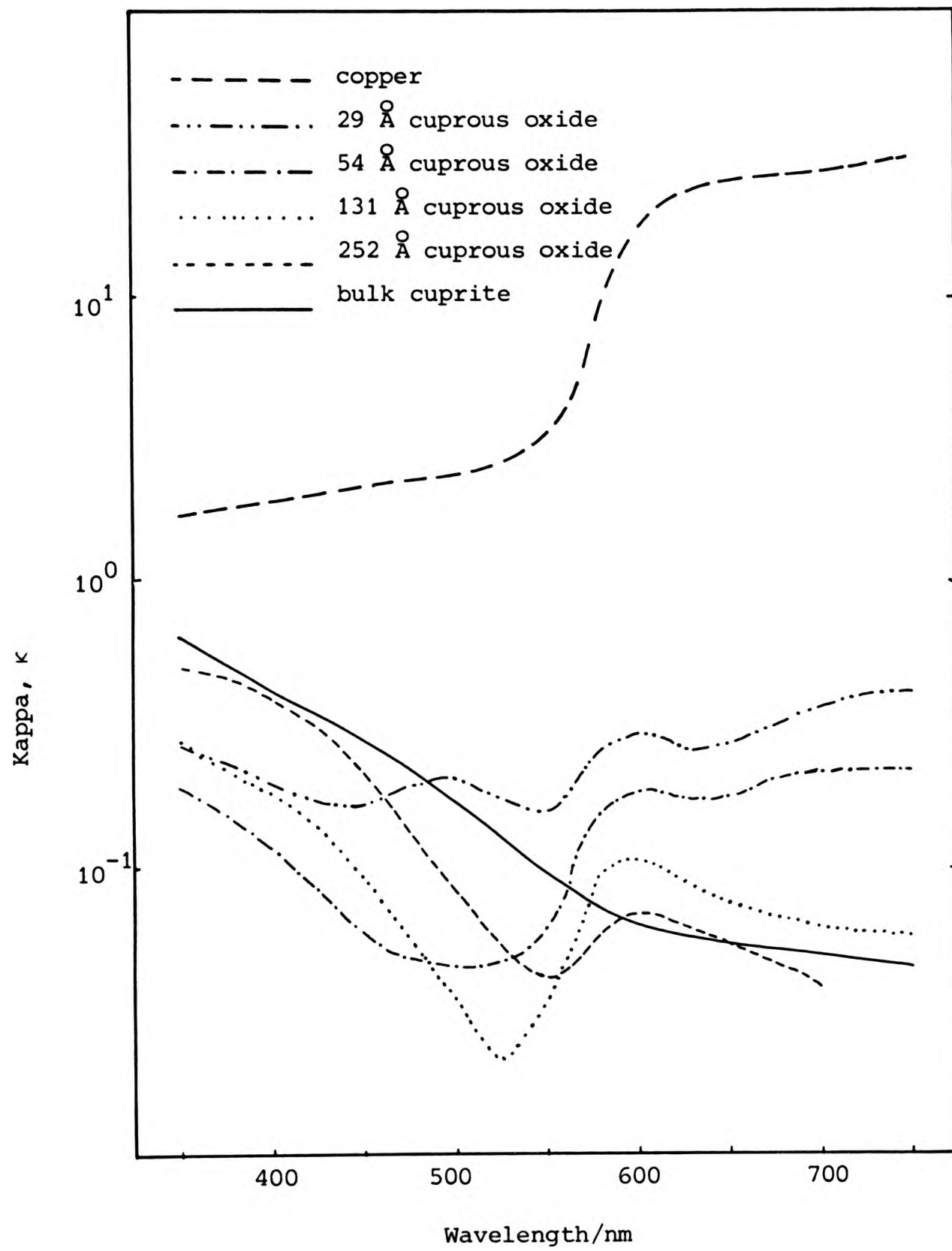
Figure 5.13 The spectral variation of log kappa for cuprous oxide

films on copper/germanium alloy
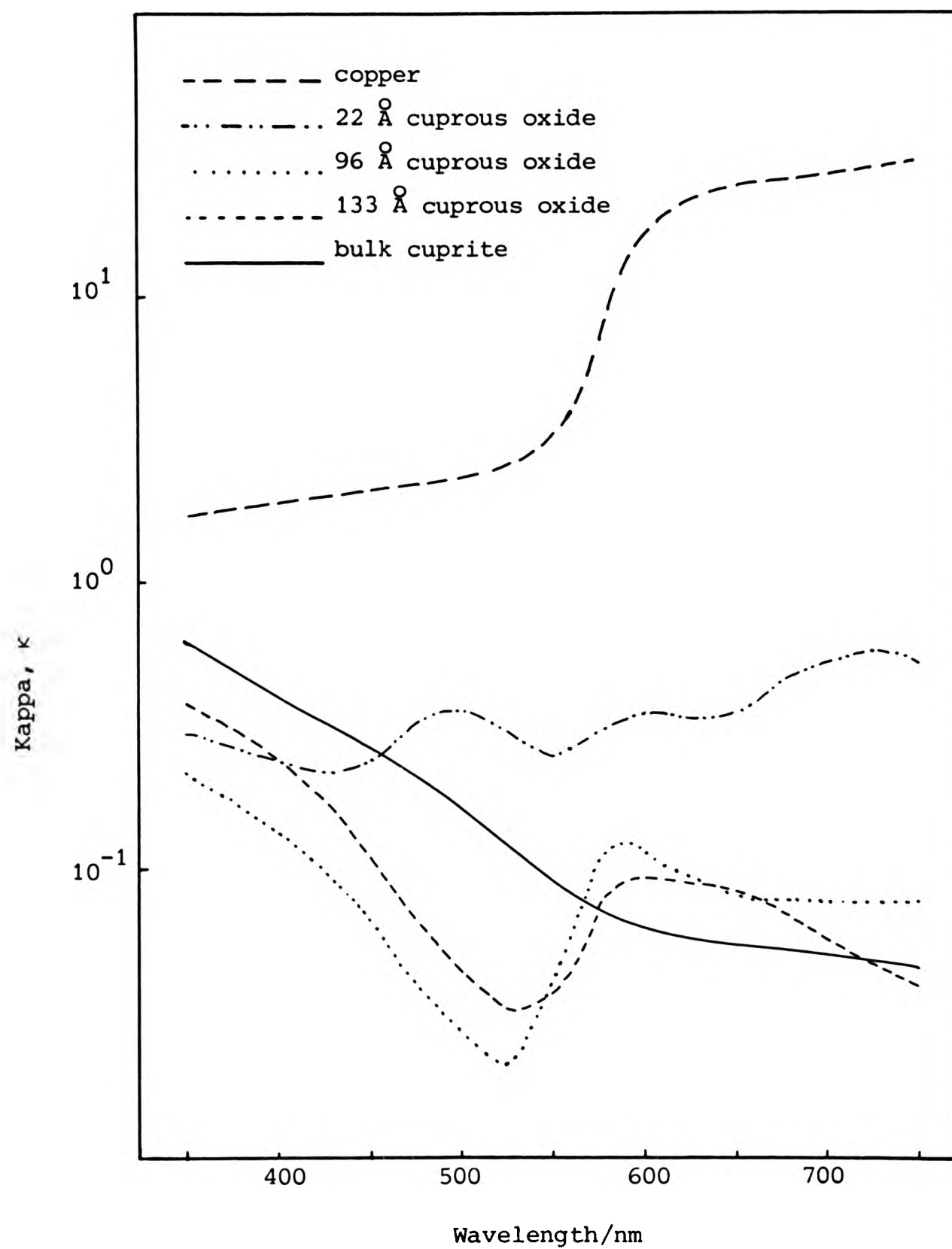
Figure 5.14 The spectral variation of log kappa for cuprous oxide films on copper/nickel alloy.
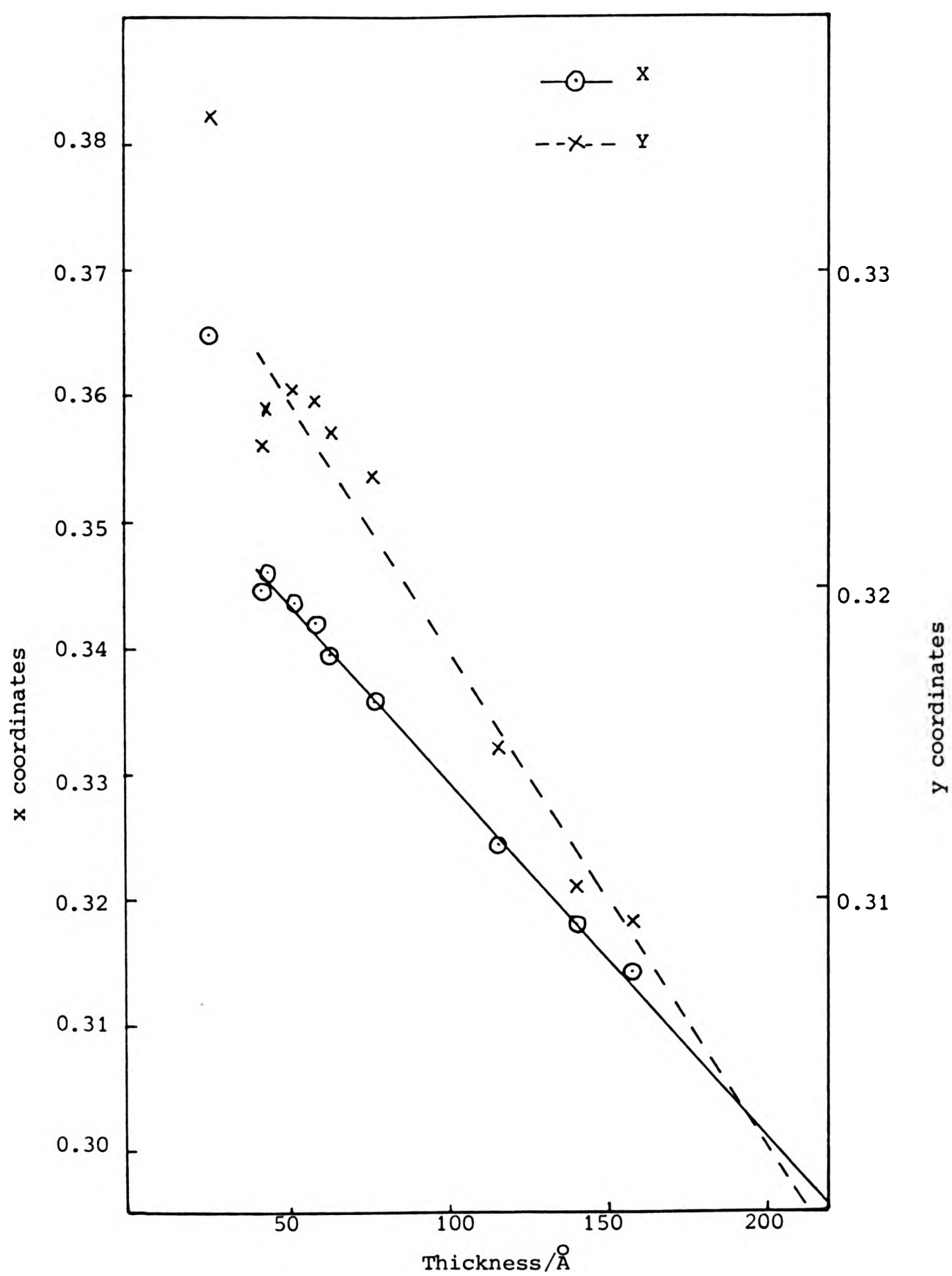
Figure 5.15   The CIE colour coordinates of oxide films on copper.
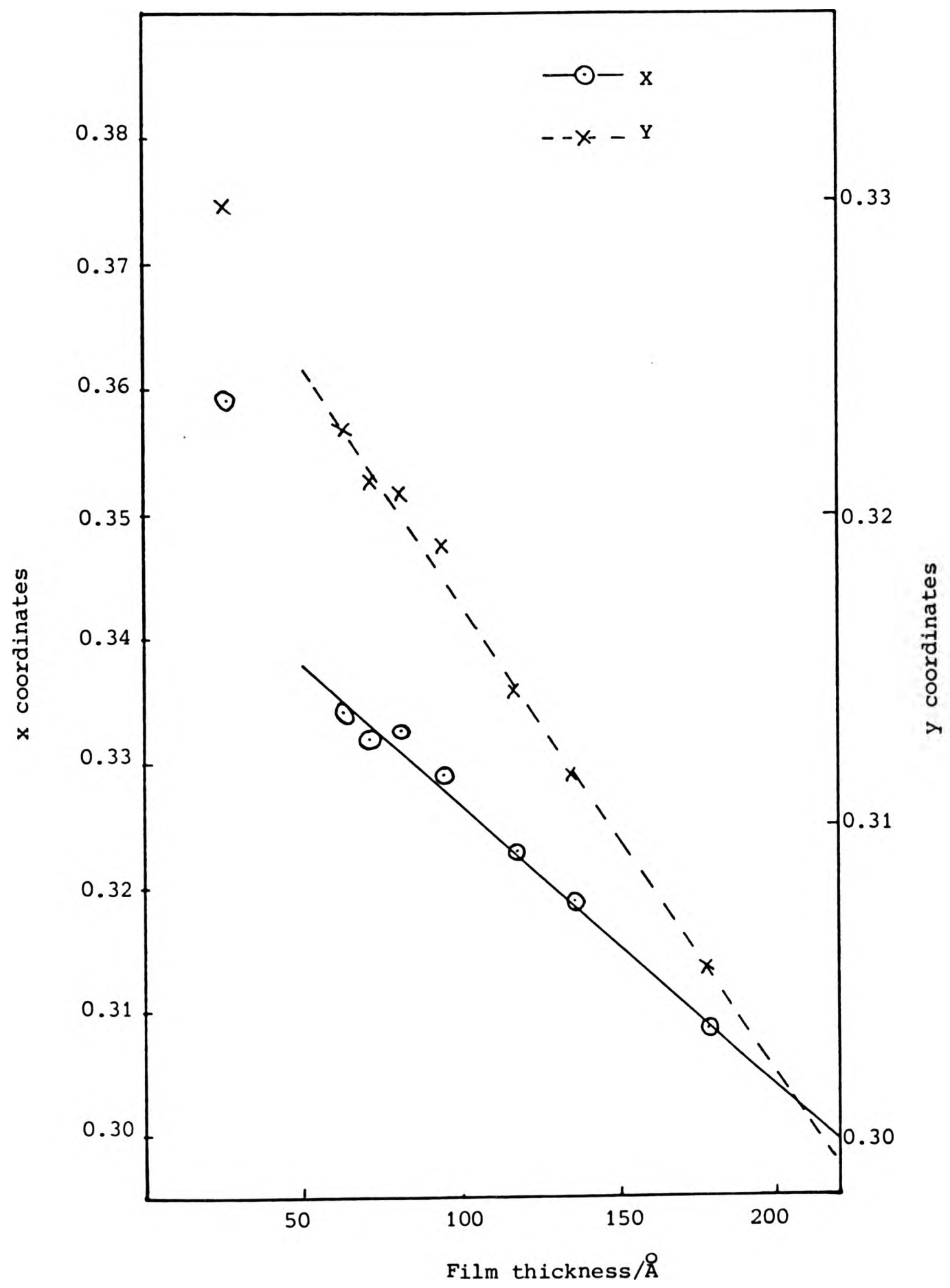
Figure 5.16 The CIE colour coordinates for oxide films on copper/
gallium alloy.
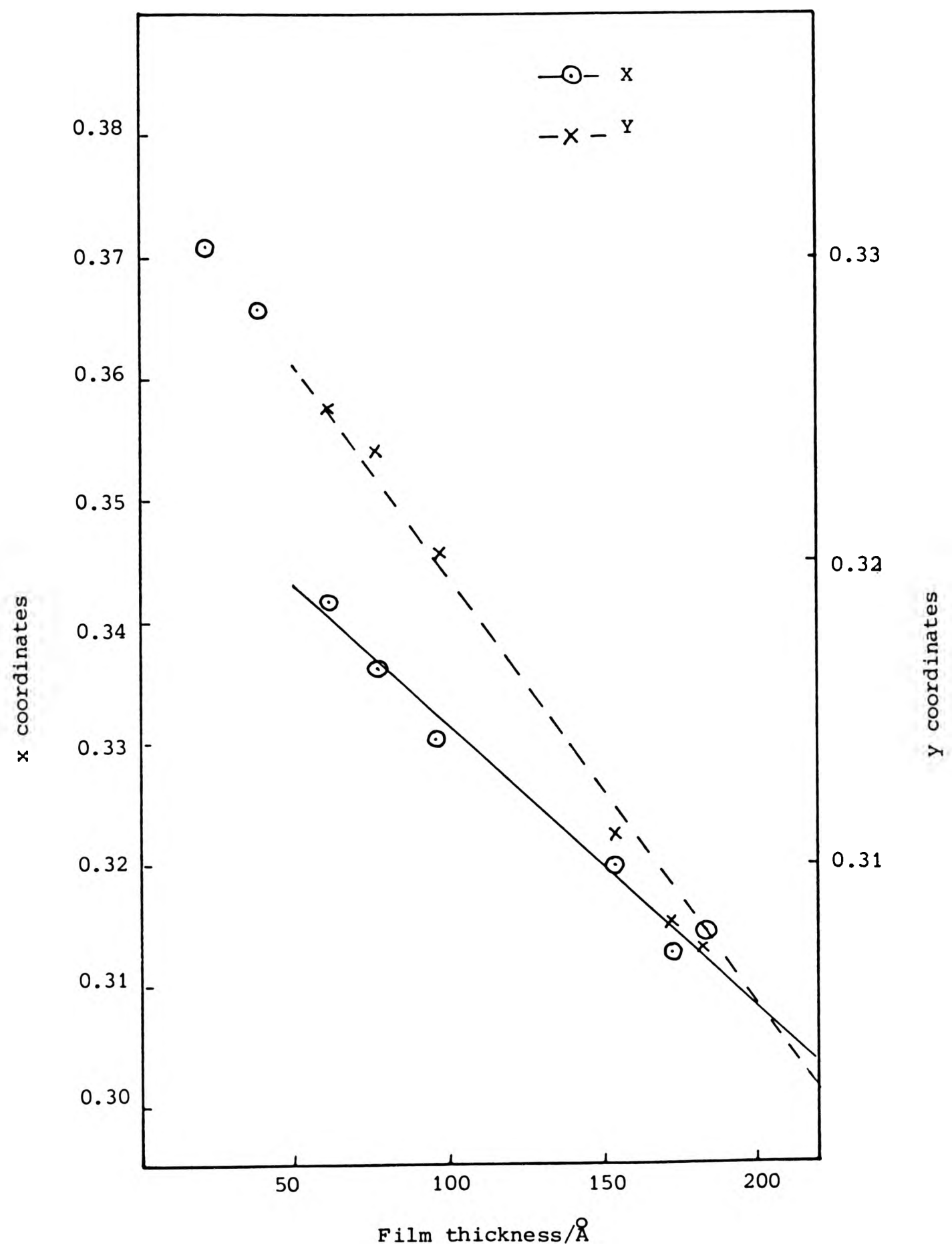
Figure 5.17 The CIE colour coordinates for oxide films on copper/

nickel alloy

of both X and Y colour coordinates on the thickness.

Extrapolation of these graphs to values of X = 0.29 and Y = 0.30

(the X and Y coordinates of bulk cuprite) indicates that films

of about 220 Å have colours close to that of the bulk oxide. If

X and Y coordinate values for films of 50, 100 and 200 Å from

Figures 5.15, 5.16 and 5.17 are combined in Figure 5.18. It

can be seen, that although the colour coordinates of the oxide

films become closer to those of bulk cuprite as the film

thickness increases, differences in the colours of the films on

the individual substrates become more pronounced (shown by the

size of the ellipse in which they are enclosed). These

differences are also visible in the photographs of specimens

oxidised in Mattsson's solution (Figure 4.10).

Figure 5.19 shows the changes in dominant wavelength with

thickness for all the oxide films.

5.5.5   Dependance of the optical properties on film thickness

Plumb (84) was one of the many workers who have suggested

explanations of the way in which the optical properties of thin

dielectric films on metal substrates change with thickness.

He found that the optical behaviour of rather thick, transparent,

dielectric films on metal surfaces can be accurately described

by an idealised model which considers the system as having

plane, parallel-sided, homogeneous phases with a discontinuous

boundary between them. Deviations occur, however, when the

dielectric phase is thinner than 100 Å. He accounted for the

anomalous absorptions encountered in the thinner films in terms

of an electrical double layer produced by a transfer of charge
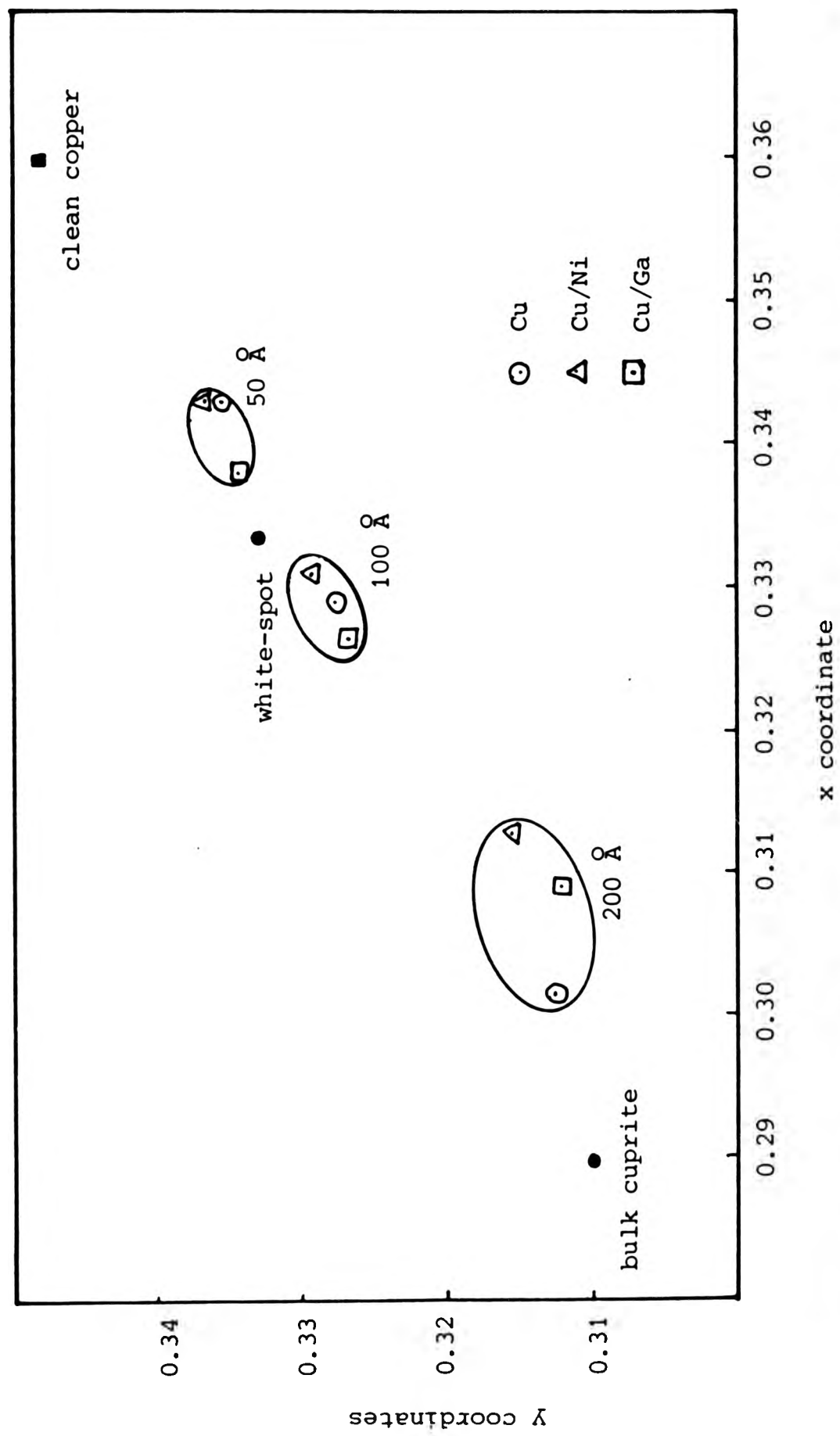
Figure 5.18   The CIE colour coordinates of oxide films of varying thicknesses on copper and dilute copper alloy substrates.
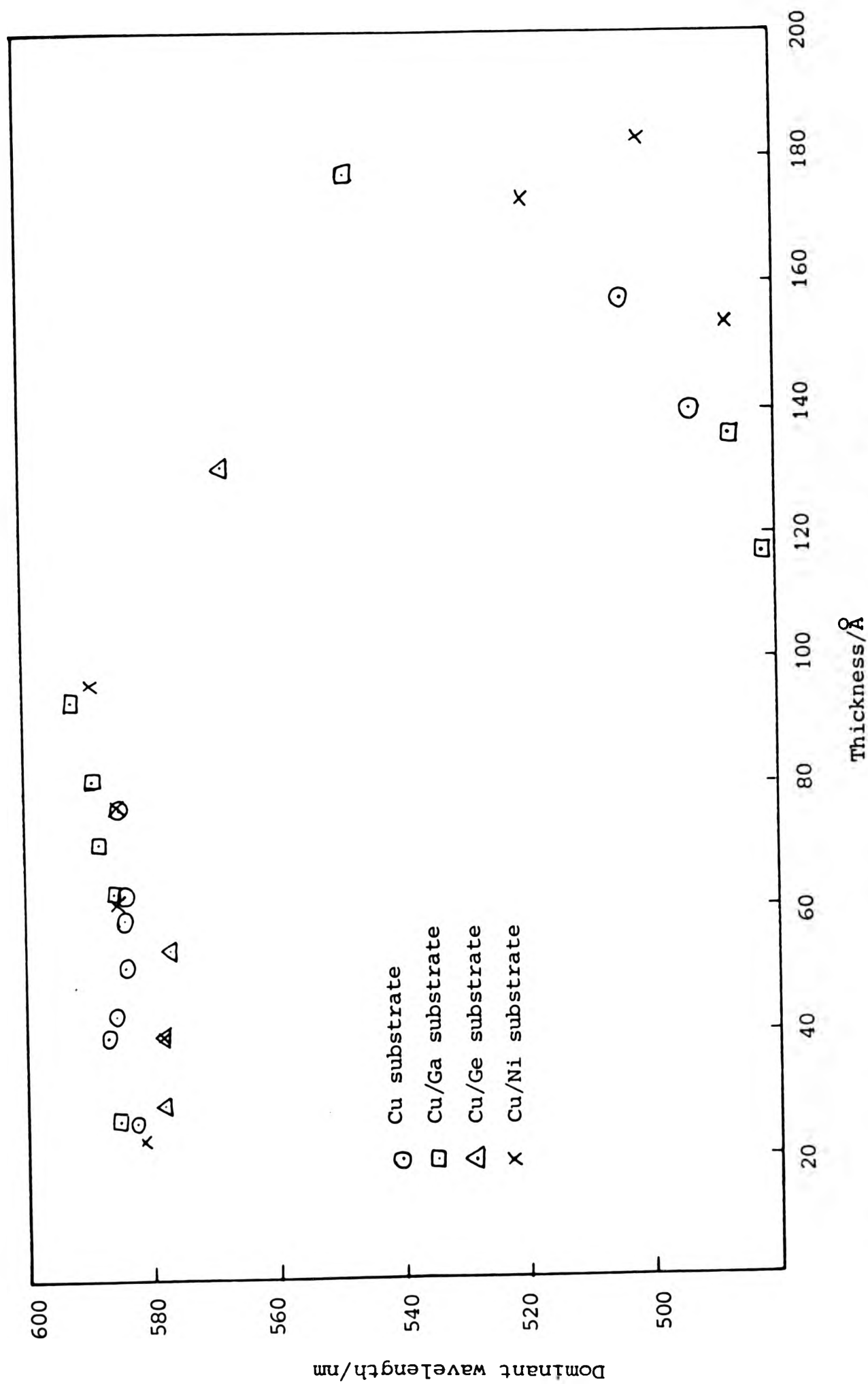
Figure 5.19 The variation of dominant wavelength with oxide film thickness.

arising from the contact of two chemically distinct phases. Thin
barium stearate films on a gold substrate were used to confirm the
theory.

Using the free electron theory of solids, Plumb derives the
expression

$$n^2 \kappa = \frac{2\Pi \, Ne^2 \, \beta}{m \, \omega(\omega^2 + \beta^2)} \tag{1}$$

where n is the refractive index

$\kappa = k/n$, the absorption index

N = concentration of charge carriers

$e = 1.60210 \times 10^{-19}$ C (the charge on the electron)

$\beta = 1/\tau$ is the damping constant for the motion of charges
under the influence of an applied field (τ is the decay
time)

ω is the frequency of the incident radiation

m is the mass of the electron.

Roberts and Ross (85) extended this work by considering three
possible effects of the space-charge region associated with a
dielectric, which depend on the height and form of the potential
energy barrier extending from the substrate Fermi level to the
bottom of the dielectric conduction band. The shape of the
potential barrier just within the dielectric would depend on
the number and type of bulk carriers and the relative magnitude
of the work functions of the metal and the insulator, ψ_m and
ψ_i respectively.

When $\psi_i < \psi_m$ electrons from the substrate will move into the
conduction bands of the dielectric. Roberts (115) now thinks
that the electrons move into the impurity levels rather than the
conduction band. The enriched region will extend into the
dielectric to a depth λ_o which for $\psi_m - \psi_i > 4kT$ has been shown
to be

$$\lambda_o \cong \frac{\pi}{2} \left[\frac{2kT \ K \ \varepsilon_o}{e^2 \ N_c} \right]^{\frac{1}{2}} \exp \left[\frac{\psi_i - \chi}{2kT} \right] \cong \left[\frac{K \ k \ T}{2\Pi N_c \ e^2} \right]^{\frac{1}{2}} \qquad (2)$$

where k is Boltzmann's constant

     T is the Kelvin temperature

     K is the dielectric constant

     ε_o is the permittivity of free space

     N_c is the effective density of states in the insulator

     at the interface

     χ is the electron affinity

This relationship is derived from solutions of the Poisson-
Boltzmann equation (84, 116, 117). Using the fact that the
density of electrons, N_c, in the insulator at the interface is
determined by the substrate (in this case the metal) interface
by the same Fermi distribution function as for the electrons in
the metal, Mott (116) shows that

$$N = N_c \left[\frac{\lambda_o}{\lambda_o + x} \right]^2 \qquad (3)$$

where N is the number of electrons per unit volume at a distance

x from the metal substrate.

When $\psi_i = \psi_m$, no charge transfer would occur, hence no space-charge region will exist and there should be no variation in electrical conductivity or optical absorption.

When $\psi_i > \psi_m$ electrons would have to flow from the dielectric to the metal substrate to establish thermal equilibrium conditions. In this situation a positively charged space-charge zone will exist in the insulator. The insulator would have to be very thick to provide sufficient electrons to satisfy the space-charge.

The expression derived by Plumb

$$n^2 \kappa = \frac{2\Pi Ne^2}{m\omega (\omega^2 + \beta^2)} \tag{1}$$

is a cubic and will therefore have two turning points. To solve the equation Roberts and Ross (85) imposed the conditions

$$\frac{dn}{d\omega} = 0$$

then

$$\frac{d\kappa}{d\omega} = \frac{1}{n} \frac{dk}{d\omega} = \frac{1}{n} \frac{2\Pi Ne^2}{nm} \beta \left[\frac{-(3\omega^2 + \beta^2)}{\omega^2(\omega^2 + \beta^2)^2} \right] \tag{4}$$

for

$$\frac{d\kappa}{d\omega} = 0, \frac{dk}{d\omega} = 0 \text{ i.e. } \omega^2(\omega^2 + \beta^2) = \infty \tag{5}$$

or

$$-(3\omega^2 + \beta^2) = 0 \tag{6}$$

Roberts and Ross (85) related these solutions to the absorbing, reflecting and transparent regions of the spectrum which were shown schematically by Abelès (118) (Figure 5.20). ω_p is the plasma frequency and is defined by

$$\omega_p = \frac{4\Pi \ Ne^2}{m_{opt}} \tag{7}$$

where N is the concentration of free carriers, m_{opt} is the optical mass at ω_p, n = k and κ = 1.

The solution $\omega \to \infty$ is found in the transparent region where $\omega \to \omega_p$ and

$$n \cong \sqrt{1 - (\omega_p/\omega)^2} \cong 1 \tag{8}$$

and

$$\kappa \cong \frac{\omega_p}{2\omega^2\tau} = 0 \tag{9}$$

Thus

$$\lim_{\omega \to \omega_p} \kappa = \lim k/n = 0$$

The other turning point occurs where $-(3\omega^2 + \beta^2) = 0$.

If ω_{crit} is the relevant frequency,

$$\omega_{crit} = i \ \beta/\sqrt{3} \tag{10}$$

If this is written in the form

$$\omega_{crit} = \beta(A + Bi)$$

it can be seen that A = 0 and B = $\beta/\sqrt{3}$ indicating that β is $\pi/2$
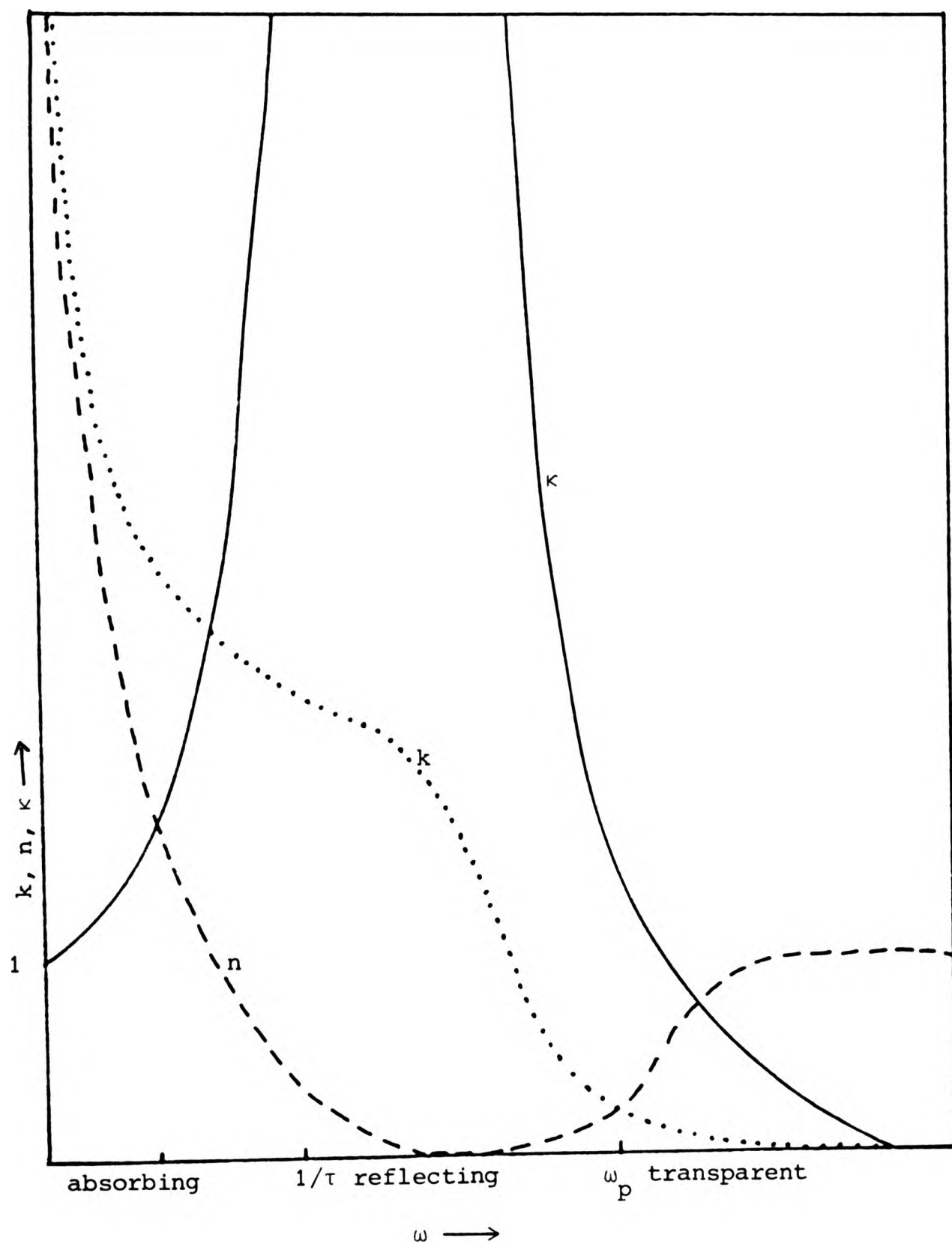
Figure 5.20   Diagram showing the variation of n, k and κ as a

function of frequency, ω (118).

out of phase with the incident radiation. But $\beta \_ 1/\tau$ and therefore ω_{crit} occurs at a frequency lower than $1/\tau$. This happens in the absorbing region where

$$0 < \omega\tau < 1 \text{ and } n^2 \cong k^2 \cong \omega_p^2 \frac{\tau}{2\omega} \tag{11}$$

hence $\qquad \kappa = \frac{k}{n} = 1 \text{ and } \frac{d\kappa}{d\omega} = 0.$

In the reflecting region

$$n = \frac{\omega_p}{2\omega^2\tau}, \; k^x \sqrt{\left(\frac{\omega_p}{\omega}\right)^2 - 1} \cong \frac{\omega_p}{\omega} \tag{12}$$

hence $\qquad \kappa = k/n = 2\omega\tau$

When κ is plotted on Figure 5.20 it is seen to pass through a maximum and to have a value of $\kappa = 1$ at the plasma frequency, ω_p.

If a dielectric on a metal surface has a space-charge region at the interface it may exhibit free-carrier behaviour and should show a maximum value of κ as a function of frequency, ω. Figures 5.11 to 5.14 show the variation of κ with frequency for oxide films of varying thickness on copper and the dilute alloys. Maxima are present at about 575 nm for films of all thicknesses although the maximum is less well defined for thicker films because the influence of the substrate is reduced. In the reflecting region

out of phase with the incident radiation. But $\beta \_ 1/\tau$ and therefore ω_{crit} occurs at a frequency lower than $1/\tau$. This happens in the absorbing region where

$$0 < \omega\tau < 1 \text{ and } n^2 \cong k^2 \cong \omega_p^2 \frac{\tau}{2\omega} \tag{11}$$

hence $\quad \kappa = \frac{k}{n} = 1 \text{ and } \frac{d\kappa}{d\omega} = 0.$

In the reflecting region

$$n = \frac{\omega_p}{2\omega^2\tau}, \quad k^x \sqrt{\left(\frac{\omega_p}{\omega}\right)^2 - 1} \cong \frac{\omega_p}{\omega} \tag{12}$$

hence $\quad \kappa = k/n = 2\omega\tau$

When κ is plotted on Figure 5.20 it is seen to pass through a maximum and to have a value of $\kappa = 1$ at the plasma frequency, ω_p.

If a dielectric on a metal surface has a space-charge region at the interface it may exhibit free-carrier behaviour and should show a maximum value of κ as a function of frequency, ω. Figures 5.11 to 5.14 show the variation of κ with frequency for oxide films of varying thickness on copper and the dilute alloys. Maxima are present at about 575 nm for films of all thicknesses although the maximum is less well defined for thicker films because the influence of the substrate is reduced. In the reflecting region

$$\frac{d\kappa}{d\omega} = \frac{-2\tau}{\omega_p^{3/2}} \left[\frac{1}{\left(\frac{\omega_p}{\omega}\right)^2 - 1} - 1 \right] \tag{14}$$

and ω_c (where $d\kappa/d\omega = 0$) $= \omega_p/2$

substituting for ω_p in (7)

$$\omega_c = \left(\frac{2\Pi \, Ne^2}{m_{opt}} \right)^{\frac{1}{2}} \tag{15}$$

since $\qquad \kappa = k/n \cong 2\omega\tau \tag{13}$

$$\tau = \frac{\kappa_c}{2\omega_c} \tag{16}$$

and since κ varies with the concentration of carriers,

substituting (3) in (1)

$$\kappa_x = \frac{k}{n} = \frac{2\Pi e^2 N_o \beta}{n^2 \, m_{opt} \, \omega(\omega^2 + \beta^2)} \cdot \left[\frac{\lambda_o}{\lambda_o + x} \right]^2 =$$

$$\frac{\omega_p^2}{2n^2} \cdot \frac{\beta}{\omega(\omega^2 + \beta^2)} \left[\frac{\lambda_o}{\lambda_o + x} \right]^2 \tag{17}$$

where κ_x represents the behaviour of κ for an insulating film

of thickness x at a frequency ω when an ohmic contact is

formed. This relationship can be tested by plotting log κ

against log $[\lambda_o/(\lambda_o + x)]^2$ which should result in a straight line

Figures 5.21 to 5.24 are plots of log κ against log $[\lambda_o/(\lambda_o + x)]^2$

with λ_o = 50 Å and 100 Å for films on copper and the dilute

copper alloys. Straight lines are obtained which converge where
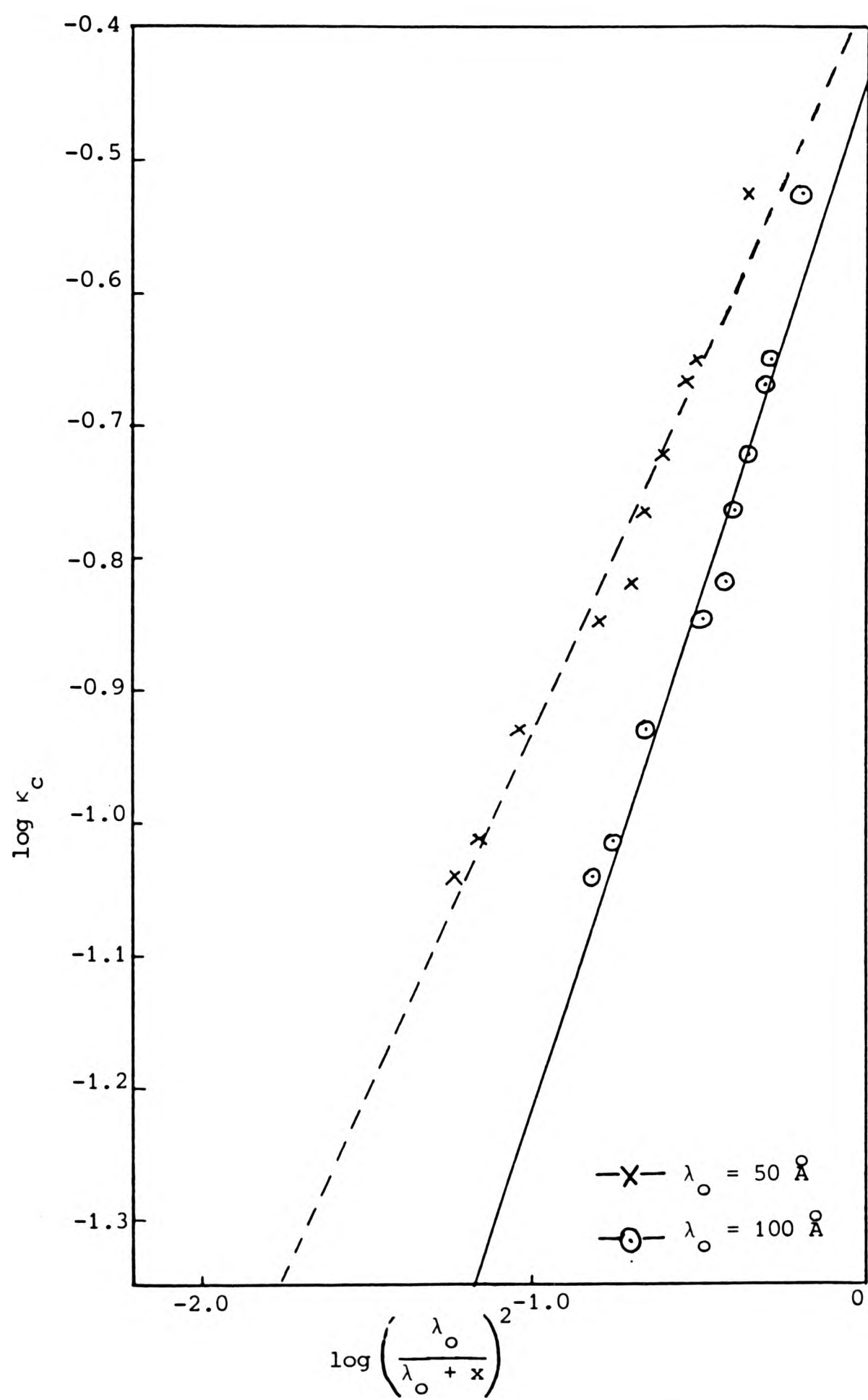
Figure 5.21   Plot of $\log \kappa_c$ versus $\log \left(\dfrac{\lambda_o}{\lambda_o + x}\right)^2$ for cuprous oxide films on copper.
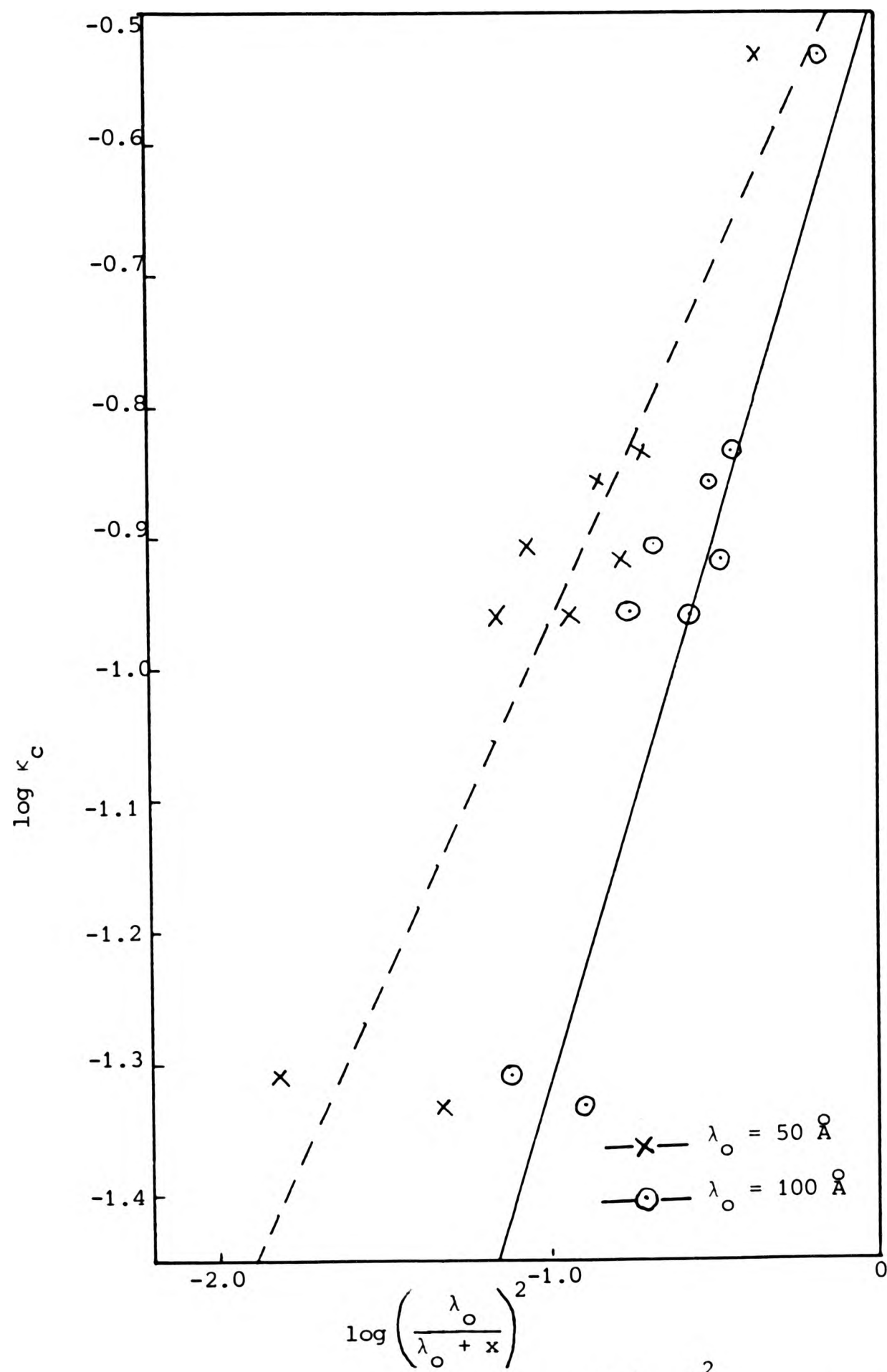
Figure 5.22 Plot of log κ_c versus log $\left(\dfrac{\lambda_o}{\lambda_o + x}\right)^2$ for oxide films on copper/gallium alloy.
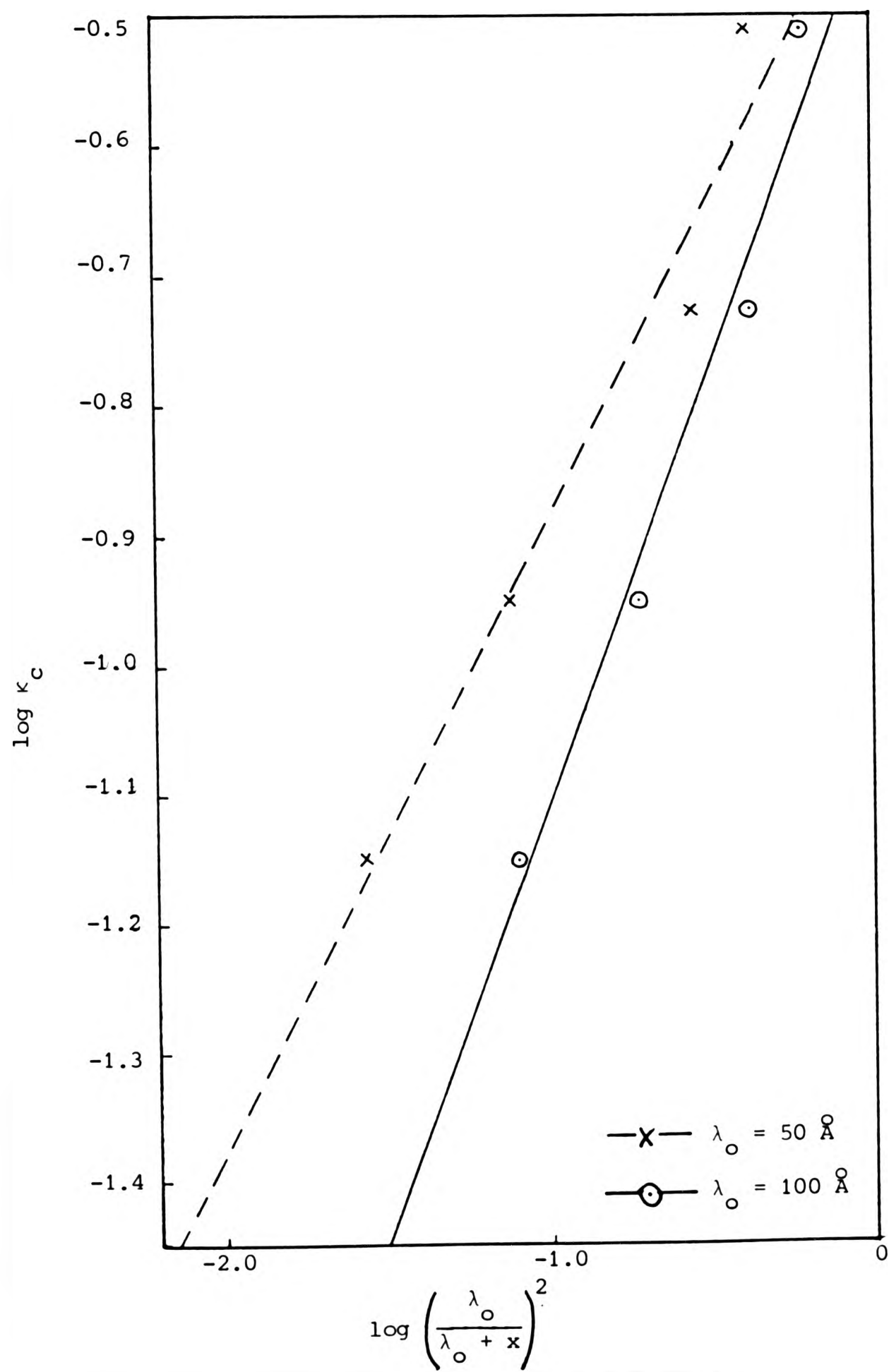
Figure 5.23 Plot of $\log \kappa_c$ versus $\log \left(\dfrac{\lambda_o}{\lambda_o + x} \right)^2$ for oxide films on copper/germanium alloy.
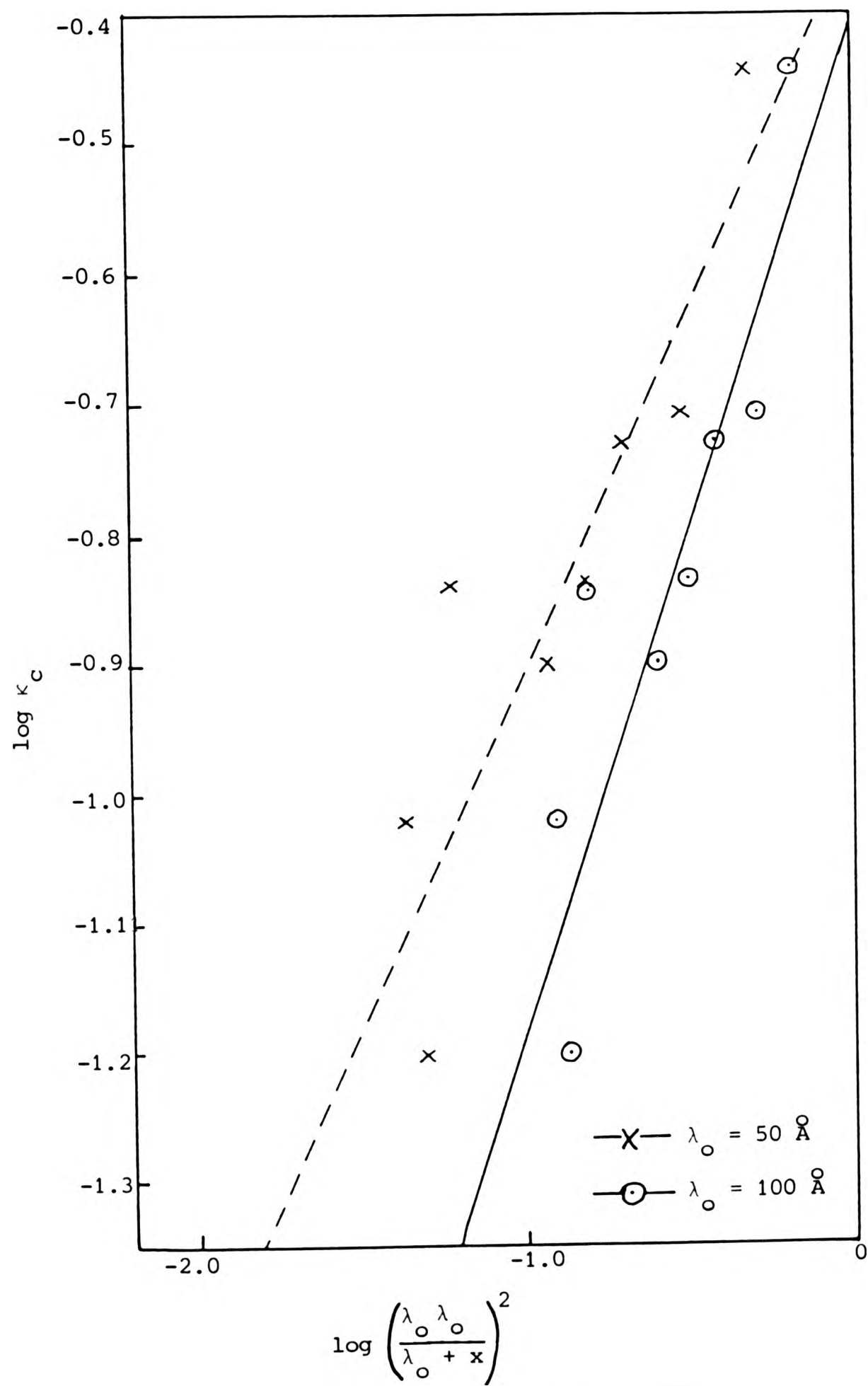
Figure 5.24 Plot of $\log \kappa_c$ versus $\log \left(\dfrac{\lambda_o}{\lambda_o + x} \right)^2$ for oxide films on copper/nickel alloy

$$\log\ (\lambda_o/\lambda_o\ +\ x)^2\ =\ 0.$$

The maximum value of kappa, κ_c and the wavelength, λ_c, at which it occurs were obtained from the computer data for each of the oxide films examined. The frequency at which the maximum occurs is given by

$$\omega_c\ =\ \frac{2\Pi\nu}{\lambda_c} \tag{18}$$

where ν is the speed of light in vacuo $=\ 3\ \times\ 10^8\ ms^{-1}$. In this region it has been shown that

$$\tau\ =\ \frac{k_c}{2\omega_c} \tag{16}$$

Tables 5.10, 5.11, 5.12 and 5.13 list the thicknesses of the oxide films, the values of κ_c, λ_c and the corresponding values of τ for oxide films on copper and dilute alloys.

Table 5.10

Values of κ_c, λ_c, ω_c and τ for oxide films on copper

Thickness/Å	κ_c	λ_c/nm	ω_c/s^{-1}	τ/s
26	0.298	610	3.09×10^{15}	4.82×10^{-17}
41	0.224	580	3.25×10^{15}	3.45×10^{-17}
43	0.215	595	3.17×10^{15}	3.39×10^{-17}
51	0.191	580	3.25×10^{15}	2.94×10^{-17}
59	0.172	580	3.25×10^{15}	2.65×10^{-17}
73	0.152	580	3.25×10^{15}	2.34×10^{-17}
77	0.142	580	3.25×10^{15}	2.18×10^{-17}
116	0.117	585	3.22×10^{15}	1.82×10^{-17}
140	0.097	585	3.22×10^{15}	1.51×10^{-17}
158	0.091	585	3.22×10^{15}	1.41×10^{-17}

Table 5.11

Values of κ_c, λ_c, ω_c and τ for oxide films on copper/gallium alloy.

Thickness/$\overset{\circ}{A}$	κ_c	λ_c/nm	ω_c/s^{-1}	τ/s
26	0.294	612	3.08×10^{15}	4.80×10^{-17}
63	0.146	584	3.23×10^{15}	2.26×10^{-17}
71	0.121	584	3.23×10^{15}	1.87×10^{-17}
81	0.139	584	3.23×10^{15}	2.15×10^{-17}
94	0.110	584	3.23×10^{15}	1.70×10^{-17}
117	0.124	584	3.23×10^{15}	1.92×10^{-17}
136	0.110	594	3.17×10^{15}	1.73×10^{-17}
178	0.046	586	3.22×10^{15}	0.71×10^{-17}
347	0.049	584	3.23×10^{15}	0.76×10^{-17}

Table 5.12

Values of κ_c, λ_c, ω_c and τ for the oxide films on copper/germanium alloy.

Thickness/$\overset{\circ}{A}$	κ_c	λ_c/nm	ω_c/s^{-1}	τ/s
29	0.308	593	3.17×10^{15}	4.83×10^{-17}
54	0.188	601	3.14×10^{15}	2.95×10^{-17}
131	0.112	587	3.21×10^{15}	1.74×10^{-17}
251	0.071	601	3.14×10^{15}	1.14×10^{-17}

Table 5.13

Values of κ_c, λ_c, ω_c and τ for the oxide films on copper/nickel alloy

Thickness/Å	κ_c	λ_c/nm	ω_c/s^{-1}	τ/s
22	0.361	595	3.17×10^{15}	5.70×10^{-17}
40	0.197	584	3.23×10^{15}	3.05×10^{-17}
62	0.186	583	3.23×10^{15}	2.88×10^{-17}
77	0.146	580	3.25×10^{15}	2.25×10^{-17}
97	0.129	584	3.23×10^{15}	2.00×10^{-17}
154	0.144	596	3.16×10^{15}	2.28×10^{-17}
173	0.063	586	3.22×10^{15}	0.98×10^{-17}
183	0.095	606	3.11×10^{15}	1.53×10^{-17}

In all cases the relaxation time decreased with the thickness of the film, which is the expected behaviour if the concentration of carriers decreases with distance from the metal substrate. The values of the relaxation times are consistent with those quoted by Greenaway and Harbeke (119). Graphs of log thickness versus $\tau^{\frac{1}{2}}$ (Figures 5.25 to 5.28) give straight lines although there is considerable scatter in the result for the copper/ gallium system. Values of τ, for films 100 Å thick and derived graphically, are tabulated in Table 5.14.
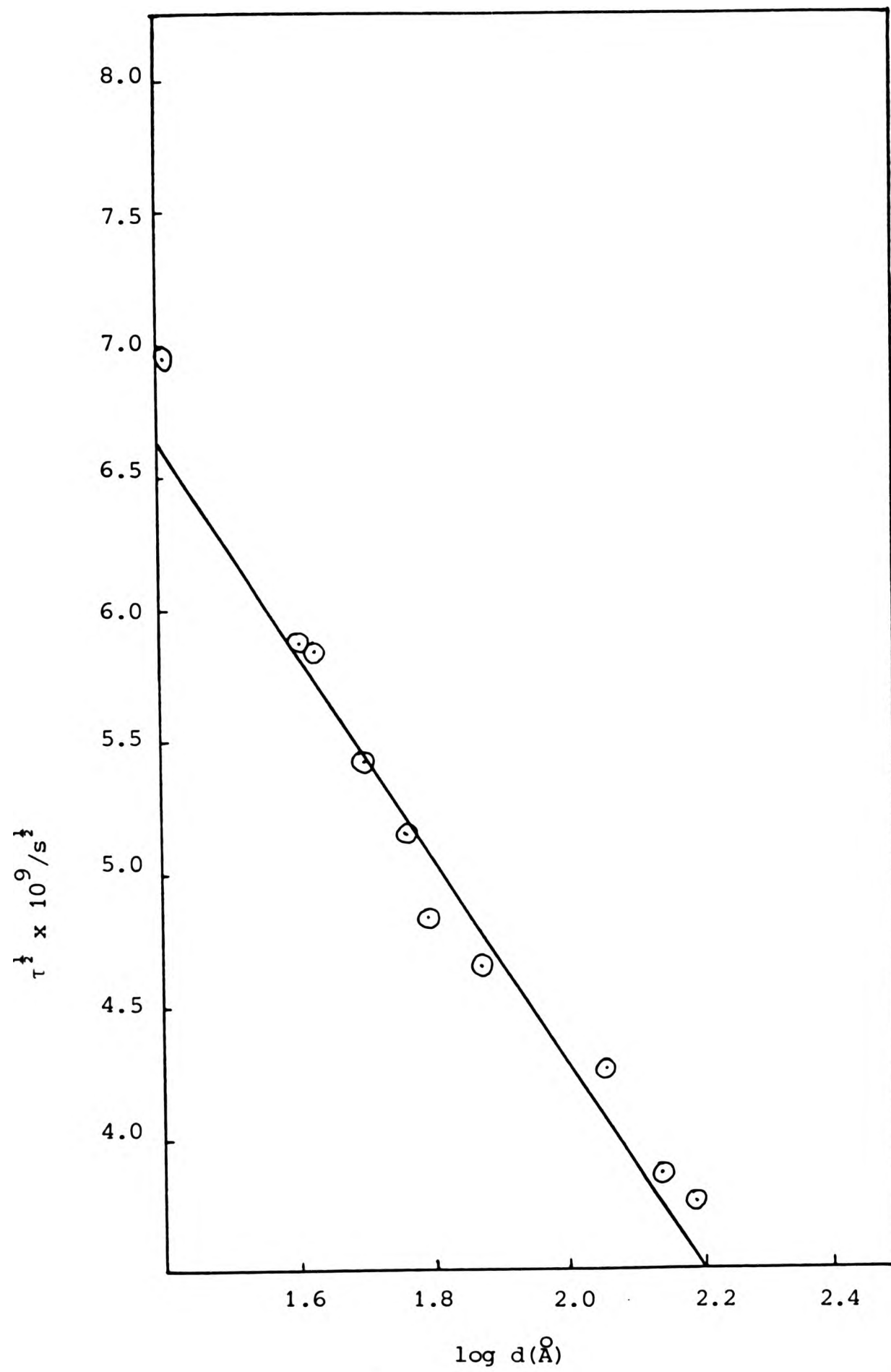
Figure 5.25   Plot of $\tau^{\frac{1}{2}}$ against log d for cuprous oxide films on copper.
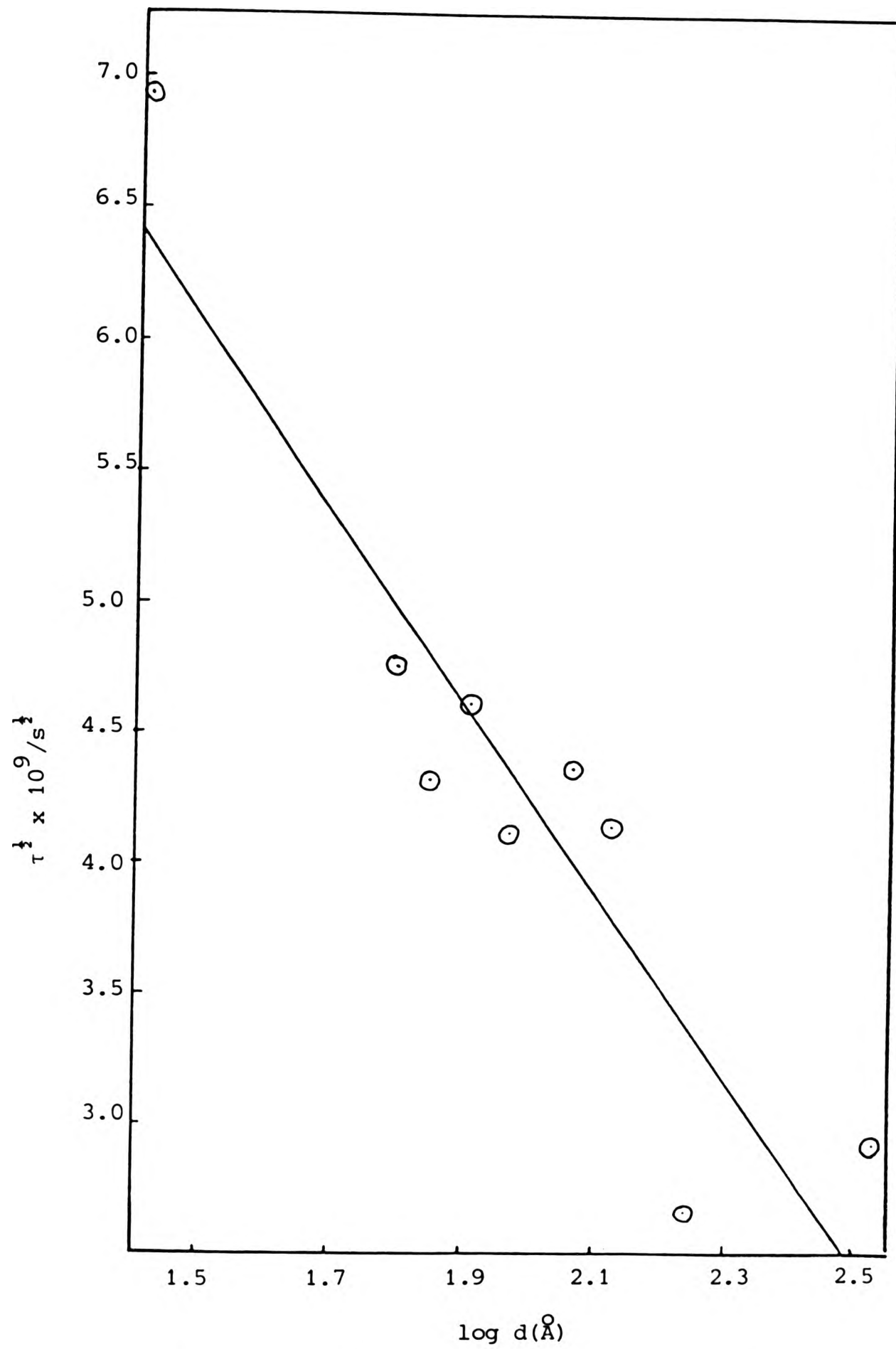
Figure 5.26   Plot of $\tau^{\frac{1}{2}}$ against log d for oxide films on copper/

gallium alloy
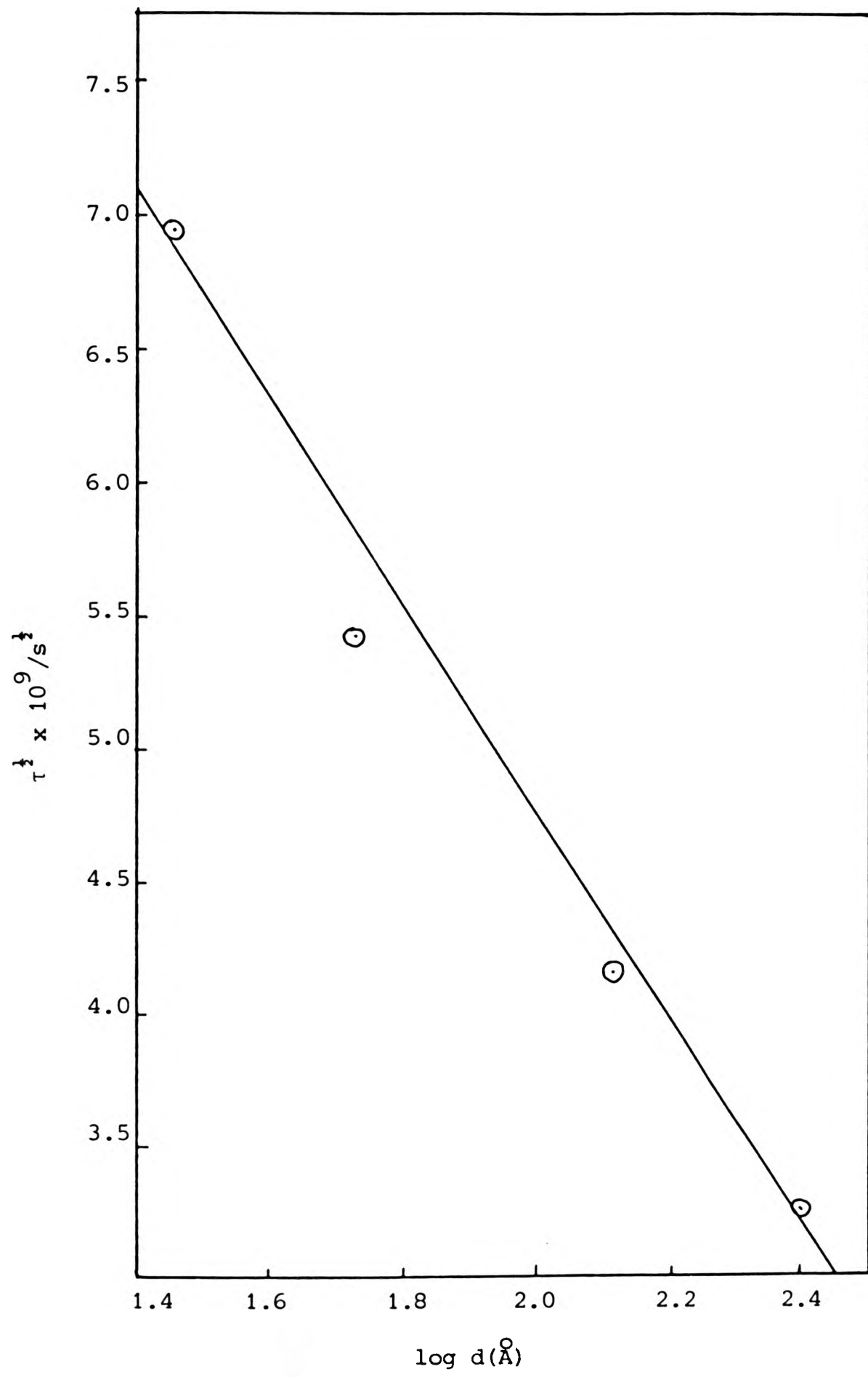
Figure 5.27 Plot of $\tau^{\frac{1}{2}}$ against log d for oxide films on copper/
germanium alloy
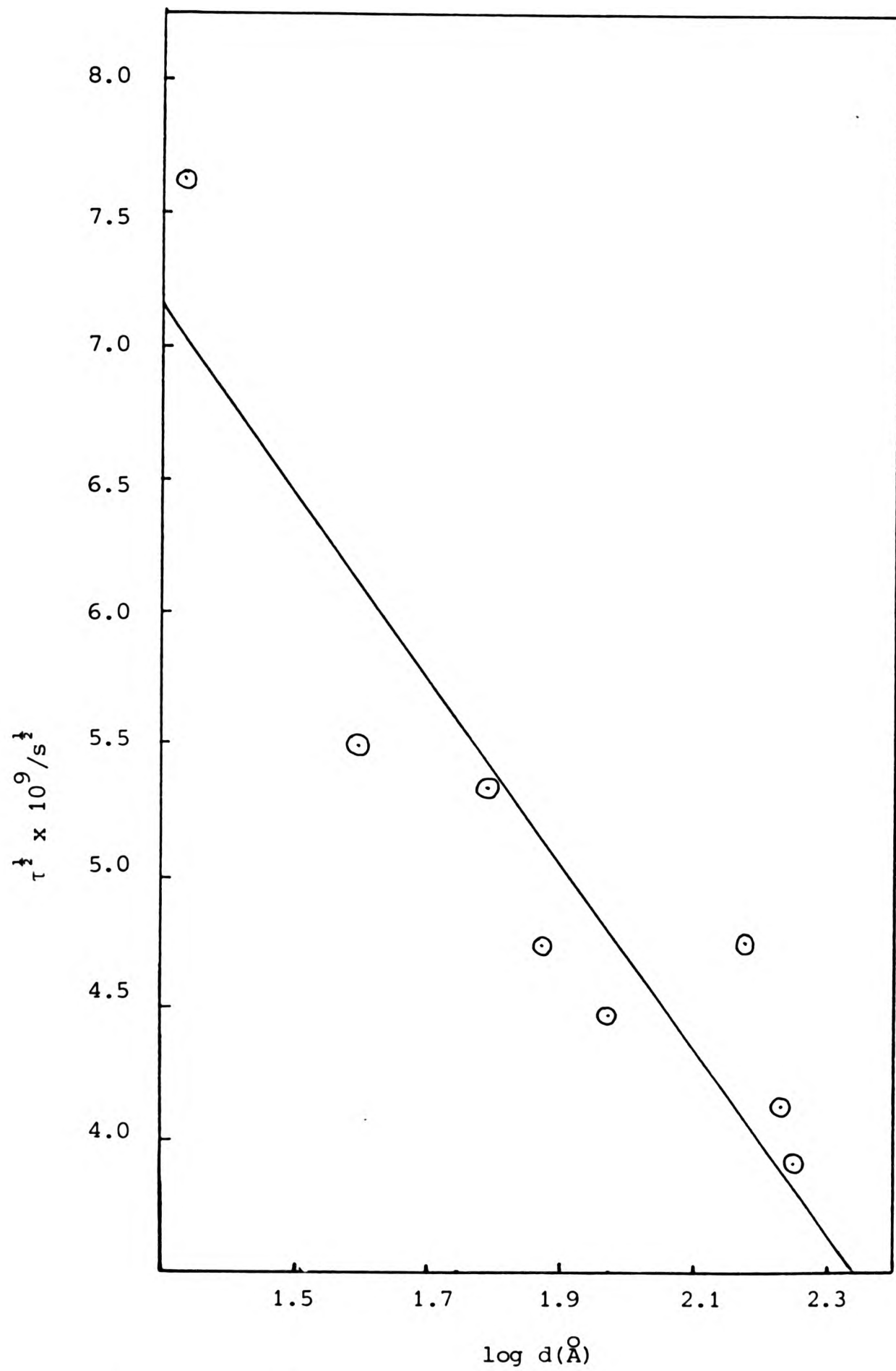
Figure 5.28   Plot of $\tau^{\frac{1}{2}}$ against log d for oxide films on copper/nickel alloy.

Table 5.14

Values of τ for films 100 $\overset{\circ}{A}$ thick

Substrate	τ/s
copper	1.92×10^{-17}
copper/nickel	2.10×10^{-17}
copper/gallium	1.94×10^{-17}
copper/germanium	2.21×10^{-17}

Apart from the copper/gallium system where there is considerable scatter, the relaxation time for films of the same thickness (100 $\overset{\circ}{A}$) is found to increase from 1.92×10^{-17} seconds for the copper substrate to 2.10×10^{-17} seconds for the copper/nickel alloy and 2.21×10^{-17} seconds for the copper/germanium alloy indicating an increased carrier concentration in the oxides on the alloy substrates compared to that on pure copper. The order of these increased relaxation times is consistent with the valencies of the alloying elements. Thus germanium with the electronic configuration $1s^2 2s^2 2p^6 3s^2 3p^6 3d^{10} 4s^2 4p^2$ has four electrons in the outer valency shell whereas nickel $(1s^2 2s^2 2p^6 3s^2 3p^6 3d^8 4s^2)$ has only two and copper $(1s^2 2s^2 2p^6 3s^2 3p^6 3d^{10} 4s^1)$ only one. Introduction of these higher valent cations into the cuprous oxide lattice produces positive holes as shown in Figure 5.29.
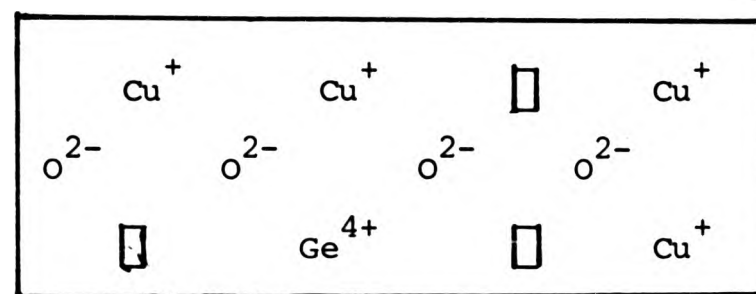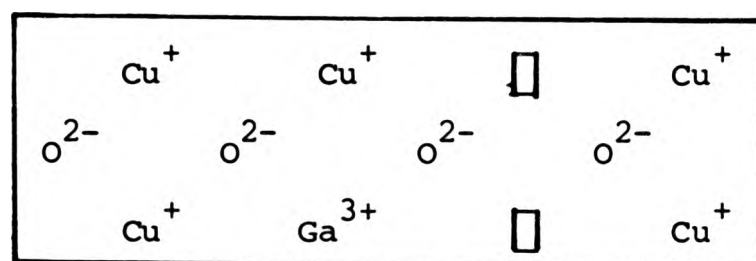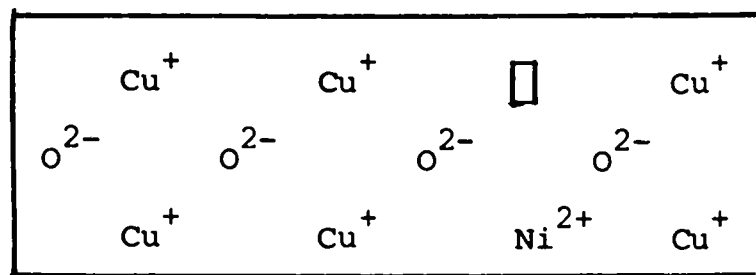
Figure 5.29   The formation of positive holes in the cuprous oxide

lattice by the introduction of higher valent cations.

Zucker (120) estimates the concentration of cation vacancies

in cuprous oxide at room temperature to be 3×10^{12} cm^{-3} for an

ideal Cu^+ concentration of 5.05 x 10^{22} cm^{-3}. A 0.5 at/o alloy would have 5 in every 1000 lattice sites occupied by atoms of the alloying element i.e. 2.5 x 10^{20} sites cm^{-3}. The ionic radii of the elements used in these experiments are listed in Table 5.15.

Table 5.15

Ionic radii of the metals

Metal	Ion	Ionic radius /Å
Cu	Cu^+	0.96
Ni	Ni^{2+}	0.72
Ga	Ga^{3+}	0.62
Ge	Ge^{4+}	0.53

The relative magnitude of the ionic radii suggest that cation substitutions are possible. To maintain electrical neutrality the introduction of a Ni^{2+} ion will result in the formation of two cation vacancies. If Ni^{2+} is present in the same concentration as it is in the alloy substrate, it will introduce 5 x 10^{20} cation vacancies cm^{-3} (far more than there are in pure cuprous oxide). This number will be even larger where lattice sites are occupied by Ga^{3+} or Ge^{4+} ions.

The relative sizes of the copper atom and those of the alloying addition will also affect the relaxation time by distorting the

lattice. Atoms smaller or larger than the copper atom will be responsible for defects in the lattice and hence increase the effective carrier concentration, although their effect is probably small as all the elements are "near neighbours" in the Periodic Table.

5.5.6 Summary

The optical constants of very thin films of cuprous oxide on any of the substrates used show appreciable differences from those of bulk cuprite. As the films thicken these differences diminish and the optical properties, including the colour, approach those of the bulk material. However, the difference in colour between oxide films on individual substrates increases.

Analysis of the optical data using a model proposed by Plumb (84) and developed by Roberts and Ross (85) suggests that the presence of the metallic substrate is responsible for the anomalous optical properties of these very thin oxide films. If this is so, the use of other metal or dielectric substrates should result in different optical properties for these thin films. The effects of gold and glass substrates are considered in the following section.

5.6 Cuprous oxide films on other substrates

5.6.1 Introduction

Thin films of cuprous oxide on glass and gold substrates were produced by oxidising thin evaporated films of copper at 80°C. In spite of repeated attempts to produce a wide range of thicknesses only a limited range was achieved. Oxide films

produced in this way are obviously not the same as those grown
on a bulk metal substrate. With evaporated films there is a
limited supply of the substrate available and this will affect
the stoichiometry and morphology of the final film. It is
unlikely therefore, that the oxide film will behave as either
bulk oxide or an oxide film in contact with an infinite
amount of the substrate. Nevertheless, the optical data
obtained for these films provided a useful comparison with
films of oxide grown on bulk alloy substrates.

5.6.2 The optical properties of thin films of cuprous oxide on glass substrates

The spectral distribution of n_f for a very thin film of oxide
is very close to that of bulk cuprite (Figure 4.32) with slight
shifting of the maximum to a lower wavelength. There is a
slight minimum in n_f at about 700 nm but nothing corresponding
to the well-defined minimum found for the cuprous oxide films
on copper-based substrates. In the case of the thicker films
the maximum is slightly shifted towards longer wavelengths.
At the red-end of the spectrum the value of n_f is appreciably
higher than that of bulk cuprite. This can not be attributed
to the effect of the substrate and may simply indicate a rough,
defective surface.

The spectral distribution of k_f for the very thin film (Figure
4.33) is also very similar to that of bulk cuprite. The minima
and maxima observed in the spectral plots of k_f for cuprous
oxide films on copper based substrates are absent in the films
on glass.

Figure 5.30 shows the variation of log kappa with wavelength for films of cuprous oxide on glass and bulk cuprous oxide. In all cases the value of kappa decreases smoothly with increasing wavelength. The numerical value of kappa for the very thin film is close to that of the bulk oxide but is appreciably higher in the case of the thicker film.

These plots show no local maxima attributable to space-charge effects and thus do not exhibit the free-carrier behaviour observable in the films on copper-based substrates.

5.6.3 The optical properties of thin films of cuprous oxide on gold substrates

The cuprous oxide films produced on the gold substrates covered a limited thickness range (51 to 67 $\overset{\circ}{A}$). When the spectral valuation of n_f and k_f for the 51 $\overset{\circ}{A}$ films is compared with an oxide film of the same thickness on copper (Figures 5.31 and 5.32) similarities are observed. The maxima and minima which have been attributed to a space-charge effect are again visible although the wavelengths at which they appear are different. This is probably due to the difference in the work functions of copper and gold. The spectral variation of log kappa for these films (Figure 5.33) shows a local maximum at about 600 nm. Table 5.16 tabulates the maximum values of kappa, κ_c, and the wavelength, λ_c, at which it occurs. The calculated values of ω_c and τ are also included.
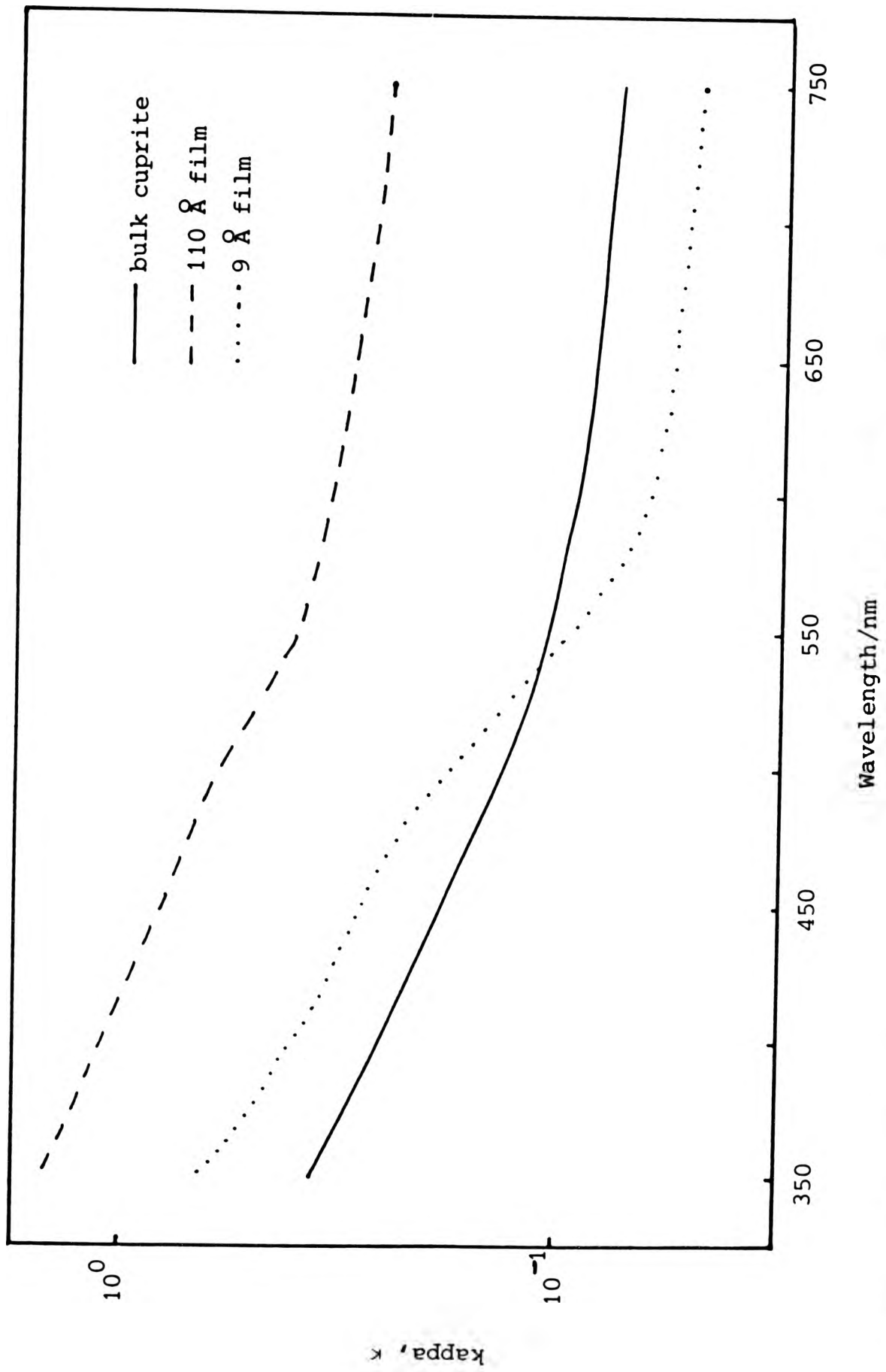
Figure 5.30   Plot of log kappa versus wavelength for cuprous oxide films on glass.
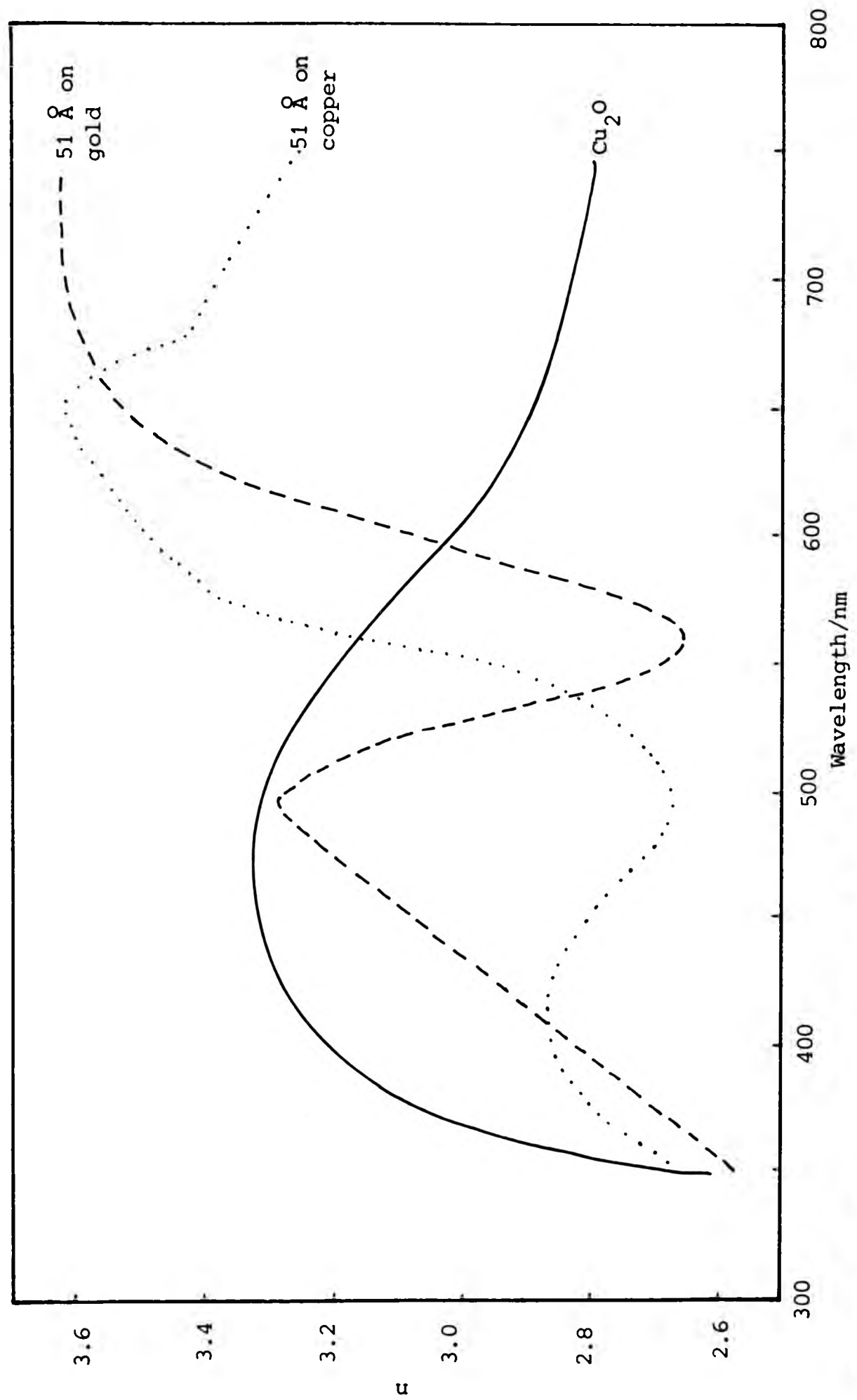
Figure 5.31 The spectral variation of n for thin cuprous oxide films on gold and copper substrates.
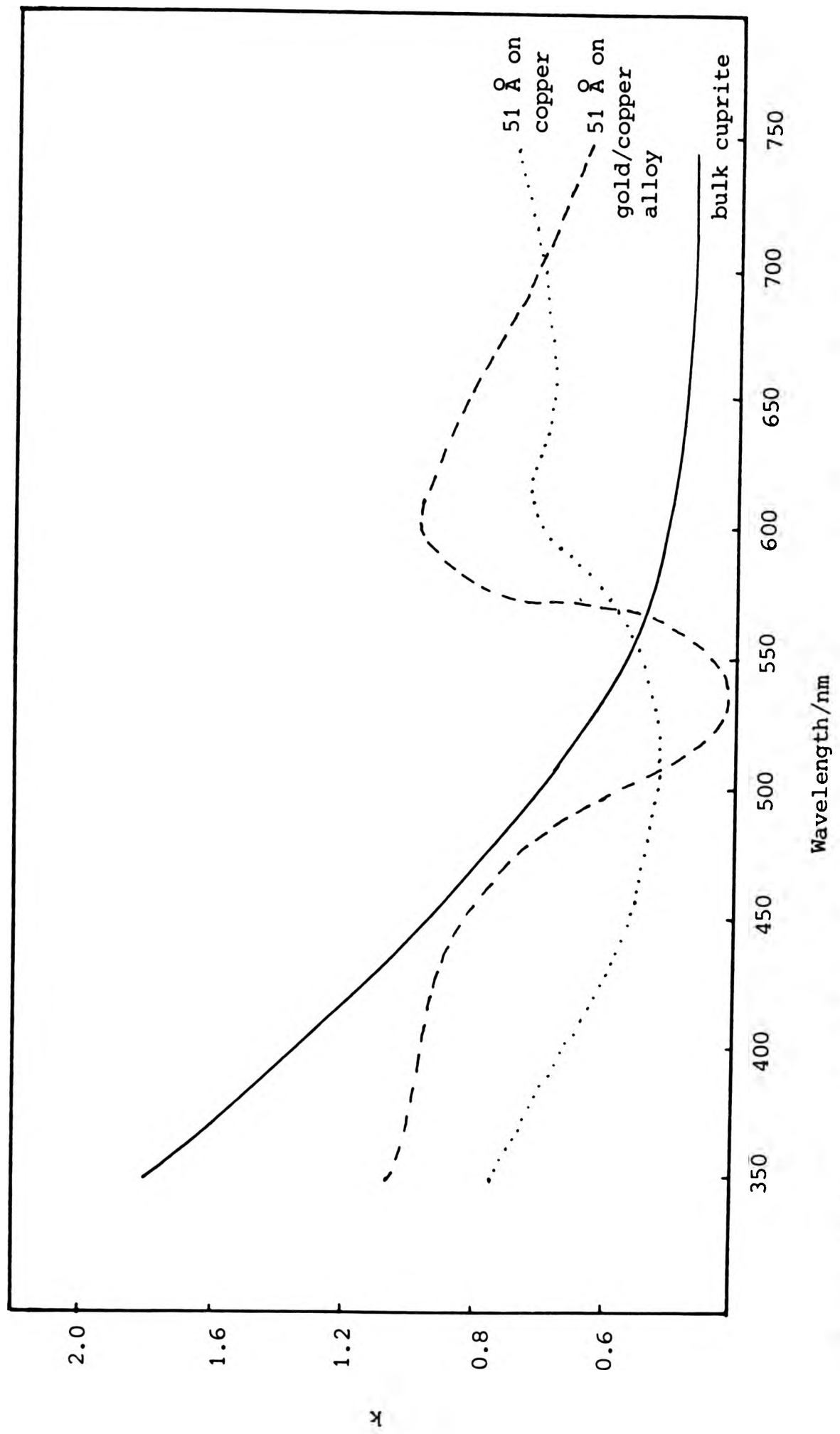
Figure 5.32 The spectral variation of k for thin cuprous oxide films on gold and copper substrates.
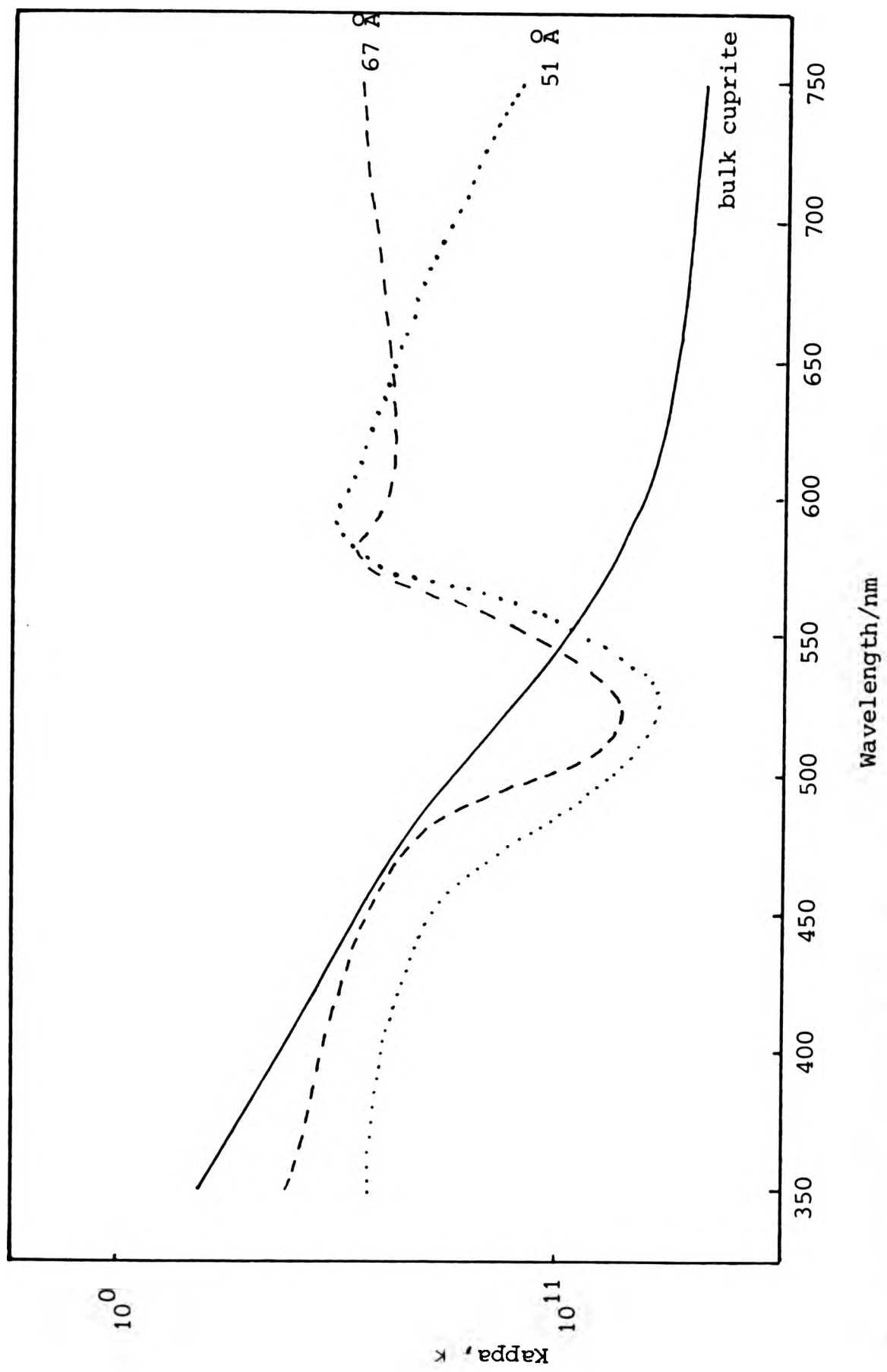
Figure 5.33 The spectral variation of log kappa for cuprous oxide films on gold substrates.

Table 5.16

The values of κ_c, λ_c, ω_c and τ for cuprous oxide films on gold substrates.

Thickness/Å	κ_c	λ_c/nm	ω_c/s^{-1}	τ/s
51	0.319	595	3.17×10^{15}	5.03×10^{-17}
60	0.301	585	3.22×10^{15}	4.67×10^{-17}
67	0.296	580	3.25×10^{15}	4.55×10^{-17}

A graph of log thickness against $\sqrt{\tau}$ (Figure 5.34) gives an interpolated value of 3.86×10^{-17} seconds for τ for a cuprous oxide film 100 Å thick. This is approximately twice the value of τ for a 100 Å cuprous oxide film on a copper substrate and indicates a greater density of carriers

Plots of log $[\lambda_o/(\lambda_o + x)]^2$ against log κ_c for λ_o = 50 Å and 100 Å respectively (Figure 5.35) are linear and converge where log $[\lambda_o/(\lambda_o + x)]^2$ = 0.

5.6.4 Summary

The model proposed by Plumb (84) and extended by Roberts and Ross (85) predicted that a dielectric film on a metallic substrate would exhibit free-carrier behaviour manifested by the appearance of a maximum in the spectral distribution of kappa, at a critical frequency, ω_c. Cuprous oxide films on metallic

204
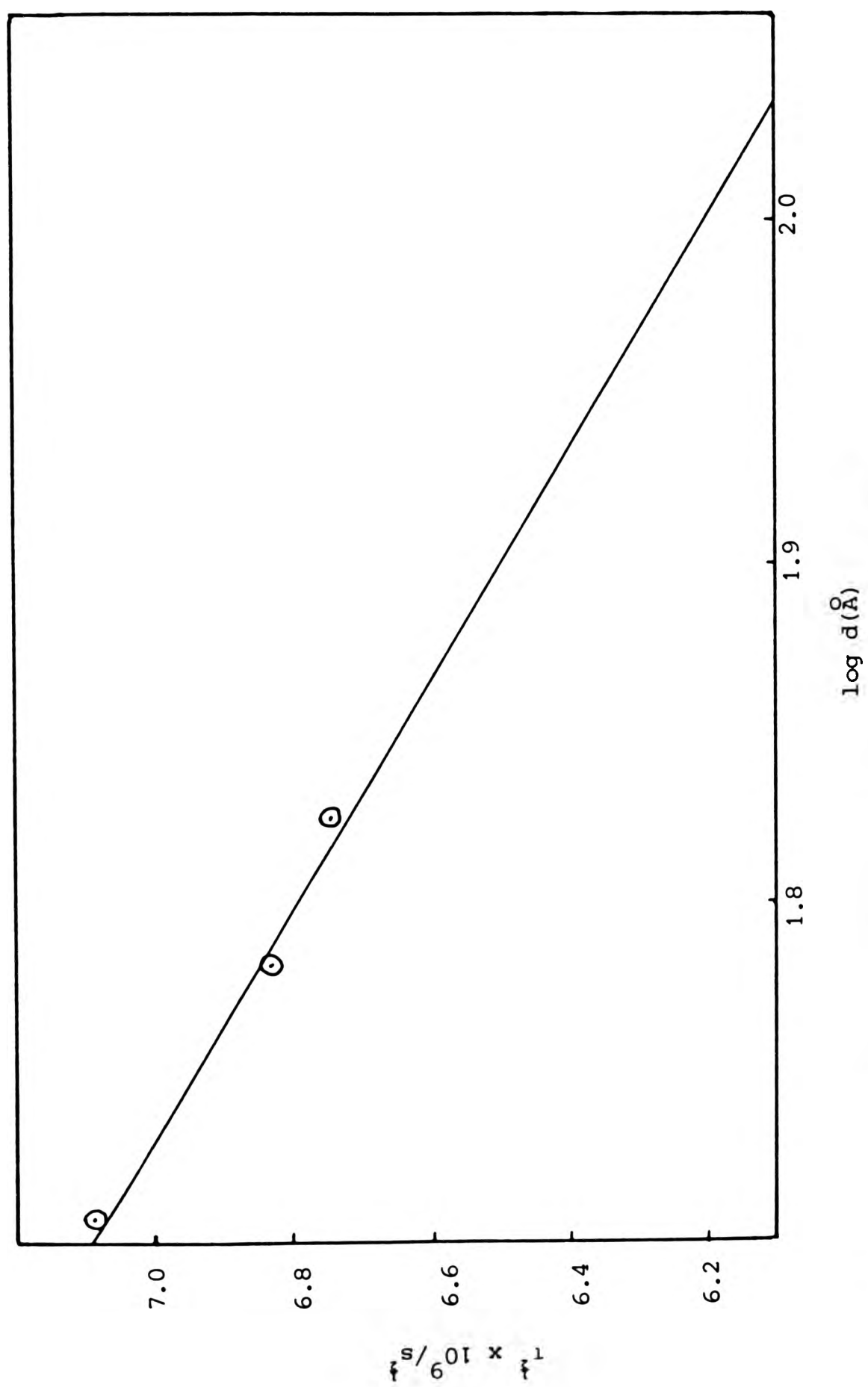
Figure 5.34   Plot of $\tau^{\frac{1}{2}}$ against log d for oxide films on gold
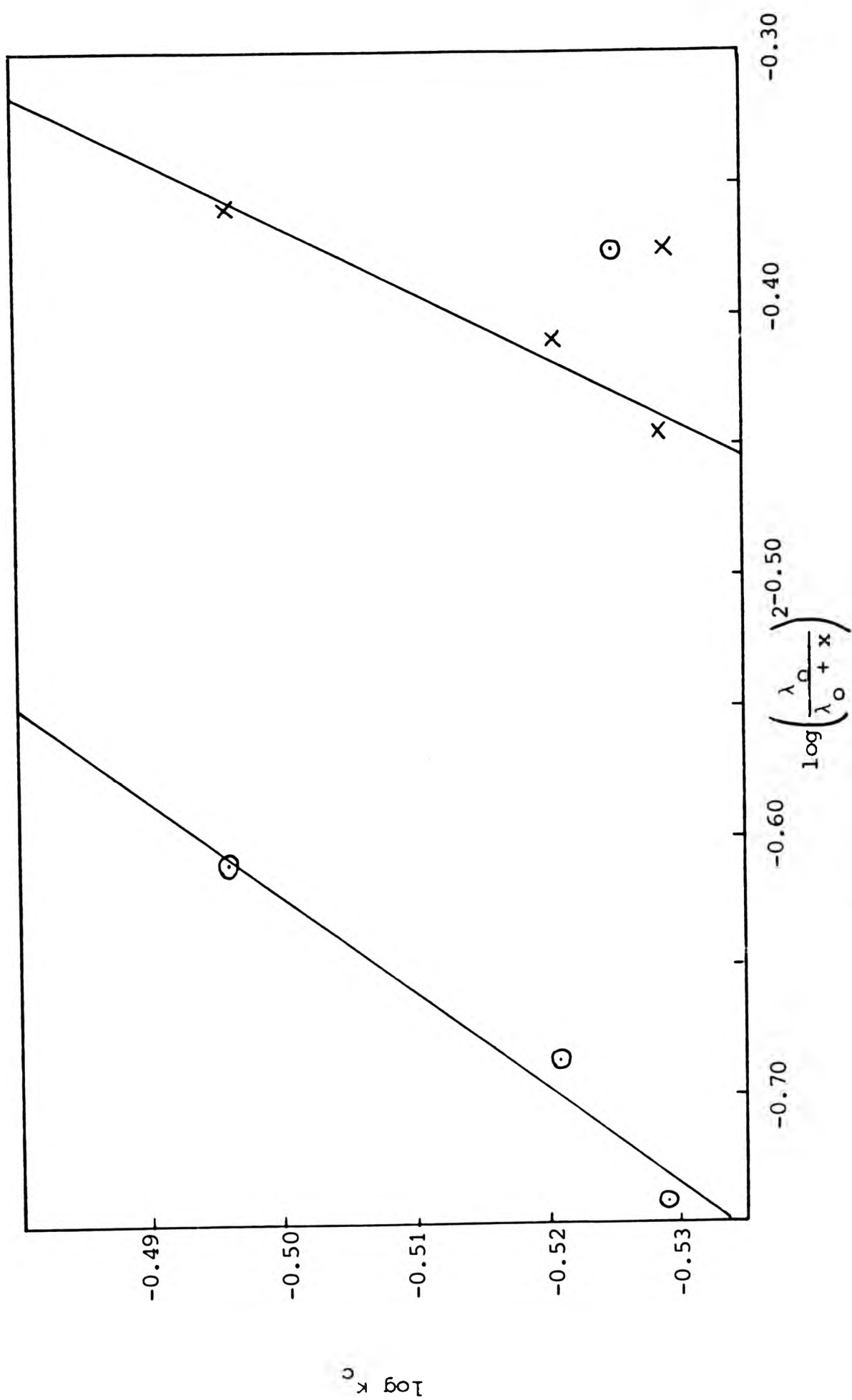
Figure 5.35 Plot of $\log \kappa_c$ versus $\log \left(\dfrac{\lambda_0}{\lambda_0 + x} \right)^2$ for cuprous oxide films on gold.

substrates (both copper and gold based) did indeed behave in
this way. The model also predicted changes in the behaviour of
metallic films on thick dielectric substrates and these were
observed in results obtained by Krautkrämer (121) and analysed
by Roberts and Ross (85). The system used in this case
consisted of a series of gold films on a glass substrate. As
the gold film thickened, the value of kappa increased and the
maximum observed in the thinner films merged into the bulk gold
curve. This system is clearly very different from that used in
this work. Cuprous oxide, even when doped with foreign cations,
has a much lower concentration of carriers than a metal. It
would seem unlikely, therefore, that a thin film of cuprous
oxide would be capable of supplying a sufficient number of
carriers to a bulk dielectric to have any measurable effect on
the optical properties of either the substrate or the film.
Thus the use of a glass substrate would not be expected to have
any appreciable influence on the optical properties of a thin
cuprous oxide film and this is supported by the experimental
results.

5.7 The effect of the substrate on the optical properties of cuprous oxide films

Most of this work has been carried out using copper as a
substrate. In all these experiments very thin films of oxide
show marked differences in their optical properties compared
to those of bulk cuprite. Well defined maxima and minima in
n_f and k_f spectra are smoothed out as the films thicken and
the spectra of the thicker films approach those of the bulk
oxide. This would be expected if the changes in spectra are the

result of an increased carrier concentration arising from the metal/oxide interface. The carrier concentration will decrease with distance from the metal/oxide interface if, as suggested, it results from the transfer of electrons from the metal to the oxide. Similar changes in spectra are seen for the other metallic substrates. For all these metal substrates k_f is consistently higher than the bulk value at longer wavelengths, indicating absorptions due to free carriers obscuring the fundamental lattice absorption.

n_f and k_f spectra for cuprous oxide films on glass are similar in shape to those of the bulk oxide especially for a very thin film. Increases in the value of k_f at the red-end of the spectrum are most likely attributable to a defective or strained oxide film. A small increase in carrier concentration is likely to occur as a result of the defective structure but without electron transfer between the substrate and film, no space-charge region will exist. Thus, thin cuprous oxide films on a glass substrate should have optical constants close to those of the bulk oxide and the experimental results show that they do.

6. CONCLUSIONS AND SUGGESTIONS FOR FURTHER WORK

   6.1 Conclusions

   The following conclusions on the nature and optical characteristics of cuprous oxide films grown on metal and dielectric substrates can be drawn from the preceeding experiments and discussion.

   1. Thermal oxidation of copper or copper alloy specimens at a low temperature proved an effective way of producing layers of cuprous oxide covering a range of thicknesses within the thin film region.

   2. The thickness and optical constants of these films were calculated from ellipsometric measurements over the spectral range 350 to 750 nm. The thickness values are supported by coulometric determinations and are consistent with the interference colours exhibited by the filmed specimens.

   3. The optical constants of the films were found to change with thickness.

   4. As the films thickened the optical constants became closer to those of the bulk oxide.

   5. Cuprous oxide films on dilute copper alloys, were found to have higher values of the absorption coefficient, k_f, particularly at the red-end of the spectrum indicating a more metallic nature.

6. Evaluation of the relaxation times for cuprous oxide films on copper and dilute copper alloys showed a greater density of carriers in oxide films on copper alloyed with higher valent elements.

7. A similar increase in carrier density was observed in cuprous oxide films which had been grown on a gold substrate.

8. No increase in carrier density was observed in the thin films of cuprous oxide on glass showing that the differences were not solely attributable to highly defective films. Thus it has been shown that cuprous oxide films on metallic substrates have increased metallic characteristics due to the nature of the ohmic contact existing between the two chemically distinct phases.

Ellipsometry has long been used as a sensitive, non-destructive method of measuring the changes occurring at a metal surface during oxidation in air or aqueous media. Such studies have often assumed that the optical constants of the appropriate bulk oxide are sufficient to calculate the film thickness even though it has been recognised that the optical constants of thin films may be very different from those of the bulk. Most of the experiments on copper have been carried out at 546.1 nm and have apparently given satisfactory results. Fortuitously, whatever the thickness of the film, the n_f and k_f spectra converge to single values - those of the

bulk at about this wavelength (Figures 4.26 and 4.27). Thus true thickness values of the films will be established at this wavelength although large discrepancies may occur elsewhere.

6.2 Suggestions for further work

The results of this work suggest that the optical properties of thin films of cuprous oxide depend on the nature of the substrate. To confirm this the following work should be undertaken.

1. The optical constants of films of cuprous oxide covering a range of thicknesses produced by active sputtering on copper, gold and glass substrates should be measured.

2. Anodic oxide films on valve metals are dielectrics and the thickness of the film depends on the applied voltage. Measurement of the optical constants of thin cuprous oxide films sputtered onto valve metal substrates bearing oxide films of various thicknesses should show that the effect of a metal substrate is diminished by a layer of dielectric oxide.

3. Iron also bears an oxide which is capable of reduction by coulometry and therefore provides another system for similar studies.

4. Doping of sputtered oxide films by ion implantation with foreign cations would allow investigation of the dependence of the concentration of the implanted species in the cuprous oxide lattice.

Appendix 1

The optical constants of copper

Spectral data for copper covering the wavelength range 350 to 750 nm were required for this work. Unfortunately most workers have taken measurements at isolated wavelengths using, for example, green light from a mercury lamp (λ = 546.1 nm) or red light from a He-Ne laser (λ = 632.8 nm). It has been necessary, therefore, to combine results obtained by three workers to give the required data. The values listed in Table A.1 were plotted to provide the optical constants listed in Table A.2. They consist of values obtained by Roberts (16), Otter (23) and Smith (24) and follow Smith's interpretation of them.

Table A.1

Experimental values of n and k for clean copper substrates

λ	n	k	condition	author
440	1.11	2.56	solidified drop	M. Otter (23)
460	1.09	2.63	"	"
480	1.09	2.72	"	"
500	1.08	2.77	"	"
520	1.04	2.78	"	"
540	0.93	2.74	"	"
560	0.65	2.72	"	"
580	0.28	2.97	"	"
600	0.13	3.45	"	"
620	0.10	3.65	"	"
640	0.10	3.92	"	"
660	0.09	4.06	"	"
365	1.07	2.07	machined, electro-polish	S. Roberts (16)
405	1.05	2.28	"	"
436	1.07	2.46	"	"
500	1.03	2.78	"	"
550	0.79	2.72	"	"
578	0.33	2.89	"	"
600	0.15	3.29	"	"
650	0.11	3.91	"	"
750	0.10	4.89	"	"
546.1	0.89	2.67	mechanical polish, anneal, ion	T. Smith (24)
632.8	0.17	3.70	bombardment	"

Table A.2

The optical constants of copper

Wavelength/nm	n	k		Wavelength/nm	n	k
350	1.14	2.00		465	1.07	2.38
355	1.14	2.03		470	1.07	2.39
360	1.13	2.04		475	1.07	2.40
365	1.13	2.05		480	1.06	2.41
370	1.13	2.08		485	1.06	2.42
375	1.12	2.10		490	1.05	2.43
380	1.12	2.13		495	1.05	2.44
385	1.12	2.14		500	1.05	2.45
390	1.12	2.15		505	1.04	2.47
395	1.11	2.18		510	1.04	2.48
400	1.11	2.19		515	1.04	2.49
405	1.11	2.20		520	1.03	2.50
410	1.11	2.23		525	1.01	2.51
415	1.11	2.24		530	1.00	2.52
420	1.10	2.25		535	0.97	2.54
425	1.10	2.28		540	0.94	2.55
430	1.10	2.30		545	0.91	2.56
435	1.10	2.31		550	0.85	2.56
440	1.09	2.32		555	0.77	2.59
445	1.09	2.33		560	0.67	2.63
450	1.09	2.34		565	0.58	2.69
455	1.08	2.36		570	0.49	2.75
460	1.08	2.37		575	0.40	2.83

Table A.2 contd

Wavelength/nm	n	k
580	0.31	2.90
585	0.26	2.98
590	0.22	3.04
595	0.20	3.11
600	0.18	3.18
605	0.17	3.25
610	0.16	3.32
615	0.16	3.39
620	0.15	3.46
625	0.15	3.54
630	0.15	3.60
635	0.15	3.66
640	0.15	3.71
645	0.15	3.76
650	0.15	3.80
655	0.15	3.83
660	0.15	3.86
665	0.15	3.89
670	0.15	3.92
675	0.15	3.95
680	0.15	3.99
685	0.15	4.02
690	0.15	4.06
695	0.15	4.09
700	0.15	4.13

Wavelength/nm	n	k
705	0.15	4.16
710	0.15	4.20
715	0.15	4.23
720	0.15	4.27
725	0.15	4.30
730	0.15	4.33
735	0.15	4.36
740	0.15	4.39
745	0.15	4.43
750	0.15	4.46

Appendix 2

The optical constants of cuprite

The optical constants of bulk cuprite used in the computations for this work are those determined by Rastall (57).

Table A3

The optical constants of bulk cuprite

Wavelength/nm	n	k	Wavelength/nm	n	k
350	2.678	1.796	430	3.250	1.050
355	2.779	1.775	435	3.266	1.016
360	2.864	1.738	440	3.278	0.987
365	2.943	1.687	445	3.293	0.952
370	3.014	1.621	450	3.307	0.913
375	3.067	1.553	455	3.318	0.874
380	3.105	1.493	460	3.325	0.842
385	3.135	1.431	465	3.330	0.802
390	3.160	1.368	470	3.332	0.762
395	3.178	1.314	475	3.331	0.725
400	3.191	1.267	480	3.328	0.691
405	3.202	1.222	485	3.324	0.659
410	3.211	1.180	490	3.319	0.627
415	3.215	1.146	495	3.316	0.597
420	3.226	1.115	500	3.311	0.568
425	3.237	1.083	505	3.309	0.540

Table A.3 contd

Wavelength/nm	n	k	Wavelength/nm	n	k
510	3.303	0.511	635	2.927	0.164
515	3.295	0.480	640	2.918	0.162
520	3.286	0.450	645	2.910	0.161
525	3.274	0.421	650	2.901	0.158
530	3.258	0.390	655	2.892	0.155
535	3.242	0.362	660	2.886	0.153
540	3.224	0.338	665	2.880	0.152
545	3.205	0.316	670	2.873	0.151
550	3.183	0.295	675	2.866	0.149
555	3.162	0.277	680	2.860	0.147
560	3.143	0.262	685	2.854	0.145
565	3.123	0.249	690	2.849	0.143
570	3.103	0.236	695	2.843	0.143
575	3.085	0.225	700	2.838	0.142
580	3.068	0.217	705	2.832	0.141
585	3.051	0.209	710	2.828	0.139
590	3.035	0.202	715	2.823	0.136
595	3.020	0.196	720	2.818	0.136
600	3.006	0.190	725	2.813	0.136
605	2.993	0.185	730	2.810	0.136
610	2.981	0.181	735	2.805	0.135
615	2.968	0.177	740	2.801	0.132
620	2.958	0.174	745	2.797	0.131
625	2.948	0.171	750	2.793	0.131
630	2.937	0.166			

Appendix 3

The film-fitting program

This appendix shows how the KCNEP1 film-fitting program has been used
to evaluate the optical constants and thickness of the oxide films on
a specimen of copper/gallium alloy. The files used are:-

    COPPER.   n and k values of the copper substrate

    CUPRIT.   n and k values of bulk cuprite

    GAOX33   experimental data.

RUN KCNEP1[,1

TYPE S FOR SPECTRAL INPUT, N FOR NON-SPECTRAL

*S

WAVELENGTH LIMITS

*350,750

SUBSTRATE FILE, ADJ.N, ADJ.K,DATASET

*COPPER. FF1

FILM GUESS FILE, ADJ.N,ADJ.K,DATASET

*CUPRIT. TT1

NO ANGLES, NO FILMS

*1.1

THICKNESS OF FILM 1 ADJ

*14T

INPUT FILE FOR FILMED SYSTEM:FILM 1 ANGLE 1 DATASET?

*GAOX33. 1

* Denotes input

Table A.4

Results of repeated iterations

No of iterations	Average thickness/nm	Average RMS error per angle	Standard deviation/nm
1	13.8143	0.025	1.8
2	13.7092	0.024	1.8
3	13.6528	0.025	1.8
4	13.6103	0.025	1.8
5	13.5873	0.024	1.8
6	13.5787	0.025	1.8
7	13.5577	0.024	1.7

The program is repeated with the same responses apart from replacing "14T" by "13.56F". This generates the film optical constants together with the root-mean-square error at each wavelength.

Table A.5

Optical constants of the oxide film

Wavelength/nm	RMS error	n	k
350	0.5278E-03	2.6804	0.9006
355	0.2754E-05	2.7346	0.8962
360	0.1182E-04	2.7799	0.8862
365	0.4152E-04	2.8290	0.8656
370	0.2092E-04	2.8808	0.8368
375	0.4490E-03	2.9267	0.8053
380	0.1400E-03	2.9650	0.7782
385	0.1242E-04	2.9939	0.7448
390	0.2200E-03	3.0205	0.7042
395	0.2989E-04	3.0484	0.6705
400	0.6496E-03	3.0702	0.6444
405	0.6850E-05	3.871	0.6131
410	0.5332E-05	3.1079	0.5780
415	0.9909E-04	3.1247	0.5465
420	0.1194E-04	3.1424	0.5206
425	0.3119E-04	3.1652	0.4920
430	0.1284E-04	3.1836	0.4550
435	0.1350E-05	3.1939	0.4200
440	0.1751E-04	3.2056	0.3911

Table A.5 contd

Wavelength/nm	RMS error	n	k
445	0.3443E-04	3.2109	0.3531
450	0.1340E-04	3.2035	0.3111
455	0.6245E-04	3.2043	0.2765
460	0.2377E-04	3.2003	0.2488
465	0.1599E-04	3.1925	0.2193
470	0.4503E-04	3.1817	0.1890
475	0.1407E-04	3.1682	0.1655
480	0.3744E-04	3.1533	0.1499
485	0.1431E-04	3.1456	0.1311
490	0.4167E-04	3.1269	0.1142
495	0.7696E-05	3.133	0.1004
500	0.4322E-05	3.1179	0.0907
505	0.4457E-05	3.1112	0.0804
510	0.1281E-04	3.1022	0.0696
515	0.4457E-04	3.1004	0.0601
520	0.9282E-04	3.1012	0.0597
525	0.1245E-04	3.1030	0.0567
530	0.1994E-04	3.1092	0.0569
535	0.5244E-04	3.1059	0.0626
540	0.6037E-06	3.1148	0.0643
545	0.2088E-04	3.1160	0.0688
550	0.2635E-04	3.1091	0.0816
555	0.2188E-04	3.1151	0.1104
560	0.4211E-04	3.1268	0.1605
565	0.2177E-05	3.1520	0.2002

Table A.5 contd

Wavelength/nm	RMS error	n	k
570	0.5211E-05	3.1657	0.2343
575	0.1009E-04	3.1918	0.2788
580	0.4838E-04	3.2214	0.3342
585	0.7923E-05	3.2478	0.3556
590	0.1539E-05	3.2596	0.3587
595	0.5211E-05	3.2902	0.3623
600	0.4269E-06	3.3254	0.3655
605	0.6453E-05	3.3463	0.3559
610	0.0000E+00	3.3893	0.3540
615	0.4269E-06	3.4120	0.3439
620	0.6750E-06	3.4505	0.3387
625	0.3924E-05	3.4834	0.3286
630	0.3019E-06	3.4982	0.3148
635	0.1708E-04	3.5208	0.3022
640	0.946E-05	3.5442	0.2951
645	0.4269E-06	3.5568	0.2845
650	0.0000E+00	3.5581	0.2767
655	0.3019E-06	3.5576	0.2675
660	0.6750E-06	3.5618	0.2610
665	0.3320E-05	3.5628	0.2531
670	0.74265E-04	3.5538	0.2451
675	0.3078E-05	3.5479	0.2396
680	0.2962E-04	3.5643	0.2367
685	0.4322E-05	3.5724	0.2303
690	0.0000E+00	3.5690	0.2277

Table A.5 contd

Wavelength/nm	RMS error	n	k
695	0.0000E+00	3.5722	0.2237
700	0.8538E-06	3.5836	0.2199
705	0.1070E-04	3.5984	0.2162
710	0.2561E-05	3.5799	0.2097
715	0.1509E-05	3.5879	0.2064
720	0.1350E-05	3.25926	0.2050
725	0.1509E-04	3.5880	0.2006
730	0.1909E-05	3.5976	0.1977
735	0.2434E-05	3.5970	0.1967
740	0.3078E-05	3.6065	0.1945
745	0.4050E-05	3.5935	0.1887
750	0.3019E-06	3.5924	0.1863

Average RMS error per angle = 0.000

Table A.6 lists the values of ψ and Δ computed by the MNEMON program for a copper substance overlaid with 13.56 nm of the film whose optical constants are listed in Table A.5 and compares them with the experimental data.

Table A.6

Comparison of experimental and computed data

Wavelength/nm	Experimental		Computed	
	ψ	Δ	ψ	Δ
350	27.00	23.60	27.00	23.63
355	26.92	22.42	26.92	22.40
360	26.95	21.16	26.95	21.15
365	27.14	19.52	27.13	19.53
370	27.56	17.84	28.55	17.84
375	28.11	16.40	28.11	16.38
380	28.66	15.46	28.66	15.46
385	29.36	14.50	29.36	14.50
390	30.29	13.74	30.30	13.76
395	31.14	13.38	31.15	13.40
400	31.71	13.14	31.82	13.15
405	32.66	13.16	32.66	13.16
410	33.63	13.38	33.63	13.38
415	34.48	13.48	34.47	13.47
420	35.21	13.78	35.20	13.80
425	36.03	14.16	36.03	14.17
430	37.08	14.84	37.08	14.82
435	38.06	15.62	38.06	15.61
440	38.87	16.40	38.87	16.38
445	39.89	17.66	39.89	17.66
450	40.93	19.78	40.94	19.76
455	41.74	21.48	41.73	21.49
460	42.27	23.38	42.26	23.39

Table A.6 contd

Wavelength/nm	Experimental		Computer	
	ψ	Δ	ψ	Δ
465	42.73	24.50	42.83	25.53
470	43.09	27.74	43.09	27.73
475	43.19	29.86	43.18	29.86
480	43.07	31.72	43.07	31.73
485	43.06	33.28	43.07	33.27
490	42.87	35.04	42.87	35.04
495	42.79	36.16	42.79	36.18
500	42.61	37.16	42.61	37.15
505	42.45	38.16	42.45	38.17
510	42.28	39.16	42.27	39.16
515	42.15	39.90	42.15	39.91
520	42.05	40.48	42.05	40.48
525	41.97	41.06	41.97	41.06
530	41.91	41.68	41.91	41.68
535	41.90	42.20	41.90	42.19
540	41.93	42.64	41.93	42.64
545	41.99	43.12	41.99	43.12
550	42.11	43.78	42.11	43.78
555	42.27	44.52	42.27	44.53
560	42.37	44.98	42.38	44.98
565	42.50	45.76	42.50	45.76
570	42.59	46.70	42.59	46.70
575	42.64	47.50	42.64	47.50
580	42.66	48.18	42.66	48.19

Table A.6 contd

Wavelength/nm	Experimental		Computed	
	ψ	Δ	ψ	Δ
585	42.65	48.94	42.65	48.94
590	42.65	49.76	42.65	49.75
595	42.64	50.38	42.64	50.38
600	42.63	50.92	42.63	50.92
605	42.64	51.66	42.64	51.66
610	42.64	52.08	42.64	52.08
615	42.65	52.76	42.65	52.76
620	42.65	53.22	42.65	53.23
625	42.66	53.76	42.66	53.76
630	42.68	54.42	42.68	54.42
635	42.68	54.42	42.68	54.42
635	42.71	54.98	42.71	54.98
640	42.72	55.42	42.72	55.42
645	42.75	55.92	42.75	55.92
650	42.76	56.56	42.76	56.56
655	42.79	57.08	42.79	57.08
660	42.81	57.54	42.81	57.54
665	42.84	58.04	42.84	58.04
670	42.87	58.66	42.87	58.66
675	42.89	59.24	42.89	59.24
680	42.90	59.60	42.90	59.60
685	42.93	60.06	42.93	60.07
690	42.94	60.66	42.94	60.66
695	42.96	61.18	42.96	61.18

Table A.6 contd

Wavelength/nm	Experimental		Computed	
	ψ	Δ	ψ	Δ
700	42.98	61.60	42.98	61.60
705	43.00	61.98	43.00	61.99
710	43.04	62.76	43.04	62.76
715	43.06	63.22	43.06	63.22
720	43.07	63.72	43.07	63.72
725	43.10	64.28	43.10	64.28
730	43.12	64.70	43.12	64.70
735	43.13	65.24	43.13	65.24
740	43.15	65.66	43.15	65.65
745	43.19	66.34	43.19	66.35
750	43.12	66.88	43.21	66.89

Table A.7 shows that the final average thickness remains 13.56 nm.
when a different estimate (perhaps derived from a different portion
of the Δ v ψ plot) is chosen.

Table A.7

Convergence of computed average thickness

No of iterations	Average thickness/nm	RMS error per angle	Standard deviation
0	23.30	0.035	3.2
1	17.6443	0.021	2.2
2	15.6112	0.026	1.9
3	14.7032	0.024	1.9
4	14.2135	0.032	1.9
5	13.9342	0.022	1.8
6	13.7763	0.025	1.8
7	13.6840	0.021	1.8
8	13.6356	0.021	1.8
9	13.5922	0.021	1.8
10	13.5802	0.025	1.8
11	13.5694	0.023	1.8
12	13.5636	0.026	1.8
13	13.5603	0.024	1.7

REFERENCES

1   H.A. Lorenz, "The theory of electrons", Dover Publications, N.Y., 1952.

2   P.K.L. Drude, "Theory of optics", Dover Publications, N.Y., 1959.

3   F. Wooten, "Optical properties of solids", Academic Press, 1972.

4   H. Ehrenreich, H.R. Philipp, Phys. Rev. 1962, 128, 1622.

5   F.M. Mueller, J.C. Phillips, Phys. Rev. 1967, 157, 600.

6   D.H. Seib, W.E. Spicer, Phys. Rev. Lett. 1969, 22, 711.

7   U. Gerhardt, Phys. Rev. 1969, 172, 651.

8   C.Y. Fong, M.L. Cohen, R.R.L. Zucca, J. Stokes, Y.R. Shen, Phys. Rev. Lett. 1970, 25, 1486.

9   R. Minor, Ann Phys. 1903, 10, 581.

10   A. Tool, Phys. Rev. 1910, 31, 1.

11   K. Foersterling, K. Freedericksz, Ann Phys. 1913, 40, 201.

12   H. Margenau, Phys. Rev. 1929, 33, 1033.

13   J. Lowery, Phil. Mag. 1936, 22, 769.

14   G. Beilby, "Aggregation and flow of solids", MacMillan, London, 1921.

15   D.M. Turley, L.E. Samuels, Metallography, 1981, 14, 275.

16   S. Roberts, Phys. Rev. 1960, 118, 1509.

17   R. Kretzmann, Ann Phys. 1940, 37, 303.

18   J.F. Archard, P.L. Clegg, A.M. Taylor, Proc. Phys. Soc. 1952, B65, 758.

19   A.B. Winterbottom, Kgl. Norske Videnskab, Selskab Fosh, 1955, Skrifter No.1, 95.

20   L.R. Ingersoll, Astrophys. J. 1910, 32, 282.

21   K. Weiss, Z. Naturforsch, 1948, A3, 143.

22   L.G. Schultz, Suppl. Phil. Mag. 1957, 6, 102.

23   M. Otter, Z. Phys. 1961, 161, 163.

24   T. Smith, J. Opt. Soc. Am. 1977, 67, 48.

25   P.C.S. Hayfield, First International Congress on Metallic Corrosion, Butterworths, 1961.

26   E.C. Butcher, A.J. Dyer, N.E. Gilbert, Brit. J. Appl. Phys.
      (J. Phys. D.) 1968, Ser. 2. 1, 1673.

27   J.A.S. Green, H.D. Mengelberg, H.T. Yolken, J. Electrochem.Soc.
      1970, 117, 433.

28   P.B. Johnson, R.W. Christy, Phys. Rev. B, 1972, 6, 4370.

29   G.W.C. Kaye, T.H. Laby, "Tables of Physical and Chemical
      Constants, 14th Edition", Longman, 1973.

30   J. Weaver, "Handbook of chemistry and physics - 64th Edition"
      Chemical Rubber Co. Press, 1984.

31   H.J. Hagemann, W. Gudat, C. Kunz, J. Opt. Soc. Am. 1975, 65,
      742.

32   H.C. Alexander, PhD Thesis, University of Alabama, 1976.

33   J.S. Hartman, App. Opt. 1981, 20, 4062.

34   M. Roychaudhuri, S. Chatterjee, Ind. J. Phys. 1982, 56A, 86.

35   P.F. Robusto, R. Braunstein, Phys. Stat. Sol. (B), 1981, 107,
      443.

36   R. Lässer, N.V. Smith, R.L. Benbow, Phys. Rev. B. 1981, 24,
      1895.

37   R. Lässer, N.V. Smith, Solid State Commun. 1981, 37, 501.

38   J.C. Phillips, Solid State Physics, 1966, 18, 56.

39   M. Hayashi, J. Faculty of Sc., Japan (II), 1952, 4, 107.

40   E.F. Gross, N.A. Karryev, Doklady, A.N. S.S.S.R. 1952, 84, 261.

41   S. Nikitine, G. Perny, M. Sieskind, J. Phys. Radium, 1954,
      15, 185.

42   I.S. Gorban, Optics and Spectrosc. (USA) 1960, 9, 398.

43   I. Pastrnyak, Sov. Phys. - Solid State, 1961, 3, 633.

44   E.F. Gross, Chang Kuang-yin, Doklady A.N. S.S.S.R., 1962,
      143, 1321.

45   J.P. Dahl, A.C. Swittendick, J. Phys. Chem. Solids, 1966,
      27, 931.

46   Z.M. Jarzebski, "Oxide semiconductors", Pergamon Press, N.Y.,
      1973.

47   Ch. Uihlein, D. Fröhlich, R. Kenklies, Phys. Rev. B. 1981, 23,
      2731.

48   N.O. Lipari, A. Baldereschi, Solid State Commun. 1978, 25, 665.

49   T.N. Rhodin, J. Amer. Chem. Soc. 1950, 72, 5102.

50   A.T. Gwathmey, A.F. Benton, J. Phys. Chem. 1942, 46, 969.

51   F.W. Young, J.V. Cathcart, A.T. Gwathmey, Acta Met. 1956, 4, 145.

52   F.W. Young, Dissertation, University of Virginia, 1950.

53   S.M. Wilhelm, Y. Tanizawa, Chang-Li Yiu, N. Hackerman, Corr. Sci. 1982, 22, 791.

54   K. Bärwinkel, H.J. Schmidt, Thin Solid Films, 1979, 59, 373.

55   V.F. Drobny, D.L. Pulfrey, Thin Solid Films, 1979, 61, 89.

56   H. Wieder, A.W. Czandera, J. Phys. Chem. 1962, 66, 816.

57   P. Rastall, C.N.A.A. PhD Thesis, 1980.

58   G. Bartz, D. Kossel "Atlas of Interference Layer Metallography" Metallography Subcommittee Deutsche Gesellschaft für Metallkunde, 1980.

59   Ernst Leitz GmbH, Wetzlar, unpublished work.

60   Bjorn Karlsson, G.G. Ribbing, A. Roos, E. Valkonen, T. Karlsson, Phys. Scripta, 1982, 25, 826.

61 L.J. Hanekamp, W. Lisowski, G.A. Bootsma, Surf. Sci. 1982, <u>118</u>, 1.

62 F.H.P.M. Habraken, O.L.J. Gijzeman, G.A. Bootsma, Surf. Sci. 1980, <u>96</u>, 482.

63 E.C. Williams, P.C.S. Hayfield, "Vacancies and other point defects in metals and alloys" Inst. of Metals Sym. No.23 1958.

64 A. Aveline, I.R. Bonilla, Solar Energy Mat. 1981, <u>5</u>, 211.

65 E. Fortin. W.M. Sears, Can. J. Phys. 1982, <u>60</u>, 901.

66 G. Garnaud, Oxidation of Metals, 1977, <u>11</u>, 127.

67 A. Daude, A. Savary, S. Robin, Thin Solid Films, 1972, <u>13</u>, 255.

68 J. O'M. Bockris, M. Gerhsaw, V. Brusic, Sym. Faraday Soc. 4, 1971, 177.

69 C.A. Fenstermaker, F.L. McCrackin, Surf. Sci. 1969, <u>16</u>, 85.

70 J. Bodesheim, A. Otto, Surf. Sci. 1974, <u>45</u>, 441.

71 O. Hunderi, Thin Solid Films, 1979, <u>57</u>, 15.

72 K. Brudzewski, Thin Solid Films, 1979, <u>61</u>, 183.

73 T.V. Vorburger, K.C. Ludema, App. Opt. 1980, <u>19</u>, 561.

74   T. Smith, J. Electroanal.Chem. 1983, 150, 277.

75   F.L. McCrackin, Nat. Bur. Stand. Tech. Note 479, 1969.

76   I. Ohlidahl, F. Lukĕs, Opt. Acta, 1975, 19, 817.

77   E.L. Church, J.M. Zavada, App. Opt. 1975, 14, 1788.

78   Z.M. Zorin and M.N. Churaeva. Opt Spectrosc. (USA), 1982, 52, 1046.

79   P. Rastall, K. Mc. Clarke and E.F.I. Roberts, Min. Mag. 1980, 43. 633.

80.   A.H. Clark, "Polycrystalline and amorphous thin films and devices", ed. L.L. Kazmerski, Academic Press, 1980.

81   I. Filinski, Phys. Stat. Sol. (b), 1972, 49, 577.

82   D.E. Aspnes, Surf. Sci. 1980, 101, 84.

83   D.E. Aspnes, Thin Solid Films, 1982, 89, 249.

84   R.C. Plumb, Journal de Physique, 1964, 25, 69.

85   E.F.I. Roberts, D. Ross, Surf. Sci. 1976, 56, 425.

86   F. Meyer, M.J. Sparnaay, "Surface physics of phosphors and semiconductors", ed. C.G. Scott, C.E. Reed, Academic Press, 1975.

87   M.A. Van Hove, Surf. Sci. 1979, 80, 1.

88   F. Meyer, Silic. Ind. 1974, 39, 181.

89   P.S. Hawge, Surf. Sci. 1980, 96, 108.

90   F.L. McCrackin, J.P. Colson, Proc. Sym. on Ellipsometry in the measurement of surfaces on thin films, Washington DC, 1963 (Washington DC, Nat. Bur. of Standards).

91   F.L. McCrackin, J.P. Colson, 1964, Nat. Bur. of Standards Tech. Note, No.242.

92   I.N. Shklyarevskii, A.F.A. El Shazli, R.G. Yarovaya, V.P. Kostyuk, Opt. Spectrosc. 1974, 36, 116.

93   D. Schueler, Surf. Sci. 1969, 16, 104.

94   M.E. Pedinoff, O.M. Stafsudd, Applied Optics, 1982, 21, 518.

95   F.L. McCrackin, Natl. Bureau of Standards (US), Tech. Note 479, Washington DC. 1969.

96   K. Mc. Clarke, C.N.A.A. PhD Thesis, 1980.

97   M.J.D. Powell, Comp. J. 1968, 11, 302.

98   E.F.I. Roberts,   A. Meadows, J. Physics, 1974, 1, 379.

99   R.H. Muller, Advances in Electrochem. and Electrochem. Eng. 1973, 9, 167.

100   P.H. Osborne, C.N.A.A. PhD Thesis, 1978.

101   M. Pourbaix, Atlas of Electrochemical Equilibria, 1966.

102   E. Mattsson, Electrochem. Acta, 1961, 3, 229.

103   E.F.I. Roberts, C.J.L. Booker, P. Osborne, H. Salim, Corr. Sci. 1974, 14, 307.

104   Handbook of Chemistry and Physics, 62nd edition, Chemical Rubber Publishing Co., 1982

105   T.A. MacMath, R.A.D. Hewko, O. Singh, A.E. Curzon, J.C. Irwin, J. Opt. Soc. Am. 1977, 67, 630.

106   J. Cassett, J. Opt. Soc. Am, 1979, 69, 725.

107   C.J.L. Booker, M. Salim, Nature, 1972, 239, 62.

108   X-ray powder data file, ASTM, 1968.

109   W.E. Campbell, U.B. Thomas, Trans. Electrochem. Soc. 1939, 76, 303.

110   M.R. Pinnel, H.G. Tompkins, D.E. Smith, Appl. Surf. Sci.
      1979, 2, 558.

111   S.L. Marchiano, C.I. Elsner, A.J. Arvia, J. Appl. Electrochem
      1980, 10, 365.

112   A.G. Akimov, I.L. Rosenfel'd, M.G. Asta'fev, Electrochimiya,
      1976, 12, 570.

113   M. Stedman, Symposium of the Faraday Society, 1970, 4, 64.

114   S. Brahms, S. Nikitine, Solid State Commun. 1965, 3, 309.

115   E.F.I. Roberts, Private communication.

116   N.F. Mott, R.W. Gurney "Electronic processes in ionic crystals"
      2nd edit. Oxford University Press, 1950.

117   J.G. Simmons "Handbook of thin film technology" edt. L.I.
      Maissel and R. Glang.

118   F. Abeles, "Optical properties of solids" edit. F. Abeles,
      North Holland Publishing Co., Amsterdam, 1972.

119   D.L. Greenaway, G. Harbeke, "Optical properties and band
      structure of semiconductors 1", Pergamon Press, 1968.

120   R.S. Zucker, J. Electrochem. Soc. 1965, 112, 417.

121   J. Krautkramer, Ann.der Physik, 1938, <u>32</u>, 537.

D66357 86

END